University of Kentucky

UKnowledge

University of Kentucky Doctoral Dissertations

Graduate School

2009

LIPID-BASED PACLITAXEL AND DOXORUBICIN NANOPARTICLES TO OVERCOME P-GP-MEDIATED DRUG RESISTANCE IN SOLID TUMORS

Xiaowei Dong
University of Kentucky, xdong2@email.uky.edu

Right click to open a feedback form in a new tab to let us know how this document benefits you.

ABSTRACT OF DISSERTATION

Xiaowei Dong

The Graduate School

University of Kentucky

2009

LIPID-BASED PACLITAXEL AND DOXORUBICIN NANOPARTICLES TO
OVERCOME P-GP-MEDIATED DRUG RESISTANCE IN SOLID TUMORS

ABSTRACT OF DISSERTATION

A dissertation submitted in partial fulfillment of the requirements for the degree of Doctor
of Philosophy in the College of Pharmacy at the University of Kentucky

By

Xiaowei Dong

Lexington, Kentucky

Co-Directors: Dr. Russell Mumper, Professor of Molecular Pharmaceutics,

University of North Carolina at Chapel Hill, North Carolina

and Dr. Val R. Adams, Associate professor of Pharmacy Practice and Science,

Lexington, Kentucky

2009

ABSTRACT OF DISSERTATION

LIPID-BASED PACLITAXEL AND DOXORUBICIN NANOPARTICLES TO
OVERCOME P-GP-MEDIATED DRUG RESISTANCE IN SOLID TUMORS

Multidrug resistance (MDR) is a major obstacle limiting chemotherapeutic efficacy. The purpose of these studies was to investigate the potential application of injectable paclitaxel (PX) and doxorubicin (Dox)-loaded nanoparticles (NPs) engineered from oil-in-water microemulsion precursors for overcoming P-glycoprotein (P-gp)-mediated drug resistance in solid tumors.

An in-vitro study was performed to test whether the oil (stearyl alcohol and cetyl alcohol) used to make lipid nanoparticles could be metabolized. The results showed that the concentrations of the fatty alcohols within nanoparticles, which were quantitatively determined over time by gas chromatography, decreased to only 10-20% of the initial concentration after 15-24 h of incubation with horse liver dehydrogenase (HLADH) and NAD^+ at 37ºC. Moreover, the surfactant Brij 78 (polyoxyethylene 20-sterayl ether) in the nanoparticles influenced the activity of the enzyme.

Novel Cremophor EL-free paclitaxel-loaded nanoparticles were developed using experimental design combining Taguchi array and sequential simplex optimization. The resulting PX G78 and PX BTM NPs were stable at 4ºC over five months and in PBS at 37ºC over 102 h. Release of PX from PX NPs was slow and sustained without initial burst release. Interestingly, PX BTM NPs could be lyophilized without cryoprotectants and without changing any physiochemical properties and bioactivities. Cytotoxicity studies in breast cancer MDA-MB-231 cells showed that PX NPs have similar anti-cancer activities compared to Taxol. Optimized Dox-loaded NPs were prepared using an ion-pair agent, sodium tetradecyl sulfate (STS), to mask Dox charge and to enhance its entrapment in NPs.

In-vitro cytotoxicity studies were carried out in both sensitive and resistant human cancer cells treated with PX and Dox-loaded NPs. All of drug-loaded NPs decreased IC50 values by 6-13-fold in resistant cells compared to free drugs. A series of in-vitro assays were used to understand the underlying mechanisms. The results, in part, showed that the NPs inhibited P-gp and transiently depleted ATP, leading to enhanced uptake and prolonged retention of the drugs in P-gp-overexpressing cancer cells.

Finally, in-vivo anti-cancer efficacy studies were performed using pegylated PX BTM NPs after intravenous (i.v.) injection and showed marked anti-cancer efficacy in nude mice bearing resistant NCI/ADR-RES tumors versus all control groups. These results

suggest that NPs may be used to both target drug and biological mechanisms to overcome MDR.

Xiaowei Dong
_____

May 20, 2009
_____

LIPID-BASED PACLITAXEL AND DOXORUBICIN NANOPARTICLES TO
OVERCOME P-GP-MEDIATED DRUG RESISTANCE IN SOLID TUMORS

By

Xiaowei Dong

Dr. Russell J. Mumper
Co-Director of Dissertation

Dr. Val R. Adams
Co-Director of Dissertation

Dr. Janice Buss
Director of Graduate Studies

May 20, 2009
Date

DISSERTATION

Xiaowei Dong

The Graduate School

University of Kentucky

2009

LIPID-BASED PACLITAXEL AND DOXORUBICIN NANOPARTICLES TO OVERCOME P-GP-MEDIATED DRUG RESISTANCE IN SOLID TUMORS

_____

DISSERTATION

_____

A dissertation submitted in partial fulfillment of the requirements for the degree of Doctor of Philosophy in the College of Pharmacy at the University of Kentucky

By

Xiaowei Dong

Lexington, Kentucky

Co-Directors: Dr. Russell Mumper, Professor of Molecular Pharmaceutics,

University of North Carolina at Chapel Hill, North Carolina

and Dr. Val R. Adams, Associate professor of Pharmacy Practice and Science,

Lexington, Kentucky

2009

To my husband, father, mother and son for their love and support and patience over the last few years

ACKNOWLEDGEMENTS

This dissertation holds far more than the culmination of years of my Ph.D. study. The printed pages in this dissertation also reflect the support and patience from many generous and inspiring people. Without their support this dissertation would not have been written. First and foremost, I wish to thank my advisor Dr. Russell Mumper for his continuous support. His unchanging confidence in me always encouraged me to face any challenges in my research. I will always remember his words for me: "you can make it!" He was always there to listen and to give guidance and encouragement. I want to thank him for bringing me so many opportunities to help me mature as a scientist and also as a person. He not only showed me different ways to approach a research problem, but also taught me how to build up a productive research team and the importance of maintaining good communication with other members of the team. His enthusiasm, passion and dedication have modeled lessons I will carry forward with me in my future work.

Besides my advisor, I would like to thank Dr. Val Adams and Dr. Michael Jay for being the co-advisors for my dissertation. I would also like to express my thanks and appreciation to the rest of my dissertation committee: Dr. Jeffrey A Moscow and Dr. James Z Hilt, who asked me challenging and thoughtful questions, and pushed me to achieve the best Ph.D. research. I would also like to thank Dr. Hollie Swanson as my outside examiner for her time and attention during this busy semester.

Collaboration also played a key role in the success of this dissertation project. I would like to thank Cynthia Mattingly in Dr. Adam's group for her support and expertise. I would also like to thank Dr. Michael Tseng at the University of Louisville for his support and many discussions.

I am also appreciative for all the previous and current students in Dr. Mumper's lab for sharing comments on my work and the collaborations.

I would also express my appreciation to Dr. Janice Buss and Catina Rossoll for assisting me with the administrative tasks necessary for completing my doctoral program, especially after I moved to UNC.

Last, but not least, I would like to thank my family: my parents, Xinlin Dong and Shuqin Zhong, for their unending love, unconditional support and trust during the long years of my education. I would like to thank my husband, Yongmin Liu, for his love and

TABLE OF CONTENTS

LIST OF TABLES

Chapter 1

Introduction and statement of problem

Cancer is a leading cause of death worldwide. The disease accounted for 7.9 million deaths (or around 13% of all deaths worldwide) in 2007 [1]. Over 85% of human cancers are solid tumors. Surgery and irradiation are the initial treatments for most cancers. However, when tumor becomes metastatic, chemotherapy plays a major role, especially for the management of recurrent disease.

There are a number of agents with established single-agent activity against cancer, with the anthracyclines [2] and taxanes [3] generally considered the most active. Selection of agents for treatment is a process relied on the patient. The relative benefits and toxicities of individual anti-cancer agent or combinations must be considered as well as the treatment history and clinical status of the patient. Toxicity is one of the most critical issues in chemotherapy since most anti-cancer agents lack selective efficacy in cancer tissue. For example, the process of development of chemotherapy in endometrial cancer is slow probably because of the toxicity of anti-cancer agents. Another problem with conventional chemotherapy pertains to the challenge of delivery. The effectiveness of cancer chemotherapy in solid tumors depends on adequate delivery of therapeutic agents to tumor cells. The biological properties of the solid tumor, which limit the penetration of drugs into neoplastic cells distant from tumor vessels, include abnormal and heterogeneous tumor vasculature, interstitium, interstitial fluid pressure (IFP), and cell density. However, even if anti-cancer drugs are located in the tumor interstitium, they can turn out to be of limited efficacy because cancer cells are able to develop mechanisms of resistance. Drug resistance has emerged as a major obstacle limiting the therapeutic efficacy of chemotherapeutic agents. These mechanisms allow tumors to evade chemotherapy. For example, multidrug resistance is one of the most important problems in chemotherapy. MDR could be due to the overexpression of the plasma membrane P-glycoprotein, which is capable of effluxing various anti-cancer drugs, such as doxorubicin and paclitaxel, out of the cells. P-gp inhibitors, e.g. verapamil or cyclosporin A, have been developed to overcome P-gp-mediated MDR. However, P-gp inhibitors do not have good selectivity and also block normal cell function of P-gp, for example, intestines and the blood-brain barrier,

and therefore increase toxicity. A refinement of this concept is the incorporation of both the therapeutic drug and the P-gp inhibiting agent into the same drug carriers, e.g. nanoparticles, for simultaneous delivery into the cell.

Nanoparticles have been developed to enhance the intracellular concentration of drugs in cancer cells while avoiding toxicity in normal cells using both passive and active targeting. The basic rational of nanoparticle delivery is attributed to their nanometer size ranges. The nano-size particles can pass through leaky and hyperpermeable tumor vasculature and accumulate in the tumor vicinity utilizing the 'enhanced permeability and retention effect' (EPR effect). The tumor interstitium is also characterized by the absence of an anatomically well-defined functioning lymphatic network. Therefore, the clearance of nanoparticles via lymphatics is generally seriously compromised in neoplastic tissues so that an additional retention of nanoparticles in the tumor interstitium has been observed. This particular concept known as the "EPR effect" results in intratumoral drug accumulation which is even higher than that observed in plasma and other tissues. In addition to passive targeting by the EPR effect, active targeting may also be pursued by targeting nanoparticles with a tumor-cell specific ligand. More importantly, it has been suggested that nanoparticles may be able to circumvent P-gp-mediated resistance. The mechanisms of carriers to overcome P-gp have been proposed based on various drug delivery systems, including *N*-(2-hydroxypropyl)methacrylamide (pHPMA) drug conjugate, Pluronic micelles, hybrid lipid nanoparticles, liposomes and cyanoacrylate type nanoparticles. Reported mechanisms included enhancement of cellular uptake of drug via endocytosis and ion-pair formation, influence of function and expression of P-gp, and change of P-gp down-stream signaling pathways.

Nanoparticles prepared in our lab from oil-in-water microemulsion precursors have been used to formulate anti-cancer drugs. Paclitaxel was entrapped into nanoparticles composed of emulsifying wax (E. wax) and Brij 78. These NPs were referred to as "PX E78 NPs". These PX E78 NPs were shown to overcome P-gp-mediated drug resistance in-vitro in a human colon adenocarcinoma cell line (HCT-15) and in-vivo in a nude mouse HCT-15 xenograft model. However, the entrapment of paclitaxel was low, about 50%, and also paclitaxel was quickly released from PX E78 NPs, about 100% release after 8 h at 37°C. Intratumoral injection was used, instead of intravenous injection, for the in-vivo anti-cancer efficacy studies mentioned above. The present research was focused on, 1)

developing new PX and Dox NPs suitable for i.v. injection to overcome P-gp-mediated drug resistance, 2) investigating the underlying mechanisms, and 3) performing in-vivo anti-cancer efficacy studies in nude mice bearing P-gp+ resistance tumors after i.v. injection. These studies are considered to be important as they could lead to a novel therapeutic strategy to overcome P-gp-mediated drug resistance and provide benefit to patients that otherwise may have limited therapeutic options.

Chapter 2

Plan of research and research hypotheses

The overall goal of this project is to investigate drug-loaded nanoparticles to overcome P-gp-mediated drug resistance in solid tumors in-vivo after intravenous injection. This research was guided by five main hypotheses:

Hypothesis #1:   The lipids used to form lipid nanoparticles could be metabolized in-vitro by horse liver alcohol dehydrogenase.

Hypothesis #2:   Nanoparticles prepared from oil-in-water microemulsion precursors can be efficiently used to formulate paclitaxel and doxorubicin.

Hypothesis #3:   Optimized nano-based paclitaxel and doxorubicin formulations will overcome P-gp-mediated tumor resistance in-vitro.

Hypothesis #4:   Paclitaxel nanoparticles will have improved anti-tumor efficacy after intravenous injection compared to free PX solution in a nude mouse xenograft model bearing P-gp-overexpressing cancer cells.

Hypothesis #5:   Epidermal growth factor receptor (EGFR)-targeted paclitaxel nanoparticles will increase the intracellular concentration of paclitaxel in cancer cells.

To evaluate these hypotheses, the research plan described in Sections 2.1 to 2.5 was carried out.

2.1 Metabolism of fatty alcohols in lipid-based nanoparticles by horse liver alcohol dehydrogenase

The main goal of this section was to investigate the metabolism of fatty alcohols in E78 NPs by horse liver alcohol dehydrogenase, a NAD-dependent enzyme. E78 NPs in this study were prepared from o/w microemulsion precursors using E. wax as the oil phase and Brij 78 as the surfactant. E. wax is composed of cetyl alcohol, stearyl alcohol and polysorbate 60. Hexadecanal and octadecanal, the intermediate products of cetyl and stearyl alcohols, were synthesized and used as the standard for the corresponding metabolic products of NPs. The metabolism of cetyl and stearyl alcohols in NPs was monitored by observing the increase in fluorescence intensity of NADH and by measuring the metabolized products using a quantitative gas chromatographic method using nonadecanoic acid as an internal standard. In parallel, NP size and turbidity were measured over time. Moreover, the influence of Brij 78 on the activity of the enzyme was tested.

2.2 Formulations of paclitaxel and doxorubicin-loaded nanoparticles for i.v. injection

The aims of this section were to, 1) develop PX-loaded NPs by combination of Taguchi approach and sequential simplex optimization, 2) develop Dox-loaded NPs by an ion-pair strategy, and 3) evaluate the cytotoxicity of PX-loaded NPs in sensitive cancer cells compared to Taxol. Experimental design by combining Taguchi approach and sequential simplex optimization was used to find new NP composition to entrap PX using Miglyol 812 or glyceryl tridodecanoate as the oil phase. Different ion-pair agents were tested to form a stable ion-pair complex with Dox. All developed PX and Dox-loaded NPs were fully characterized by particle size, zeta potential and stability. Entrapment efficiencies, drug loading and release profiles were also investigated. Cytotoxicity studies in breast cancer MDA-MB-231 cells were performed to evaluate the biological activity of PX NPs compared to Taxol$^{®}$.

2.3 In-vitro assessment of paclitaxel and doxorubicin nanoparticles to overcome P-gp-mediated resistance and possible mechanisms

The main objective of this section was to test the potential abilities of PX NPs and Dox NPs to overcome P-gp-mediated drug resistance in-vitro and to elucidate possible

mechanisms. To address P-gp-mediated drug resistance, in-vitro cytotoxicity studies were carried out based on PX and Dox-loaded NPs in two pairs of parental and MDR tumor cell lines. To understand the mechanism of inhibition of P-gp, a resistant cell line, NCI/ADR-RES, was used for quantitative measurement of uptake and efflux studies with Dox NPs. Fluorescence microscopy was also used to observe the uptake of Dox NPs. In addition, the effects of blank NPs and excipients used to prepare NPs on both calcein AM uptake and ATP levels were studied. In parallel, membrane integrity and cell apoptosis were tested for cells treated with NPs and excipients. MTT assay, mitochondrial membrane potential and TEM analysis were performed to understand the influence of NPs on cell mitochondria.

2.4 In-vivo anti-cancer efficacy of paclitaxel-loaded nanoparticles in mice bearing P-gp + resistant tumor

The goal of this section was to evaluate the anti-cancer efficacy of PX NPs in mice bearing NCI/ADR-RES resistant tumors. New PX BTM NPs composed of Miglyol 812 as the oil phase and Brij 78 and D-alpha-tocopheryl polyethylene glycol 1000 succinate (TPGS) as the surfactants were used for these studies. P-gp+ resistant NCI/ADR-RES cells were implanted into female nude mice by subcutaneous injection. When tumors reached a defined size range, 4.5 or 2.25 mg PX/kg was administered by i.v. injection via the tail vain every 7 days for three weeks. Tumor size and mice weight were monitored over time.

2.5 Formulation of transforming growth factor-α (TGF-α)-coated nanoparticles and in-vitro assessment for active targeting delivery

The main objective of this section was to develop TGF-α-coated nanoparticles for EGFR-targeted delivery. TGF-α was conjugated to polyoxyethylene 100-stearyl ether (Brij 700) and then the Brij 700-TGF-α conjugate was coated on the surface of nanoparticles. The coating efficiency of the Brij 700-TGF-α conjugate was measured after membrane separation of coated NPs with the free conjugate. To confirm the binding activity of Brij 700-TGF-α conjugate, a competition binding assay of the conjugate was performed in A431 cells and compared to that of the free TGF-α. TGF-α-coated NPs were fluorescently labeled with BODIPY 558/568 C12 to determine the cellular uptake of TGF-α-coated NPs in EGFR-overexpressing ovarian NCI/ADR-RES cells.

Chapter 3

Background and significance

3.1   Cancer chemotherapy

Cancer remains one of the leading killers of humans in the world with the number of global cancer deaths projected to increase 45% from 2007 to 2030 in spite of the great efforts in the oncology field over the past two decades [1]. The majority of cancer-related deaths are a result of complications from recurrent or metastatic disease. When patients are diagnosed with cancer, they want to know whether their disease is local or has spread to other locations – metastasis, the process whereby cancer cells penetrate into lymphatic and blood vessels, circulate through the bloodstream, and then invade and grow in the secondary sites elsewhere. Once cancer becomes metastatic, chemotherapy as a systemic therapy is a major option for many patients. Moreover, chemotherapy may be the only systemically therapeutic option for some types of cancer, for example, for women with ER- and HER-2-negative, endocrine-resistant disease [4, 5]. The most active anti-cancer drugs are the taxanes and anthracyclines. However, cancer can generate drug resistance induced by chemotherapy. One of mechanisms for drug resistance is overexpression of a transmembrane protein P-gp. Paclitaxel and doxorubicin are well known to be P-gp substrates. In this present research, paclitaxel and doxorubicin were chosen as model drugs for the studies.

3.1.1   Paclitaxel and its formulations

Paclitaxel is one of the most effective anti-cancer agents against a broad spectrum of human cancer, including breast, lung, and ovarian caner. Paclitaxel is a natural taxane originally extracted from the bark of the Pacific yew tree, *Taxus brevifolia* [6]. The development of paclitaxel was suspended for over a decade because of problems in drug formulation, drug supply and controversies regarding the mechanism of action. A semi-synthesis method was developed to provide the quantities needed for commercialization. In this method, a precursor of paclitaxel, 10-deacetyl-baccation III, from the common yew *Taxus baccata* was converted to paclitaxel by chemical synthesis. Horwtiz first

reported the mechanism of action for paclitaxel in 1979 [7]. It is known that paclitaxel interferes with microtubule depolymerization in tumor cells [7-11] resulting in an arrest of the cell cycle in mitosis [12, 13] as well as induction of cell death by apoptosis [14, 15]. Interestingly, in addition to exerting its more widely accepted anti-cancer effects, paclitaxel has also been shown to lower tumor interstitial fluid pressure, decompress blood vessels and improve oxygenation in patients [16, 17]. The ability of paclitaxel to lower interstitial fluid pressure is a bonus effect of this chemotherapy agent as it has a potential to improve penetration of drugs into the interior tumor mass. However, as will be discussed in the next paragraph, the physical/chemical properties of paclitaxel present many challenges for formulations and advanced drug delivery systems.

Currently, only two commercial dosage forms of injectable paclitaxel, Taxol® and Abraxane®, are available. The high lipophilicity and the high lattice energy of paclitaxel result in very limited aqueous solubility. The chemical structure of paclitaxel is shown in Figure 3.1. The solubility of paclitaxel has been reported as 0.7 μg/ml and 30 μg/ml [18, 19]. It is difficult to formulate paclitaxel into a delivery system acceptable for human administration. After investigation of a large variety of excipients to enable parenteral administration of paclitaxel, the formulation approach using the polyoxyethylated castor oil derivative Cremophor EL represented the most viable option [20]. The first commercial formulation of paclitaxel was Taxol which contains a solvent system of Cremophor EL and dehydrated ethanol in a ratio of 50:50 (v/v) for intravenous infusion. A number of pharmacological, pharmacokinetic and pharmaceutical drawbacks are associated with this formulation. The pseudo-non-linear pharmacokinetic behavior of paclitaxel and serious side effects, such as hypersensitivity reactions, attributable to Cremophor EL have been reported [21-26]. In clinical therapy, high doses of anti-histamines and gluococorticoids are co-administered to manage these adverse effects, but this strategy has raised the possibility of additional pharmacokinetic and pharmacodynamic interactions with paclitaxel. The possible precipitation of paclitaxel after dilution in infusion fluids requires the presence of a 0.22 micron in-line filter in the administration set. The drawbacks presented by the presence of Cremophor EL in Taxol stimulated extensive research to develop alternative Cremophor EL-free formulations of paclitaxel.

Several strategies were used to develop Cremophor EL-free paclitaxel formulations, including oral administration of paclitaxel [27], prodrugs and modified

taxoids, and various formulation techniques. To avoid vehicle-related adverse effects, Cremophor EL-free dosage forms of paclitaxel have been taken by using alternative cosolvent/surfactant systems, emulsion systems, microparticles, nanoparticles, cyclodextrins, and liposomes [28, 29]. The summary of alternative formulations of paclitaxel and their status in clinical development is presented in Table 3.1. Among them, Abraxane is the first Cremophor EL-free paclitaxel product approved by the FDA for the treatment of relapsed breast cancer or as second-line therapy in metastatic breast cancer in 2005. This novel formulation is prepared by high-pressure homogenization of paclitaxel in the presence of human serum albumin at a concentration of 4.5%, similar to that of albumin concentration in the blood, resulting in a nanoparticle colloidal suspension with a mean particle diameter of 130-150 nm [30]. The results of a multicenter phase II trial of Abraxane at a maximum tolerated dose of 300 mg/m^2/week on metastatic breast cancer patients showed no severe hypersensitivity reactions without premedication [31]. Another phase III trial on patients with metastatic breast cancer demonstrated that Abraxane significantly improved response rates compared with Taxol [32]. However, in this phase III trial, Abraxane did not show a statistically significant difference on median survival compared to Taxol for the patients with metastatic breast cancer receiving first-line therapy. Thus, it is true that Cremophor EL-free formulation of paclitaxel do have certain advantages in cancer therapy in that the side effect caused by Cremophor EL was eliminated; however, it is still unknown as to whether this formulation will improve the life-span of patients [28]. It is also worthy to be noted that Abraxane costs over $4200 per dose. Therefore, alternative and cost-effective formulations of paclitaxel are still needed for novel therapeutic opportunities in cancer.

3.1.2 Doxorubicin and its formulations

Doxorubicin is one of the first identified anthracyclines and was isolated from the pigment-producing *Streptomyces peucetius* in the 1960s. It is also known as Adriamycin and hyrdoxydaunorubicin. The structure of doxorubicin is shown in Figure 3.2. Doxorubicin is an essential component in the treatment of a wide variety of cancers, including hematological malignancies, many types of carcinoma and soft tissue sarcomas. The exact mechanisms of action of doxorubicin in cancer cells remain a matter of controversy despite extensive clinical utilization. In general, it is thought that intercalation

of doxorubicin into DNA base pairs inhibits the progression of the enzyme, topoisomerase II, to stabilize topoisomerase II complex and eventually impedes DNA resealing. The resulting DNA fragmentation leads to cell death [33-35]. However, the clinical use of doxorubicin soon proved to be hampered by such serous problems as the development of resistance in tumor cells or toxicity in healthy tissues. Notably, the main limitation of doxorubicin is chronic cardiotoxicity, leading to congestive heart failure.

The development of effective approaches to limit cardiac toxicity while maintaining anti-cancer efficacy of doxorubicin has become a focus in recent years. Basically, the efforts were made to either develop tumor-targeted formulations and/or develop new analogs. The rationale to use the formulation strategy to reduce cardiac toxicity is based on the study of the mechanism by which doxorubicin induces cardiotoxicity. Studies have shown that cardiomyocytes are more susceptible than other tissues to apoptosis induced by doxorubicin because cardiomyocytes exhibit different enzyme expression and antioxidant properties [36-38]. For example, cardiomyocytes expresses low levels of catalase and undergo inactivation of selenium-dependent glutathione (GSH)-peroxidase-1 after exposing to doxorubicin. This inactivation could eliminate an important defense against doxorubicin [37, 38]. Doxorubicin itself dose not have tumor-targeting properties. Tumor-targeting delivery could be achieved by putting tumor-specific ligands on colloidal carriers such as nanoparticles or liposomes containing doxorubicin to achieve active targeting delivery, or by using such carriers themselves which have been shown under optimized conditions to preferentially distribute to tumors (passive targeting delivery). Currently, there are several doxorubicin formulations based on targeting delivery on the market or in clinical trials. Two main liposomal formulations of doxorubicin have been marketed: a sterically stabilized polyethyleneglycol (PEG)-coated liposomal formulation, Doxil® (Caelyx® in Europe) and a non-pegylated liposomal formulation, Lipodox®. In a clinical phase III trial in first-line treatment of women with metastatic breast cancer, the liposomal formulation Caelyx showed comparable efficacy and significantly reduced cardiac toxicity as compared with free doxorubicin [39]. Ten patients of the 254 patients received Caelyx 50 mg/m^2 (every 4 weeks) developed cardiotoxicity versus 48 patients of the 255 patients received doxorubicin 60 mg/m^2 (every 3 weeks). The success of Caelyx may depend on passive targeting delivery of liposomes by taking advantage of the EPR effect. This effect will be discussed in greater details in the

sections below. Another interesting approach is active targeting delivery. Although this approach is attractive, so far only one such formulation of doxorubicin, *N*-(2-hydroxypropyl)methacrylamide (HPMA) copolymer-doxorubicin-galactosamine (PK2, FCE28069), has progressed into a phase I trial designed to treat hepatocellular carcinoma or secondary liver disease. PK2, bearing a galactosamine residue as a ligand that is recognized by the hepatic asialoglycoprotein receptor, showed evidence of clinical activity and induced no or considerably less severe cardiotoxicity than equivalent doses of free doxorubicin in rats [40, 41]. To date, no doxorubicin analogs have been shown to have clearly superior activity compared with doxorubicin. Liposomal formulations of doxorubicin are currently the best known alternative to improve the therapeutic index and spectrum of activity of doxorubicin with less cardiotoxicity in clinical practice.

3.2 Barriers in chemotherapy for the treatment of solid tumors

The development of therapeutic drugs against cancer has been focused on finding innovative approaches to selectively deliver anti-cancer drugs to solid tumors, while minimizing injury to healthy tissues. However, the efforts are confronted by physiological barriers at the tumor level and drug resistance at the cellular level.

3.2.1 Tumor Physiological - tumor-level barriers for drug delivery in solid tumors

Physiological characteristics of solid tumors related to drug delivery include, 1) abnormal blood vessel architecture and function, 2) interstitial fluid pressure, also known as interstitial hypertension, and 3) lack of lymphatics [42, 43]. Unlike normal microvessels, tumor vessels resulting from angiogenesis are dilated, tortuous and heterogeneous in their spatial distribution [44-46]. The flow of blood through tumor vessels varies according to tumor types and microenvironment so that the penetration of drugs in solid tumors is difficult. The disorganized structure of solid tumors causes poor drug delivery to the central region in large tumors. Nonetheless, large inter-endothelial junctions, increased numbers of fenestrations and abnormal basement membrane are often found in tumor vessels. The "leakiness" of tumor vessels generates gap openings that are significantly larger than those observed in normal tissues [47-50]. This vascular permeability in solid tumors leads one to develop tumor targeted-carriers that are small enough to enter through tumor vascular openings without passing through those in normal

11

tissues. The abnormal structure and function of blood and lymphatic vessels in solid tumors cause IFP elevation whereas IFP in normal tissues is around zero mmHg. An increase in tumor IFP reduces the transcapillary pressure gradient from the vascular compartment to interstitial space of tumors [51]. Furthermore, uniform elevation of IFP results in a negligible flow inside tumors [52]. Thus, the uniformly elevated IFP impedes the delivery of therapeutic drugs both across the blood vessel wall and interstitium in solid tumors. Studies have shown that there are no functional lymphatic vessels inside solid tumors [53-55]. Functional lymphatic vessels are present in the tumor margin and the peri-tumoral tissue to mediate tumor growth and metastases. The lack of lymphatics in tumors reduces the effective outflow of interstitial fluid, partially contributing to the increase of tumor IFP. However, the positive aspect of the absence of lymphatics for drug delivery is that drugs can not be drained out of tumors via the lymphatic system once they locate inside tumors. Moreover, since a blood supply is crucial for growth, tumor cells have the ability to recruit new blood vessels in various ways through a process called angiogenesis. The fact that a survival of tumor critically depends on its blood supply provides a common opportunity for the destruction of solid tumors if drug concentrations in the bloodstream remain high for an appropriate period.

3.2.2 Multidrug resistance – cell-level barriers for drug delivery in solid tumors

Therapeutic drugs will face another big barrier, drug resistance, after they penetrate in tumors. Multidrug resistance remains the main cause of the failure of the use of conventional chemotherapy to treat common solid tumors [56]. Frequently, resistance is intrinsic to the cancer, but as therapy becomes more and more effective, acquired resistance has also become common. A variety of mechanisms contribute to acquired drug resistance to a broad range of anti-cancer drugs including, 1) expressing one or more energy-dependent transporters that bind to and efflux anti-cancer drugs from cells, leading to insensitivity to drug-induced apoptosis [57], 2) altered targets, and 3) induction of drug-detoxifying mechanisms [58]. A summary on the reported mechanisms of drug resistance is presented in Figure 3.3. Among them, overexpression of drug transporters is the most common reason. P-glycoprotein is the important and best-known membrane transporter involved in MDR. The focus of this research is P-gp-mediated MDR.

3.2.2.1 P-glycoprotein

The initial MDR was reported in the late 1960s and early 1970s. Drug-resistant mammalian cell lines were then established for studying this phenomenon. A common feature of these drug resistant cell lines was the overexpression of P-gp when compared to the drug sensitive parent cell lines [59, 60]. In humans, two closely related genes, MDR1 and MDR2 or MDR3, encode highly homologous P-gp. However, only the MDR1 gene has been linked to the MDR. The MDR1 gene is highly expressed in many clinically resistant tumors. In some cases its expression at diagnosis has been proven to be an adverse prognostic factor. In other cases, MDR1 appeared after relapse from remission, suggesting that P-gp was a survival mechanism in a subclone of cancer cells that eventually regrew [61-66]. Studies in leukemias, myelomas and some childhood cancers showed that P-gp expression correlated with poor response to chemotherapy. Moreover, the early clinical trials testing P-gp modulation in acute leukemia in the presence of P-gp modulators resulted in clinical relapse and reduction of P-gp expression [67, 68]. These clinical evidences demonstrated that P-gp plays a significant role in clinical drug resistance.

P-gp is an ATP-dependent transmembrane transporter which can transport a broad range of structurally unrelated compounds out of the cells. The human P-gp is a 170 kDa protein containing 1280 amino acids. The topology of P-gp was proposed to contain 12 transmembrane domains with 6 extracellular loops and 2 hydrophilic regions (ATP-binding domains) containing nucleotide-binding domains which are characteristics of the ATP-binding cassette (ABC) family of transporters (Figure 3.4.) [69-72]. P-gp is expressed at significant levels in human normal tissues, such as the biliary canaliculi of the liver, the proximal tubules of the kidneys, the small intestine, colon and adrenal cortex [73, 74]. The activity of P-gp in normal tissues suggested an important role in transepithelial transport to prevent cytotoxic compounds in the environment and diet from entering the body, although the physiological role of P-gp still is a subject of speculation. The studies on P-gp knockout mice showed that P-gp had no essential physiological function on fertility. The mice grew and developed into adulthood normally. However, these mice were very sensitive to MDR-related anti-cancer drugs. Moreover, more of these drugs accumulated in the central nervous systems of the mice, indicating a major role of P-gp at the blood-brain barrier [75-77].

P-gp can remove many different hydrophobic drugs from cells to decrease intracellular accumulation of anti-cancer drugs. Drugs may be pumped out by P-gp as they enter the plasma membrane, or even as they are inside the cells. These drugs include many of the commonly used natural-product anti-cancer drugs such as doxorubicin, vinblastine, etoposide and paclitaxel, as well as many commonly used pharmaceuticals ranging from anti-arrhythmics and anti-histamines to cholesterol-lowering statins and HIV protease inhibitors [78]. Although the detailed mechanism of drug efflux by P-gp is unknown, the predicted transport cycle of P-gp involves the change of structure of ATP-binding domains after binding of drug substrates, stimulation of ATP hydrolysis, and rearrangement of P-gp shape caused by ATP binding and hydrolysis. The final step involving the conformational change of P-gp results in the release of the drug into the extracellular space. ATP hydrolysis is necessary for resetting of P-gp [79].

3.2.2.2 Strategies to overcome P-gp-mediated drug resistance

The strategies to overcome P-gp-mediated resistance can be summarized as follows: 1) *modification of chemotherapy regimens*. Non-cross-resistant chemotherapeutic regimens utilize the largest number of active agents at the highest doses possible, assuming that mutations conferring drug resistance will not convey resistance to all of the agents in the regimen, and, also, high-dose chemotherapy regimens could be given to cancer patients. This approach assumes that despite resistance to standard doses of anti-cancer drugs, a dose-response relationship still exists for these tumors and that high doses of chemotherapy might overcome this resistance; 2) *protein and gene-directed therapy*. The aim of this strategy is to specifically target overexpressing cells with anti-MDR1 antisense oligonucleotides, anti-MDR1 ribozymes or anti-MDR1 monoclonal antibodies. One of the most recent developments in cancer gene therapy is the transduction of small interfering RNA (siRNA). Some issues are associated with these approaches. For example, anti-MDR1 antibodies, such as MRK-16, also may target MDR1-expressiong cells in normal tissues although it is specific for human P-gp. Thus, the potential to lead to unacceptable toxicities could be missed in a murine model. Moreover, anti-MDR1 antibody and anti-MDR1 ribozymes encountered the problems related to effective delivery to tumors; 3) *development of new anti-cancer drugs which are not substrates of P-gp*. The modified drug analogues can affect the binding of analogues to P-gp and consequently P-gp can not

recognize the analogues. Two taxane analogues, DJ-927 (phase I) [80, 81] and Ortataxel (phase II) [82, 83], designed to overcome drug resistance have been evaluated in clinical trials. Other new taxane analogues such as BMS-184476 (phase I) [84, 85] and RPR 109881A (phase II) [86, 87] also were claimed to have a broad spectrum of activity both in sensitive and resistant tumor cell lines; 4) *the use of inhibitors of P-gp to reverse P-gp-mediated drug resistance*. This is an approach receiving the most attention. The inhibitors of P-gp can be classified into two groups. Some inhibitors can transport themselves, and then act as competitive antagonists. The others are not transported but affect P-gp function. The mechanism of reversal of P-gp by these agents is not fully understood at the moment; 5) *the use of drug carrier moieties and delivery systems to overcome P-gp-mediated drug resistance*. Currently, several different formulations encapsulating anti-cancer drugs which are P-gp substrates are being developed. Paclitaxel vitamin E emulsion (TOCOSOL) containing a P-gp inhibitor TPGS in excipients was evaluated in a clinical phase II trial for drug resistance. The results showed promising efficacy when TOCOSOL was administrated weekly in patients with refractory cancers [28]. Partial reversal of drug resistance has been observed also when liposomal Dox was given to cell cultures [88]. A detailed discussion on this approach will be given in the sections below; 6) *inhibition of P-gp-mediated drug resistance using monoclonal antibodies or peptides* [89-91]. Synthetic P-gp-derived peptides corresponding to fragments from the extracellular loops of the murine P-g were coupled to PEG and inserted into liposomes. These peptides have been shown to reverse MDR. After immunization with these peptide-loaded liposomes and treatment with Dox, an increase of 83% survival time was observed in mice inoculated with P388R cells. No auto-immune responses were detected in immunized mice. However, complete eradication of tumors did not occur. These results indicate a new approach to break immune tolerance towards MDR1 protein and consequently modulate sensitivity of resistant tumors to chemotherapy [89].

The clinical success has been limited in the attempts to overcome P-gp-mediated drug resistance. A large number of new generations of drug analogues were developed as non P-gp substrates. However, most taxane analogues can not demonstrate greater therapeutic indexes in-vivo, or showed toxicity to normal tissues although they were proposed to be not P-gp substrates [85]. Another means to overcome P-gp-mediated drug resistance is to develop P-gp inhibitors. The study on the compounds including the calcium

channel blocker verapamil to reverse vincristine resistance in murine leukemia cells opened the door for the development of inhibitors of P-gp to overcome P-gp-mediated drug resistance [92, 93]. To date, clinical trials with the third generation inhibitors are ongoing, including trials with compounds LY335979, R101933 and XR9576. However, the therapeutic results from previous clinical trials using first- and second-generation inhibitors of P-gp have been generally negative or only modestly positive and have not fulfilled the promise of the preclinical data. There are probably two major reasons for the failure of many of these P-gp inhibitors to show beneficial effects. One of the reasons is that they are weak and nonspecific inhibitors. The requirement on high dose of inhibitors, e.g. > 10 μg verapamil, was not achievable in clinical trials. Additional toxicities of anti-cancer drugs due to the inhibition of P-gp in normal tissues remain a concern for the more potent P-gp inhibitors. The other reason is a programmed pharmacokinetic drug interaction resulting from co-administration of P-gp inhibitors and anti-cancer drugs. A modest pharmacokinetic interaction between verapamil and doxorubicin in humans was observed [94]. Also, one clinical trail reported excessive vincristine neuropathy associated with the use of cyclosporin A to inhibit P-gp [95]. Increased toxicity of the anti-cancer drugs may occur due to both pharmacokinetic effects and inhibition of a protective function of P-gp in normal tissues. Certain third generation of P-gp inhibitors as mentioned above showed minimal pharmacokinetic interactions with anti-cancer drugs. However, the contribution of these inhibitors to reverse clinical drug resistance needs to be defined in clinical trials.

3.3 Nano-based drug delivery systems for cancer

Nanotechnology has a long history. The first description of nanoparticles, in scientific terms, is back to 1857 in a paper about the optical properties of nanometer-scale metals [96]. In pharmaceutical field, the development of the first nanocarrier dates back approximately 40 years, when the first example of a liposome was described [97]. However, the most important scientific advancements on development of nanoscale vehicles with distinct physical and biochemical properties for drug delivery applications have only taken place with the last two decades. In its strictest definition from the National Nanotechnology Initiative, nanotechnology refers to structures roughly in the 1 to 100 nm size in at least on dimension. Nanoparticles for the purpose of drug delivery are more commonly defined as submicron (<1 μm) particles. The most common examples of these

nanoparticles include polymeric nanoparticles, dendrimers, nanoshells, liposomes, lipid-based nanoparticles, magnetic nanoparticles and virus nanoparticles. One of the most appealing properties of nanoparticles is their sizes, resulting in distinct properties that are not available from individual molecule alone or equivalent materials as a larger scale. Nanoparticles have the potential to improve the therapeutic index of currently available drugs by increasing drug efficacy, lowering drug toxicity, and achieving steady state therapeutic levels of drugs over an extended period of time. Nanoparticles can also improve drug solubility and drug stability, allowing the development of potentially effective new chemical entities that have been stalled during the preclinical or clinical development because of suboptimal pharmacokinetic or biochemical properties. Finally, nanoparticles may also facilitate the development of multifunctional systems for active targeting drug delivery. Nanoparticles are expected to benefit all branches of medicine. The focus of the remaining chapter will be to review the applications of nanoparticles for cancer chemotherapy.

3.3.1 Nanoparticles for solid tumor delivery

The effectiveness of cancer therapy in solid tumors depends on adequate delivery of the therapeutic agent to tumor cells. Many anti-cancer drugs have a marginal selectivity for malignant cells because they target the reproductive apparatus in cells having high proliferation rates. However, anti-cancer drugs having this mechanism of action result in high toxicities against rapidly dividing normal cells such as hair follicles, germ cells and hematopoietic cells. Other anti-cancer drugs are distributed non-specifically in the body where they affect cancer and normal cells. Therefore, the side effects associated with chemotherapy limit the dose achievable with the tumor and also result in suboptimal treatment due to excessive toxicities. Delivery of drugs to solid tumors also remains difficult because of the physiological barriers in solid tumors, as described in Section 3.2.1. Nanoparticles have emerged as one approach to overcome the lack of specificity of conventional drugs and delivery barriers in solid tumors [98-101]. The small physical dimensions of nanoparticles enable them to partially penetrate through biological and physiological barriers of tumors that are unique to tumors and normally impermeable for larger particles. By this way, passive targeting delivery to tumors could be achieved due to the physicochemical properties of a carrier and the pathophysiological condition of a

17

target. The flexible surface chemistry of nanoparticles also allows the ability to conjugate targeting ligands for active targeting delivery. Then ligand-coated nanoparticles may be specifically taken up by cancer cells by receptor-mediated endocytosis. A schematic representation for different mechanisms by which nanoparticles enhance drug delivery to solid tumors is shown in Figure 3.5. [101].

3.3.1.1 Passive targeting delivery by EPR effect

The role of tumor vasculature as a potential target for solid tumors has been elucidated since the late 1970's. The studies exploited the ability of nanosize polymeric anti-cancer agents selectively to target tumor tissues due to extensive vascular leakage or permeability in tumor capillaries. Moreover, vascular permeability enhancing factors, such as bradykimin, nitric oxide and vascular endothelial growth factor, facilitate extravasation of macromolecular drugs within tumor tissues as well as surrounding normal tissues. Furthermore, an impaired lymphatic system in solid tumors leads to prolonged retention of macromolecules in tumor tissues. Thus, this enhanced permeability and retention effect of macromolecules in tumor tissues has been termed the EPR effect. Later, other nanosize anti-cancer drugs, such as the copolymer HPMA-doxorubicin conjugate [102], pegylated liposomal doxorubicin [103], and SMA-doxorubicin micelles [104, 105], showed selective accumulation of anti-cancer drugs in solid tumors. Treatment of solid tumors has undoubtedly been the main research area for nanoparticles because of the targeting advantage offered by EPR effect. In nanoparticle delivery research, the EPR effect becomes a hallmark concept that differentiates a tumor from normal tissue to make passive targeting delivery possible to solid tumors.

For such a passive targeting mechanism to take place, physiochemical parameters of nanoparticles including particle size and surface properties are crucial. The desirable nanoparticles should have a certain particle size with long circulation. The leaky vasculature at the solid tumor site is a critical advantage in treating solid tumors with nanoparticles despite other impeding factors as described in Section 3.2.1. The pore cutoff size of extravasation through transvascular gaps in most experimental tumors is in the range between 380 nm and 780 nm depending on the tumor types, whereas the tight endothelial junctions of normal vessels typically are between 1 to 10 nm [47, 106]. It was proposed that transvascular transport of the particles in the tumors resulted from

interendothelial or transendothelial open junctions rather than by endothelial phagocytosis or vesicles. To achieve this extravasation in solid tumors, average particle size less than 300 nm was suggested [47].

Another important prerequisite for the passive targeting delivery is that the plasma concentration of the drug must remain high and long; that means, drug-coated nanoparticles must be sustained in the bloodstream long enough to reach or recognize solid tumors. Nanoparticles, unlike microspheres (> 1μm), are small enough to be dosed via i.v. administration. In the bloodstream, the major defense system of the body, reticuloendothelial system (RES), also known as mononuclear phagocytes system (MPS), could rapidly remove nanoparticles and becomes a major obstacle to long circulation of nanoparticles. The first step of clearance of nanoparticles by RES is opsonization in which nanoparticles recognized as foreign particles are coated with opsonin proteins to make them more visible to phagocytic cells. After opsonization, phagocytosis occurs to destruct or remove foreign materials from the bloodstream. Phagocytic cells mainly include Kupffer cells of the liver and macrophages of the spleen. A large number of researchers were motivated to develop "stealth" nanoparticles to avoid uptake of nanoparticles by the RES. It has been repeatedly demonstrated that the opsonization of hydrophobic particles occur more quickly than that of hydrophilic nanoparticles owing to the enhanced absorbability of blood serum proteins on hydrophobic surfaces [107, 108]. Modification of the nanoparticle surface with chains of hydrophilic and flexible polymers can shield nanoparticles from the opsonins and therefore prevent elimination by the cells of the RES. The polymer chains create a barrier layer to block the adhesion of opsonins and make the nanoparticles 'invisible' to phagocytic cells. The most commonly used polymers are PEG types, such as poly(ethylene oxide) and poly(propylene oxide). Polymers could be put on the nanoparticle surface by covalently grafting, entrapping, and adsorption. However, there are no absolute rules or methods available to completely and effectively block the opsonization of nanoparticles although research in this area has been on-going for over 30 years. Modification of nanoparticle surface is complicated and case-dependent. For example, the study on biodegradable albumin nanoparticles showed that neutrally charged albumin nanoparticles reduced phagocytic uptake by macrophages in-vitro in comparison with charged particles, especially those with a positive charge. A further study on the in-vivo distribution of albumin nanoparticles in rats indicated that blood circulation times and

organ accumulation was not influenced by surface charges of nanoparticles. Thus, the in-vivo fate of albumin nanoparticles did not correlate with the in-vitro cell culture model [109]. Moreover, Polymer chains here create a barrier layer to block the adhesion of opsonins. The thickness of the layer is crucial but hard to control and varies within different types of nanoparticles and coating strategies. However, it is noteworthy that the effective stealth properties provided by these barrier layers depend largely on the PEG molecular weight, surface chain density and conformation [110]. For example, PEG chains are incorporated into liposomes using a PEG-lipid, a highly asymmetric amphiphile. However, generally, less than 10% of PEG2000-lipid can be incorporated in liposome without inducing vesicle micellularization [111]. The configuration of PEG layers changed from "mushroom" to "brush" depending on the density of PEG chains on the surface. It is considered that the optimal configuration for stealth nanoparticles is to create a PEG coating configuration that is somewhere between the mushroom and brush. A general guide for liposomes is to coat the liposomes with 3-5% (w/w) of PEG. However, this guide may not apply in the case for other delivery systems as the configuration of PEG layers primarily depends on the surface properties of the colloidal delivery system. For example, "soft" surface nanoparticles, such as hydrogel nanoparticles and nanocapsules, make the PEG coating layers less effective [110]. Therefore, for different nanoparticles, the effective modification method needs to be developed individually based on the physicochemical properties of the nanoparticles.

In addition to clearance of nanoparticles by phagocytosis, nanoparticles are also subjected to splenic filtration, a non-phagocytic uptake. The width of interendothelial cell slits of the spleen is about 200 nm to 500 nm [112]. A study of the biodistribution of polystyrene nanospheres (60 to 250 nm) coated or uncoated with hydrophilic polymers was carried out in rats. In this study, coating of nanospheres with hydrophilic polymers dramatically reduced uptake of particles by liver, regardless of particle sizes. However, coated nanospheres were sequestered by the spleen apparently depending on the particle size. The size and deformability of nanoparticles play critical roles in their clearance by this mechanism in human spleens. For rigid nanoparticles, the size to achieve long circulation should not exceed 200 nm. Otherwise, nanoparticles should be deformable enough to pass splenic filtration [113, 114].

Surface modification of nanoparticles using conventional chemicals could alter and tune their pharmacokinetic or pharmacodynamic properties, such as to increase the circulation time within the body.

3.3.1.2 Active targeting delivery

The basic principle of active targeting delivery is that the delivery of drugs to cancer cells or cancer-associated tissues can be selectively increased by associating the drugs with targeting ligands that bind to surface antigens or receptors that are either uniquely expressed or overexpressed in the target cells relative to normal tissues. Unlike passive targeting delivery discussed above which is due to the nature of the nanoparticles and the pathophysiology of solid tumors, active targeting delivery is based on specifically molecular recognition. When nanoparticles are targeted to the extracellular portion of transmembrane tumor antigens or receptors, they may be specifically taken up by cancer cells through receptor-mediated endocytosis. Nanoparticles are able to selectively carry higher payloads of anti-cancer drugs with fewer ligands to target cancer cells compared to other delivery systems such as active targeting drug-conjugate. The target receptor is an important key for targeting delivery. The receptor should be either selectively expressed or over-expressed in cancer cells compared to normal cells. The internalization of the ligand-receptor binding complex and availability of the receptor after the first association with the ligands are also important selection criterions for the receptor. Overexpression of the receptor in normal tissues is an obstacle for targeting to cancer. For example, folic acid is a small molecule popularly used to target folic acid receptors in cancer cells. However, it was demonstrated that folic acid receptors are also expressed in normal tissues like placenta and kidneys. The clinical translation of this targeting delivery was impeded although folate-targeted nanoparticles showed effectiveness in several tumor models [115, 116]. Thus, the search for new ligands for cancer targeting concentrates around specific receptors.

To choose a ligand, it is now well accepted that the binding affinity, stability, the size of the ligand, and the density of the ligand on the surface of nanoparticles play a critical role for successful targeting [98, 117]. Antibodies [118], aptamer [119], peptide and small molecules [120] have been reported as targeting ligands for selective targeting delivery. The ligand could be attached to the surface of nanoparticles by covalent binding

or non-covalent binding [121]. Covalent binding is the general method in which ligands are bound to the surface of nanoparticles through hydrophobic anchors. To avoid steric barriers on the nanoparticle surface and to retain the binding activity of ligands, the hydrophobic anchors contain PEG moiety with high molecular weight and the ligands are coupled to the PEG terminus. One approach, via pre-insertion, is to functionalize nanoparticles by entrapping functionalized lipid-PEG into nanoparticles, and then the ligands are coupled to the surface of nanoparticles by a covalent bond. The other approach, via post-insertion, is to first conjugate functionalized lipid-PEG and the ligands, and then the conjugate is post-inserted into nanoparticles to form ligand-coated nanoparticles. Obviously, the final coupling reaction in the pre-insertion approach introduces a chance to alter the drug loading if components of nanoparticles are not stable during the reaction. However, the purification of the conjugate of lipid-PEG-ligand may be an issue in the post-insertion, especially when using small molecules as the ligands, since the conjugate may have similar molecular weight and properties as with the lipid-PEG. Thus, the choice of method depends on the properties of nanoparticles and the ligands. However, there are several requirements for the coupling. In general, the desirable coupling approach should be simple, efficient and reproducible. The method should also not alter the binding affinity of the ligands, and not alter the drug entrapment efficiency and drug release profiles in a negative manner. Moreover, ligand-coated nanoparticles should be able to circulate a long time in the bloodstream to achieve appropriate targeting.

Active drug targeting delivery is attractive but has not been extensively investigated in human clinical trials. There are very few clinical trials in this area although the proof of concept is established. Most of studies on active targeting delivery were performed using liposomes. In-vivo outcomes are quite dependent on all criteria as discussed above. Anti-MUG-1 immunoliposomal doxorubicin targeted to human MUC-1 gene did not show improved efficacy in solid tumors compared to non-targeted liposomes although they were more effective in treating early lesions in both the pseudometastatic and metastatic models [122]. Other controversial results in this area are related to the question: Dose active targeting delivery increases tumor localization (accumulation)? Enhancement of tumor accumulation has been demonstrated in some studies, for example, liposomes coated with vasoactive intestinal peptide to target breast cancer [123], folate-coated polyelectrolyte complex micelles to target folic acid receptors in solid tumors [124],

and peptide-coated liposomes to target EFGR [125]. However, in other studies, tumor accumulation was not different between targeted and non-targeted liposomes even though enhanced therapeutic efficacy was observed using the targeted liposomes. The explanation for the enhanced therapeutic efficacy includes the alteration of target caused by the active targeting of angiogenic homing peptide coated liposomes [126], the acceleration of cellular uptake of antibody-modified liposomes [118, 127] and effective penetration of sigma receptor-targeted siRNA nanoparticles in tumors [128]. In this research, TGF-α was chosen as a ligand to coat on the surface of nanoparticles to target EGFR in solid tumor cells.

3.3.1.2.1 EGF receptor

Overexpression of EGFR has been detected in more than 90% of human head and neck squamous cell carcinomas [129], and also is frequently detected in other major cancers of epithelial origin, including carcinomas of the lung, breast, prostate, ovary and bladder [130-132]. Increased expression of EGFR and its ligands in cancers often correlates with poor prognosis stemming from advanced disease [133]. EGFR has been a molecular target for cancer therapy as it is overexpressed in cancer cells and is a central element for cell proliferation, differentiation and apoptosis [134]. There are two general strategies to inhibit EGFR: antagonistic antibodies targeting the extracellular domains and small soluble tyrosine kinase inhibitors competing with ATP for binding to the catalytic domain [135].

The EGFR is a 170 kDa cell surface transmembrane receptor with receptor tyrosine kinase activity. EGFR is one of the members in ErbB family which includes four closely related members: EGFR/ErbB1/HER1, ErbB2/Neu/HER2, ErbB3/HER3, and ErbB4/HER4. EGFR is characterized by a modular structure consisting of an extracellular ligand-binding domain, a single hydrophobic transmembrane region, and the intracellular part harboring the highly conserved tyrosine kinase domain. Ligand binding induces homodimerization or heterodimerization and subsequently conformational change which triggers autophosphorylation of C-terminal tyrosines. It is phosphorylation of tyrosine residues that leads to a series of intracellular signaling events [130, 136]. After binding of the ligand to EGFR, the ligand-receptor complex enters cells by receptor-mediated endocytosis [137]. Activation of EGFR initiates to a multitude of signaling pathways such as the highly conserved MAP kinase pathway, phosphatidylionsitol-2-kinase pathway and

cytoplasmic tyrosine kinase c-Src signaling. These diverse cellular pathways lead to proliferation, migration, gene transcription, cell cycle progression and cell survival.

EGFR-targeted drug delivery systems have been investigated for active targeting delivery because of the overexpression of EGFR in cancers. Radiopharmaceutical ^{111}In-labeled-EGF exhibited strong anti-cancer effects against MDA-MB-468 (EGFR+) breast cancer xenografts, and had modest inhibition of tumor growth against MCF-7 (EGFR-) breast cancer xenografts in comparison. The highest tumor localization and growth inhibition were achieved for small, nonestablished tumors [138]. Also, EGF was conjugated on copolymer micelles for active targeting delivery [139]. Confocal laser scanning microscopy revealed that EGF-conjugated micelles, labeled by the fluorescent probe CM-Dil, accumulated intracellularly in MDA-MB-468 cells after incubation for 2 h, whereas no detectable cell uptake was observed for the non-targeted micelles. It suggests that EGFR-targeted delivery formulation could enhance cellular uptake by the endocytosis pathway. EGFR-targeted liposomes have been developed using EGF [140], monoclonal antibody fragment of C225 [141], or a peptide ligand [125]. The antibody-conjugated drug-loaded liposomes showed greater cytotoxicity than the corresponding non-targeted liposomal drugs in EGFR-overexpressing cancer cells while equivalent potency was observed in cells that lacked EGFR overexpression. The biodistribution of peptide ligand-mediated liposomes performed by using fluorescence imaging techniques demonstrated preferential accumulation of the liposomes in the tumor site, suggesting active targeting delivery in-vivo.

3.3.1.2.2 TGF-α as a targeting ligand

TGF-α is a biological active polypeptide containing 50 amino acids with a molecular weight of 5616 Da. TGF-α was first isolated from retrovirus-transformed cells [142] and specifically binds to the EGFR. The structure of TGF-α is represented in Figure 3.6. The three disulfide bonds separate the amino acid sequence to three loops: A, B and C loops. The data from NMR analysis suggested that A and C loops and the C-terminal tail of TGF-α contain residues that form the major binding interface with the EGFR and that the N-terminal amino acids outside the A loop remain flexible in the receptor-bound species that make the N-terminal not play an important role in the receptor-ligand interaction [143, 144].

After TGF-α binding, ligand-occupied EGFR is rapidly internalized in a process termed ligand-induced endocytosis. TGF-α dissociates from EGFR in the early endosomes (pH= 5.9-6.0) very shortly after internalization, which favors receptor recycling and results in more potent mitogenic signaling. The recycling of EGFR to the cell surface will sustain the original ligand-binding ability of the cells [8]. Unlike TGF-α, EGF-EGFR complex remains stable in the mildly acidic early endosomes. Most of EGF is degraded in lysosomal compartment (pH= 5.0-6.0) thus reducing the cell surface content of the receptor and its signal capacity. This pH-dependent stability difference is attributed to the fate of EGFR during endocytosis. TGF-a may dissociate from EGFR at pH 7 whereas EGF may dissociate from EGFR at pH 5.5, according to the isoelectric point (pI) values of both ligands. Comparing TGF-α and EGF as the ligand for active targeting delivery, the use of TGF-α as a ligand will theoretically allow for retention of EGFR on the cell surface for targeting. The aberrant expression of TGF-α was associated with a highly aggressive phenotype in human colon cancer cell lines. In addition, TGF-α could be an autocrine for EGFR network [145, 146]. Thus, the possibility to stimulate proliferation of tumor cells by TGF-α is a concern.

TGF-α levels in cancer patients are higher than those in healthy individuals. The concentration of TGF-α ranged from 210 to 740 pg/ml in 83 breast cancer patients as compared to a range from 120 to 207 pg/ml in 74 healthy individuals [147]. The endogenous TGF-α may not interfere with TGF-α-coated nanoparticles to bind with the receptors. In a study, human placental membranes were pre-incubated with human EGF or human TGF-α. The results indicated that the presence of these ligands in a membrane preparation did not affect the apparent number of binding sites, but only resulted in an increase in the apparent dissociation constant for EGFR [148]. Therefore, exogenous TGF-α, like TGF-α coated on nanoparticles, could be able to bind with EGFR even in the presence of endogenous TGF-α.

TGF-α has been used to target toxins to cancer cells overexpressing EGFR. In-vitro and in-vivo studies demonstrated that TGF-α-*Pseudomonas* exotoxin (PE40) exhibited cytotoxicity that correlated to the expression of EGF. The exotoxin caused only minimal damage to normal tissues despite the presence of EGFR on many normal cell types [149, 150]. However, there are no reports in literatures examining the utilization of TGF-α for

targeting delivery of nanoparticles. Thus, we propose to deliver paclitaxel nanoparticles to breast tumors using TGF-α as a ligand to target cell surface EGFR.

3.3.2 Lipid-based nanoparticles to formulate anti-cancer drugs

Nanomedicine is based on nanotechnology to aim at developing effective clinical treatments. In cancer research, nanomedicine covers diagnostics, biosensors and drug delivery. There are many reviews written on nanoparticles used for drug delivery. Here, the following section will focus on the lipid-based nanoparticles and present some of their potential applications for anti-cancer drug delivery. The term lipid is taken in the general sense to include wax, glycerides and phospholipids.

The innovations in combinatorial chemistry and high throughput screening focused on potency and high activity of small molecule anti-cancer drugs are leading to a shift of the properties of new chemical entities towards more lipophilic and poorly water-soluble molecules. As a result, about 40% of potential drug candidates never enter further development including a formulation development stage due to their poorly water solubility [151]. An urgent need has always existed for the safe and effective delivery of poorly soluble drugs. Water insolubility can be defined as more than 10,000 parts of water needed to dissolve one part of solute, corresponding to a solubility of <0.1 mg/ml. Drug insolubility is caused by either hydrophobicity impeding the drug to form hydrogen bonds with water or by a high lattice energy of the drug resulting in the ability to reduce intermolecular drug interactions in the solid state. Typically, hydrophobicity and crystal lattice energy are indicated by the octanol-water partition coefficient (P) and melting point (MP), respectively. The conventional formulation strategies for water-insoluble drugs include the conversion of a water-insoluble drug to a more soluble salt form, pH adjustment, the use of co-solvents, and inclusion complexation, i.e. the use of cyclodextrin [152]. However, for drugs with high P and/or MP, or if a high dose is required, the conventional approaches mentioned above are limited. In addition to insolubility, drug candidates may have additional problems pertaining to stability, acute toxicity and side effects. When taken together, all of these become a bottleneck in the drug development process. The advances of lipid-based nanoparticle systems for improved drug delivery offer a great potential for the administration of anti-cancer drugs. The main advantages of this system include low toxicity of carriers themselves, solubilization of poorly water-

soluble drugs, high drug loading, protection of drugs against chemical and biological degradation related to the administration route, prolonged circulation, targeting delivery, and controlled release. In addition, more than one anti-cancer drug may be co-encapsulated into colloidal carriers for combined cancer chemotherapy [153]. Lipid-based nanoparticles are generally comprised of biocompatible and biodegradable lipids and therefore may be less toxic than many types of polymeric nanoparticles prepared from synthetic polymers. Once the particle size is reduced to submicron levels, the surface area of the nanoparticles increases substantially, and also the saturation solubility increases with the reduction of particle size, leading to an increase in the dissolution rate. The encapsulation of drugs into the carriers provides protection of the drugs from the influence of physiological conditions. Also, the carrier may have prolonged circulation; thus, the required therapeutic levels of the drugs in the blood for the extended time interval and a better targeting effect may be more readily achieved. Additionally, by choosing the excipients and compositions of the nanoparticles, controlled release can be explored to further reduce acute toxicity. As described above, nanoparticles could perform passive targeting delivery to solid tumors by the EPR effect or even active targeting by placing the ligand on the surface of nanoparticles. Lipid-based nanoparticles have become an increasingly important field of research for delivering anti-cancer drugs in terms of these potential benefits. The primary types of lipid-based nanoparticles investigated are micelles, liposomes, nanoemulsions, nanocapsules, and solid lipid nanoparticles. These systems will be discussed in the following sections. All of them are potential drug carriers administered by different routes including oral [154, 155], topical [156, 157] and parenteral [158, 159].

3.3.2.1 Micelles

Micelles are the most basic colloidal drug delivery systems and are formed spontaneously in nature. In the body, colloidal micellar species comprising endogenous surfactants and lipid digestion products, i.e. bile salt mixtures, facilitate the absorption of highly insoluble fatty acids and fat soluble vitamins. Micelles with particle size normally within 5 to 100 nm range are thermodynamically stable and form spontaneously by association of amphiphilic molecules such as surfactants under defined concentrations and temperatures. The concentration of a monomeric amphiphile at which micelles appear is called the critical micelle concentration (CMC). The formation of micelles is driven by the

decrease of free energy in the system because of the removal of hydrophobic fragments from the aqueous environment and the re-establishment of the hydrogen bond network in water. Hydrophobic fragments of the amphiphilic molecules form the core of a micelle, while hydrophilic moieties form the shell of the micelle. When used as drug carriers in aqueous media, micelles solubilize molecules of poorly soluble nonpolar drugs within the micelle core, while polar drugs could be adsorbed on the micelle surface and substances with intermediate polarity distribute along surfactant molecules in intermediate positions. One limitation of micellar systems is the relatively low hydrophobic volume of the interior of micelles, leading to limited drug loading. Consequently micellar formulations may often comprise a surfactant and solvent mixture, such as the formulation of the injection Taxol consisting of Cremophor EL and ethanol at a 1:1 ratio. Another limitation of conventional micellar systems is the danger of drug precipitation upon the dilution of the solubilized drug with physiological fluids after parenteral administration. The dilution of the formulation by physiological fluids may cause the disassociation of the micelles as the concentration of the surfactants used to solubilize the drugs may be lower than their CMC.

More recently, polymer micelles prepared from amphiphilic copolymers for solubilization of poorly soluble drugs as an alternative to lipid-based surfactant systems have attracted much attention. Polymer micelles offer a more versatile structure, biodegradability, and lower CMC that may lead to better in-vivo stability and more conjugation chemistries for linking ligands to the surface of the colloidal system. Polymer micelles are self-assembled from block copolymers comprising a hydrophobic block such as poly-lactic acid with a hydrophilic block. As a result of a common progression of development of 'stealth' systems for intravenous administration, pegylation approaches were used to form stealth micelles to enhance circulation time. Also, the PEG corona can act as a diffusion barrier for hydrophobic drugs to reduce burst release characteristic of micelles [160]. Thus, the hydrophilic block on the copolymer typically contains PEG segments with a molecular weight from 1 to 15 kDa. Similar to micelles formed with conventional surfactants, polymeric micelles comprise the core of the hydrophobic blocks stabilized by the corona of hydrophilic chains in water. However, compared to the conventional micelles, polymeric micelles are more stable upon the relatively high dilution conditions experienced in-vivo. For example, some amphiphilic copolymers have CMC values as low as 10^{-6} M [161]. PEG-phosphatidylethanolamine (PEG-PE) conjugates were

used to self-assemble the micelles with the particle size of 7 to 35 nm [162, 163]. Two long-chain fatty acyl groups of phospholipids provided greater hydrophobic cores compared to the conventional polymeric micelles. CMC and the particle size of the micelles formed from lipid-polymer conjugates depend on the length of the polymers. These lipid-core micelles are hybrid between polymeric micelles and lipid-based micelles. The hydrophobic block can represent a hyperbranched backbone chain to which hydrophilic PEG chains were attached to make a water-soluble polymer exhibiting micellar properties [164]. To further reduce the clearance by RES system and perform active targeting delivery, multifunctional micelles either through conjugation of targeting ligands on the micelle surface or through a triggered release mechanism (pH-sensitive polymeric micelles) were developed [163, 165, 166]. Antibody, peptide, transferrin and folate residues have been attached to the micelle surface. The drug loading efficiency apparently correlates with the hydrophobicity of a drug and is usually in the range from 1.5 to 50% by weight. Although many drug-loaded polymeric micelles have been developed, most of the results have described in-vitro studies. Such in-vitro results do not necessarily imply that these systems will be efficacious in-vivo. For example, recently, methoxy poly(ethylene glycol)-block-poly(caprolactone) (MePEG-b-PCL) amphiphilic diblock copolymers were synthesized as a water-soluble form or a water-insoluble form based on the lengths of PCL block. Water-insoluble copolymers were used to make nanoparticles while water-soluble copolymers were used to make micelles. It was demonstrated that the polymeric nanoparticles possessed a higher core microviscosity than the polymeric micelles. Interestingly, although the in-vitro release of paclitaxel from both paclitaxel-loaded polymeric nanoparticles and micelles in PBS were similar and slow, in-vivo biodistribution showed that the association of paclitaxel solubilized by micelles with the lipoprotein deficient plasma caused a similar plasma distribution as with free paclitaxel, resulting in a rapid release of the micellar drug during the in-vivo study, whereas nanoparticles retained more of paclitaxel with less association with the lipoprotein deficient plasma [167].

3.3.2.2 Liposomes

Liposomes have been and continue to be the most intensively researched colloidal drug delivery systems even four decades after their discovery. There are some excellent reviews and books covering all aspects of liposome technology. Liposomes are normally

composed of phospholipids that spontaneously form multilamellar, concentric bilayer vesicles with layers of aqueous media separating the lipid layers. The particle size of small unilamellar vesicles which are comprised of a single, lipid outer layer with an aqueous core is in the range 20 – 80 nm. The surface of liposomes may be charged or uncharged based on the selection of different phospholipids. There are many methods to prepare liposomes including precipitation [168]. Liposomes may be used to load both hydrophobic and hydrophilic drugs. Hydrophilic drugs reside in the aqueous core whereas hydrophobic drugs tend to remain in the lipid layers. Hydrophobic drugs are added during the formation of liposomes. Hydrophilic drugs may also be loaded during formation, but for charged drugs the pH-gradient method may be used wherein a pH gradient between the internal and external aqueous domains drives the drug into the interior of the liposomes by partitioning through the membrane. Liposomes have poor loading capacity for hydrophobic drugs that can not be dissolved in sufficient amounts in the phospholipid bilayer or sequestered in the liposome core. Furthermore, after i.v. administration, such drugs often rapidly partition from the bilayers into cells or bind to serum proteins preventing accumulation at the target site. Several liposomal drugs are now marketed including Ambisome® (amphotericin B), Doxil® (doxorubicin hydrochloride) and Visudyne® (verteporfin) to name a few. As discussed previously pegylation using a PEG conjugated lipid is routine to sterically stabilize liposomes for escaping the RES and altering pharmacokinetics. Pegylation is described in details in Section 3.3.1.1. However, based on the recent studies, a potential limitation of pegylated liposomes is the complement activation that can lead to anaphylactic response, causing hypersensitivity reactions in patients receiving pegylated liposomes. Another recent finding on pegylated liposomal drugs reported the accelerated blood clearance (ABC) phenomenon, resulting in pegylated liposomes to be cleared very rapidly from the circulation upon repeated injection [169]. IgM was secreted into the bloodstream after the first dose. The abundant binding of IgM to liposomes was responsible for the induction of the ABC phenomenon, and it appeared that the spleen may play an important role in this phenomenon. As was described in Section 3.3.1.2, various ligands, such as folate, peptides and antibodies have also been conjugated to liposomes to achieve active targeting delivery to solid tumors. On-going limitations of liposomes relate to stability and the ease and cost of manufacturing liposomal products

3.3.2.3 Nanoemulsions

Emulsions with particle size in the nanometer scale (typically between 50 nm and 200 nm) are often referred to nanoemulsions. To prepare an emulsion, oil, water, surfactant and energy are required. The total free energy of formation of an emulsion, ΔG, can be represented as the following:

$$\Delta G = \Delta A \gamma - T\Delta S \qquad \qquad \text{Ref. [170]}$$

where ΔA is the increase in interfacial area, γ is the interfacial tension, T is temperature and ΔS is the increase of entropy. When the bulk oil produces a large number of droplets, the interfacial area greatly increases. The small energy term, $T\Delta S$, can not compensate for the energy change from $\Delta A \gamma$ and consequently ΔG is positive. Thus, nanoemulsions cannot form spontaneously and the energy is required. In contrast to microemulsions, nanoemulsions are thermodynamically unstable. The methods used to produce nanoemulsions mainly include high-energy processes, low-energy emulsification and the phase inversion temperature (PIT) method [158, 159, 171]. High-energy methods include high-pressure homogenization and microfluidization which can be used at both the laboratory and industrial scale, as well as ultrasonification which is primarily used at the laboratory scale. The low-energy emulsification method was developed in a study of the phase behavior of water/oil/surfactant systems. Three different methods were studies based on the various emulsification processes: method (1) addition of oil to aqueous surfactant dispersion, method (2) addition of water to a surfactant solution in oil, and method (3) mixing preequilibrated samples of the components [172]. Only method 2 generated nanoemulsions with sizes about 50 nm. It appeared that the formation of nanoemulsions depended not only on the thermodynamic conditions but also on preparation methods and the order of addition of the components. The PIT method is the most widely used in the industry among all methods. It is based on the changes of the hydrophilic lipophilic balance (HLB) of the system by modifying factors such as temperatures, electrolyte concentrations, and using mixtures of surfactants which influence HLB [173]. It was thought that the key to nanoemulsion formation using low-energy emulsification and PIT methods could be attributed to the phase transitions occurring during the emulsification process. In addition to the three common methods mentioned above, a 'spontaneous' emulsification method named the Ouzo method also was reported to form nanoemulsions. The limitation of this method is the low oil content (typically 1%) and requirement for

using water-miscible solvents resulting in systems with somewhat limited utility for drug delivery [174].

Nanoemulsions are transparent or translucent systems and possess stability against sedimentation or creaming since the Brownian motion and the diffusion rate are greater than the sedimentation rate induced. The major mechanism for nanoemulsion destabilization is Ostwald ripening, an observed phenomenon in solid (or liquid) solutions which describes the evolution of an inhomogeneous structure over time and results from the difference in solubility between small and large droplets. Ostwald ripening can be quantitatively assessed from the Lifshitz-Slezov and Wagner (LSW) theory. According to this theory, the Ostwald ripening rate in oil-in-water emulsions is directly proportional to the solubility of the oil in the aqueous phase. However, experimental Ostwald ripening rates have been reported to be about three orders of magnitude higher than those calculated. Therefore, it is debatable to use LSW theory to predict Ostwald ripening rates [175]. Ostwald ripening can be reduced by the addition of the second oil with a low solubility in the aqueous phase and modification of the interfacial film at the oil/water interface using a second surfactant [170]. Nanoemulsions have been used as drug delivery systems for various routes of administration including parenteral [159, 176] and oral [177]. The anti-HER2 monoclonal antibody (Herceptin) was covalently linked to paclitaxel-palmitate-loaded cationic immunoemulsion to target HER2 receptors on prostate cancer cells [178]. The improved anti-cancer efficacy of this immunoemulsion was observed at day 56 after three treatments (once weekly for 3 weeks) at dose of 10 mg/kg compared to non-targeted paclitaxel-palmitate-loaded cationic emulsion and paclitaxel-palmitate solution in mice bearing orthotopic prostate tumors. A vitamin E-based nanoemulsion of paclitaxel (TOCOSOL) is currently in phase III clinical development. TOCOSOL is produced by a high-shear homogenization method. Tumor growth over time was monitored using TOCOSOL at 20, 40 and 60 mg/kg and Taxol at its MTD of 20 mg/kg. TOCOSOL had improved anti-tumor activity compared to Taxol in mice implanted with B16 murine melanoma [179].

3.3.2.4 Nanocapsules

Nanocapsules are ultrafine particles with a diameter of less than 1 μm with a liquid core (generally an oil) surrounded by a polymeric membrane structured by polymers or a

combination of hydrophilic/lipophilic surfactants. The structural feature and concept of nanocapsules are different form nanoemulsions which have surfaces stabilized by the adsorption of some surfactants [180-182]. Vegetable oils and triglycerides with medium- and long- chain fatty acids are the common components for the lipid cores. The drugs are confined to the lipid core which serves as a reservoir to allow a high drug loading for hydrophobic drugs and a slow release profile. Thus, nanocapsules are pharmaceutically attractive for water-insoluble drugs. Four techniques have been reported to prepare nanocapsules to date and include (1) interfacial polymerization of monomers [183], (2) interfacial deposition of preformed polymers [184], (3) an emulsification-diffusion technique [180], and (4) a phase inversion-based process [185]. Only the phase inversion-based process did not require the use of organic solvents for preparation of the nanocapsules. Although nanocapsules have been studied over the last 20 years, progress toward the use of nanocapsules for delivering anti-cancer drugs has been slow. Very few reports of in-vivo studies can be found in literature. A possible reason for this is that, as mentioned above, many of the processes used to prepare nanocapsules requires the use of organic solvents which may present toxicity issues. Paclitaxel-loaded nanocapsules were proved to be toxic in mice bearing P388 leukemia. The toxicity was apparently due to the composition of the nanocapsules which were comprised of poly(lactic acid), benzyl benzoate and Pluronic F68 [186]. Another problem that has been reported for nanocapsules is their stability in an aqueous environment. Drug leakage out of the nanocapsules can happen. Lyophilization, also known as freeze drying, has been investigated to extend the shelf-life of nanocapsules. However, lyophilization of nanocapsules is not easy as nanocapsules have a very thin and fragile envelop that may not withstand the mechanical stress of freezing [187, 188]. Etoposide and paclitaxel were encapsulated into nanocapsules and relatively high drug loadings and sustained drug release were achieved over a period of several days for etoposide and up to a few weeks for paclitaxel [189]. Lipophilic derivatives of gemcitabine, which is an anti-cancer drug and suffers from a rapid plasmatic metabolism, were incorporated into polycyanoacrylate nanocapsules in order to physically and chemically protect gemcitabine [190]. PEG was used to form a hydrophilic layer on the surface of nanocapsules to escape the RES system [191, 192]. Pegylated lipid nanocapsules exhibited long circulating properties. A promising in-vivo study was carried out using paclitaxel-loaded nanocapsules prepared from a phase inversion-based process in

a chemically induced hepatocellular carcinoma model in Wistar rats. Groups treated with paclitaxel and with PX-loaded nanocapsules showed significant increases in mean survival times compared to control, demonstrating an equivalent therapeutic efficiency of paclitaxel and paclitaxel-load nanocapsules that avoided the use of Cremophor EL in the formulation. Paclitaxel-loaded nanocapsules formulated using the phase inversion-based process also showed reversal of multidrug resistance in glioma cells in-vitro and reduction of tumor progression in rats bearing F98 glioma cells [193].

3.3.2.5 Solid lipid nanoparticles

Solid lipid nanoparticles made from biodegradable or biocompatible solid lipids were developed in the beginning of 1990s as an alternative colloidal carrier system for controlled drug delivery. Solid lipid nanoparticles are matrix systems in which the drug is physically and uniformly dispersed. The release of a drug incorporated in the lipid matrix occurs due to degradation of the particles by lipases present at the site of injection, leading to a prolonged release of drugs from the solid lipid nanoparticles [194]. A comprehensive review on solid lipid nanoparticles can be found in the literature [195]. As with other lipid colloidal systems, solid lipid nanoparticles have advantages including good tolerability due to the use of relatively safe lipids, protection of drugs against chemical degradation, and manageable issues with respect to large scale production by high pressure homogenization. Different water-insoluble drugs have been incorporated into solid lipid nanoparticles by choosing appropriate lipids for the drugs [196, 197]. However, the high temperatures used in the process of high pressure homogenization may increase the degradation rate of the drug and the carriers. Also, solid lipid nanoparticles have shown somewhat limited drug loading capacity and drug expulsion during storage. Moreover, the majority of lipophilic spin probes were found to be located not in the core of solid lipid nanoparticles but at the interface between the lipid layers and the core [198]. This may be the reason for the burst release of the drug which often happens for drug-loaded solid lipid nanoparticles. Selection of lipids is important for development of solid lipid nanoparticles. Lipids containing less ordered crystal lattices favor high drug loading capacity, slow release and prevention of drug leakage during the storage. For example, paclitaxel nanoparticles (PX E78 NPs) were previously developed in our lab. The nanoparticles were composed of emulsifying wax and Brij 78. Low drug entrapment efficiency (<50%) and a fast release profile (100% release

within 8 h) were associated with these PX E78 NPs. To solve this problem, nanostructured lipid carriers (NLC) have been developed as a new generation of solid lipid nanoparticles [199]. The lipid core of NLC was composed of a mixture of solid and liquid lipids in order to obtain a reduced crystal lattice. The choice of the lipids forming the core of NLC was considered as the most important factor determining drug incorporation efficiency. The solid lipid and the liquid lipid may not be very miscible, possibly resulting in a separate compartment in the core. In this case, the core is no longer a viscous semisolid and the drug will be excluded. For example, lipophilic drugs including bupivacaine base, bupivacaine stearate or indomethacin were incorporated into NLC with a lipid core composed of a mixture of triglycerides containing Precirol (solid) and Miglyol 812 (liquid) at a 4:1 ratio. None of the studied drugs were successfully incorporated in the lipid core. Moreover, the choice of lipids can not be based on the solubility of drugs in the bulk lipids since the exclusion effect did not correlate with the solubility [200].

3.3.3 Experimental design to optimize nanoparticle composition

To achieve targeting delivery to tumors, the preparation of nanoparticles is a critical step. In general, the components of the nanoparticles including lipids and surfactants are selected based on the physical and chemical properties of the model drug. A scientist then faces the challenge of finding the right composition of nanoparticles that will have the optimal properties for that specific drug. The basic goal is to develop nanoparticles of required stability, particle size range and uniform distribution and to ensure robust parameters for production. The classical approach used to optimize nanoparticle formulations is one-factor-at-a-time which is to vary the levels of one factor while keeping the others constant. This approach generally leads to a large number of experiments and ignores the possibility of factor interactions whereby the optimum for one variable may depend on the particular level of other variables.

Experimental design can be defined as the strategy for setting experiments in such a manner that the information required is obtained as efficiently and precisely as possible. The objective of experimental design is to plan and conduct experiments in order to extract the maximum amount of information from the collected data in the smallest number of experimental runs [201]. The optimization, which is a process to choose the best alternative from a set of possibilities, is facilitated based on experimental design. In the

search for the best nanoparticle formulation, the excipients are the independent variables or factors which are controllable and the dependent variables or responses are the factors to be optimized. When optimization includes different excipients and various responses, the combined response optimization is preferable. Desirability function is a way to combine multiple responses into one function for the simultaneous evaluation [200, 201]. In this function, each response is transformed to a d value. The overall contribution of all responses (d values) is combined to a D value which is used as an overall response to evaluate the outputs of the experiments.

Optimization methods could be considered as two different groups [202]. The first group is called the simultaneous approach and depends on mathematical models. The setting of all the variables in the mathematical models is preselected and consequently the number of experiments to be performed is known beforehand. Factorial design belongs to this group and has been used in the development of formulations [203-207]. A full factorial experimental design which studies the effect of all factors at various levels includes a large number of experiments. For example, for a study involving five factors at two levels of each factor, the number of experiments is 2^5. To reduce the number of experiments, fractional factorial design is developed using only a fraction of the experiments specified by the full factorial design. Various strategies are used to ensure an appropriate choice of experiments which could cover all possibilities in a full factorial design. Taguchi approach is based on fractional factorial designs, combining mathematical and statistical techniques. Orthogonal arrays are chosen for experimental design in this approach [208]. This approach was used to optimize solid lipid nanoparticles in which camptothecin was incorporated. The solid lipid nanoparticles were prepared by high pressure homogenization. Four independent variables including drug concentration, types and concentrations of emulsifiers, and homogenization pressure at three levels of each variable were studied for their influence on nanoparticle sizes. After nine experiments, the optimized condition resulted in monodispersed camptothecin-loaded nanoparticles with particle size about 200 nm. The carboxylate form of camptothecin was found to be significantly less potent than the lactone form in in-vivo tumor models. The resultant camptothecin-loaded nanoparticles greatly increased the stability of camptothecin toward hydrolysis and retention of the active lactone form [197].

The second group of optimization methods is model independent. The optimization is completed via a "searching" process. Sequential simplex optimization is the common approach in this group of optimization. The sequential simplex optimization was original developed in 1965 [209]. A simplex is a geometric figure with k + 1 corners, where k is equal to the number of independent variables. In this method, the optimum is tracked by evaluating the responses from the experiments at a set of points forming a simplex in the factor-space. New simplices are continually formed by reflecting one point in the hyperplane of the remaining points. The setting is not known beforehand. Thus, the current experiment is based on previous experiments. Each movement of the simplex involves changing all factor levels but factor interaction is accommodated in this scheme. This method has been demonstrated to be an efficient strategy for rapid optimization of multi-factor systems in chemistry and biochemistry [210-212]. In pharmaceutical product development, it is worthy to note that this search method allows setting up the range of independent variables and restricting the responses, e.g. particle size, in a very simple way besides the optimization. However, very few studies in literature have reported on the use of this method to optimize formulations. Essentially there are no reports on optimization of nanoparticle formulations using simplex optimization. The few use of simplex optimization may result from the unexpected number of experiments to reach an optimum because the number of experiments to be performed is unknown before the optimization in this method. When the starting simplex is far away from the optimum, optimization needs a long way to search for the best case. Therefore, the optimization process may be longer compared to simultaneous methods. A relevant study used a genetic algorithm and a downhill simplex technique to optimize a dry powder blend comprised of six lubricant/glidant agents and containing 500 mg of alpha methyl dopa to fill into hard gelatin capsules [213].

3.3.4 Safety issue for nanoparticles including their fate and metabolism

While targeted drug-loaded nanoparticle formulations have been shown to greatly improve anti-cancer efficacy of anti-cancer drugs in-vivo or in the clinic, there have been increasing concerns regarding the risks that nanoparticles may pose [214, 215]. To avoid risks, biodegradable and biocompatible excipients are commonly selected to produce nanoparticles for medical uses. These relatively safe materials includes lipids,

polysaccharides and biodegradable aliphatic polyesters, such as poly(lactic acid) (PLA), poly(glycolic acid) (PGA) and poly(ε-caprolactone) (PCL) [216]. Still, the properties of nanoparticles are different from those of bulk excipients. A decrease in the size of particles results in an increase in the total surface area of particles while keeping the mass unchanged. Although these intrinsic properties of nanoparticles may help improve drug delivery as discussed above, chemical alternations on the surface of the nanoparticles may occur. The nano-scale size of nanoparticles may lead to additional physicochemical and biological activities which are lacking in large, micron-sized particles. Moreover, the entrapment of bulk excipients into the matrix of nanoparticles may change their properties. For example, the surfactants are generally used to make lipid-based nanoparticles. It is known that the surfactants as surface active agents can affect membrane integrity [217]. To understand the blood compatibility of E78 nanoparticles composed of emulsifying wax (oil) and Brij 78 (surfactant), the hemocompatibility of E78 NPs was evaluated including hemolytic activity, platelet function and blood coagulation [218]. E78 NPs showed potential blood compatibility at clinically relevant doses. In addition, the platelet function was not affected up to 1 mg/ml of E78 NPs. Moreover, whereas Brij 78 alone led to a significant dose-dependent and time-dependent red blood cell lyses at the tested concentration range from 0-4 mM, E78 NPs made with 4 mM Brij 78 did not cause red blood cell lyses.

The metabolism of excipients in nanoparticles or the metabolism of nanoparticles themselves has not been studied in detail. A few in-vitro studies have been carried out to understand the degradation of solid lipid nanoparticles [219, 220]. During storage time and in in-vivo conditions, drug release from solid lipid nanoparticles could take place by diffusion and by matrix degradation. Thus, the main purpose of these studies was to optimize the compositions of solid lipid nanoparticles by choosing different lipids based on degradation velocity by enzymes and surfactants which influenced the biodegradation process. The results showed that the longer the fatty acid chains in the glycerides, the slower the degradation rate. Also, some surfactants, e.g. Poloxamer 407, slowed down the degradation due to steric stabilization whereas others, e.g. Tween 80, did not. There are very few studies on the metabolism of nanoparticles in-vivo. It is possible that insoluble nanoparticles accumulate in the body. The biological effect will depend on the properties and dose of nanoparticles. Nanoparticles also may interact with biological molecules [221].

Therefore, there remains the need to study metabolism of excipients in nanoparticles and the nanoparticles themselves to understand the potential issues pertaining to the fate and safety of nanoparticles for drug delivery.

3.4   Drug delivery systems to overcome P-gp-mediated drug resistance and their possible mechanisms

Multidrug resistance is a major impediment to the success of cancer chemotherapy. P-glycoprotein is the first discovered multidrug transporter and best characterized and most clinically relevant. P-gp is the product of the MDR1 gene and effluxes drugs without chemically modify. Approximately 50% of the anti-cancer drugs used clinically today are substrates of P-gp [222]. The emergence of drug resistance has made many of the chemotherapy drugs ineffective. Different strategies attempting to overcome P-gp-mediated drug resistance have been developed as described above. This section focuses on overcoming P-gp-mediated drug resistance using drug delivery systems. Unlike the potentially more serious effects of the active P-gp inhibitors, drug delivery systems may be inhibitors of P-gp with low pharmacological activity and reduced side-affects. The formulations discussed below to overcome MDR are summarized in Table 3.2.

3.4.1   P-gp inhibition by lipid formulations

In 1972, the study showed that Tween 80 enhanced the effect of actinomycin D and daunomycin in Chinese hamster resistant cells [223]. Since this report, a number of lipid and polymeric excipients present in pharmaceutical formulations have been reported to modulate the activity of P-gp. P-gp as an efflux pump located in the apical membranes of intestinal absorptive cells can reduce the absorption of drugs and consequently decrease the oral bioavailability. Thus, the lipid formulation strategy for enhancing absorption of drugs which are P-gp substrates become an attractive topic and has been extensively reviewed for oral delivery [222, 224-226]. Caco-2 and MDCK cells expressing P-gp are the most widely used cell models to study the oral absorption. Most of surfactants inhibiting P-gp are non-ionic. They can be divided into two classes according to the chemical structure [224]. The first class of surfactants exhibit a hydrophobic tail responsible for membrane anchoring and a hydrophilic head-group, including triglycerides, Cremophor EL, Solutol HS-15, TPGS, Tween 80, and Brij 35. The second class of surfactants, which lack a typical

membrane anchor, includes polyethylene glycol (PEG) and poly(ethylene oxide) (EO)-poly(propylene oxide) (PO) block copolymers (Pluronics or poloxamers). All surfactant inhibitors contain a unit which comprises hydrogen bond acceptor groups such as ester groups and polyoxyethylene sequences that could form hydrogen bonds with the transmembrane sequences of P-gp which are rich in hydrogen bond donor groups. Provided that the binding affinity of surfactants is higher than that of the drug, the surfactants become P-gp inhibitors and enhance the absorption. The inhibitory effects of surfactants on P-gp efflux are related to the structure of surfactants such as the length hydrophilic chain and hydrophilic lipophilic balance. TPGS 1000 has been reported to influence drug efflux well below its reported CMC of 0.02 wt. % [227]. A structure-activity relationship (SAR) study was carried out to understand the influence of PEG chain length on apical efflux transporters in Caco-2 cell monolayers [228]. TPGS analogs containing different PEG chain length (MW from 200-6000 Da) were synthesized. The results suggested that PEG chain length was essential to influence Rhodamine 123 efflux in-vitro. Commercial TPGS 1000 turned out to be one of the most potent analogs to inhibit P-gp efflux. The effect of HLB values of excipients on P-gp modulation was also studied for uptake of epirubicin in Caco-2 cells [229]. Surfactants with optimal net efficacy in this study including Tween 20, Tween 80, Brij 30 and Myrj 52 consist of a polyethylene and intermediate hydrocarbon chain. The characteristics of the surfactants allow them to partition between lipid bilayers and P-gp domains. The optimal HLB value to enhance epirubicin uptake was in the range of 10 to 17. A relative study on Pluronic block copolymers with varying length of EO and PO segments was performed in bovine brain microvessel endothelial cells (BBMEC) cells [230]. The most efficacious block copolymers exhibited intermediate length of 30 to 60 PO blocks and a relatively hydrophobic structure (HLB < 20), e.g. Pluronic P85 with 40 PO blocks and an HLB of 16. The common mechanisms of surfactants to inhibit P-gp may include binding competition of drugs with surfactants resulting from an interaction between surfactants and P-gp, and membrane fluidization leading to an indirect protein destabilization [230-233]. However, the latter mechanism may not be the case for some surfactants. For example, TPGS tends to rigidify lipid bilayers, not fluidizes them. [232].

3.4.2   Liposomes to address P-gp

Liposomal delivery systems have been shown to inhibit P-gp efflux [88, 234-238]. The proposed mechanisms included escaping P-gp through an endocytosis pathway [238] and direct interaction with P-gp. The interaction of liposomes with P-gp was proved by completely inhibition of photoaffinity labeling of P-gp by azidopine [235]. However, other studies showed that liposomes had limited effectiveness in addressing P-gp-mediated resistance in laboratory in-vitro models of cellular resistance and in clinical studies [239-242]. Liposome formulations containing both an anti-cancer drug and a P-gp inhibitor have been studied recently. The results showed that liposomal co-encapsulated drugs had better responses in both in-vitro and in-vivo resistant models compared to a single drug [243-245]. Moreover, liposomal targeting delivery systems have been investigated to overcome P-gp-mediated drug resistance [244]. For example, doxorubicin and verapamil were co-encapsulated into liposomes with 95% and 70% loading efficiency, respectively. To achieve targeting, human transferring (Tf) targeted to the Tf receptors which are overexpressed in leukemia cells was further conjugated to the liposomes. In resistant leukemia K562 cells (Tf receptor +), Tf-conjugated co-loaded liposomes showed 5.2 and 2.8 times greater cytotoxicity than non-targeted co-loaded liposomes and Tf-conjugated Dox liposomes, respectively. It was concluded that TfR-targeted liposomes co-loaded with Dox and verapamil were effective in selective targeting and reversal of drug resistance in cells [244].

3.4.3 Polymer and lipid nanoparticles (or nanocapsules) to address P-gp

A number of studies have investigated encapsulation of anti-cancer drugs into polymer nanoparticles and lipid nanoparticles (or nanocapsules) to overcome P-gp-mediated drug resistance [246-251]. Among them, polyalkylcyanoacrylate nanoparticles were the earliest ones investigated in resistant cell lines [249]. The results showed that non-biodegradable polymethacrylate nanoparticles can be internalized by an endocytosis process and reverse P-gp-mediated drug resistance in-vitro [252]. For in-vivo studies, biodegradable Dox-loaded polyisohexylcyanoacrylate (PIHCA) nanoparticles were developed. These PIHCA nanoparticles showed more cytotoxicity than free Dox in Dox-resistant C6 cells. Later on, more rapidly biodegradable PIBCA NPs were formulated to load Dox. Dox uptake from PIBCA NPs was different with that from PIHCA NPs as Dox-loaded PIBCA NPs caused higher cellular Dox uptake than free Dox. Also, it was

demonstrated that PIBCA NPs did not enter cells via an endocytosis pathway and efflux of Dox in NPs had a similar profile with free Dox. Mechanistic studies found that, 1) nanoparticles could deliver high concentration of Dox close to or adhered to the cell membrane, resulting in saturation of P-gp, and 2) the formation of an ion-pair between cyanoacrylic acid (a nanoparticle degradation product) and Dox could mask the positive charge of Dox and facilitate diffusion of Dox across cell membranes [253, 254]. However, in-vivo studies using MDR tumors showed that these nanoparticles were not efficacious in-vivo perhaps due to poor delivery to the tumors [255]. A new polymer-lipid hybrid nanoparticle (PLN) system was used to increase the cytotoxicity of Dox in resistant cells [251]. Dox uptake and retention from Dox-loaded NPs were significantly enhanced compared to free Dox. Blank PLNs did not improve Dox uptake and retention in resistant MDA-MB-435/LCC6MDR1 cells. These results indicated that the PLNs did not influence P-gp activity by themselves. The results also revealed that phagocytosis was an important pathway for PLN to enter the cells. Based on this pathway, Dox-loaded PLNs could bypass P-gp, leading to enhanced Dox uptake in resistant cells [256]. Recently, AerosolOT (AOT)-alginate nanoparticles were evaluated for their potential to overcome P-gp-mediated drug resistance. Dox-loaded AOT-alginate NPs enhanced cytotoxicity of Dox in resistant NCI/ADR-RES cells. It was observed that: 1) the uptake of rhodamine was significantly increased using rhodamine-entrapped nanoparticles in resistant cells, 2) blank NPs also improved rhodamine accumulation in a dose-dependant manner in resistant cells, and 3) the enhancement in rhodamine accumulation was not due to membrane permeabilization. However, the mechanism of AOT-alginate NPs to overcome P-gp-mediated drug resistance has not been established [248]. As mentioned above, the surfactant Solutol HS15, a mixture of free PEG 660 and PEG 660 hydroxystearate, could inhibit P-gp. Solutol HS-15-based lipid nanocapsules (LNC) containing paclitaxel or etoposide were studied for their potential to overcome MDR [193, 257]. PX-loaded LNCs were shown to significantly reduce cancer cell survival in comparison with Taxol in 9L cells and F98 cells. Solutol HS15 on its own did not improve the effects of paclitaxel. Similarly, PX-loaded LNCs significantly reduced tumor mass in-vivo whereas Taxol did not have a significant effect in an MDR-expressing F98 s.c. glioma model. The mixture of Solutol HS15 and PX did not improve tumor responses in this in-vivo model. This indicated that the importance of the nanocarrier itself for the anti-cancer effect on MDR.

The study also showed that LNC internalization could not be mediated by clathrin-dependent endocytosis. It was assumed that LNC endocytosis involves one or both of the two known cholesterol enriched membrane microdomains. The consecutive intracellular cholesterol movements would constitute the core of the LNC inhibitory effects on MDR. Thus, according to these mechanism studies, the investigators proposed that the inhibition of MDR efflux pump by LNCs could result from the interaction of the released intracellular free Solutol HS15 with MDR efflux pump and redistribution of intracellular cholesterol [193]. It is noteworthy that the drugs delivered into MDR cells by PLGA NPs are susceptible to efflux by P-gp [258]. PLGA NPs were taken up by cells by endocytosis, resulting in an increase of cellular concentration of the drug encapsulated into the NPs. Following entry, NPs were retained in the cytoplasm for a sustained period of time and slowly released the drug in the cellular cytoplasm. However, PX-loaded PLGA NPs did not show significant cytotoxicity in resistant NCI/ADR-RES cells. It was proved that P-gp activity did not affect the uptake and retention of NPs themselves. Thus, the inefficiency of PX-loaded PLGA NPs could result from the active efflux of the drug in cytoplasm by P-gp. Therefore, P-gp could not only extract the drug when the drug diffused into the cell through the lipid bilayer, but also pump out the drug present in the cytoplasm. Consequently, the efficiency of overcoming P-gp based on endocytosis of NPs may be limited.

3.4.4 Polymer conjugates to address P-gp

Poly[N-(2-hydroxypropyl)methacrylamide] (polyHPMA) and HPMA copolymers have been proposed by several groups as potential drug delivery systems. HPMA is a water-soluble, nonimmunogenic, synthetic polymer. HPMA copolymer-Dox conjugates have shown the potential to overcome drug resistance [259-261]. A series of studies on HPMA-Dox conjugates addressed multiple mechanisms of MDR in addition to P-gp-mediated drug resistance. After HPMA-Dox conjugate was internalized by an endocytosis pathway, the spacer between the polymer and the drug was cleaved by an enzymatic hydrolysis reaction in the lysosomal compartment of the cells, resulting in the release of the drug from the conjugate. Chronic exposure of sensitive A2780 cells to HPMA-Dox conjugates did not induce MDR as measured by quantification of MDR-1 gene expression, the inhibition of MPR gene expression and a decrease of resistance against Taxol [262]. In

contrast, repeated exposure to free Dox led to an increased resistance to Dox and Taxol and upregulation of the MDR-1 gene. Further in-vitro mechanistic studies on overcoming MDR revealed that HMPA-Dox conjugates inhibited drug detoxification systems by suppressing the expression of genes encoding glutathione and UDP transferase, cellular defensive mechanism by activating apoptosis signaling pathways and down-regulating the expression of the bcl-2 protein family and mechanisms of DNA repair, replication and synthesis leading to more DNA damage [263, 264]. These results indicated that underlying mechanisms triggered by macromolecular carriers can modulate the biological response of the cell at a molecular level, resulting in an overall increased cytotoxicity. The ability of HMPA-Dox conjugates to overcome MDR in-vivo was demonstrated in solid tumor mouse models of sensitive human ovarian carcinoma A2780 and resistant A2780/AD tumors [265]. HMPA-Dox conjugates significantly decreased tumor size 28 times in sensitive tumors and 18 times in resistant tumors whereas free Dox only reduced tumor size 2.8 times in sensitive tumor and had no effect in the resistant tumor model as compared to the control. The underlying mechanisms were also investigated for the in-vivo study. An enhanced accumulation of HMPA-Dox conjugates in the tumor was observed, and attributed to the EPR effect. The permeability of blood vessels decreased concomitantly with the downregulation of vascular growth and permeability (VEGF) gene in polymer-treated tumors. The other mechanisms proposed in-vitro, such as downregulation of the expression of genes responsible for the activity of efflux pumps, detoxification and apoptosis, were also demonstrated in the in-vivo studies.

3.4.5 Pluronic micelles to address P-gp

Pluronic is an inert block copolymer comprising of poly(ethylene oxide) (EO) (hydrophilic) and poly(propylene oxide) (PO) (hydrophobic). Pluronics are different than HMPA copolymers due to their amphiphilic nature. Their surfactant properties allow them self-assemble into micelles with a hydrophobic PO inner core and a hydrophilic EO outer shell. However, similar with HMPA copolymers, Pluronic block copolymer micelles also have been shown to overcome drug resistance. Extensive studies with Pluronic block copolymer micelles have been reviewed [266-268]. SP1049C containing Dox in the mixed micelles of Pluronic L61 and F127 is in clinical trials to treat metastatic adenocarcinoma of the upper gastrointestinal tract. Also, SP1049C showed more efficient accumulation in

tumors than free Dox, while distribution of SP1049C in normal tissues is similar to that of Dox [269]. Efficacy of SP1049C was confirmed in in-vivo experiments in both sensitive and resistant tumor models including P388 and P388/ADR murine leukemia, Sp2/0 and Sp2/0-Dnr murine myeloma, 3LL-M27 Lewis lung carcinoma, MCF-7 and MCF-7/ADR human breast carcinomas and KBv human oral epidermoid carcinoma [267, 269]. However, the toxicity of SP1049C was similar to that of free Dox. This suggested that SP1049C did not improve toxicity of free Dox, e.g. cardiotoxicity which is improved by liposomal Dox. However, there were no additional side-effects reported for SP1049C. Disintegration of micelles in biological fluids upon dilution to a concentration below its CMC is one of common concerns about using micelles for drug delivery. The biodistribution and pharmacokinetics of Pluronic P85 micelles suggested that the elimination of P85 was controlled by the renal elimination of P85 unimers and not by the rate of micelle disintegration [270]. However, micelle disintegration had been reported with other Pluronic micelles. To further address the potential of micelle disintegration, Pluronic L121 and Pluronic P-105 micelles were chemically modified to form a network or crosslink. Therefore, the CMC of the micelles was greatly reduced and the stability was enhanced while their ability to inhibit P-gp function still remained [271, 272].

The complex mechanisms associated with the effects of Pluronic block copolymers on MDR cells have been thoroughly studied. These mechanisms include, 1) altering membrane microviscosity [273, 274]. It was suggested that unimers (single block copolymer molecules) are responsible for biological modification as the effect of Pluronic copolymer occurred at the concentrations below their CMC. The hydrophobic PO chains of Pluronic unimers insert into the hydrophilic regions of the membrane, resulting in alterations of the membrane structure, and decrease in its microviscosity (membrane fluidization); and 2) inhibiting drug efflux transporters, such as P-gp and MRPs, through inhibition of P-gp ATPase activity; and 3) depleting intracellular ATP levels [273, 275]. As these pumps are energy dependent, attenuation of these pumps was related to energy deprivation and abolishment of pump associated ATPase activity. Thus, it can be surmised that Pluronic mediating direct and indirect energy depletion leads to operation cessation of efflux pumps and consequently sensitizes resistant cell lines to chemotherapeutic agents. A linear correlation between the extent of ATP depletion and chemosensitization elicited was established; and 4) influencing cell apoptosis signaling. Dox-loaded Pluronic block

copolymer P85 significantly enhanced the pro-apoptotic activity of the drug and prevented the activation of the anti-apoptotic cellular defense [276]; and 5) decreasing GSH intracellular levels and glutathione-s-transferase (GST) activity, indicating the inhibition of the GSH-GST detoxification system [277].

Table 3.1. Summary of alternative parenteral formulations of paclitaxel in clinical development (Adapted from Hennenfent and Govindan [28])

Delivery strategy	Agent	Development stage	Dose-limiting toxicity	References
Nanoparticles	Paclitaxel protein-bound particles (Abraxane[TM])	FDA-approved (300)[a]	neuropathy, stomatitis, superficial keratopathy	[30]
Prodrugs	DHA-paclitaxel (Taxoprexin[®])	Clinical (phase III) (1100)[a]	neutropenia	[278]
Co-solvents	Polymeric-micellar paclitaxel (Genexol-PM[®])	Clinical (phase I)[a] (390)	neuropathy, myalgia, neutropenia	[279]
Liposomes	Liposome-encapsulated paclitaxel	Clinical (phase I) (175)[a]	mucositis, neutropenia	[280]
Emulsions	Paclitaxel vitamin E? emulsion (Tocosol/S-8184)	Clinical (phase II)	neutropenia	[281]

[a]: maximum tolerated dose (mg/m^2)

Table 3.2. Formulations to overcome MDR and their proposed mechanisms

Formulations	Proposed mechanisms	Status	References
Liposomes	Endocytosis	In-vitro	[238]
	Interaction of liposomes with P-gp	In-vitro	[235]
	Co-encapsulation of a P-gp inhibitor (verapamil)	In-vitro	[244]
Polymethacrylate NPs	Endocytosis	In-vitro	[252]
Polyisohexylcyanoacrylate NPs	(1) No endocytosis (2) Saturation of P-gp by high concentration of the drug (3) Formation of an ion-pair between NP degradation product and the drug	In-vitro in-vivo	[253-255]
Polymer-lipid hybrid NPs	Phagocytosis	In-vitro	[251]
AerosolOT (AOT)-alginate NPs	Not established	In-vitro	[248]
Solutol HS-15-based lipid nanocapsules	(1) Interaction of the released intracellular free Solutol HS-15 with MDR efflux pump (2) Redistribution of intracellular cholesterol	In-vitro in-vivo	[191, 257]
HPMA copolymer-Dox conjugates	(1) Endocytosis (2) Inhibition of drug detoxification systems (3) Inhibition of cellular defensive mechanisms	In-vitro in-vivo	[259-265]
Pluronic block copolymer micelles	(1) Change in membrane microviscosity (2) Inhibition of drug efflux transporters (3) ATP depletion (4) Influence of cell apoptosis signaling (5) Inhibition of the GSH-GST detoxification system	In-vitro in-vivo phase II	[266-275]
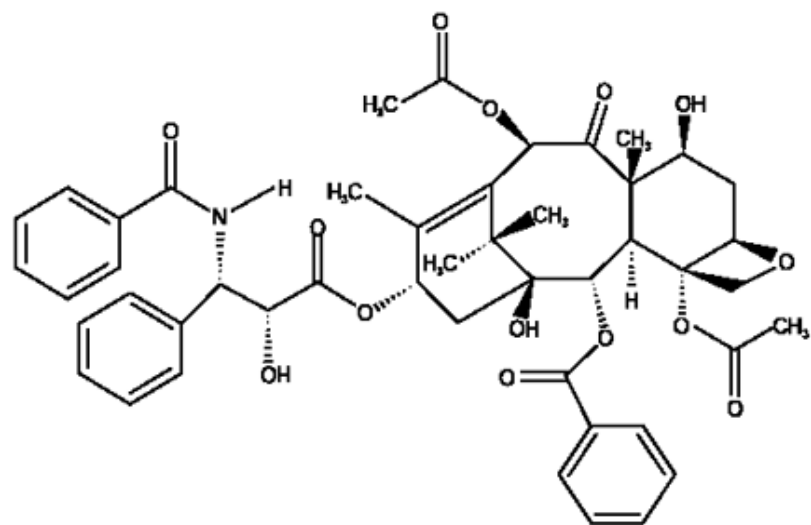
Figure 3.1: The chemical structure of paclitaxel

Figure 3.2: The chemical structure of doxorubicin.
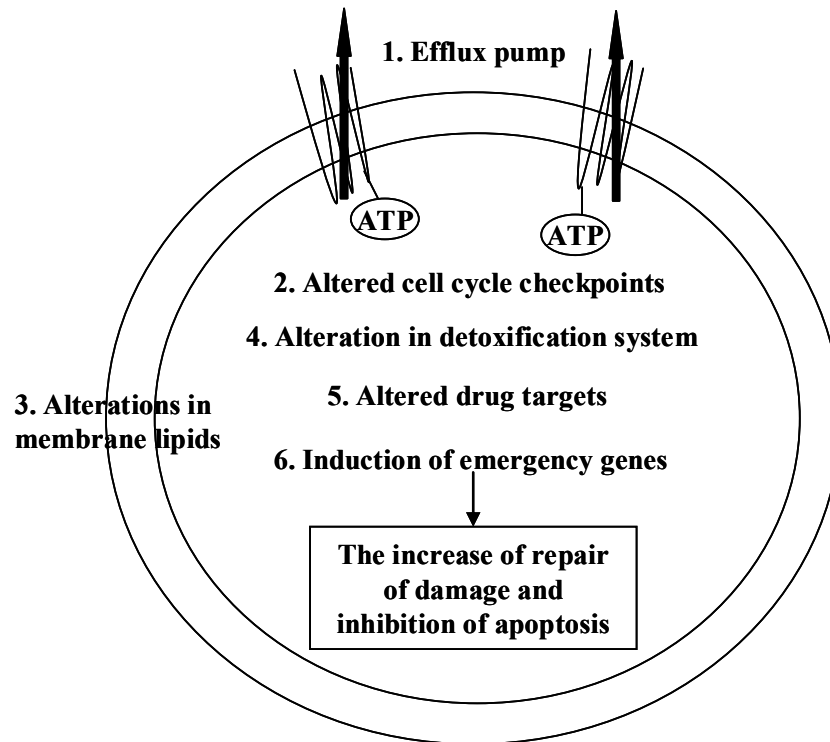
Figure 3.3: The summary of the mechanisms in which cultured cancer cells have been shown to become resistant to cytotoxic anti-cancer drugs. The efflux pumps shown schematically at the plasma membrane include MDR-1, MRP family members, and MXR (ABC G2), which is presumed to function as a dimer (Adapted from Gottesman [77]).
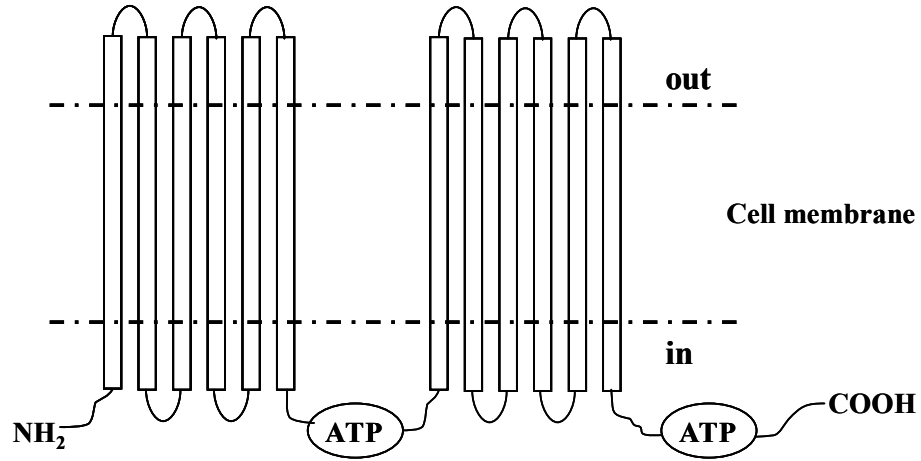
Figure 3.4: Topology model of P-glycoprotein. Each hydrophobic domain is followed by a hydrophilic domain (ATP binding domain) containing a nucleotide-binding site that is located at the cytoplasmic face of the membrane and couples ATP hydrolysis.
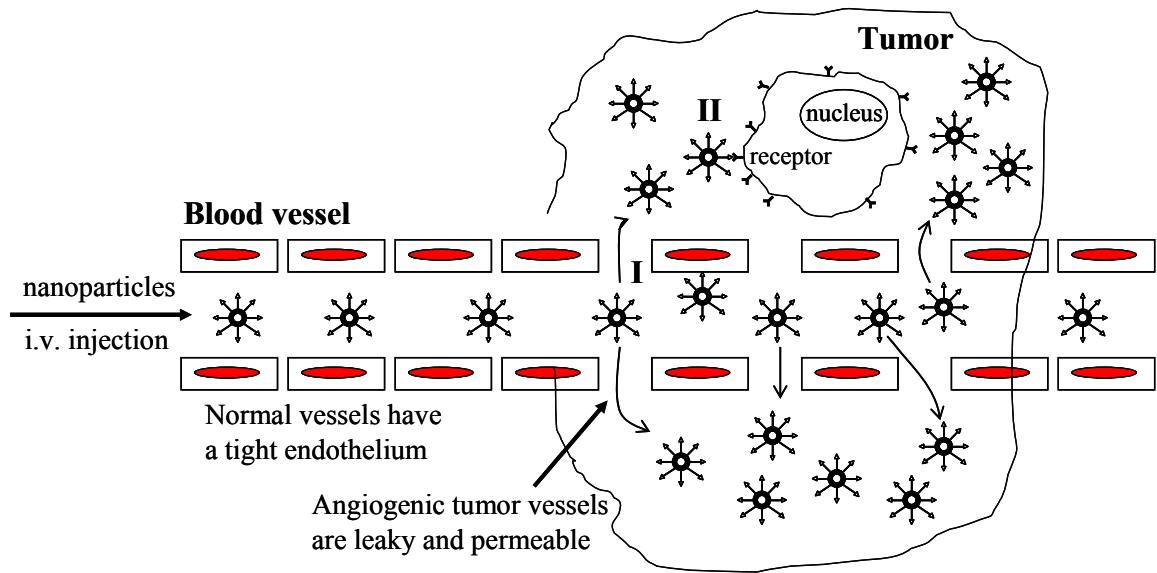
Figure 3.5: A schematic representation of enhanced drug delivery to solid tumors using nanoparticles. (I) Passive targeting delivery. After i.v. injection, nanoparticles accumulate in tumors through leaky and permeable tumor vasculature and impaired lymphatic system (EPR effect). (II) Active targeting delivery. Ligand-coated nanoparticles can bind with the receptor resulting in cell-specific recognition and improved drug delivery to solid tumors.
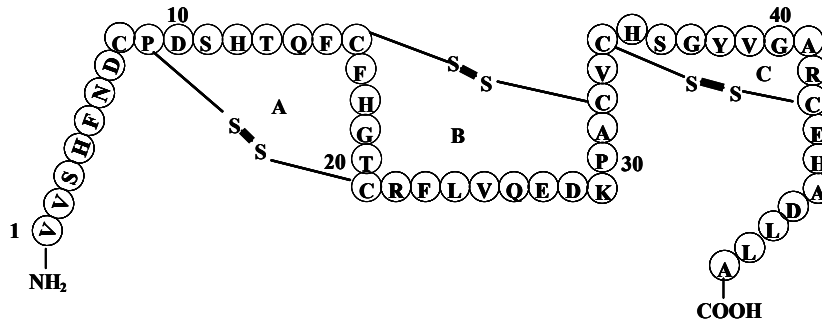
Figure 3.6: A schematic representation of the primary and loop structure of TGF-α.
Te six cysteines form the three disulfide loops. The disulfide bonds are represented as *thick lines*, and the *loops* formed by these are labeled as *A*, *B*, and *C*.

Chapter 4

The metabolism of fatty alcohols in lipid nanoparticles by horse liver alcohol dehydrogenase

4.1   Summary

Fatty alcohols are commonly used in lipid-based drug delivery systems including parenteral emulsions and solid lipid nanoparticles. The purpose of these studies was to determine whether horse liver alcohol dehydrogenase, a NAD-dependent enzyme, could metabolize the fatty alcohols within the NPs and thus serve as a mechanism to degrade these NPs in the body. Solid nanoparticles (<100 nm) were engineered from oil-in-water microemulsion precursors using emulsifying wax as the oil phase and Brij 78 as the surfactant. Emulsifying wax contains both cetyl and stearyl alcohols. NPs were incubated with the enzyme and NAD^+ at 37°C for up to 48 h, and the concentrations of fatty alcohols were quantitatively determined over time by gas chromatography (GC). The concentrations of cetyl alcohol and stearyl alcohol within the NPs decreased to only 10-20% remaining after 15-24 h of incubation. In parallel, NP size, turbidity and the fluorescent intensity of NADH all increased over time. It was concluded that horse liver alcohol dehydrogenase/NAD^+ was able to metabolize the fatty alcohols within the NPs, suggesting that NPs made of fatty alcohols may be metabolized in the body via endogenous alcohol dehydrogenase enzyme systems.

4.2   Introduction

Nanoparticles have received considerable attention as potential drug delivery systems for over 30 years. There are some general advantages to the use of nanoparticles for drug delivery: (1) Due to their small sizes, nanoparticles help to solve many challenging problems in drug formulation. For example, nanoparticles are ideal carriers for poorly soluble drugs, especially when the drugs lack solubility in both aqueous and non-aqueous media. Reducing the particle size of poorly soluble drugs may enhance the dissolution rate and drug bioavailability since the available surface area per given mass of particles is increased [282]; (2) The toxicity and side effects of certain anti-cancer drugs such as doxorubicin [283] and cisplatin [284] may be considerably reduced by entrapping the drugs in nanoparticles; (3) In addition, nanoparticles have been shown to provide benefit in enhancing the circulation time of drugs in the body [285, 286]; (4) Finally, nanoparticles have been used to target specific cells and tissues in the body [287] and to control the release rate of drugs [288].

One of the major considerations in the use of nanoparticles as delivery systems is the selection of the composition of the components. Typically, nanoparticles are made from either biodegradable and/or biocompatible polymers or lipids [289, 290]. Recently, lipids such as fatty alcohols have been used to form colloidal carriers such as microspheres [291, 292], liposomes [293, 294] and nanoparticles [295]. However, there are few or no reports on the metabolism of fatty alcohols within formed nanoparticles. It was previously shown by DeAngelis and Findlay that synthetic ^{14}C-cetyl alcohol was widely distributed in the body after intratracheal administration. ^{14}C-cetyl alcohol was oxidized to palmitic acid which was then used in the phospholipid biosynthesis pathway [296]. Additionally, another report has shown that lipase was able to metabolize fatty acids used to make solid lipid nanoparticles [219].

Our laboratories have reported on a novel method to engineer stable nanoparticles from oil-in-water microemulsion precursors. In this method, melted nonionic emulsifying wax which is composed of cetyl alcohol ($C_{16}H_{34}O$), stearyl alcohol ($C_{18}H_{38}O$) and polysorbate 60 was used to form the oil phase. These nanoparticles have been utilized for brain targeting [297], dendritic cell targeting [298, 299] and tumor targeting [300-302]. In a recent study, it was demonstrated that these lipid-based nanoparticles did not cause in-vitro red blood cell lyses at concentrations up to 1 mg/ml [218]. In addition, these

nanoparticles did not activate or aggregate platelets; however, the nanoparticles were shown to inhibit agonist induced platelet activation and aggregation in a dose-dependent manner. Although these NPs appear to have blood compatibility at clinically relevant doses, little is known about the metabolism of the NPs.

The purpose of the present studies was to investigate whether horse liver alcohol dehydrogenase (alcohol: AD^+ oxidoreductase, EC 1.1.1.1) could metabolize cetyl and stearyl alcohols present in the lipid-based nanoparticles. The metabolism of the fatty alcohols in the nanoparticles was monitored by the increase in fluorescence intensity of NADH and by quantitative measurements of the metabolized products using a quantitative gas chromatographic method.

4.3   Materials and Methods

Materials

Cetyl alcohol (1-hexadecanol, 95%) was purchased from Sigma (St. Louis, MO). Stearyl alcohol (1-Octadecanol, 99%), stearic acid (99.5%), pyridinium chlorochromate (PCC), nonadecanoic acid (98%), diethyl ether, dichloromethane (CH_2Cl_2), NAD^+ (β-nicotinamide adenine dinucleotide) (99%) and horse liver alcohol dehydrogenase (HLADH) (0.89 units/mg lyophilized powder containing sodium phosphate buffer salt and NAD^+) were purchased from Sigma-Aldrich (St. Louis, MO.). Celite$^®$ 545, 1 N hydrochloric acid and 1 N sodium hydroxide were obtained from Fisher (Fairlawn, NJ.). Silica gel 60 was obtained from Macherey-Nagel (Düren, Germany). Hexane was purchased from EM (Darmstadt, Germany). Brij 78 was purchased from Uniqema (New Castle, DE.). Emulsifying wax, palmitic acid, monobasic sodium phosphate and dibasic sodium phosphate were purchased from Spectrum (New Brunswick, NJ.).

Methods
Synthesis of hexadecanal and octadecanal

Hexadecanal and octadecanal were prepared by oxidation of the corresponding alcohols using pyridinium chlorochromate (PCC). The initial concentrations of pyridinium chlorochromate and fatty alcohols were 0.9 mM and 0.1 mM, respectively. Pyridinium chlorochromate was dissolved in 85 ml dichloromethane with Celite 545 (PCC: Celite 545, 1: 1 w/w). The fatty alcohol dissolved in 15 ml dichloromethane was slowly added to a well stirred PCC solution and reacted for 4 h. The reaction mixture was passed through a column (3 cm × 8 cm) packed with silica gel 60. The products were eluted with dichloromethane and the fraction was evaporated to dryness. The structures of hexadecanal and octadecanal were confirmed by GC-MS and NMR.

Preparation and characterization of nanoparticles from microemulsion precursors

Solid nanoparticles were engineered from oil-in-water microemulsion precursors using emulsifying wax as the oil phase and Brij 78 as the surfactant. Twelve (12) milligrams of emulsifying wax were accurately weighed into a glass vial and melted together with 20.7 mg Brij 78 at 60°C. Next, 6 ml of 50 mM phosphate buffer (pH 7.5) were added under

magnetic stirring. After 30 min of continuing stirring at 60°C, a homogeneous and clear oil-in-water microemulsion formed. The warm microemulsion was then cooled to room temperature while stirring to form a 6 ml solid nanoparticle suspension. After the nanoparticles formed, an additional 4 ml of 50 mM phosphate buffer (pH 7.5) were added to dilute the nanoparticles to 10 ml. Nanoparticle size was measured by photon correlation spectroscopy (PCS) using a Coulter N4 Plus Submicron Particle Sizer (Coulter, Miami, FL) by scattering light at 90° at 25°C for 1 min. Each 1 ml sample for PCS was prepared by diluting 100 μl nanoparticle suspension with 900 μl deionized and 0.22 μm filter water.

Incubation of nanoparticles with horse liver alcohol dehydrogenase and NAD$^+$

Horse liver alcohol dehydrogenase and NAD$^+$ were added to nanoparticle suspensions so that the final concentrations were 1 mg/ml and 5 mg/ml, respectively. The amount of alcohol dehydrogenase and NAD$^+$ added was based on a previous reported study (Hinson & Neal, 1975.). The samples were incubated with shaking at 37°C for 48 h. Nanoparticle suspensions in the absence of alcohol dehydrogenase and NAD$^+$ were used as controls. To measure the metabolism of the fatty alcohols, 100 μl and 1000 μl aliquots were removed from the samples at different time points during the 48 h incubations. For the 100 μl aliquots, 900 μl water was immediately added to perform particle size, turbidity, and fluorescence intensity measurements (see below). For the 1000 μl aliquots, the enzymatic reaction was terminated by adding 100 μl of 1 N HCl. Next, 300 μl of the internal standard, nonadecanoic acid (1000 μg/ml), were added to the mixture. The mixture was then heated at 60°C for 30 min, cooled to room temperature, and then extracted with 1 ml diethyl ether (× 2) and 1 ml hexane (× 2). The combined extract was dried under N$_2$, and dissolved with 1 ml hexane for GC analysis.

Measurement of particle size, turbidity and fluorescence intensity

The nanoparticle size was measured as described above. The turbidity of the nanoparticle suspensions was detected by UV spectroscopy using a Beckman DU 7500i Spectrophotometer at 320 nm using water as the blank. The fluorescence intensity of NADH was measured using a Hitachi Model F-2000 Fluorometer (excitation wavelength was 350 nm and emission wavelength was 460 nm). To obtain the corrected fluorescent measurement

of each sample, the fluorescent intensity of a fresh mixture of 1 mg/ml alcohol dehydrogenase and 5 mg/ml NAD^+ was subtracted at each time point.

The influence of Brij 78 on the HLADH/NAD^+ enzyme reaction of fatty alcohols

Cetyl alcohol (1 mg/ml) without Brij 78 and with 1 mM Brij 78 or 3 mM Brij 78 was incubated with 1 mg/ml horse liver alcohol dehydrogenase and 5 mg/ml NAD^+ at 37°C for 48 h. The enzymatic reactions were monitored by detecting NADH (as described above). As controls, the mixtures of alcohol dehydrogenase and NAD^+ in the absence and present of Brij 78 were used.

Quantitative analysis of cetyl alcohol and stearyl alcohol by gas chromatography

GC analysis was performed using a Thermoquest Trace 2000 System equipped with a flame ionization detector (FID) and AS 2000 Autosampler. Separation of samples was carried out on a 30 m column (0.53 mm i.d.) coated with SPB-1 phase (poly (dimethylsiloxane), 1.5 μm film thickness) from Supelco (Bellefonte, PA). The injector was used in the splitless mode, and the sample injection volume was 1 μl. The injector and detector temperatures were kept at 220°C and 270°C, respectively. The initial temperature of the column was 80°C and was held for 0.06 min, and then increased at 20°C/min to 250°C. The temperature was then held at 250°C for 6 min. The total run time was 14.56 min. Helium was used as the carrier gas. Data acquisition and processing were performed with a Chromquest (Version 2.53) software for GC system.

The identification of sample peaks was determined by comparing the relative retention time to that of known standards. Quantification was aided using nonadecanoic acid as an internal standard. The purity of each standard was determined by GC in triplicate. The revised concentration was used for subsequent calculations. The stock solutions of hexadecanal, octadecanal, cetyl alcohol, stearyl alcohol, palmitic acid, stearic acid and nonadecanoic acid were prepared at a concentration of 1000 μg/ml in *n*-hexane. From the stock solutions of cetyl alcohol and stearyl alcohol, working standards of 600, 400, 300, 100 and 10 μg/ml containing 300 μg/ml nonadecanoic acid in *n*-hexane were made. Each sample was measured in triplicate, and average areas were used to obtain calibration curves of the standards. Consequently, quantitative linear ranges were determined and relative response factors (f_i) were calculated. The stock solutions of hexadecanal, octadecanal, palmitic acid

and stearic acid were used to identify the corresponding peaks. The concentrations of samples from the incubations were determined in triplicate and calculated as $W_i = (f_i \times A_i \times W_s)/As$: where W_i and W_s are the weighed amounts of sample (i) and internal standard (s), respectively; A_i is the peak area of sample, A_s is the peak area of the internal standard, and f_i is the relative response factor of sample (i).

4.4 Results and discussion

Fatty alcohols present in the body can be incorporated into wax esters and ether lipids via the fatty acid-fatty alcohol cycle [303]. Fatty alcohols are oxidized to the corresponding fatty acids by fatty alcohol: NAD^+ oxidoreductase (FAO, EC 1.1.1.192). FAO is a complex enzyme that consists of at least two separate enzymes, fatty alcohol dehydrogenase (FADH) and fatty aldehyde dehydrogenase (FALDH). Fatty alcohol dehydrogenase (FADH) metabolizes fatty alcohols to fatty aldehydes and fatty aldehyde dehydrogenase (FALDH) metabolizes fatty aldehydes to fatty acids [303-305]. Previous literature studies with this enzyme system have been performed in a heterogeneous enzyme 'cocktail' derived from the liver, and thus it was not an isolated enzyme system. However, in these present studies, a commercially available purified enzyme, HLADH was utilized. The general reaction of HLADH is shown in Figure 4.1 [306]. As a single enzyme, Horse liver alcohol dehydrogenase catalyzes the reversible interconversion of fatty alcohols and their corresponding aldehyde/ketone products, and also catalyzes the dismutation and oxidation of the fatty aldehydes to the corresponding fatty acids. The activity of horse liver alcohol dehydrogenase for aldehyde oxidation is low due to the high K_m and low V_{max} of the reaction of fatty alcohols to fatty acids. Thus, alcohol dehydrogenase plays a more important role in the oxidation of alcohols to aldehydes. Related, aldehyde dehydrogenase may then convert the formed aldehydes to the corresponding acids [306, 307].

In order to choose the appropriate operational parameters for the quantitative gas chromatographic method, several temperature programs were studied. The optimized chromatographic method balanced efficiency, sample capacity, and peak resolution. In initial GC method development studies, peaks of palmitic acid and stearyl acid showed some tailing. Thus, methods were adapted to increase resolution and resolve tailing. The final optimized temperature program was held at 80°C for 0.06 min, then increased to 250°C at a rate of 20°C/min and held for 6 min at 250°C. Seven compounds (hexadecanal, cetyl alcohol, palmitic acid, octadecanal, stearyl alcohol, stearic acid and nonadecanoic acid) were fully separated with good resolution in the optimized operational condition. A representative GC chromatogram is shown in Figure 4.2.

The purity of cetyl alcohol, stearyl alcohol, and nonadecanoic acid was determined by GC and is listed in Table 4.1. Nonadecanoic acid was chosen as the internal standard for quantitative measurement by GC. All three compounds had purity in the range of 98.3-

99.4%. Table 4.2 shows the calibration parameters of both cetyl and stearyl alcohols. A minimum of five concentrations were examined for each calibration curve (see Figure 4.3). The results demonstrate that the calibration curves for both cetyl and stearyl alcohols were linear from 10 µg/ml to 600 µg/ml. The R^2 value for cetyl alcohol and stearyl alcohol were 0.9969 and 0.9941, respectively.

The in-vitro metabolism of lipid-based NPs is shown in Figure 4.4 as a function of time. The GC assay was used to quantify the loss of both cetyl and stearyl alcohols from the NP suspension incubated with the HLADH/NAD$^+$ system at 37°C for up to 48 h. The concentrations of cetyl alcohol and stearyl alcohol decreased by more than 80% of each initial one of fatty alcohols after 15-24 h. However, from 24-40 h, the concentrations of both cetyl alcohol and stearyl alcohol increased by 2-3 fold. This phenomenon was very reproducible and was repeated in multiple experiments. Most likely, the subsequent increase in alcohol concentrations at approximately 24 h could be explained by the unique property of the enzyme (see Figure 4.1) whereby the equilibrium supports the regeneration of the alcohols from the aldehydes by the reversible reactions [306, 308].

Experiments were also performed to quantify the corresponding fatty aldehydes (hexadecanal and octadecanal) and fatty acids (palmitic acid and stearic acids). In fact, as shown in Figure 4.2, the presence of these metabolic products could be identified by GC. However, due to extraction difficulties and stability limitations of the fatty aldehydes, additional studies were not performed to develop a quantitative GC method for these compounds.

Increase in size, turbidity and fluorescence intensity when NPs are incubated with HLADH/NAD$^+$

In addition to quantitative studies assessing the loss of the primary NP components, cetyl and stearyl alcohols, evidence to prove NP metabolism was sought. It was hypothesized that NPs exposed to HLADH/NAD$^+$ would undergo an expansion in particle size coupled with an increase in turbidity due to the presence of metabolic products. As shown in Figure 4.5, HLADH/NAD$^+$ caused the NPs to more than double in size over 48 h at 37°C versus a NP control. In addition, as shown in Figure 4.6, there was a corresponding increase in the turbidity of the metabolized NP suspension. It was also noted that the

metabolized NP suspension exhibited an increase in foaming likely a result of free Brij 78 that was liberated from the NPs over time.

As shown in Figure 4.1, the conversion of a fatty alcohol by HLADH results in the reduction of NAD^+ to NADH. NADH is fluorescent and thus its concentration over time would be expected to increase upon fatty alcohol metabolism. As shown in Figure 4.7, NADH fluorescence in the suspension substantially increased over the first 24 h providing additional evidence of the enzymatic reaction. Notably, the rate and extent of NADH fluorescence very closely matched the rate and extent of the loss of fatty alcohols as shown in Figure 4.4.

Effect of the Brij 78 surfactant on the enzyme reaction

During the engineering of the nanoparticles, the Brij 78 surfactant was added to form the oil-in-water microemulsion at an elevated temperature. It is known that the addition of even low concentrations of surfactants influence the structure and activity of enzymes [309, 310]. No previous literature reports on the effect of Brij-based surfactants on the $HLADH/NAD^+$ enzyme system were identified. Thus, studies were undertaken to assess the effect of Brij 78 on the activity of this enzyme system. In these studies, cetyl alcohol was incubated with $HLADH/NAD^+$ in the presence and absence of Brij 78. The increase of NADH fluorescence was monitored over time. As shown in Figure 4.8, the incubation of $HLADH/NAD^+$ with or without 2 mM Brij 78 resulted in no increase in NADH fluorescence intensity. The fluorescence intensity increased when $HLADH/NAD^+$ was incubated with 1 mg/ml cetyl alcohol. However, the rate of increase of fluorescence intensity was considerably lower than the rate when $HLADH/NAD^+$ was incubated with lipid-based NPs (as shown in Figure 4.7). This suggested that Brij 78 may be enhancing the activity of HLADH. In fact, when $HLADH/NAD^+$ was incubated with both Brij 78 and cetyl alcohol, the fluorescent intensity markedly increased similar to that of the NPs shown in Figure 4.7. Moreover, the enhancement of fluorescent intensity was related to the concentration of Brij 78. These results indicate that the activity of HLADH was enhanced in the presence of Brij 78 and this enhancement accelerated metabolism of fatty alcohols present as either free fatty alcohols (cetyl alcohol alone) or fatty alcohols entrapped in a solid nanoparticle.

In conclusion, the results of these studies demonstrate that an alcohol dehydrogenase enzyme metabolized fatty alcohols present in solid lipid-based nanoparticles. In fact,

entrapping the fatty alcohols into solid nanoparticles did not hinder the reaction of the fatty alcohols with the enzyme. Under the conditions tested, over 80% of cetyl alcohol and stearyl alcohol in the NP suspension were metabolized within 15 h. The results also showed that Brij 78 increased the activity of the enzyme. These studies suggest that lipid-based systems comprised of fatty alcohols are likely to be readily metabolized in the body by endogenous fatty alcohol dehydrogenase.

Table 4.1. The average purity of each standard as measured by gas chromatography (n=3)

Standard	Cetyl Alcohol	Stearyl Alcohol	Nonadecanoic acid
Purity (%)	99.37	98.29	98.52
R.S.D. (%)	0.222	0.031	0.178

Table 4.2. Calibration parameters of cetyl and stearyl alcohols in the quantitative gas chromatographic assay

Standard	Calibration curve	Linear range (μg/ml)	R^2	Relative response factor (f_i)
Cetyl Alcohol (n=3)	y = 3.2438x – 0.1284	10-600	0.9969	0.30828
Stearyl Alcohol (n=3)	y = 3.4693x – 0.1838	10-600	0.9941	0.28824

Nonadecanoic acid was used as an internal standard. $y = A_i/A_s$ and $x = C_i/C_s$; where A_i and A_s are the peak areas of the fatty alcohols and internal standard, respectively, and C_i and C_s are the concentrations of the fatty alcohols and internal standard, respectively.

Figure 4.1

$$CH_3(CH_2)_n\text{-OH} \;+\; NAD^+ \;\underset{}{\overset{HLADH}{\rightleftharpoons}}\; CH_3(CH_2)_n\overset{\displaystyle O}{\overset{\|}{C}}\text{-H} \;+\; NADH$$

$$CH_3(CH_2)_n\overset{\displaystyle O}{\overset{\|}{C}}\text{-H} \;+\; NAD^+ \;\xrightarrow{HLADH}\; CH_3(CH_2)_n\overset{\displaystyle O}{\overset{\|}{C}}\text{-OH} \;+\; NADH$$
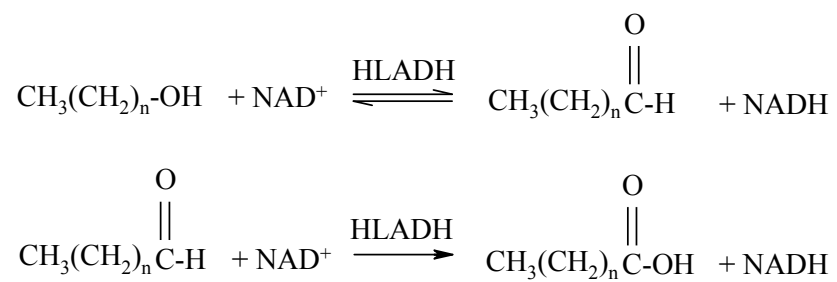
Figure 4.1: The reaction of fatty alcohol and fatty aldehyde with horse liver alcohol dehydrogenase (HLADH)/NAD$^+$ enzyme system.

Figure 4.2
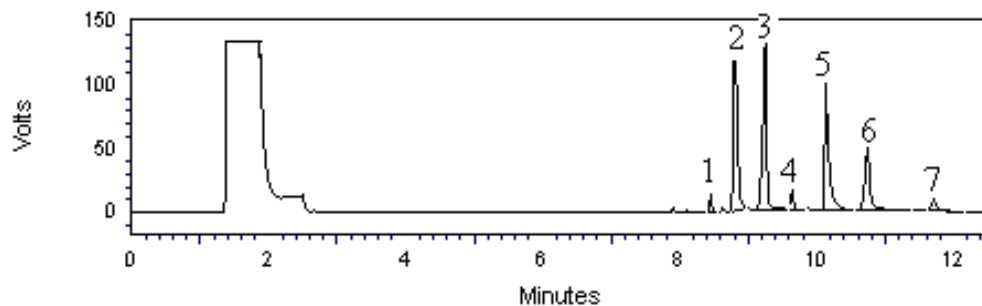
Figure 4.2:   Gas chromatography (GC) chromatogram of seven standards: (1) hexadecanal, (2) cetyl alcohol, (3) palmitic acid, (4) octadecanal, (5) stearyl alcohol, (6) stearic acid and (7) nonadecanoic acid.

Figure 4.3
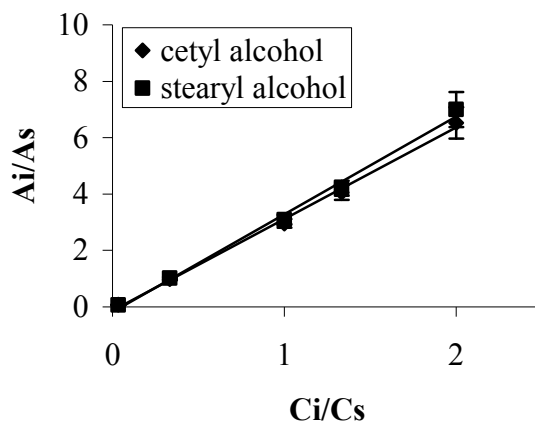
Figure 4.3: Calibration curves (C_i/C_s vs A_i/A_s) of cetyl alcohol and stearyl alcohol as measured by gas chromatography. A_i and A_s are the peak areas of the fatty alcohols and internal standard, respectively. C_i and C_s are the concentrations of the fatty alcohols and internal standard, respectively. Each point is the mean ± SD (n=3). The internal standard was nonadecanoic acid.

Figure 4.4
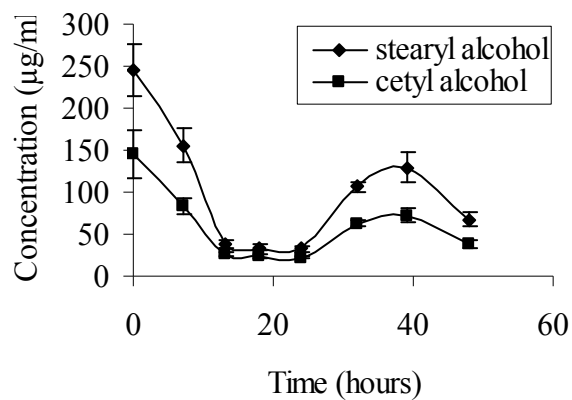
Figure 4.4: **In-vitro metabolism of cetyl alcohol and stearyl alcohol in lipid nanoparticles as a function of time when nanoparticles were incubated with horse liver alcohol dehydrogenase and NAD$^+$ at 37°C for 48 h.** Each point is the mean ± SD (n=3).

Figure 4.5
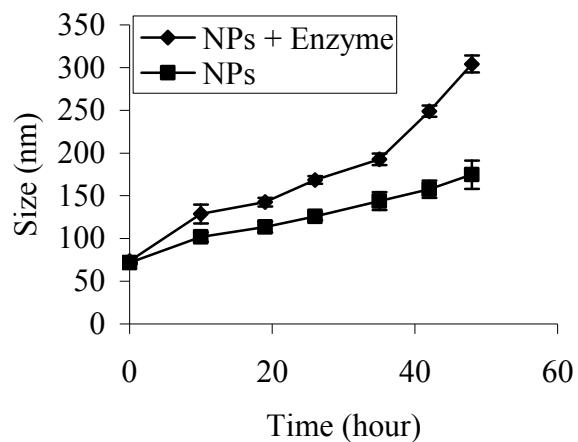
Figure 4.5: **The change in particle size when lipid nanoparticles were incubated with horse liver alcohol dehydrogenase and NAD$^+$ at 37°C for 48 h.** Each point is the mean ± SD (n=3).

Figure 4.6
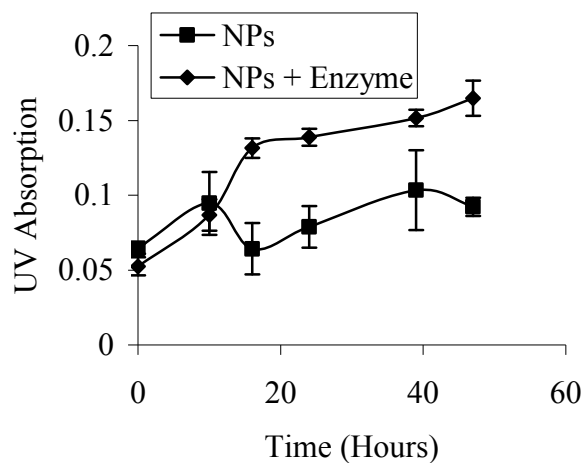
Figure 4.6: The change in turbidity when lipid nanoparticles were incubated with horse liver alcohol dehydrogenase and NAD$^+$ at 37°C for 48 h. Each point is the mean ± SD (n=3).

Figure 4.7
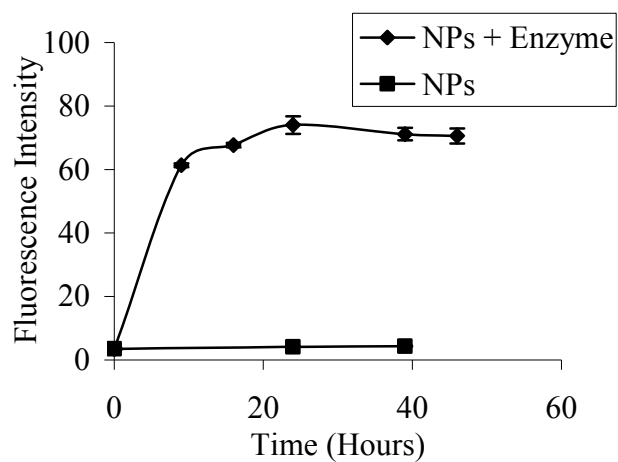
Figure 4.7: **The change in fluorescence intensity when lipid nanoparticles were incubated with horse liver alcohol dehydrogenase and NAD$^+$ at 37°C for 48 h.** Each point is the mean ± SD (n=3).

Figure 4.8
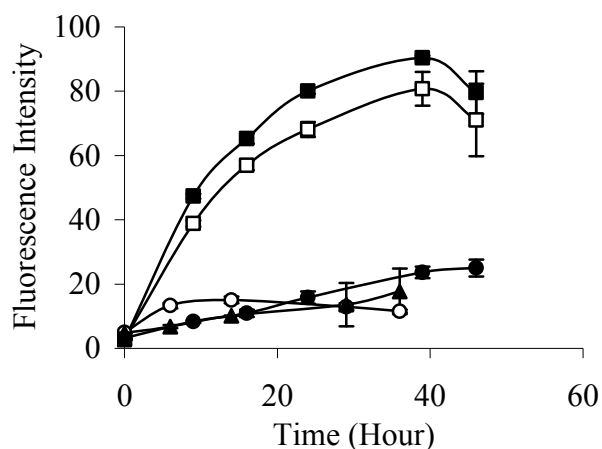
Figure 4.8: The effect of Brij 78 on the enzymatic reaction of cetyl alcohol in lipid nanoparticles with horse liver alcohol dehydrogenase (HLADH) and NAD$^+$ for 48 h. (○) 2 mM Brij 78 + HLADH/NAD$^+$, (▲) HLADH/NAD$^+$, (●) Cetyl alcohol + HLADH/NAD$^+$, (□) 1 mM Brij 78 + cetyl alcohol + HLADH/NAD$^+$, (■) 3 mM Brij 78 + cetyl alcohol + HLADH/NAD$^+$. For all samples, the concentrations of HLADH, NAD$^+$, and cetyl alcohol were 1 mg/ml, 5 mg/ml, and 1 mg/ml, respectively. Each point is the mean ± SD (n=3).

Chapter 5

Development of new lipid-based paclitaxel nanoparticles using sequential simplex optimization

5.1   Summary

The objective of these studies was to develop Cremophor-free lipid-based paclitaxel nanoparticle formulations prepared from warm microemulsion precursors. To identify and optimize new nanoparticles, experimental design was performed combining Taguchi array and sequential simplex optimization. The combination of Taguchi array and sequential simplex optimization efficiently directed the design of paclitaxel nanoparticles. Two optimized paclitaxel nanoparticles were obtained: G78 NPs composed of glyceryl tridodecanoate (GT) and Brij 78, and BTM NPs composed of Miglyol 812, Brij 78 and TPGS. Both nanoparticles successfully entrapped paclitaxel at a final concentration of 150 µg/ml (over 6% drug loading) with particle sizes less than 200 nm and over 85% of entrapment efficiencies. These novel paclitaxel nanoparticles were stable at 4ºC over five months and in PBS at 37ºC over 102 h as measured by physical stability. Release of paclitaxel was slow and sustained without initial burst release. Cytotoxicity studies in MDA-MB-231 cancer cells showed that both nanoparticles have similar anti-cancer activities compared to Taxol. Interestingly, PX BTM nanocapsules could be lyophilized without cryoprotectants. The lyophilized powder comprised only of PX BTM NPs in water could be rapidly rehydrated with complete retention of original physicochemical properties, in-vitro release properties, and cytotoxicity profile. Sequential simplex optimization has been utilized to identify promising new lipid-based paclitaxel nanoparticles having useful attributes.

5.2   Introduction

Paclitaxel is one of the most effective anti-cancer agents used in the treatment of various tumors. It is a taxane which interferes with microtubule depolymerization in tumor cells resulting in an arrest of the cell cycle in mitosis followed by the induction of apoptosis. However, the high lattice energy of paclitaxel results in very limited aqueous solubility (approximately 0.7-30 μg/ml) [18, 19] contributing to only two commercialized dosage forms of injectable paclitaxel, Taxol and Abraxane. Taxol is composed of a 50:50 (v/v) mixture of Cremophor EL (polyethoxylated castor oil) and dehydrated alcohol. Serious side effects, such as hypersensitivity reactions, attributable to Cremophor EL, have been reported [26]. In clinical therapy, high doses of anti-histamines and gluococorticoids are co-administered to manage these adverse effects, but this strategy has raised the possibility of additional pharmacokinetic and pharmacodynamic issues with paclitaxel. To eliminate Cremophor EL from the paclitaxel formulation, many alternative Cremophor EL-free formulations of paclitaxel have been investigated. Abraxane is one of those Cremophor EL-free paclitaxel formulations and was registered with the FDA in 2005. Despite its improved clinical profile, Abraxane is generally not replacing Taxol in cancer chemotherapy, mostly due to its high cost. Therefore, alternative and cost-effective parenteral formulations of paclitaxel are still needed.

Nanoparticles offer an alternative delivery system for cancer therapy that have the potential to control the release rate of drug, improve the drug pharmacokinetics and biodistribution, and reduce drug toxicity. Due to their small size, nanoparticles with entrapped drugs may penetrate tumors due to the discontinuous and leaky nature of the microvasculature of tumors [47, 311]. Also, the characteristically poor lymphatic drainage of tumors may result in slower clearance of nanoparticles that accumulate in tumors. This well-known effect is referred to as the EPR effect [283, 312].

Lipid-based particulate delivery systems, including liposomes, micelles, nanocapsules, and solid lipid nanoparticles, have been developed especially to solubilize poorly water-soluble and lipophilic drugs. These lipid-based systems have the advantage that comprises bio-derived and/or biocompatible lipids that often result in lower toxicity. In general, the lipid-based systems are made from the combination of lipophilic (oil), amphiphilic (surfactant) and hydrophilic (water) excipients. Formulation approaches typically involve a highly interactive process of experimentally investigating many

variables including type and amount of excipients, excipient combinations, and processes (i.e., high-pressure homogenization, microfluidization, extrusion, microemulsion precursors, etc.). Appropriate type and amount of excipients are critical variables, especially in the case of microemulsion precursors to prepare lipid-based systems. Typically, phase diagrams with the blends of different excipients are first developed using the water titration method. Then, combinations of excipients and the drug substance are further optimized for their phase behavior and thermodynamic stability [313, 314]. However, when several surfactants and/or oils are used, construction of phase diagrams becomes quite tedious, expensive, and time consuming.

Experimental design is a statistical technique used to simultaneously analyze the influence of multiple factors on the properties of the system being studied. The purpose of experimental design is to plan and conduct experiments in order to extract the maximum amount of information from the collected data in the smallest number of experimental runs. Factorial design based on response surface method has been applied to design formulations [203, 315]. However, an increase in the number of factors markedly increases the number of experiments to be carried out. The so-called Taguchi approach proposes a special set of orthogonal arrays to standardize fractional factorial designs [208]. By this approach, the size of factorial design is reduced. As shown in Figure 5.1, sequential simplex optimization is a step-wise strategy for optimization that can adjust many factors simultaneously to rapidly achieve optimal response. The optimization is preceded by moving of a geometric figure (the "simplex"). The starting simplex is composed of k + 1 vertex (experiments) wherein k is the number of variables. Then, the experiments are performed one by one. The new simplex is obtained based on the results from the previous simplex and the procedure is repeated until the simplex has rotated and optimum is encircled. The variable-size simplex algorithm is the modified simplex algorithm which allows the simplex to change its size during movement (Figure 5.1). For detailed principles and applications, the reader is referred to the specialized literature [316, 317]. Thus, this process of sequential simplex optimization allows for simultaneous formulation development and optimization.

Our laboratory has already reported on the engineering of stable solid lipid-based nanoparticles from oil-in-water microemulsion precursors. Nanoparticles (E78 NPs) composed of E. wax as the lipid matrix and Brij 78 as the surfactant were reproducibly

prepared with particle sizes less than 150 nm. These E78 NPs were found to have excellent hemocompatibility [218] and were shown to be metabolized in-vitro by HLADH/NAD$^+$ [318]. Paclitaxel E78 NPs were shown to overcome Pgp-mediated tumor resistance in-vitro in a human HCT-15 colon adenocarcinoma cell line [300] and in-vivo in athymic nude mice bearing solid HCT-15 xenograft tumors [319]. However, a shortcoming of the PX E78 NPs used in the above studies was that the entrapment efficiency of paclitaxel in the NPs was only 50% which resulted in relatively rapid in-vitro release (over 80% in 8 h). These shortcomings were directly attributable to the relatively poor solubility of PX in the melted E. Wax.

In light of the above, the objective of these studies was to develop Cremophor-free lipid-based paclitaxel nanoparticle formulations that (1) utilized acceptable oil phases having improved solvation ability for PX, (2) had PX entrapment efficiency >80% with a minimum final concentration of 150 μg/ml with over 5% drug loading, (3) resulted in slow(er) release profiles of PX from NPs, and (4) had comparable in-vitro cytotoxicity to Taxol. To achieve these objectives, two medium-chain triglycerides, glyceryl tridodecanoate and Miglyol 812, were selected as the oil phases to engineer nanoparticles from o/w microemulsion precursors. Triglycerides are biocompatible/biodegradable excipients [320]. It has been reported that paclitaxel has a high partition coefficient (Kp) in medium-chain triglycerides [321]. Glyceryl tridodecanoate is solid at room temperature whereas Miglyol 812 is liquid at room temperature. Thus, it was thought that the uses of glyceryl tridodecanoate and Miglyol 812 as oil phases may result in the formation of solid lipid nanoparticles and nanocapsules, respectively. As discussed above, simplex optimization or the combination of Taguchi array and sequential simplex optimization was used to identify optimized systems based on initial response variables (criteria) of particle size and polydispersity index. Identified leads were then fully characterized for stability, entrapment efficiency, in-vitro release, and cytotoxicity in human MDA-MB-231 breast cancer cells.

5.3   Materials and Methods

Materials and cell culture

Paclitaxel, glyceryl tridodecanoate, PBS, and Tween 80 were purchased from Sigma-Aldrich (St. Louis, MO). Emulsifying wax and stearyl alcohol were purchased from Spectrum Chemicals (Gardena, CA). Brij 78 was obtained from Uniqema (Wilmington, DE). TPGS was purchased from Eastman Chemicals (Kingsport, TN). Miglyol 812 is a mixed caprylic ($C_{8:0}$) and capric ($C_{10:0}$) fatty acid triglyceride and was obtained from Sasol (Witten, Germany). Dialyzers with a molecular weight cutoff (MWCO) of 8000 Da were obtained from Sigma-Aldrich (St. Louis, MO). Microcon Y-100 with MWCO 100 kDa was purchased from Millipore (Bedford, MA). Ethanol USP grade was purchased from Pharmco-AAPER (Brookfield, CT). Taxol[®] was obtained from Mayne Pharma Inc. (Paramus, NJ). The human breast cancer cell line, MDA-MB-231, was obtained from American Type Culture Collection (ATCC) and was maintained in DMEM supplemented with 10% fetal bovine serum (FBS). Cells were cultured at 37ºC in a humidified incubator with 5% CO_2 and maintained in exponential growth phase by periodic subcultivation.

Methods

Preparation of nanoparticles from microemulsion precursors

Nanoparticles were prepared from warm o/w microemulsion precursors as previously described with some modification [322]. Defined amounts of oil phases and surfactants were weighed into glass vials and heated to 65ºC. One (1) ml of filtered and deionized (D.I.) water pre-heated at 65ºC was added into the mixture of melted oils and surfactants. The mixture were stirred for 20 min at 65ºC and then cooled to room temperature. To prepare PX NPs, 150 µg of PX dissolved in ethanol was added directly to the melted oil and surfactant and ethanol was removed by N_2 stream prior to initiating the process described above. Particle size and size distribution of NPs were measured using a N5 Submicron Particle Size Analyzer (Beckman). Ten microliters of nanoparticles were diluted with 1 ml of D.I. water to reach within density range required by the instrument, and particle size analysis was performed at 90º light scattering at 25ºC.

Development of prototype nanoparticles by sequential simplex optimization

(1)   BTM Nanoparticles comprised of Miglyol 812, Brij 78 and TPGS

Miglyol 812 and stearyl alcohol were chosen as oil phases, and Brij 78 and TPGS were selected as the surfactants. Taguchi array L-9 (3^4) was first used to help set up the starting simplex for sequential simplex optimization. Particle size and polydispersity index (P.I.) were used to evaluate the results. Three levels for each excipient and Taguchi array are presented in Table 5.1.A. As directed by the results from Taguchi array, the starting simplex was constructed based on the results of trials 3, 5, and 9 with a slight change for each component in each trial (Table 5.1.B). Sequential simplex optimization then was performed as previously described following the variable-size simplex rules [317]. Desirability functions previously developed for the simultaneous optimization of different response variables (criteria) [323] were used to transform response variables (particle size and P.I.) into a measure d (d_{size} or $d_{P.I.}$) that could be adequately compared and combined with each other. Then, the d of the individual response variable was combined into an aggregated value (D value) by using a weighted geometric average. Definitions of d and D value are presented in the equation (1) and equation (2), respectively:

$$d_i = \begin{cases} 0 & Y_i \leq a \ or \ Y_i \geq b \\ \left[\dfrac{Y_i - a}{b - a}\right]^s & a < Y_i < b \end{cases} \qquad \text{Equation (1)}$$

In Equation (1), i indicates particle size or P.I. The limits were from a = 70 nm to b = 250 nm for particle size, and from a = 0.05 to b = 1.2 for P.I. As the optimization in Table 5.1.B was complex, a larger range of P.I. were chosen in order to avoid too many "worst" trials in the simplex, which could stop the optimization. In addition, the larger range of P.I. also helped to seize all possible compositions in the optimization process. For these optimization experiments, particle size and P.I. were given equal importance; thus, the constant s = 1.

The overall contribution of all responses is presented as a single aggregated D value as calculated by Equation (2):

$$D = (d_{\text{particle size}} \times d_{\text{P.I.}})^{1/2} \qquad \text{Equation (2)}$$

A comparison of each trial in the simplex optimization was based on this aggregated D value which contained information from both particle size and P.I.

After the sequential simplex optimization, Miglyol 812, Brij 78 and TPGS were chosen to form BTM NPs. Four different compositions based on the results from sequential simplex optimization were tested (Table 5.1.C) and were prepared to further optimize BTM NPs.

(2)   G78 nanoparticles comprised of glyceryl tridodecanoate and Brij 78

G78 nanoparticles were optimized using MultiSimplex software (CambridgeSoft Corporation, Cambridge, MA). The variable-size simplex rules were also used in this optimization, and response variables included particle size, P.I. and the peak numbers in nanoparticle distribution. The starting simplex was based on our previously optimized E78 NP composition (2 mg E. wax and 4 mg Brij 78 in 1 ml NP suspension). Thus, the limits for particle size and P.I. were naturally smaller than those for the sequential simplex optimization in Section 2.3.1. The limits were from a = 50 nm to b = 200 nm for particle size, and from a = 0.01 to b = 0.4 for P.I., and from a = 1 to b = 2 for peak numbers. Two milliliters of NP formulations were prepared for each composition.

Lyophilization of PX NPs

To determine the effect of lyophilization on the NPs, blank and PX NPs in the presence or absence of 5% lactose were lyophilized using a VirTis® lyophilizer (SP Industries, Gardiner, NY). Two milliliters of each sample was rapidly frozen at -40ºC and then lyophilized using a program of 7.5 h at -10ºC for primary drying and 7.5 h at 25ºC for secondary drying at 100 mTorr. The resultant lyophilized products were reconstituted in 2 ml of D.I. water using a plate shaker for 5 min. The particle sizes of reconstituted lyophilized NPs from six different batches were measured as described above.

Characterization of paclitaxel G78 and BTM nanoparticles
(1)   Particle size and zeta potential measurement

Nanoparticles were analyzed for particle size and size distribution as described above. Ten microliters of blank NPs and PX NPs were diluted with 1 ml of D.I. water and was added 10 µl of PBS buffer (pH 7.4) for the measurement of zeta potentials using Zetasizer Nano Model ZEN2600 (Malvern Instruments, Worcs, U.K).

(2)   Determination of drug loading and entrapment efficiency

The concentration of PX was quantified by HPLC using a Thermo Finnigan Surveyer HPLC System and an Inertsil ODS-3 column (4.6 × 150 mm) (GL Sciences Inc.) preceded by an Agilent guard column (Zorbax SB-C18, 4.6 × 12.5 mm). The mobile phase was water-acetonitrile (40:60, v/v) at a flow rate of 1.0 ml/min with PX detection at 227 nm. For the paclitaxel standard curve, paclitaxel was dissolved in methanol. To quantify PX in NPs, 1 part of PX NPs in water was dissolved in 8 parts of methanol. PX BTM NPs containing 30% of 7-*epi* PX was dissolved in methanol and then serially diluted in methanol to prepare the standard curve of 7-*epi* PX. Drug loading and entrapment efficiencies were determined by separating free PX from PX-loaded NPs using a Microcon Y-100, and then measuring PX in NP-containing supernatants as described above. To ensure mass balance, the filtrates were also assayed for PX. PX loading and PX entrapment efficiency were calculated as follows:

% drug loading = [(drug entrapped in NPs) / (weight of oil)] × 100% (w/w)

% drug entrapment efficiency = [(drug entrapped in NPs) / (total drug added into NP preparation)] × 100% (w/w)

(3)   Particle size stability of NPs in 4ºC and 37ºC

The physical stability of G78 and BTM nanoparticle suspensions was assessed over storage at 4ºC for five months. Prior to particle size measurement, NP suspensions were allowed to equilibrate to room temperature. The stability of all NP suspensions was also assessed at 37ºC in 10 mM PBS, pH 7.4 by adding 100 µl NP suspensions to 13 ml PBS buffer with a water bath shaker mixing at 150 rpm. At each time interval, 1 ml aliquots were removed and allowed to equilibrate to room temperature prior to particle size measurement.

(4)   DSC analysis of G78 NPs

Differential scanning calorimetry (DSC) analysis was performed to determine the physical state of the core lipid (glyceryl tridodecanoate). Blank G78 or PX G78 nanoparticle suspensions were concentrated about 20-fold using Microcon Y-100 at 4ºC. The concentrated NPs were (1) analyzed by DSC immediately or (2) transferred to an

aluminum pan and that was placed in a desiccator for two days at room temperature prior to DSC analysis. As controls, bulk glyceryl tridodecanoate (5 mg), Brij 78 (5 mg) and the bulk mixture of glyceryl tridodecanoate (3.4 mg) and Brij 78 (8 mg) were placed in aluminum pans for DSC analysis (PerkinElmer, Norwalk, CT). Heating curves were recorded using a scan rate of 1ºC/min from 15ºC to 66ºC.

(5)   In-vitro release studies

PX release studies (n = 4) were completed at 37ºC by the dialysis method using PBS with 0.1% Tween 80 as release medium. Before release studies, the solubility of PX in release medium was measured. Briefly, extra amounts of paclitaxel were added into 2 ml of release medium until saturation was attained. After centrifuge, the concentration of PX in the supernatant was determined by HPLC as described above. For release studies, one milliliter (1 ml) of PX G78 NPs was purified with a Microcon Y-100 and re-suspended into 1 ml D.I. water. The concentration of PX in re-suspended PX G78 NPs was measured by HPLC as described above. Eight hundred microliters of purified PX G78 NPs, PX BTM NPs and reconstituted lyo PX BTM NPs were placed into a regenerated cellulose dialysis membrane (MWCO 8000 Da) submerged in 40 ml PBS with 0.1% Tween 80, respectively, and then shaken in a water bath at a speed of 150 rpm at 37ºC. Free PX was also used as a control. At predetermined times, 200 µl aliquots were taken from outside of the dialysis membrane, and replaced with 200 µl fresh media. PX was measured by HPLC as described above. Mass balance was confirmed by measuring PX concentration inside the dialysis membranes after 72 h. In addition, the particle sizes of PX NPs inside the dialysis membranes were measured when release studies were terminated (at 72 h).

In-vitro cytotoxicity studies

The cytotoxicity of PX NPs was tested in human MDA-MB-231 breast cancer cells using the sulforhodamine B (SRB) assay [324]. Cells were seeded into 96-well plates at 1.5×10^4 cells/well and cells were allowed to attach overnight. Cells were incubated for 48 h with drug equivalent concentrations ranging from 10,000 nM to 0.01 nM for Taxol, PX-loaded NPs and blank NPs. The SRB assay was performed and IC50 values were determined. Briefly, the cell lines were fixed with cold 10% trichloroacetic acid and stained using 0.4% SRB dissolved in 1% acetic acid. The bound dye was solubilized with

10 mM tris base, and the absorbance was measured at 490 nm using a microplate reader. IC50 values were calculated based on the percentage of treatment over control. All groups included three independent experiments (N = 3) with triplicates (n = 3) for each experiment.

Statistical analysis

Statistical comparisons were made with ANOVA followed by pair-wise comparisons using Student's *t*-test using GraphPad Prism software. Results were considered significant at 95% confidence interval ($p < 0.05$).

5.4   Results

Development of BTM nanoparticles by Taguchi array and sequential simplex optimization

It has previously been reported that a combination of liquid and solid lipid oils enhances drug loading and stability in nanoparticles as compared to only a solid lipid core [195, 199]. In the initial development of NPs, a combination of the oil phase of Miglyol 812 (liquid oil) and stearyl alcohol (solid oil) was selected, in addition to two potential surfactants, Brij 78 and TPGS. Thus, based on these four variables (excipients), Taguchi array was carried out to determine the extent of compositions to which the starting simplex could be formed efficiently. Taguchi's orthogonal array for 3 levels 4 variables (L-9 3^4) is shown in Table 5.1.A. As depicted, trials 3, 5 and 9 gave the most promising results. Thus, the compositions of these three trials (3, 5, and 9) were used to construct the starting simplex in the sequential simplex optimization (Table 5.1.B). As described in the method section, there were two basic criteria for current nanoparticle formulation: particle size (<200 nm) and P.I. (< 0.35). D value from desirability functions including particle size and P.I. as response variables was used to evaluate the result of each experiment. Interestingly, the simplex (trial 6 in Table 5.1.B) identified an initial NP formulation that did not contain stearyl alcohol (the solid oil component), but comprised of Miglyol 812, Brij 78 and TPGS. Thus, as directed by simplex, subsequent experiments focused on these three excipients. Four different compositions were used to prepare nanoparticles as shown in Table 5.1.C. Among them, trial 2 resulted in optimized NPs having a mean particle size of 149 nm and P.I. of 0.328. Interestingly, due to the relatively low concentration of the resulting NPs, 150 μg/ml of paclitaxel could not be entrapped into these NPs. However, when each component was increased by a factor of 2.5, the more concentrated NP formulation was able to accommodate the desired concentration of PX without changes in particle size and P.I. This final PX BTM NP formulation consisted of 2.5 mg of Miglyol 812, 1.5 mg of TPGS and 3.5 mg of Brij 78 in 1 ml water with 150 μg/ml of paclitaxel.

Development of G78 nanoparticles by sequential simplex optimization

A solid lipid, glyceryl tridodecanoate, was selected as an alternative to lipid-based NPs. Glyceryl tridodecanoate was selected as a possibly direct replacement of E. Wax in the previously described E78 NPs due to the enhanced solubility of PX in glyceryl

tridodecanoate. Thus, in this simplex optimization, there were two variables, glyceryl tridodecanoate (oil) and Brij 78 (surfactant). The initial simplex was directed by the MultiSimplex software based on the reference values of 2 mg for glyceryl tridodecanoate and 4 mg for Brij 78 in 1 ml water. Simplex optimization then proceeded as shown in Table 5.2. After 8 trials, the optimized composition reached nearly constant values in trials 9-11 of 1.6-1.9 mg for glyceryl tridodecanoate and 4-4.2 mg for Brij 78 in 1 ml NP suspension. Finally, trial 11 was identified as the most optimized composition since the composition gave the smallest particle size and the formulation could easily accommodate 150 μg/ml of paclitaxel.

Lyophilization of BTM and G78 nanoparticles

The lyophilization of blank BTM NPs and PX BTM NPs in water alone resulted in the formation of dry white cakes that were rapidly rehydrated with water within <15 s to produce clear NP suspensions wherein the NPs showed complete retention of original physicochemical properties and in-vitro release properties (Figure 5.2 and Figure 5.6). In contrast, lyophilized blank G78 NPs or PX G78 NPs in the presence or absence of 5% lactose as a cryoprotectant could not be rehydrated in water and produced aggregates/agglomerates after rehydration.

Particle size and zeta potential

All tested nanoparticles had mean particle size diameters less than 200 nm with zeta potentials of about -6 mV regardless of PX entrapment. The entrapment of paclitaxel had no influence on the mean particle size of G78 and BTM nanoparticles (Table 5.3). Interestingly, rehydrated lyophilized NPs had smaller particle sizes for both blank BTM NPs and PX BTM NPs (Figure 5.2).

Drug loading and entrapment efficiencies of paclitaxel in nanoparticles

HPLC analysis showed that the 7-*epi* isomer of PX was present at about 30% when PX was formulated in NPs in water. Further analysis showed that the epimerization occurred during preparation of the PX NPs [325]. However, epimerization at C7 is reversible and can be prevented by forming PX NPs at slightly acidic pH [326]. 7-*epi* isomer of PX did not form when PX BTM NPs were prepared in 10% lactose (pH = 5) or

50 mM sodium acetate buffer (pH = 6). The slope of the standard curve for 7-*epi* PX was not statistically different from that for PX (data not shown). Thus, the standard curve for PX was used to determine the total PX concentration (PX plus 7-*epi* PX).

The entrapment efficiencies for PX G78 NPs and PX BTM NPs were 85% and 97.5% as shown in Table 5.3. The mass balance of PX was 85.4 ± 3.3 % and 97.5 ± 2.6 % (mean ± SD, n = 3) for PX G78 NPs and PX BTM NPs, respectively. The results showed that paclitaxel was incorporated into nanoparticles at weight ratio of over 6% of the selected lipid core. Finally, rehydrated lyophilized PX BTM NPs showed 93.1% of entrapment efficiency, which was not statistically different to that of non-lyophilized PX BTM NPs ($p > 0.05$).

Physical stability of nanoparticles

The physical stability of paclitaxel nanoparticles was evaluated by monitoring changes of particle sizes at 4ºC upon long-term storage as well as short-term stability at 37ºC in PBS to simulate physiological conditions. The particle sizes of G78 and BTM nanoparticles with or without paclitaxel did not significantly change at 4ºC for five months (Figure 5.3). To test stability of nanoparticles in physiological conditions, G78 NPs, BTM NPs and reconstituted lyophilized BTM NPs were incubated in PBS at 37ºC for 102 h. Particle sizes of PX-loaded and blank nanoparticles slightly increased after 72 h incubation. The data for PX-loaded NPs are shown in Figure 5.4 whereas the data for blank NPs are not shown.

Physical state of the core lipid in G78 nanoparticles

It has been reported that glyceryl tridodecanoate (also called "trilaurin") existed as super-cooled melts rather than in a solid state in nanoparticles [327, 328]. Thus, in the present studies, DSC analysis was used to determine the physical state of glyceryl tridodecanoate in G78 nanoparticles. Bulk glyceryl tridodecanoate showed the melting peak at 46ºC while Brij 78 had two melting peaks at 35ºC and 40ºC. The concentrated blank and PX G78 NPs clearly showed an endothermal peak at 43ºC (Figure 5.5.B). After drying of the NPs, two other peaks at 35ºC and 40ºC appeared for blank or PX G78 NPs (Figure 5.5.A). The endothermal peaks of Brij 78 intensified after drying suggesting that more Brij 78 existed in the solid state. The melting peak of glyceryl tridodecanoate in

nanoparticles shifted to lower temperature and broader compared to that of bulk material. However, the endothermic peak at 43ºC for glyceryl tridodecanoate indicated that glyceryl tridodecanoate retained a solid state in G78 nanoparticles.

In-vitro release of paclitaxel from nanoparticles

Paclitaxel has been reported to have aqueous solubility of 0.7-30 µg/ml. Therefore, to maintain sink conditions, PBS with 0.1% Tween 80 was used as the release medium for the in-vitro release studies of paclitaxel. The solubility of paclitaxel in the release medium at room temperature was 10.8 ± 0.3 µg/ml (mean ± SD, n = 3) as measured by HPLC. Thus, for the release studies, 800 µl of PX NPs containing 150 µg/ml of paclitaxel were placed into 40 ml of the release medium. There was no 7-*epi* PX observed during the release study of free paclitaxel. The cumulative release of paclitaxel from PX NPs was calculated based on the total PX (PX plus 7-*epi* PX) released and is shown in Figure 5.6. Free PX was released completely within 4 h. For all tested PX NPs, although the initial release rates were greater between 0 and 8 h, no initial burst of PX was observed. After 8 h, the release rates were much lower. The results showed that the mean cumulative release of PX after 72 h was 40%, 50% and 53% from PX G78 NPs, PX BTM NPs and reconstituted lyophilized PX BTM NPs, respectively. Mass balance analysis for PX G78 NPs, PX BTM NPs and lyophilized PX NPs showed that 79.2 ± 8.6 %, 98.3 ± 24.2 %, and 73.4 ± 16.6 % (mean ± SD, n = 4) of the PX was recovered, respectively. There were no other PX degradation peaks, except for 7-*epi* PX, observed by HPLC during the course of the studies. Moreover, lyophilized PX BTM NPs showed the same release profile as compared to PX BTM NPs ($p > 0.05$ at each time point). Also, the particle sizes of all tested nanoparticles did not change significantly after 72 h.

In-vitro cytotoxicity studies

The cytotoxicity of PX NPs was tested in human breast cancer MDA-MB-231 cells using the SRB assay (Table 5.4). PX NPs showed a clear dose-dependent cytotoxicity in MDA-MB-231 cells. There was no statistical significance in the IC50 values of PX BTM NPs and lyophilized PX BTM NPs compared to commercial Taxol. However, the IC50 of PX G78 NPs had comparable but statistically different IC50 values compared to Taxol. Blank NPs showed some cytotoxicity but only at the paclitaxel equivalent dose of 617.3

nM and 354.6 nM of PX which corresponds to a total NP concentration of 26.4 µg/ml and 15.1 µg/ml for blank G78 NPs and BTM NPs, respectively.

5.5   Discussion

Paclitaxel is an important agent in the treatment of metastatic breast cancer. However, the optimal clinical use of paclitaxel is limited due to its poor aqueous solubility. Commercial paclitaxel formulation, Taxol, is generally associated with hypersensitivity reactions which results from the excipient Cremophor EL in Taxol. To overcome the problems, numerous lipid-based and Cremophor EL-free paclitaxel formulations have been investigated, such as liposomes [329], solid lipid nanoparticles [330, 331], micelles [332, 333], and emulsions [176, 334].

In the present study, two median chain triglycerides, glyceryl tridodecanoate and Miglyol 812, were used to investigate new lipid-based nanoparticles for paclitaxel. Relative to other candidate oil phases, these two oils have high solvation abilities for PX. Glyceryl tridodecanoate has a relatively low melting point of 46ºC, which theoretically facilitates the preparation of lower crystalline cores which may accommodate a greater concentration of drug [195]. Miglyol 812, being a liquid, forms a reservoir-type drug delivery system in which poorly water-soluble drugs remain dissolved inside the liquid oil core and consequently a high payload and reduced release profile may be achieved [184, 335]. As expected, the final optimized nanoparticles, G78 NPs and BTM NPs, successfully entrapped paclitaxel with high loading and entrapment efficiency (Table 5.3). However, the selection of these two alternative oil phases required the development of optimized NP formulations. To facilitate, we used a methodology that combined Taguchi array and sequential simplex optimization. The simplex is made of k + 1 vertex. The response of the experiment in each vertex is ranked and the "worst" response is replaced by the new set of variables for the next experiment. To efficiently move the simplex, there should be limited "worst" responses in the staring simplex. As new excipients were investigated and no prior composition was used as a reference (Table 5.1), Taguchi array was first performed to explore and provide the framework of the starting simplex. The final optimization was then completed using sequential simplex optimization. Trial 6 in Table 5.1.B identified a new nanoparticle formulation composed of the liquid oil Miglyol 812. After further optimization, new BTM nanoparticles were developed. In the case of G78 NPs, it was closely resembled with the E78 NPs (Table 5.2). Thus, sequential simplex optimization was directly used for the investigation of G78 NPs. The results for both PX NPs indicate that this new methodology combining Taguchi array and sequential simplex optimization

could efficiently and effectively be used to identify optimized nanoparticles. Finally, a total of 19 trials and 11 trials were used to obtain optimized BTM NPs and G79 NPs, respectively. In contrast, even for 4 factors and 3 levels design, e.g. optimization in Table 5.1.A and 5.1.B, complete factorial design would require $3^4 = 81$ experiments. To our best knowledge, this is the first report to use the combination of Taguchi array and sequential simplex optimization for the development of nanoparticles.

Choosing appropriate lipids could help increase the entrapment efficiency of drug and slow the release rate of the drug from the nanoparticles. As compared with PX E78 NPs previously developed in our laboratory, the optimal PX BTM and G78 nanoparticles were very reproducible with high drug loading and showed much slower release of PX achieving about 50% and 40% after 72 h, respectively (Figure 5.6). The slow and sustained release of paclitaxel without burst release from PX BTM and PX G78 nanoparticles indicated that paclitaxel was likely not present at or near the surface of nanoparticles but instead within the core of the NPs as ideally predicted by the enhanced solvation abilities of Miglyol 812 and glyceryl tridodecanoate for PX. Moreover, entrapment of paclitaxel into nanoparticles did not change the sizes of nanoparticles. All PX NPs had particle sizes less than 200 nm, even after 102 h of incubation in PBS at 37ºC. These data indicate potential stability of PX NPs in-vivo after intravenous injection (Figure 5.4). Cytotoxicity studies showed that both PX G78 and BTM nanoparticles had the same or comparable anti-cancer activity compared to commercial Taxol in human MDA-MB-231 breast cancer cells. Therefore, both of these identified PX NP formulations may be good candidates for ligand-mediated tumor-targeting delivery of PX.

Several studies have reported that glyceryl tridodecanoate retained in lipid-based NPs in a super-cooled liquid state. If true, this semi-stable state of glyceryl tridodecanoate will likely affect the stability of nanoparticles due to the predicted phase transition of the super-cooled core to the crystalline phase. However, the present studies showed using DSC analysis that glyceryl tridodecanoate remained as a solid state in G78 NPs (Figure 5.5), suggesting that the phenomenon of super-cooled glyceryl tridodecanoate in nanoparticles may be dependent on the process and compositions (i.e., surfactant) used to prepare the nanoparticles. Blank and PX G78 nanoparticles stored as liquid suspensions at 4ºC remained stable for several months and exhibited no change in particle sizes. There was some concern that G78 nanoparticles, made with the lower melting GT, may be adversely

affected by body temperature. However, either blank or PX G78 nanoparticles showed no change in particle sizes after 102 h of incubation in PBS at 37ºC.

It is thought that BTM NPs may be a novel liquid reservoir, or nanocapsule-type formulation. The liquid reservoir containing paclitaxel dissolved in Miglyol 812 is stabilized with the polymeric surfactants Brij 78 and TPGS. Higher drug loading of PX BTM nanoparticles indicates the advantage of this nanocapsule-type formulation as compared to the solid-core type G78 NP system. The BTM NPs were spontaneously formed after cooling from the warm o/w microemulsion precursors. It is thought that the BTM NPs are nanocapsules and not nanoemulsions since nanoemulsions are non-equilibrium and thermodynamically unstable systems that cannot, by definition, form spontaneously without agitation or significant mechanical/shear mixing [336]. Another very interesting discovery was serendipitously made during the course of the present studies. In one attempt to concentrate NP formulations to analyze for entrapped PX, NPs were lyophilized in water. The BTM NP formulations produced uniform white cakes that could be rapidly rehydrated with complete retention of original physicochemical properties, in-vitro release properties, and cytotoxicity profile. Our experience, as well as others, is that it is often difficult to freeze-dry colloidal suspensions in the presence of cryoprotectants. To our knowledge, there are few or no reports on the successful lyophilization of colloidal suspensions without the use of a cryoprotectant which protects the nanoparticles from the stresses of the freezing and thawing process. Moreover, the lyophilization of nanoemulsions or nanocapsules is thought to be even more challenging due to the existence of the very thin and fragile envelope that may not withstand the mechanical stress of freezing [187, 188]. Even in the presence of cryoprotectants, an increase of particle size is likely to occur [185]. In the present studies, the optimal BTM nanoparticles were successfully lyophilized without cryoprotectants. The non-collapsed uniform cakes of PX BTM NPs in water alone were rehydrated and spontaneously produced particle sizes that were, in fact, slightly smaller than the original particle sizes. In addition, there was a complete retention of the in-vitro release properties and cytotoxicity profile.

In conclusion, the combination of Taguchi array and sequential simplex optimization efficiently guided the development and optimization of lipid-based nanoparticulate formulations for paclitaxel. Injectable paclitaxel nanoparticles, PX G78

93

NPs and PX BTM NPs, were successfully prepared via a warm o/w microemulsion precursor engineering method. Both paclitaxel nanoparticle suspensions were physically stable at 4ºC over five months, and PX BTM could be lyophilized without cryoprotectants. PX G78 and BTM nanoparticles showed comparable or same anti-cancer activity compared to Taxol in MDA-MB-231 breast cancer cells. Therefore, these paclitaxel-loaded nanoparticles may be candidates for ligand-mediated tumor-targeting delivery of paclitaxel after intravenous injection.

Table 5.1.A. Taguchi array for the development of BTM nanoparticles. Listed are the compositions per 1 ml nanoparticle suspension.

Trial	Brij 78 (mg)	TPGS (mg)	Stearyl alcohol (mg)	Miglyol 812 (mg)	Particle size (nm)	P.I.
1	1.6	1.2	0.6	1.4	35	1.21
2	1.6	0.9	0.4	1.0	193.5	0.978
3	**1.6**	**0.6**	**0.2**	**0.6**	**118.4**	**0.159**
4	1.2	1.2	0.4	0.6	25	1.435
5	**1.2**	**0.9**	**0.2**	**1.4**	**212.9**	**0.307**
6	1.2	0.6	0.6	1.0	282.6	0.897
7	0.7	1.2	0.2	1.0	130.5	0.826
8	0.7	0.9	0.6	0.6	315	1.685
9	**0.7**	**0.6**	**0.4**	**1.4**	**234.6**	**0.355**

Bold font indicates promising lead formulations

Table 5.1.B. Sequential simplex optimization for the development of BTM nanoparticles. Listed are the compositions per 1 ml nanoparticle suspension.

Trial	movement	Brij 78 (mg)	TPGS (mg)	Stearyl alcohol (mg)	Miglyol 812 (mg)	Particle size (nm)	P.I.	d_{size}	$d_{P.I.}$	D
1	\	1.6	0.6	0.4	0.6	35.6	0.070	0	0.017	0
2	\	1.2	0.9	0.4	1.4	197.6	0.449	0.709	0.347	0.496
3	\	0.7	0.6	0.8	1.4	186.3	0.360	0.646	0.270	0.417
4	\	1.6	0.9	1.6	1.2	309.2	1.079	0	0.895	0
5	\	0.7	2.1	1.6	1.2	182.7	1.028	0.626	0.85	0.730
6	**R (1, 2, 3, 5)**	**0.5**	**1.2**	**0**	**1.1**	**192.4**	**0.230**	**0.680**	**0.157**	**0.326**

Bold font indicates promising lead formulations

95

Table 5.1.C. Development of BTM nanoparticles. Listed are the compositions per 1 ml nanoparticle suspension.

Trial	Brij 78 (mg)	TPGS (mg)	Miglyol 812(mg)	Particle size (nm)	P.I.
1	0.5	1.2	1.1	192.4	0.23
2	**1.4**	**0.6**	**1**	**149**	**0.328**
3	0.9	0.6	1.4	190	0.103
4	1.2	1.5	1.2	309.2	1.079

Bold font indicates promising lead formulations

Table 5.2. Simplex optimization for the development of G78 nanoparticles. Listed are the compositions per 1 ml nanoparticle suspension

Trial	Brij 78 (mg)	Glyceryl tridodecanoate (mg)	Particle size (nm)	P.I.	Peak # [a]	Current membership [b]
1	3.5	1.5	157.2	0.3	2	0
2	4.5	1.8	153.5	0.36	1	4.77E-02
3	3.8	2.5	194.6	0.275	1	1.73E-02
4	4.8	2.8	195.3	0.25	2	0
5*	3.8	1.8	161.9	0.258	1	0.138
6	4.5	1.1	-- [c]	--	--	--
7	4.0	2.1	199	0.282	1	3.03E-03
8	3.3	2.2	--	--	--	--
9*	4.2	1.9	161.3	0.274	1	0.125
10	4.0	1.6	156.4	0.325	1	8.38E-02
11*	**4.0**	**1.7**	**143.6**	**0.369**	**1**	**4.48E-02**

[a] The peak numbers in nanoparticle distribution

[b] Current membership has the same meaning and definition with D value in desirability functions.

[c] Impossible to form nanoparticles based on this composition

* indicates the composition of the final simplex

  Bold font indicates promising lead formulations

Table 5.3. Physiochemical properties of

PX G78, PX BTM, and lyo PX BTM nanoparticles (n=3)

Formulations	Theoretical loading (µg/ml)	Mean[a] diameter (nm)	P.I.	Zeta potential (mV)	% Drug loading (w/w, drug/oil)	% Drug entrapment efficiency
PX G78 NPs	150	169.2 ± 8.1	0.302 ± 0.027	-6.6 ± 2.6	7.5	85.4 ± 3.3
PX BTM NPs	150	190.5 ± 7.8	0.279 ± 0.054	-5.9 ± 1.78	6	97.5 ± 2.6[#]
Lyo PX BTM NPs	150	130.0 ± 7.8	0.284 ± 0.042	-5.1 ± 1.00	6	93.1 ± 4.1[#]

[a] The data are presented as the mean of the mean particle size of nanoparticles in different batches ± SD (n = 3).

$p > 0.05$

Table 5.4. IC50 values of paclitaxel nanoparticles in MDA-MB-231 cells at 48 h

Formulations	Taxol[®]	G78 NPs		BTM NPs #1		BTM NPs #2 [a]		Lyo BTM NPs #2 [a]	
		PX NPs[*]	BL NPs	PXNPs[#]	BL NPs[##]	PX NPs[#]	BL NPs[##]	PX NPs[#]	BL NPs[##]
IC50 (nM)	7.2 ± 2.9	21.0 ± 1.5	617.3 ± 356	7.6 ± 1.2	354.6 ± 59.0	15.1 ± 6.8	342.7 ± 119.6	15.6 ± 10.6	256.1 ± 128.6

Data are presented as the mean ± SD of three independent experiments (N=3) with triplicate (n=3) measurements for each sample/concentration tested.

[a] Lyo BTM NPs #2 were directly lyophilized from BTM NPs #2. Lyophilized powder was stored at 4°C for overnight prior to completing the cytotoxicity studies.

$p > 0.05$ compared to IC50 of Taxol[®]

$p > 0.05$ within the group

* $p < 0.05$ compared to IC50 of Taxol[®]

Figure 5.1
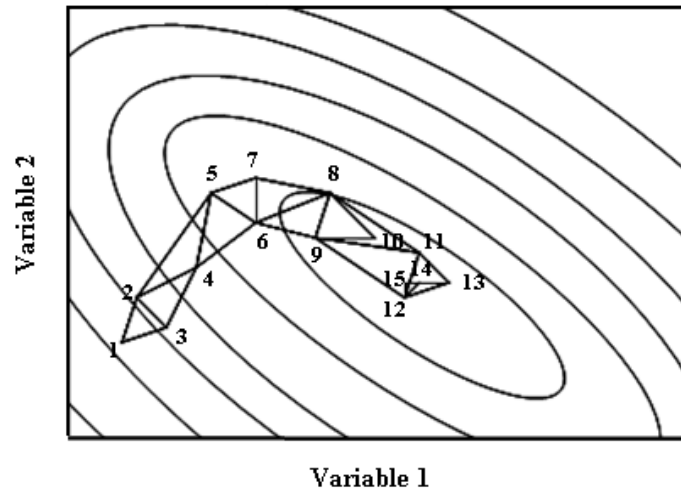
Figure 5.1: **The principles of sequential simplex optimization for two variables using variable-size simplex rules on the response surface** [317]. The starting simplex consists of vertexes 1, 2 and 3 where 1 gives the worst response. The second simplex consists of vertexes 2, 3, and 4 after a reflection and expansion. Finally, the movement of the simplex results in the simplex 12, 14, and 15 which indicates the optimum.

Figure 5.2
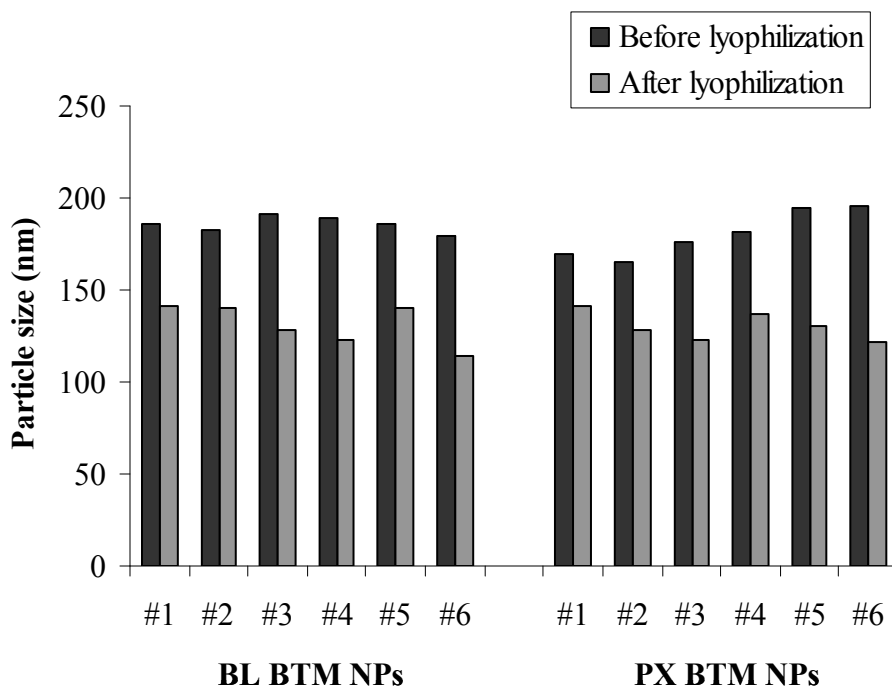
Figure 5.2: Particle size of BTM nanoparticles before and after lyophilization (and rehydration). Six different batches were tested for both blank BTM nanoparticles and PX-loaded BTM nanoparticles. For all tested NP formulations, P.I. values ranged from 0.03 to 0.35 indicating uniform, mono-dispersed NPs. Data are presented as the mean particle size of three separate measurements of each batch.

Figure 5.3
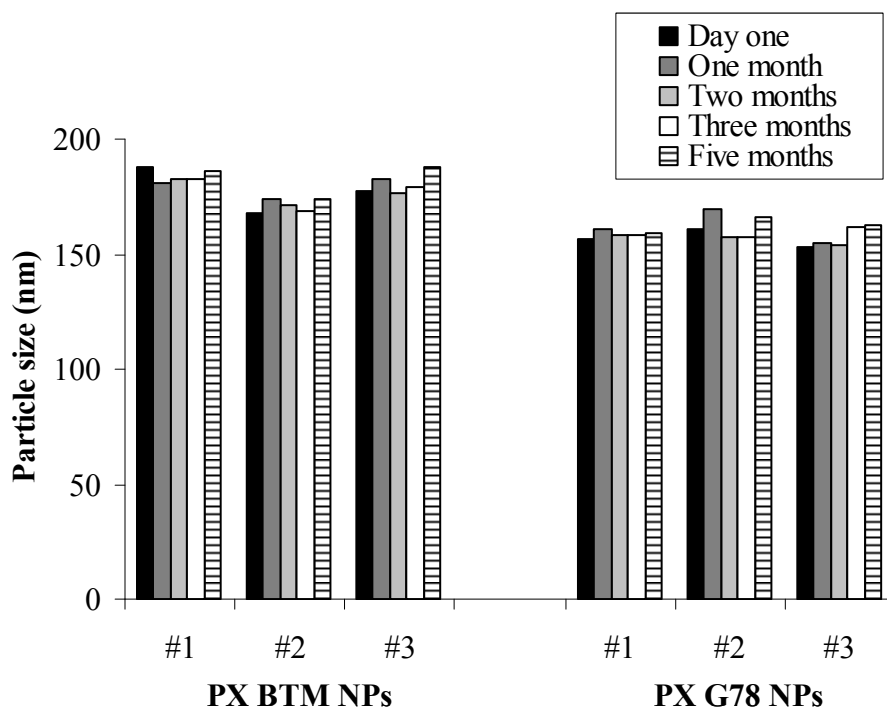
Figure 5.3: Long-term stability of paclitaxel nanoparticles stored at 4°C. Three different batches of PX-loaded BTM and G78 nanoparticles were monitored for particle sizes over five months. For all tested samples, P.I. <0.35. Data are presented as the mean particle size of three separate measurements of each batch.

Figure 5.4
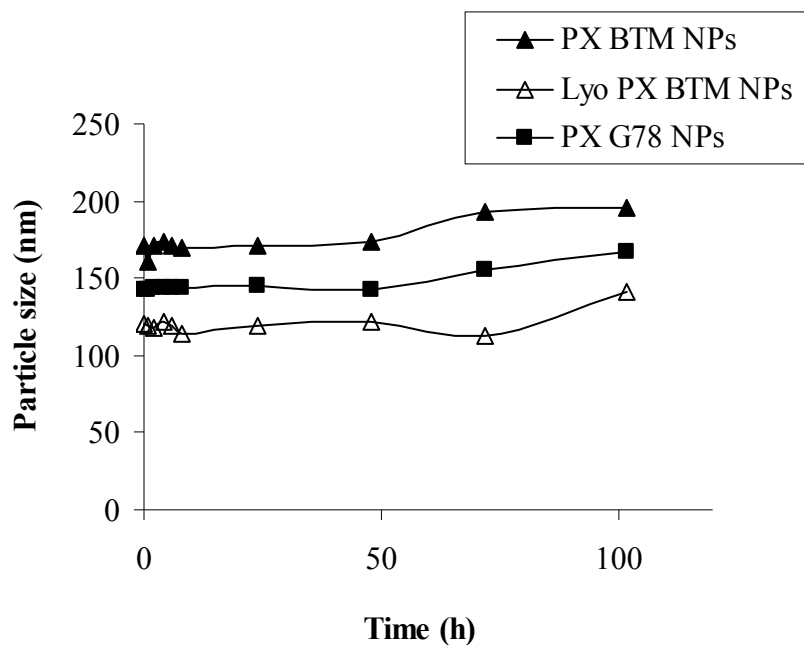
Figure 5.4: **Stability of paclitaxel nanoparticles in PBS at 37ºC.** PX BTM nanoparticles, reconstituted lyophilized PX BTM nanoparticles and PX G78 nanoparticles were monitored for particle sizes for 102 h. For all tested samples, P.I. <0.35. Data are presented as the mean particle size of three separate measurement of each batch.

Figure 5.5

A

Bulk GT

Bulk Brij 78

Mixture of bulk Brij 78 and GT

Blank G78 NPs (dry)

PX G78 NPs (dry)

20 25 30 35 40 45 50 55 60 65

B

Bulk GT

Bulk Brij 78

Mixture of bulk Brij 78 and GT

Blank G78 NPs (wet)

PX G78 NPs (wet)

20 25 30 35 40 45 50 55 60 65

Temperature (°C)
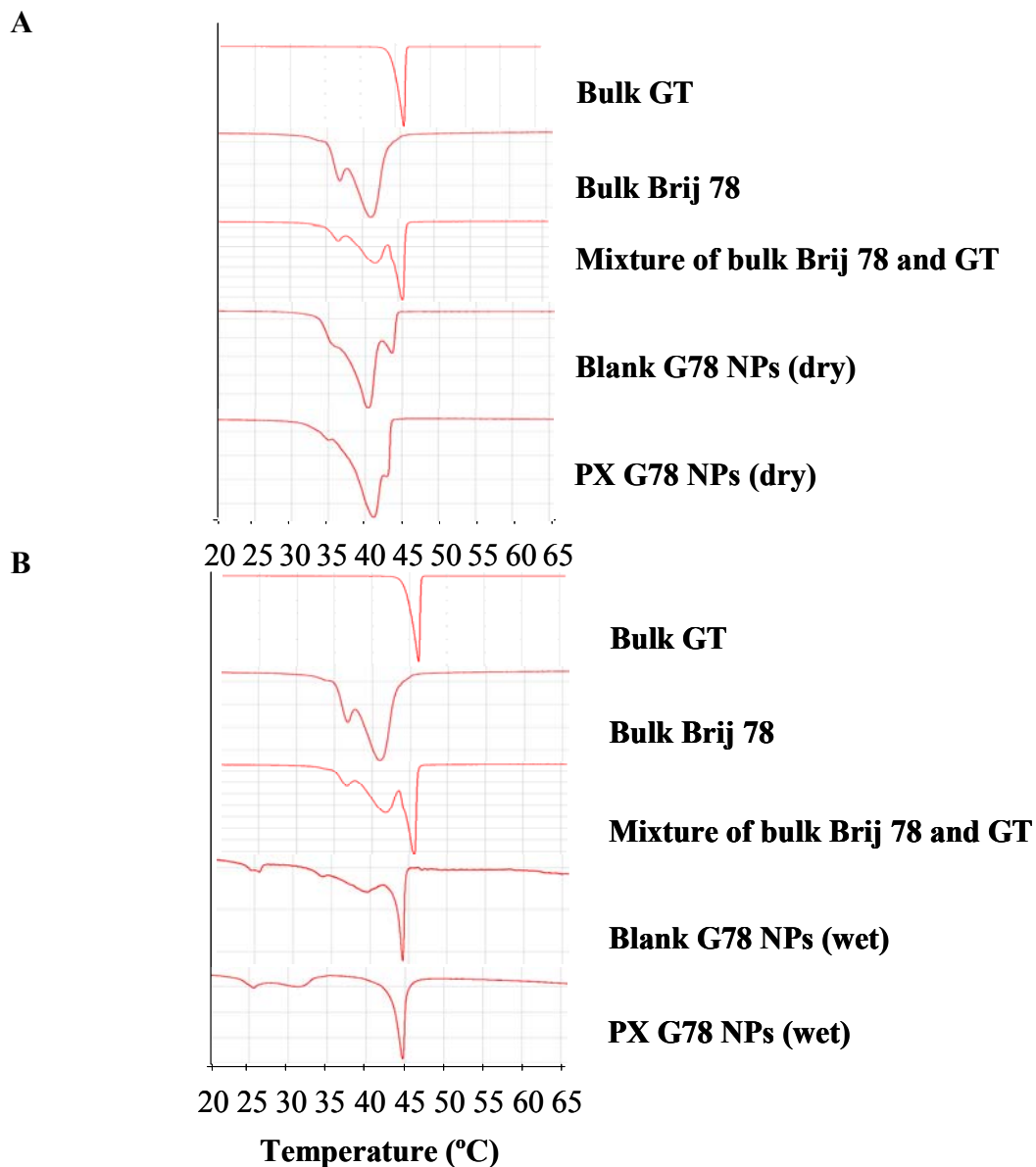
Figure 5.5: DSC for G78 nanoparticles. (A) The concentrated nanoparticles were dried by desiccations for two days prior to DSC analysis ("dry"). (B) DSC analysis of nanoparticles was performed immediately after concentrating nanoparticles ("wet"). GT means glyceryl tridodecanoate.

Figure 5.6
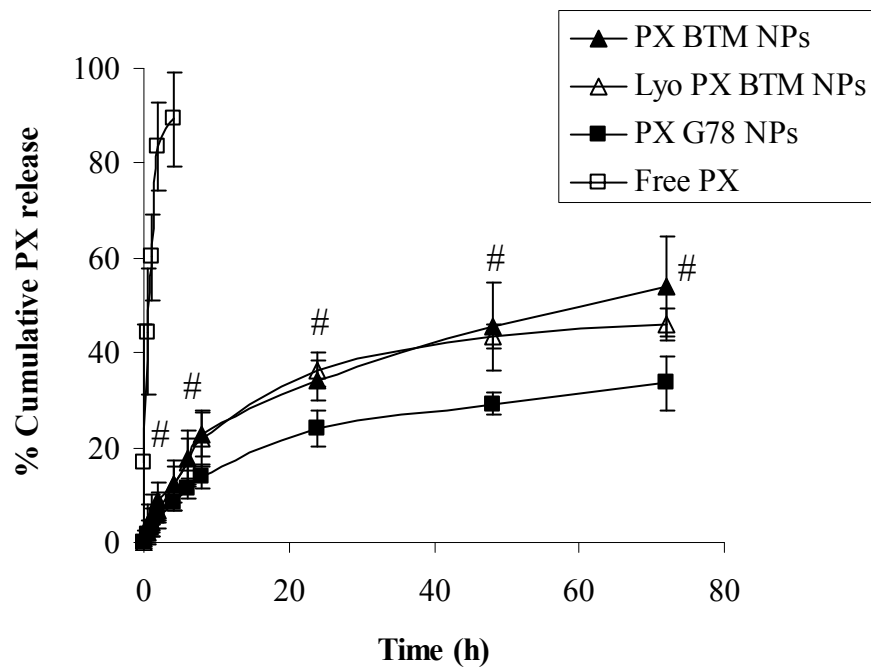
Figure 5.6:   Release of PX from PX nanoparticles at 37ºC. Paclitaxel release was measured using the dialysis method in PBS (pH 7.4) with 0.1% Tween 80 as described in the Method section. Data are presented as the mean ± SD (n = 4). # $p > 0.05$ as compared between PX BTM NPs and lyo PX BTM NPs.

Chapter 6

Development of new solid lipid doxorubicin nanoparticles to treat P-gp-mediated resistance in-vitro

6.1   Summary

Doxorubicin has a wide range of anti-cancer activity. Also, it is a P-gp substrate. The purpose of these studies was to develop and characterize a doxorubicin-loaded solid lipid nanoparticle delivery system to treat P-gp-mediated drug resistance in-vitro. Solid lipid nanoparticles were prepared from microemulsion precursors. An ion-pair strategy was used to enhance the loading of doxorubicin into nanoparticles. Different potential ion-pair agents were investigated. STS was found to be the best choice for the ion-pair agent. Further, drug release and drug entrapment efficiency of Dox NPs were measured. To optimize the composition of nanoparticles to get a slow release profile, various compositions of nanoparticles were investigated using STS as the ion-pair agent. Doxorubicin was released from solid lipid nanoparticles about 65% at 8 h in PBS at 37ºC. Dox-loaded solid lipid nanoparticles containing different compositions of oils and surfactants provided several promising formulations to test for efficacy in P-gp-overexpressed resistant cancer cells.

6.2   Introduction

Current tumor chemotherapy faces several challenges which include the lack of tumor selectivity, and intrinsic or acquired drug resistance, such as overexpression of a membrane transporter P-gp on the surface of cancer cells. To improve the therapeutic efficacy and minimize the side effects, various drug delivery and targeted systems have been investigated, such as polymer conjugates, liposomes, micelles, and lipid nanoparticles [238, 251, 253, 257, 263, 268]. Nano-sized delivery systems could passively accumulate drugs in solid tumors by taking advantage of the EPR effect. Moreover, some of the delivery systems showed the ability to overcome MDR. Therefore, the combination of using EPF effect and overcoming MDR by drug delivery systems could provide a new strategy to solve the challenges of tumor chemotherapy.

Doxorubicin is a P-gp substrate with a broad-spectrum anti-cancer activity. Although it continues to be used extensively in the treatment of different cancers, its clinical value is limited due to its acute myelotoxicity, development of cardiomyopathy and development of drug resistance. Two commercial formulations of doxorubicin are Dox Hydrochloride for Injection and liposomal Dox, Doxil®. Dox has two pK_as, 7.8 and 10.7. Its free base at high pH (>10) is water-insoluble. However, at neutral pH, its salt form is water-soluble with a positive charge. Dox Hydrochloride for Injection was formulated by directly dissolving Dox·HCl salt into water. This formulation is not beneficial for targeting tumors. Thus, the selectivity of the formulation is low. The cationic charges of these salts may pose an obstacle for efficient drug incorporation into lipid particles or liposomes. To entrap Dox into liposomes, current liposomal Dox formulation uses a pH-gradient strategy. The pH outside of the liposomes is increased to allow formation of free Dox base. Due to water-insolubility of free Dox base, it could pass the hydrophobic bilayer of the liposomes. After getting into the core liposomes (hydrophilic and neutral pH), Dox returns to its salt form with a positive charge which can not pass through the hydrophobic bilayer of the liposomes, resulting in the incorporation of Dox into liposomes. Liposomal Dox formulations have been reported to significantly reduce cardiotoxicity in a phase III study as compared to free doxorubicin [39]. However, none of these commercial Dox formulations claims to overcome MDR. An ion-pair strategy has been used to entrap Dox into solid lipid nanoparticles [337]. Based on this strategy, counterions (ion-pair agents) with negative charges were used to form the ion-pair complex with Dox·HCl. Formed ion-

pair complex could shield the positive charge of Dox and increase lipophilicity of Dox, leading to entrapping Dox into solid lipid nanoparticles.

In this study, different ion-pair agents for Dox were screened in an attempt to form a stable ion-pair complex. We expected that the formation of stable ion-pair complex could enhance Dox loading and reduce the release of Dox from Dox-loaded nanoparticles. In following studies, Dox-loaded NPs were then tested to overcome P-gp-mediated drug resistance in-vitro.

6.3   Materials and Methods

Materials

Doxorubicin hydrochloride, taurocholic acid sodium salt hydrate, (±)-α-Tocopherol phosphate disodium salt, sodium taurodeoxycholate (STDC), sodium lauryl sulfate (SDS), Niaproof 4 (7-Ethyl-2-methyl-4-undecyl sulfate sodium salt), and sodium tetradecyl sulfate (STS) were purchased from Sigma-Aldrich (St. Louis, MO). Cellulose sulfate 3500,000, Poly(vinylsulfonic acid) sodium salt, E. Wax and stearyl alcohol were purchased from Spectrum Chemicals (Gardena, CA). Brij 78 was obtained from Uniqema (Wilmington, DE). TPGS was purchased from Eastman Chemicals (Kingsport, TN). Dextran sulfate sodium salt 2500 was purchased from ABCR GmbH & Co. KG (Karlsruhe, Germany). Dextran sulfate sodium salt 5000, Dextran sulfate sodium salt 8000, and Dextran sulfate sodium salt 100,000 were purchased from Sigma-Aldrich (St. Louis, MO).

Methods

Preparation of doxorubicin-ion-pair complex

A titration method was used to select the suitable ion-pair agent with a negative charge to form stable Dox-loaded solid lipid nanoparticles. Doxorubicin hydrochloride was dissolved into D.I. water to make a Dox stock solution at the concentration of 1 mg/ml. Fifty microliters of Dox stock were titrated with various ion-pair agents which were dissolved in water, respectively, until red precipitates (ppts) appeared indicating the formation of Dox-ion-pair complex. The water was removed after centrifugation. One ml of PBS pH 7.4 was added to the red ppts and kept for 4 h at room temperature to test if ppts could dissolve in PBS.

Preparation of doxorubicin-loaded solid lipid nanoparticles

Nanoparticles were prepared from warm o/w microemulsion precursors as previously described with some modification. Doxorubicin was first precipitated with the ion-pair agent in water to form the ion-pair complex. Then, the ion-pair complex was dried with N_2 stream and dissolved into ethanol. Defined amounts of oil phases and surfactants were weighed into glass vials and melted at 65ºC. The Dox ion-pair complex/ethanol

solution was added into melted excipients and ethanol was removed using a N_2 stream. One ml of D.I. water pre-heated at 65ºC was added into the mixture and stirred for 20 min at 65ºC. The mixture was then cooled to room temperature. The particle size of NPs was measured by photon correlation spectroscopy (PCS) using a Coulter N4 Plus Submicron Particle Sizer (Coulter) with scattering light at 90° at 25°C for 1 min. Zeta potentials were measured using the Zetasizer Nano ZEN2600 (Malvern Instruments, Worcs, U.K).

Particle size stability of nanoparticles at 4ºC and 37ºC

The physical stability of Dox-loaded NP suspension was tested over one month at 4ºC by monitoring particle size of NPs. The size stability of NPs also was tested in PBS pH 7.4 for 6 h at 37ºC. Four hundred microliters of Dox NPs were put into 10 ml PBS pH 7.4 and incubated at 37ºC. At each time point, 1 ml of the NP suspension was taken out to measure particle size. Prior to particle size measurement, NP suspensions were allowed to equilibrate to room temperature.

Quantitative measurement of Dox by Microplate reader and HPLC assay

Quantitative assay methods were performed to measure concentration of doxorubicin. Doxorubicin standard solutions were prepared in water for injection and could be stored at -80ºC over six months without any changes on chemical properties. A Dox standard curve was developed using the Bio-Tek Synergy 2 Microplate Reader either at 487 nm or at fluorescence mode with 480 nm excitation and 550 nm emission. In addition, the concentration of Dox was quantified by HPLC using a Thermo Finnigan Surveyer HPLC System and an Inertsil ODS-3 column (4.6 × 150 mm) (GL Sciences Inc.) preceded by an Agilent guard column (Zorbax SB-C18, 4.6 × 12.5 mm). Separation was carried using a mobile phase consisting of 0.1 M ammonium formate containing 0.14 % triethylamine (adjusted pH to 2.4 by addition of formic acid)-acetonitrile-methanol-tetrahydrofuran (60:25:17.5:2.5, v/v/v/v) at a flow rate of 1.0 ml/min. Dox was measured either with a fluorescence detector with an excitation wavelength of 480 nm and an emission wavelength of 550 nm, or a PDA detector at 487 nm. To measure Dox entrapped into NPs, 50 ul of Dox-loaded NPs were mixed with 150 ul of methanol prior to HPLC injection. The assay methods were compared using Dox-loaded NPs.

Determination of Dox loading and entrapment efficiency

Dox loading and entrapment efficiencies were determined by separating free Dox from Dox-loaded NPs using a Microcon Y-100 (MWCO 100 kDa, Millipore) at 4ºC, and then measuring Dox in supernatants and filtrates. Concentrations of Dox were measured using a microplate reader at 487 nm. The mass balance was then calculated. Drug loading and drug entrapment efficiencies were calculated as follows:

% drug loading = [(drug entrapped in nanoparticles) / (weight of oil)] × 100% (w/w)

% drug entrapment efficiency = [(drug entrapped in nanoparticles) / (total drug added into nanoparticle preparation)] × 100% (w/w)

In-vitro release studies of Dox-loaded NPs

Dox release studies from different Dox-loaded NPs (n=3 for each) were completed at 37ºC using the dialysis method. Two hundred microliters of Dox NPs were placed into a cellulose ester dialysis membrane (MWCO 100 kDa, Spectrum Lab) submerged in 6 ml PBS at pH 7.4 for 24 h. The release medium was then shaken in a water bath at a speed of 150 rpm at 37ºC. At defined times, two hundred microliter aliquots were taken from outside the dialysis membrane, and fresh media were replaced. Dox was measured using the microplate reader in the fluorescence detection mode (480 nm excitation and 550 nm emission). Free Dox and Dox ion-pair complex (ppts) were used as controls.

6.4   Results

Selection of the ion-pair agent for doxorubicin complex

NPs #2, composed of 2 mg/ml of E. wax, 2 mg/ml of Brij 78 and 2.6 mg/ml of TPGS in 1 ml of D.I. water, were used as the prototype of NPs to screen the suitable ion-pair agent for Dox. The twelve tested ion-pair agents are listed on Table 6.1. The final optimized ion-pair agent for Dox was STS which quantitatively precipitated Dox at a mole ratio of 1:1.2 (Dox: STS) (Figure 6.1). Dox-STS complex had low solubility in PBS and also formed good NPs with the mean diameters less than 120 nm. The highest loading of Dox was 600 µg/ml by using STS as the ion-pair agent. Therefore, the rest of the studies in this section was focused on STS as the ion-pair agent for Dox.

Quantitative measurement of Dox by a microplate reader and HPLC assays

Various quantitative assays were developed for doxorubicin, including a microplate reader assay and a HPLC assay with either UV-Vis or fluorescence detection (Table 6.2). Dox recovery in Dox NPs using the HPLC assay was 102.8%. To compare the measurement from the HPLC assay and microplate reader assay, the concentrations of Dox in Dox-loaded NPs were measured by both methods at 486 nm. The results did not show a significant difference: 124 µg/ml of Dox by the microplate reader assay versus 111 µg/ml of Dox by the HPLC assay. Thus, in the latter studies, the microplate reader assay was chosen as the major assay method for measuring either Dox concentration in Dox-loaded NPs or free Dox concentration.

Optimization of compositions of NPs for Dox-STS-loaded NPs

To find the optimized NP formulation, two new Dox NPs, Dox NPs #3 composed of 2 mg/ml of E. wax and 4 mg/ml of Brij 78 and Dox NPs #4 composed of 2 mg/ml of stearyl alcohol and 4 mg/ml of Brij 78, were prepared using the Dox-STS complex. These Dox-loaded NPs were characterized in the rest studies and compared to identify the best NP formulation.

Particle size stability of nanoparticles

The physical stability of Dox-loaded NP suspension was monitored by measuring particle size of NPs over one month at 4ºC for the storage condition. All Dox-loaded NPs

increased their size over 45% from their initial starting point (Figure 6.2). However, particle size of Dox-loaded NPs did not change within 6 h at 37ºC in PBS, which simulated physiological conditions (Figure 6.3).

Dox loading and entrapment efficiency

The Dox loading and entrapment efficiencies in three Dox-loaded NPs are shown in Table 6.3. The entrapment efficiencies of all Dox-loaded NPs were higher than 80%. The mass balance gave about 100% of Dox recovery. This indicated that the method for measuring entrapment efficiencies of Dox was reliable, and that STS was a good ion-pair agent. The formed Dox-STS ion-pair complex had very good solubility with oils and surfactants in NPs.

In-vitro release studies of Dox-loaded NPs

The cumulative release of Dox from Dox-loaded NPs is shown in Figure 6.4. Over 90% of free Dox were released from dialysis tubes within 4 h. This suggested that the dialysis method was suitable to make a sink condition and measure Dox release from Dox-loaded NPs. At 8 h, about 70% of Dox were released from Dox-loaded NPs. This rapid release was observed in all Dox NPs with different compositions. A burst release was observed in all Dox NPs, with about 15% of Dox being released at the first 0-5 min. After the initial release, 50% of Dox was released in next 8 h and the rest of Dox (35% of Dox) was slowly released up to 24 h.

6.5   Discussion

Dox is a positively-charged drug and the hydrochloride salt has appreciable aqueous solubility. Thus, an ion-pairing strategy was utilized to neutralize the charge on Dox and increase its affinity for the melted oil phase. Various ion-pair agents were tested (Table 6.1). There are at least three criteria for the suitable ion-pair agent: 1) the most ideal agent should be able to quantitatively precipitate Dox from water, 2) the formed ion-pair complex should not be soluble in PBS, and 3) the formed ion-pair complex could be used to form stable NPs utilizing the method described herein. However, most of the ion-pairing complex of Dox either rapidly dissolved in PBS and/or were not soluble in the melted oil phases used to prepare the solid lipid nanoparticles. For example, STDC formed ion-pair complex with Dox quantitatively, and also gave good Dox-loaded NPs with a high drug loading efficiency. However, Dox-STDC complex is soluble in PBS, resulting in a very rapid release profile of Dox from Dox-STDC-loaded NPs. About 85% of Dox were released from Dox-STDC NPs within 15 min. The final optimized ion-pair agent for Dox was STS. All Dox NPs made from STS in the present work were reproducibly produced with mean diameters of particle sizes less than 120 nm, and had high drug loading and entrapment efficiency (Table 6.2). In addition, all NPs were stable over one month at 4°C, though particle size increased (Figure 6.2). By forming ion-pair complex, water-soluble and positive-charged Dox was successfully entrapped into solid lipid NPs. Ion-pair strategy may be a potential approach to entrap other ionic anti-cancer drugs into solid lipid nanoparticles.

The series of quantitative assays were developed for doxorubicin (Table 6.2). The assay method was chosen based on the concentration of samples in the experiment. The HPLC assay using a fluorescence detector could measure the concentration of Dox as low as 0.0023 µg/ml. Therefore, this method could be used as the assay method for future Dox uptake studies in cells or in-vivo biodistribution study. In the HPLC assay, Dox-loaded NPs were pre-destroyed by methanol to release free Dox. However, in the microplate assay, Dox-loaded NPs were directly measured at the microplate reader. The results from these two different assay methods did not show a significant difference. This also indicated that entrapping Dox into NPs did not influence the absorbance of Dox.

The release profile of Dox from Dox-loaded NPs consisted of a rapid release phase within 0-8 h and a slower release phase after 8 h (Figure 6.4). This indicated that some

Dox may locate near the surface of nanoparticles and readily diffuse out into the release medium. The reason for the rapid release may be related to the components in NPs which competed with Dox to bind with STS, so that the ion-pair complex partially dissociated during the process to make Dox-STS NPs. Thus, another two NPs with different compositions were studied. All Dox NPs gave high entrapment efficiency (Table 6.3). However, they showed similar release profiles. Moreover, Dox release from Dox-loaded NPs was similar with Dox release from Dox-STS complex (Figure 6.4). Actually, the current Dox release profiles are comparable with those reported in literature [337]. The unchanged particles sizes in PBS at 37ºC over time demonstrated that the physical stability of NPs was not the reason for the rapid release. It is possible that ions in PBS competed with Dox or STS to form new ion-pair complex, or the excipients competed with Dox to bind with hydrophobic STS during NP preparation. Thus, the major reason causing rapid release of Dox from Dox NPs within 8 h may be related to the stability of Dox-STS complex which could dissociate either in PBS over time or in the process of NP preparation.

Table 6.1. Ion-pair agents screened for doxorubicin

Ion-pair agents	Precipitates (ppts)	ppts dissolved in PBS	Form NPs
Taurocholic acid sodium salt hydrate	no		
(±)-α-Tocopherol phosphate disodium salt	no		
STDC (sodium taurodeoxycholate)	yes	yes	yes
SDS (sodium lauryl sulfate)	yes	yes	yes
Dextran sulfate 2500	yes	no	yes
Dextran sulfate 5000	yes	no	yes
Dextran sulfate 8000	yes	no	yes
Dextran sulfate 100,000	yes	no	no or difficult
Cellulose sulfate 3500,000	yes	no	no
Poly(vinylsulfonic acid) sodium salt	yes	yes	no
Niaproof 4 (7-Ethyl-2-methyl-4-undecyl sulfate sodium salt)	yes	no	yes
STS (sodium tetradecyl sulfate)	yes	no	yes

Table 6.2. Standard curve of doxorubicin (N=3)

Assay method	Detection	Standard curve	Linear range (µg/ml)	R^2
Microplate reader	486 nm	y = 0.0111x	0.939-93.9	0.9999
	Fluorescence	y = 504x – 87.7	0.282-4.69	0.9999
HPLC assay	486 nm	y = 116082x – 159253	1-100	0.9992
	Fluorescence	y = 1000000x	0.00229-2.35	0.9993

Table 6.3. Physiochemical properties of Dox-loaded nanoparticles (n=3)

Formulations	Theoretical loading (µg/ml)	Mean[a] diameter (nm)	P.I.	Zeta potential (mV)	% Drug loading (w/w, drug/oil)	% Drug entrapment efficiency (EE%)	% Mass balance for measuring EE%
Dox NPs #2	300	103.3 ± 1.2	0.284± 0.009	-27	15	86.2± 5.9	94.7± 0.6
Dox NPs #3	300	84.9 ± 3.3	0.313± 0.06	-27.4	15	91.0± 5.9	108.8 ± 7.9
Dox NPs #4	300	68.8 ± 2.5	0.064± 0.02	-26.6	15	91.8± 4.6	115.5 ± 1.8

[a] The data are presented as the mean of the mean particle size of nanoparticles in different batches ± SD (n = 3).
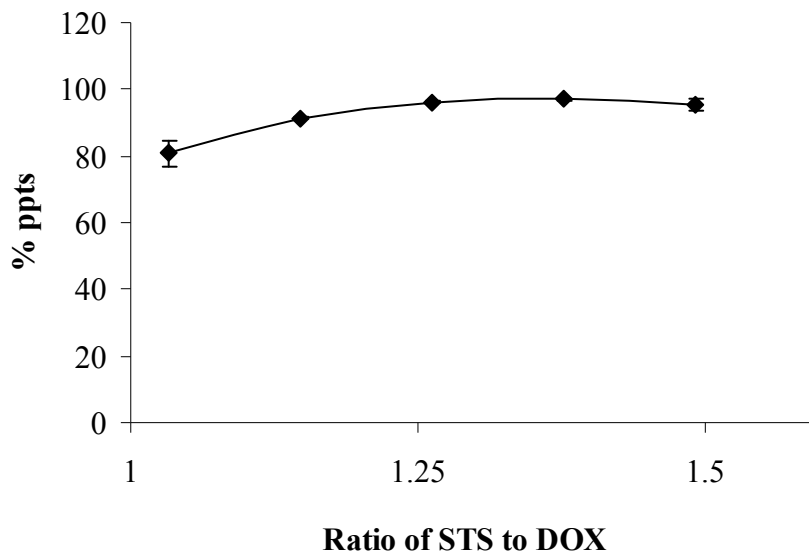
Figure 6.1

Figure 6.1: Formation of Dox-ion-pair complex using STS as the ion-pair agent. Red precipitates (ppts) indicated that the ion-pair complex was formed in water when Dox solution was titrated with STS solution. At the specific ratio of STS to Dox (between 1.25 to 1.5, mole/mole), over 95% of Dox formed the ion-pair complex.

Figure 6.2
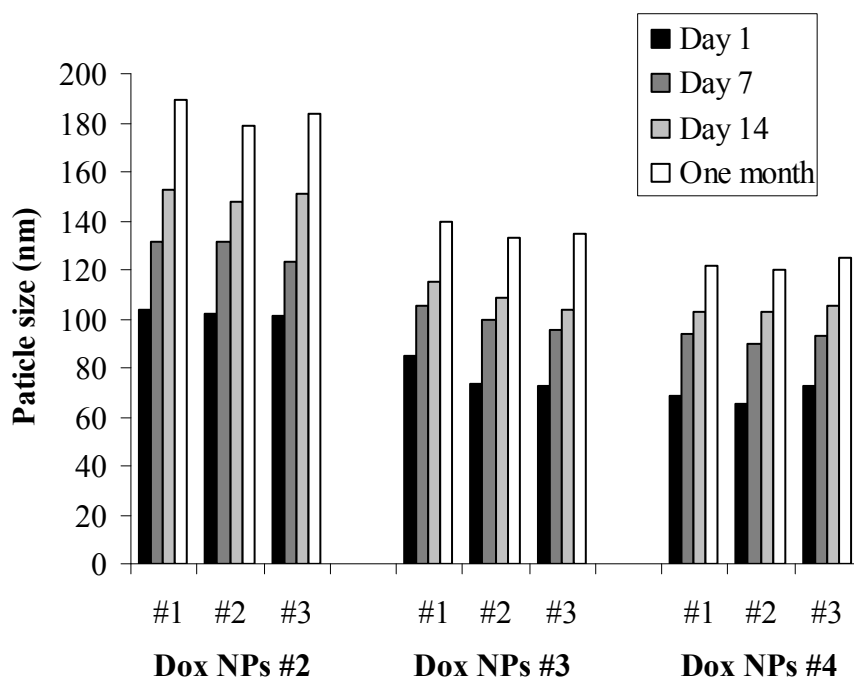
Figure 6.2: **Physical stability of Dox-loaded nanoparticles stored at 4ºC.** Three different batches of Dox-loaded NPs with different compositions were monitored for particle size over one month. For all tested NPs, P.I. < 0.35. Data are presented as the mean particle size of three separate measurements for each batch.

Figure 6.3

Figure 6.3: Physical stability of Dox-loaded nanoparticles in PBS at 37ºC. Dox-loaded NPs were diluted with PBS and incubated at 37ºC. Particle size was monitored over time. For all tested NPs, P.I. < 0.35. Data are presented as the mean particle size of three separate measurements for each batch.

Figure 6.4

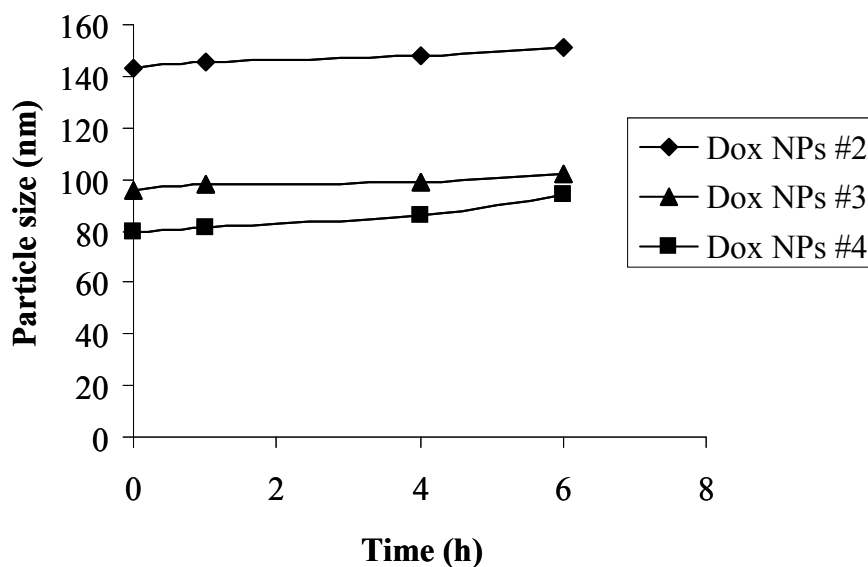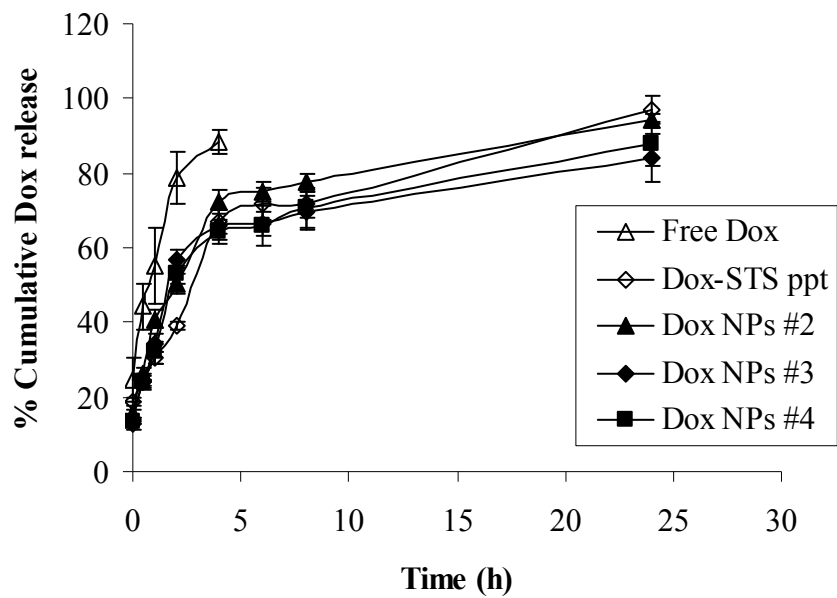**Figure 6.4: Release of Dox from Dox-loaded nanoparticles in PBS at 37ºC.** Dox release was measured using the dialysis method in PBS. Data are presented as the mean ± SD (n=3).

Chapter 7

Doxorubicin and paclitaxel-loaded lipid-based nanoparticles overcome multidrug resistance by inhibiting P-glycoprotein and ATP depletion

7.1   Summary

To test the ability of nanoparticle formulations to overcome P-gp-mediated multidrug resistance, several different doxorubicin and paclitaxel-loaded lipid NPs were prepared. Dox NPs showed 6-8-fold lower IC50 values in P-gp overexpressing human cancer cells than those of free Dox. The IC50 value of PX NPs was over 9-fold lower than that of Taxol in P-gp-overexpressing cells. A series of in-vitro cell assays were used including quantitative studies on uptake and efflux, inhibition of calcein acetoxymethylester (calcein AM) efflux, alteration of ATP levels, membrane integrity, mitochondrial membrane potential, apoptosis and cytotoxicity. Enhanced uptake and prolonged retention of Dox were observed with NP-based formulations in P-gp-overexpressing cells. calcein AM and ATP assays confirmed that blank NPs inhibited P-gp and transiently depleted ATP. Intravenous injection of pegylated PX BTM NPs showed marked anti-cancer efficacy in nude mice bearing resistant NCI/ADR-RES tumors versus all control groups. NPs may be used to target both drug and biological mechanisms to overcome MDR via P-gp inhibition and ATP depletion.

7.2 Introduction

Drug resistance is the major cause of failure of cancer chemotherapy. Multidrug resistance is a term used to describe the broad-spectrum resistance to chemotherapy in human cancer, which is a complex phenomenon that can result from several biochemical mechanisms that are still not fully understood [338]. A widely studied mechanism of MDR is that resulting from altered cell membrane transport. P-glycoprotein encoded by the mdr1 gene is well-characterized and known to be a clinically important transporter protein belonging to the ATP-binding cassette family of membrane transporters [339]. It has been shown to pump substrates, including doxorubicin and paclitaxel, out of tumor cells through an ATP-dependent mechanism that reduces the effective drug concentrations and consequently decreases the cytotoxic activity. A large number of P-gp inhibitors have been developed. However, clinical trials have been disappointing due to the high inherent toxicities of P-gp inhibitors and/or changed pharmacokinetics and biodistribution properties of anti-cancer drugs co-administrated with P-gp inhibitors [340].

Formulation strategies have been developed to potentially address P-gp-mediated resistance including colloidal delivery systems, polymer-drug conjugates, and polymeric-micelles. Certain drug-loaded liposomes [235, 239] and solid lipid nanoparticles [251, 341] have been shown to decrease the resistance of P-gp-expressing cells in-vitro, which has been attributed to increased cellular accumulation of the drug. However, importantly, intracellular drug was still removed by P-gp efflux because formulations did not affect P-gp function [256, 258]. Anti-cancer drugs conjugated to polymers such as pHPMA have been shown to effectively kill both sensitive and resistant cancer cells. Proposed mechanisms for these conjugates in resistant cells include internalization by endocytosis, partial inhibition of P-gp gene expression [342], and modification of caspase-dependent apoptosis signaling pathways [264]. Polymeric-micelles based on Pluronic¸ co-block polymers composed of poly(oxyethylene)-poly(oxypropylene), have been used to modulate P-gp in cancer cells [268, 276]. Pluronic micelles have been used to selectively inhibit the P-gp efflux system by ATP depletion in P-gp cells, as well as to reduce the GSH / GST detoxification system and to alter apoptotic signal transduction.

Our laboratory has previously developed paclitaxel NPs wherein the drug was entrapped into NPs having E. wax as the oil phase and Brij 78 as the surfactant. These PX NPs were used to overcome P-gp-mediated resistance in-vitro in a human colon

adenocarcinoma cell line (HCT-15) [300] and in-vivo in a nude mouse HCT-15 xenograft model [319]. The purpose of the present study was to determine how improved PX NPs and new Dox NPs overcome P-gp-mediated resistance.

7.3   Materials and Methods

Chemicals

Doxorubicin hydrochloride, paclitaxel, sodium tetradecylsulfate (STS), sodium taurodeoxycholate (STDC), glyceryl tridodecanoate, calcein AM, Brij 700 and cyclosporin A were purchased from Sigma-Aldrich. E. Wax and stearyl alcohol were purchased from Spectrum Chemicals (Gardena, CA). Brij 78 was obtained from Uniqema (Wilmington, DE). TPGS was purchased from Eastman Chemicals. Polystyrene nanoparticles were purchased from Polysciences, Inc.

Tumor cell lines and cell culture

The P-gp-overexpressing human ovarian carcinoma cell line NCI/ADR-RES and sensitive cell line OVCAR-8 were both obtained from National Cancer Institute. The P-gp-overexpressing human melanoma cell line MDA-MB-435/LCC6MDR1 and matching sensitive cell line MDA-MB-435/LCC6 were kindly provided by Dr. Robert Clarke (Georgetown University, Washington, DC). The sensitive human breast cancer cell line MDA-MB-468 was obtained from ATCC. All cells were maintained in exponential growth phase by periodic subcultivation.

Preparation and characterization of Dox and PX nanoparticles

Drug-loaded nanoparticles were prepared directly from warm o/w microemulsion precursors. PX NPs and Dox NPs were prepared and characterized as previously described in Chapter 4 and in Chapter 6, respectively.

Preparation and characterization of concentrated pegylated PX BTM NPs

To utilize PX BTM NPs for animal studies, PX BTM NPs containing a high concentration of PX were required to obtain the dose of 4.5 mg PX/kg with 200 µl of injection/mouse. PX BTM NPs were tested for their ability to be concentrated. Briefly, the concentrated NPs were prepared using 3-5 times of the amounts of all excipients and PX with the volume of water remaining unchanged. The resulting concentrated PX BTM NPs were measured for particle size. To test the ability of concentrated PX BTM NPs to pass 0.2 µm sterile Millex-LG filters (Millipore), the light scattering counts of nanoparticles

were directly measured without any dilution. The concentration of PX in NPs was also measured by HPLC before and after passing through the 0.2 μm filters. To prepare concentrated pegylated PX BTM NPs for the in-vivo efficacy studies, 3-time concentrated PX BTM NPs containing 450 μg/ml of PX were chosen for pegylation using Brij 700 (8% w/w ratio of Brij 700 to Miglyol 812). To make an isotonic NP suspension and to avoid the generation of 7-*epi* isomer of PX, NPs were prepared in 10% lactose dissolved in water for injection. The pH value of the final 10% lactose solution was 5.4. Briefly, Brij 78 (2.8 mg/ml), TPGS (1.5 mg/ml), and Miglyol 812 (2.5 mg/ml) were weighed out into a glass vial and heated to 70ºC. One (1) ml of 10% lactose solution pre-heated to 70ºC was added into the mixture of melted oils and surfactants. Spontaneously formed microemulsions were stirred for 15 min at 70ºC. Then, 200 μg Brij 700 dissolved in 10% lactose solution pre-heated to 70ºC were added to the warm microemulsions. The warm microemulsions were continually stirred for 10 min at 70ºC and then stirred for 4 h at room temperature to complete the insertion of Brij 700 into NPs. To prepare PX NPs, 450 μg of PX dissolved in ethanol were added directly to the melted oil and surfactant. After ethanol was evaporated using a nitrogen stream, the method described above was followed. The final NPs were passed through the sterile 0.2 μm filters. The concentrations of PX in NPs were measured before and after passing 0.2 μm filters, and PX entrapment efficiency was also measured after passing 0.2 μm filters using the HPLC assay.

In-vitro cytotoxicity studies

Cells were seeded into 96-well plates at 1.5×10^4 cells/well and allowed to attach overnight. Cells were incubated for 48 h with drug equivalent concentrations of all test articles ranging from 10,000 nM to 0.01 nM of free drug (corresponding to 5.45 μg/ml to 5.45 pg/ml for Dox, and 8.54 μg/ml to 8.54 pg/ml for PX). The sulforhodamine B (SRB) assay was performed and IC50 values were calculated based on the percentage of treatment over control [324].

Cellular uptake and efflux of Dox in cells

Cells were seeded in 48-well plates at a density of 2×10^5 cells/well and incubated overnight. Confluent cell monolayers were washed with Earle's balanced salt solution (EBSS) and treated with test articles. All samples were diluted with EBSS buffer and

adjusted to 5 µg Dox/ml or the Dox equivalent concentration. Cells were treated with samples at 37ºC for 0.5, 1 and 2 h. Cells were washed twice with ice-cold PBS pH 7.4 and lysed with PBS containing 1% Triton X-100 at 37ºC for 30 min. For efflux studies, cells were treated with each sample for 2 h, washed, and then cells were incubated with EBSS buffer at 37ºC for another 1, 2 and 4 h. Dox concentrations in cell lysates were measured by HPLC on an Inertsil ODS-3 column with a mobile phase consisting of 0.1 M ammonium formate containing 0.14 % triethylamine (adjusted pH to 2.4 by addition of formic acid)-acetonitrile-methanol-tetrahydrofuran (60:25:17.5:2.5, v/v/v/v) at a flow rate of 1.0 ml/min, and Dox was detected by fluorescence with 480/550 nm excitation/emission. Dox concentrations were normalized for protein content as measured with the BCA assay (Pierce) [343]. The cell efflux rate was calculated as: (uptake at 2 h – efflux at 4 h)/4.

Calcein AM assay for P-gp function

A calcein AM assay was performed using a modified method [344]. Briefly, cells were seeded in black 96-well plates at a density of 1×10^5 cells/well overnight and treated with 50 µl of various doses of test articles diluted in EBSS buffer. After 0.5 h at 37ºC, 50 µl of 0.25 µM calcein AM (Sigma-Aldrich) were added into each well and the fluorescence of calcein was immediately measured every 5 min for 1 h using a microplate reader with 485/589 excitation/emission at room temperature. For pre-treatment experiments, cells were exposed to blank NPs #2 for 0.5 h and washed, and then 50 µl of fresh EBSS buffer was added before addition of calcein AM. The % relative fluorescence in the cells was expressed as: % Relative Fluorescence (FL) = [($FL_{treatment}$ − $FL_{nontreatment}$)/ $FL_{nontreatment}$] × 100%

To assess cell membrane integrity, cells were treated with the same samples for 0.5 h at 37ºC, and then incubated for 1 h at room temperature. Then, cells were trypsinized and 50 µl of 0.4 % trypan blue solution was added. Membrane integrity was normalized to untreated control and expressed as (viable cells/total cells) × 100%.

ATP and Apoptosis assays

An ATP assay was performed as described previously [275]. Cells were seeded in 48-well plates at a density of 2×10^5 cells/well and incubated overnight. Various doses of

test articles in EBSS buffer were added to cells and incubated at 37ºC for 2 h. After treatment, cells were washed twice with ice-cold PBS and lysed with PBS containing 1% Triton X-100 at 37ºC for 30 min. ATP in cell lysates was then measured using ATPlite 1step Assay Kit (PerkinElmer) and normalized for protein content. Cell apoptosis under the tested conditions above was measured using the Annexin V-FITC Apoptosis Detection Kit I (BD Biosciences).

To assess whether cells could recover from ATP depletion, cells were incubated with various concentrations of test articles for 2 h, washed, and then incubated for another 4 h and 13 h, and then ATP levels and total proteins were measured.

Histology studies by transmission electron microscopy (TEM)

Cells were washed, scraped, and fixed in 4% buffered formalin, post-fixed in 2% osmium tetraoxide, and dehydrated in ascending concentrations of ethanol before embedded in Araldite 502. Blocks were sectioned at 1 µm and 800 Å for light and electron microscopy. Thin sections were stained with lead citrate and uranyl acetate before examined using a Philips 10 electron microscope operated at 60 kV.

Mitochondrial potential measurement

Cells were seeded in black 96-well plates at a density of 1×10^5 cells/well overnight and treated with test articles for 2 h at 37ºC. After washing, mitochondrial potential was detected using the JC-1 Mitochondrial Membrane Potential Detection Kit (Biotium). 1.5 or 0.15 µg/ml of PX BTM NPs and 6 µg/ml of cyclosporin A were used as positive and negative controls. Mitochondrial potential was expressed as (red FL/ green FL) $_{treatment}$/ (red FL/ green FL) $_{nontreatment} \times 100\%$.

3-(4, 5-Dimethylthiazol-2-yl)-2, 5-diphenyltetrazolium bromide (MTT) assay

Resistant cells and their sensitive parental cells were seeded in 96-well plates as a density of 4×10^4 overnight and incubated with MTT and samples for 2 h at 37ºC. Two hundred microliters of reagent containing 20% SDS and 50% dimethyl formamide in water were added and incubated for 1 h at room temperature and plates were read at 570 nm (test) and 650 nm (reference).

In-vivo anti-cancer efficacy study using pegylated PX BTM NPs

Female nude (nu/nu) mice, 4-5 weeks (Harlan Laboratories) were housed in a pathogen-free room. All experiments involving the mice were carried with an approved protocol by the University of North Carolina Animal Care and Use Committee. Two separate sets of in-vivo anti-cancer efficacy studies were performed.

The first anti-cancer efficacy study:

The mice were injected subcutaneously in the interscapular region with 4×10^6 NCI/ADR-RES cells suspended in DMEM medium. When the tumors exhibited volume between $50 - 150$ mm^3 (Day -7), the mice were randomly assigned to different treatments at two different PX doses of 4.5 mg/kg and 2.25 mg/kg. Mice were injected with either 100 or 200 μL of isotonic treatment article by intravenous injection. Tumors were measured in two perpendicular dimensions every two days for 12 days, and the tumor volume was calculated using the formula: $V = (L \times W^2)/2$, where L and W are the longest and shortest diameters, respectively.

The second anti-cancer efficacy study

Tumor models were set up as described above. When the tumors became a defined solid with the volume between $60 - 200$ mm^3 (Day -38), the mice were randomly assigned to different treatments at PX dose of 20 or 4.5 mg/kg. Mice were injected with 200 μL of isotonic treatment article by intravenous injection on day 0, 7, 14 and 21. On Day 30 after treatment, mice were sacrificed except the two Taxol groups and PX BTM NP group. On Day 31, mice in Taxol groups were treated with pegylated PX BTM NPs (4.5 mg PX/kg) every three days for a total of three times. Then, on Day 48, mice were retreated with pegylated PX BTM NPs (7.5 mg PX/kg) every three days for a total of three times. For PX BTM NP group, mice were monitored for tumor growth. On Day 48, mice were retreated with pegylated PX BTM NPs (7.5 mg PX/kg) every three days for a total of three times. Tumors were measured in two perpendicular dimensions and the tumor volume was calculated using the formula as above.

Statistical analysis

Statistical comparisons were made with ANOVA followed by pair-wise comparisons using Student's t test using GraphPad Prism software. Results were considered significant at 95% confidence interval ($p < 0.05$).

7.4   Results

Dox and PX nanoparticles

The compositions and physicochemical properties of Dox and PX NPs are shown in Table 7.1.A and 7.1.B, respectively. PX could be entrapped directly into G78 NPs and BTM NPs. Dox ion-pair complexes with STDC were somewhat soluble in PBS that led to increased rates of Dox release from the NPs. In comparison, STS fully precipitated Dox at a mole ratio of 1:1.2 (Dox: STS) and resulted in an ion-pair complex that had both low solubility in PBS and high solubility in the melted oil phases. All NPs were stable over one month at 4°C (Figure 5.3 and Figure 6.2).

Concentration and pegylation of PX BTM NPs for in-vivo efficacy studies

Blank BTM NPs and PX BTM NPs were concentrated to 3, 4 and 5 times of the original composition as presented in Chapter 4. The concentrated 3× NPs had particle sizes in the range between 170 nm and 200 nm, and the particle size 5× NPs was in the range between 200 to 230 nm. After passing through 0.2 μm filters, the light scattering counts for nanoparticle suspensions and the concentrations of PX changed less than 4%, indicating that concentrated blank BTM NPs and PX BTN NPs could pass 0.2 μm filters without the loss of nanoparticles (Table 7.2). Three-time (3×) concentrated PX BTM NPs containing 450 μg/ml of PX were optimized to add Brij 700 for the in-vivo efficacy studies. The final optimized pegylated PX BTM NPs had particle sizes about 180 nm. Four batches of pegylated PX BTM NPs were prepared. The pegylated PX BTM NPs passed through 0.2 μm filters without the loss of PX and the filtered pegylated PX BTM NPs had entrapment efficiency of PX higher than 95% (Table 7.3).

In-vitro cytotoxicity studies

Cytotoxicity data in two pairs of parental (sensitive) and P-gp cell lines are reported in Figure 7.1. As expected, in the tested Dox concentration range, free Dox showed no toxicity in NCI/ADR-RES cell line in the tested concentration range (IC50 > 5.45 μg/ml, corresponding to > 10,000 nM) and very low toxicity in MDA-MB-435/LCC6MDR1 cell line (IC50= 3.62 μg/ml, corresponding to 6643 nM) (Figure 7.1.A and 7.1.B). Dox-loaded NPs showed a clear dose-dependent cytotoxicity against all tested cell lines. In sensitive cell lines, the IC50 values of Dox-loaded NPs were comparable with those of free Dox. In

comparison, the IC50 values of Dox NPs #2 were 8-fold lower in NCI/ADR-RES cells (IC50s < 0.61 µg/ml, corresponding to 1111 nM) and in MDA-MB-435/LCC6MDR1 cells (IC50 < 0.45 µg/ml, corresponding to 821 nM) than those of free Dox. Blank NPs did not cause significant cytotoxicity against all cell lines up to a total NP dose of 30 µg/ml.

Interestingly, the post-addition of Dox to blank NPs showed similar cytotoxicity to Dox NPs in both sensitive and resistant cell lines. Thus, to ascertain if this phenomenon was drug specific, PX G78 NPs and PX BTM NPs were tested for cytotoxicity in OVCAR-8 and NCI/ADR-RES cells and compared with Taxol. As shown in Figure 7.1.C and Figure 7.1.D, the IC50 value of Taxol in NCI/ADR-RES cells was 495-fold greater (IC50= 3.26 µg/ml, corresponding to 3814 nM) than that in sensitive cells (IC50= 0.00658 µg/ml, corresponding to 7.7 nM). Also, the IC50 value of both PX NPs was over 9-fold lower than that of Taxol in P-gp cells. Both blank NPs did not show significant cytotoxicity in these cell lines. Similar to when free Dox was post-added to blank NPs, the post-addition of free PX to blank G78 NPs or blank BTM NPs had comparable cytotoxicity to that of PX entrapped in NPs. The IC50 values of the post-addition were slightly lower than those of PX NPs in both cell lines; however, the difference was statistically significant ($p < 0.05$) only in the sensitive cells.

Cellular uptake and efflux of Dox

The uptake and efflux of Dox with various formulations containing 5 µg/ml of Dox was examined in both NCI/ADR-RES and MDA-MB-468 cells at different temperatures (Figure 7.2). Dox NPs #2 were chosen as the basic NP formulation for these studies. The uptake of Dox was time-dependent except when cells were pre-treated with blank NPs #2. In NCI/ADR-RES cell line at 37°C, NPs led to over a 2-fold increase in the extent of uptake compared with treatment with free Dox (Figure 7.2.A). Similarly, all treatments with NP formulations enhanced the retention of Dox. After cells were treated with Dox NPs #2, greater than 15-fold Dox remained in the P-gp cells and the efflux rate was 1.5-fold lower compared with free Dox after 4 h of efflux. Importantly, the post-addition of Dox to blank NPs #2 also showed enhanced uptake and retention. To eliminate the possibility that Dox was quickly bound to the surface of blank NPs #2, cells were pre-treated with blank NPs #2 and washed before the addition of free Dox. In this treatment, the uptake of Dox was very rapid and reached a maximum within 0.5 h and 7-fold greater

Dox was retained in cells compared with free Dox. However, the efflux rate of this treatment (0.19 [Dox](ng)/[protein](μg)/h) was significantly greater than that of free Dox (0.13 [Dox](ng)/[protein](μg)/h) ($p < 0.05$) (Figure 7.2.A). The uptake of Dox in NCI/ADR-RES cells at 4ºC with Dox NPs #2 and free Dox was 24-fold lower and 10-fold lower, respectively, than those at 37ºC. Unlike the uptake at 37°C that showed marked differences between NP groups and free Dox, the differences at 4°C were significantly reduced (Figure B.1). The extent of Dox uptake was also carried out in sensitive MDA-MB-468 cells at 37°C. NP formulations showed greater uptake than free Dox as shown in Figure 7.2.B. In fact, the Dox NPs #2 very rapidly entered MDA-MB-468 cells and Dox from NPs quickly and extensively localized inside the nuclei of cells by fluorescence microscopy (Figure B.2).

To confirm that Brij 78 could also enhance Dox uptake and decrease efflux, NCI/ADR-RES cells were pre-treated with various concentrations of Brij 78 (Figure 7.2.C). At the concentrations of Brij 78 that showed ATP depletion, pre-treatment of cells with Brij 78 led to comparable Dox uptake enhancement and efflux reduction compared with blank NPs #2 (Figure 7.2.A).

Calcein AM assay

The ability of blank NPs #2, and the Brij 78 and TPGS surfactants to inhibit P-gp was evaluated using the calcein AM assay in five resistant and sensitive cell lines (Figure 7.3). Under all conditions tested, the trypan blue assay confirmed that there was no significant loss of cell membrane integrity (Figure B.3). In resistant cells, the fluorescence caused by intracellular calcein significantly increased in a dose-dependent manner either in the presence of blank BTM NPs (Figure B.4), blank NPs #2 (Figure 7.3.A and Figure 7.3.B) or when cells were pre-treated with blank NPs #2 for 0.5 h (Figure B.5). Brij 78 and TPGS surfactants also led to a dose-dependent increase in calcein fluorescence over 1 h. In contrast, polystyrene NPs did not increase intracellular fluorescence. In stark contrast, no treatments led to increased intracellular fluorescence compared with calcein AM alone in the sensitive MDA-MB-468 cells (Figure B.6), OVCAR-8 cells (Figure 7.3.C) and MDA-MB-435/LCC6 cells (Figure 7.3.D). However, the human melanoma MDA-MB-435/LCC6 cells showed greater permeability as the uptake of calcein AM was higher in these cells.

ATP and Apoptosis Assays

To further understand the mechanisms by which blank NPs and surfactants inhibited P-gp, intracellular ATP levels in cells were measured after exposure to various concentrations of blank NPs #2, Brij 78 and TPGS. In resistant NCI/ADR-RES and MDA-MB-435/LCC6MDR1 cells, ATP levels decreased in a dose-dependent manner after treatment with blank BTM NPs (Figure B.7), blank NPs #2 and Brij 78 to 40%, 35% and 20% of the initial value, respectively; however, there was no change in ATP levels after treatment with TPGS (Figure 7.4.A). Importantly, cyclosporin A and polystyrene NPs did not decrease ATP levels in the tested concentration range in NCI/ADR-RES cells. In contrast, over all tested concentrations in sensitive MDA-MB-468 and OVCAR-8 cells, only 0.5 and 1 μg/ml of Brij 78 and blank NPs #2 (Dox equivalent doses) decreased ATP levels to 86% and 65% of the initial value, respectively (Figure B.8). However, ATP levels decreased in MDA-MB-435/LCC6 cells, which had no significant difference with those in corresponding resistant cells (Figure B.8). Also, TPGS decreased ATP levels in this sensitive cell line (Figure B.8). In the presence of 17 μg/ml of cyclosporin A, ATP levels further decreased by an additional 20-40% at each concentration tested (Figure B.9). Finally, ATP recovery studies showed that after blank NPs #2 and Brij 78 were removed from NCI/ADR-RES cells, cellular ATP levels returned to 100% after 4 h for the lower concentrations tested and were completely restored after 13 h for all concentrations (Figure 7.4.B).

Under the conditions analogous to the ATP depletion experiments, four concentrations of Dox-equivalent doses (0.5, 1, 2, and 5 μg/ml) for the Brij 78 and TPGS surfactants and blank NPs were tested for their ability to induce apoptosis versus control cells at 2 h in NCI/ADR-RES cells. Only blank NPs at 5 μg/ml showed significance versus control ($p < 0.05$), and these differences were modest (8% versus 6.7% for control).

TEM

MDA-MB-468, OVCAR-8 and NCI/ADR-RES cells are anchorage-dependent epitheloid cells. The effects of Dox on these cells seemed similar with the major changes in the degree of nuclear chromatin compaction. In NCI/ADR-RES and OVCAR-8 cells, Dox NPs #2 or blank NPs #2 treatment induced the most severe changes that included cytoplasmic accumulation of multivesicular bodies, chromatin condensation, and varying

degree of mitochondrial swelling. After 1 h of incubation, swollen mitochondria were frequently observed in the resistant cells treated with Dox NPs #2 or blank NPs #2 (Figure 7.4.C). However, this effect was not observed in the sensitive MDA-MB-468 cells. In comparison, Brij 78 also produced mitochondrial swelling in NCI/ADR-RES and OVCAR-8 cells (Figure B.10). In human melanoma cells, MDA-MB-435/LCC6 and MDA-MB-435/LCC6MDR1, swollen mitochondria were also observed with the treatment of blank NPs #2 or Brij 78 (Figure B.10).

Mitochondrial potential measurement

Mitochondrial potential changed in all tested cells treated with blank NPs #2 and Brij 78 at the same concentrations that depleted ATP (Figure 7.4.D). TPGS did not change mitochondrial potential in all cell lines except in MDA-MDB-435/LCC6. All tested samples changed mitochondrial potential in MDA-MB-435/LCC6 cells except the treatment with 0.15 µg/ml of PX BTM NPs.

MTT assay

To a certain extent, all tested samples including blank NPs #2, Brij 78 and TPGS decreased MTT reduction in a dose-dependent manner, except at the lowest concentration of tested samples (0.05 µg/ml of Dox equivalent dose) (Figure B.11). The minimum value of MTT reduction at 1 µg/ml of Dox equivalent dose was $71 \pm 8\%$ (versus control) and observed in MDA-MB-435/LCC6 cells treated with blank NPs #2 (30 µg/ml).

In-vivo anti-cancer efficacy study

In the first study, tumor volume increased with control, Taxol and blank BTM NPs administration at the two PX or PX-equivalent doses tested. In comparison, a marked anti-cancer effect of the pegylated PX BTM NPs was clearly observed (Figure 7.5). The tumor volume in the two tested pegylated PX BTM NPs groups almost did not change during the course of the study. A statistically significant difference of pegylated PX BTM NPs from all other treatments was observed from day 5 and continued to the end of the study. Blank BTM NPs did not show any clinical signs of toxicity even at the highest dose of 210 mg NPs/kg.

In the second study, tumor volume increased with control, blank BTM NPs, Taxol and the mixture of blank BTM NPs and Taxol administration. Taxol, at 20 mg PX/kg, is the maximum tolerate dose of Taxol in mice. However, only pegylated PX BTM NPs at the dose of 4.5 mg PX/kg, again, inhibited tumor growth (Figure 7.6.A). A statistically significant difference of pegylated PX BTM NPs from all other treatments was observed from day 7 and continued to the end of the study. After mice in Taxol groups were treated with pegylated PX BTM NPs, tumors became smaller ($p < 0.05$) (Figure 7.6.B). Although tumors continued growing after treatment ended, the second cycle of treatment with pegylated PX BTM NPs caused the tumors to shrink. The tumors in the PX BTM NP group started to grow after treatment (Figure 7.6.A). However, retreatment with pegylated PX BTM NPs in this group decreased tumor volume (Figure 7.6.C).

7.5   Discussion

The objective of the present studies was to investigate the potential of drug-loaded lipid nanoparticles to overcome P-gp-mediated drug resistance, and to elucidate possible mechanisms. The results of the cytotoxicity studies indicate that all tested drug-loaded NPs significantly reduced IC50 values in P-gp-overexpressing ovarian and melanoma cell lines over free drug. Of interest was that the post-addition of free Dox to blank NPs also showed similar IC50 values compared to Dox-loaded NPs (Figure 7.1). This is a similar observation as reported by Némati and colleagues in which Dox-loaded polyalkylcyanoacrylate nanoparticles were used to treat sensitive and resistant leucemic murine cells [345]. This observation could be the result of two possibilities: 1) due to strong adhesive properties, Dox is adsorbed onto the surface of NPs [346], and 2) blank NPs could affect P-gp and therefore enhance the cytotoxicity of Dox. To test these two possibilities, PX was used because the neutral PX would be less likely to adhere to the slightly negatively charged NPs. In a similar manner as Dox NPs, free PX post-added to blank NPs showed comparable cytotoxicity as PX-loaded NPs. Temperature-dependent uptake of Dox NPs #2 in NCI/ADR-RES cells indicates an endocytosis pathway of NPs uptake. Obviously, nanoparticles not only enhanced the uptake of Dox but also improved the retention of Dox in resistant cell lines even if Dox was entrapped into NPs or physically present with blank NPs. More importantly, the uptake and retention of Dox increased when cells were pre-treated with blank NPs or free Brij 78 and then free Dox was added (Figure 7.2.A and Figure 7.2.C). These results are in contrast to a previous study that showed that the uptake and retention of Dox in MDA-MB-435/LCC6MDR1 cells were not improved when free Dox was added to PLNs [256]. These contrasting studies seem to indicate a different and preferential mechanism of our NPs from the PLNs on P-gp. Taken as a whole, these studies prove that the lipid-based NPs described in the present studies inhibit the function of P-gp. Although a prior study suggested that an ion-pair complex of Dox and polycyanoacrylic acid, a degradation product of polyalkylcyanoacrylate NPs, may increase the intracellular diffusion of Dox and result in increased efficacy of Dox NPs in resistant cells [347], the present study suggested that the ion-pairing agents likely did not affect P-gp directly since the IC50 of PX NPs prepared without ion-pair agents was also low (Figure 7.1.C and 7.1.D). According to the data, the factor that was the most influential was the inclusion of the surfactant Brij 78, but not

necessarily TPGS. In fact, it has been shown that some surfactants reverse the activity of P-gp and MRP2 [348]. In these studies, we showed that both Brij 78 and TPGS were able to increase calcein AM influx in P-g cells, but only Brij 78 was found to deplete ATP. Calcein AM is a non-fluorescent substrate of P-gp that, once in the cells, is irreversibly converted by cytosolic esterase to calcein, a non-permeable and fluorescent molecule. Thus, the increased intracellular fluorescence of calcein when P-gp cells were exposed to lipid-based NPs indicates the inhibition of P-gp function. Moreover, the integrity of membrane confirmed that the inhibition resulted from a selective interaction with P-gp rather than an unspecific membrane alteration which may increase doxorubicin transport in resistant cells. Additionally, the inhibition of P-gp by blank NPs was not related to nanoparticle size since polystyrene nanoparticles having the same particle size had no effect on the intracellular fluorescence (Figure 7.3.A). Since P-gp efflux is an energy-dependent process, intracellular ATP levels were investigated. The results of the present studies demonstrate that exposure to blank NPs #2 induces a significant decrease in ATP levels in two resistant cells without inducing cell apoptosis. The effect of individual surfactant on ATP levels also was examined. It is clear that Brij 78, not TPGS, decreased ATP levels in resistant cell lines (Figure 7.4.A). Even at a very low actual concentration of 4.5 µg/ml, which is well below the critical micelle concentration (CMC) of Brij 78 (860 µg/ml), Brij 78 reduced the ATP levels after 2 h to 78% of the initial value. The ATP levels in sensitive cells responded differently to different cells. ATP levels only slightly changed in MDA-MB-468 and OVCAR-8 cells whereas ATP levels in MDA-MB-435/LCC6 cells decreased to the same extent as with the corresponding resistant cells after treatment with either blank NPs #2 or Brij 78. Our findings on ATP depletion are in agreement with the previous reports from the Kabanov group that concluded that ATP depletion caused by Pluronic P85 block copolymer was one of the major reasons for reversal P-gp activity and dominant in P-gp cells [344, 349]. Moreover, Brij 78 had similar influence on enhanced Dox uptake and retention as compared to blank NPs #2 (Figure 7.2.C). The results of the present study also suggested that reversal of P-gp function by ATP depletion caused by NPs was transient and reversible, based on ATP recovery studies (Figure 7.4.B) and uptake and efflux studies (Figure 7.2.A and Figure 7.2.C).

Our previous studies suggested that Brij 78 could influence the activity of an alcohol dehydrogenase/NAD+ enzyme system in-vitro [318]. The mitochondria are

responsible for regulation of cellular metabolism, and also are the ATP factory in cells. Increase in matrix volume of mitochondria can be due to energetic stress inside cells [350, 351]. It is important to note that the MTT reduction may not result from cell death because the apoptosis data and ATP recovery data showed that cells did not undergo apoptosis and that the ATP depletion was transient. Therefore, the MTT assay data more likely suggested a change in the cell metabolic activity or enzyme activity in the mitochondrial respiratory chain in treated cells [352, 353]. Therefore, it is likely that the metabolic activity was decreased in all cells treated with blank NPs #2 and Brij 78. Moreover, mitochondrial potential in resistant and sensitive cell lines changed at the same concentrations of blank NPs #2 or Brij 78 that depleted ATP. However, the change in mitochondrial potential and mitochondrial swelling did not destroy mitochondrial function as ATP levels returned to normal within 4-13 h depending on the dose (Figure 7.4.B). It is worthy to note that MDA MB-435/LCC6 cells showed both changes in ATP levels and mitochondrial potential. These effects may be related to the high permeability of the cell membrane as observed by the relatively high uptake of calcein AM (Figure 7.3.D). The change in the mitochondrial potential was correlated with mitochondrial swelling in all tested cells in these studies. Thus, it is possible that Brij 78 and NPs influence the enzymes involved in mitochondrial respiratory chain, and consequently produce energy stress in cells. As a consequence, the mitochondrial potential changes and the mitochondria swell to meet the energy requirement. These effects are likely pronounced in Pgp-overexpressing cells as they require more energy for P-gp expression and function.

The current study suggested that there are at least two major reasons for enhanced cytotoxicity of Dox or PX-loaded lipid-based NPs in P-gp-mediated resistant cells: 1) increased extent of drug uptake by endocytosis of NPs which helps to partially bypass P-gp; 2) decreased efflux rate of drug through inhibition of P-gp function and ATP depletion caused by Brij 78, a component of NPs. Both increase intracellular drug concentrations which is the key to overcome transporter mediated resistance.

Pegylation is a common method to prepare "stealth" NPs to escape the RES system. Brij 700 containing a PEG moiety with a molecular weight 4400 was used to prepare pegylated PX BTM NPs. To achieve the high concentration of PX in NPs required for the in-vivo efficacy studies, PX BTM NPs were concentrated up to 5-times the original concentration. Pegylated PX BTM NPs containing 450 μg/ml of PX were successfully

prepared with the ability to pass through the 0.2 μm sterile filters. Two in-vivo anti-cancer efficacy studies in mice bearing resistant NCI/ADR-RES cell xenografts demonstrated that pegylated PX BTM NPs significantly inhibited tumor growth versus all tested controls. Taxol even at its maximum tolerate dose (20 mg PX/kg) did not inhibit tumor growth in current xenograft model. The blank BTM NPs also showed the ability to inhibit P-gp function and deplete ATP in-vitro. However, co-administration of blank BTM NPs and Taxol also did not inhibit tumor growth (Figure 7.6.A). Therefore, it is important to keep PX inside the NPs so that blank BTM NPs and PX could reach tumors at the same time for tumor inhibition, because ATP depletion caused by blank NPs is transient and reversible. For Taxol-failed groups, PX BTM NPs caused the tumors to shrink (Figure 7.6.B). It indicated that PX BTM NPs could be used to treat recurrent tumors. It was hypothesized that pegylated PX BTM NPs with a slow and sustained release profile of PX greatly took the advantage of the EPR effect to accumulate in tumors. By combining the benefit of blank BTM NPs to inhibit P-gp and deplete ATP, PX and P-gp inhibitors (blank BTM NPs) had synergized activity against tumor cells in order to overcome the resistance and inhibit tumor growth. Importantly, the BTM NPs were well tolerated by mice as mice did not show any clinical signs of toxicity even at the highest dose of 210 mg NPs/kg given weekly over four weeks and after several cycle treatments (Figure 7.6). This specific apparent lack of toxicity of BTM NPs distinguishes them from the common P-gp inhibitors which interact with drugs and have often resulted in additional side effects. Additional in-vivo studies are on-going including pharmacokinetic and biodistribution studies, as well as additional efficacy studies in resistant and sensitive tumor mouse tumor models.

In conclusion, both Dox and PX-loaded lipid-based NPs containing the Brij 78 surfactant were shown to overcome P-gp-mediated drug resistance. The mechanism of P-gp inhibition and ATP depletion distinguishes these Brij 78-based NPs from other known nanoparticles and liposome-based carrier systems. To the best of our knowledge, this is the first report on nanoparticles which can inhibit P-gp efflux and deplete ATP. Most importantly, NP-based carriers that effectively target both the drug and biological mechanisms to overcome MDR (P-gp inhibition and ATP depletion) appear to be a novel therapeutic strategy and additional in-vivo work is warranted.

Table 7.1

Table 7.1.A. Compositions of Dox and PX NPs

Formulations	Ion-pair	Oil phases (mg/ml)				Surfactants (mg/ml)	
		E. wax	Stearyl alcohol	Glyceryl tridodecanoate	Miglyol 812	TPGS	Brij 78
Dox NPs #1	STDC	2.0	-	-	-	2.6	2.0
Dox NPs #2	STS	2.0	-	-	-	2.6	2.0
Dox NPs #3	STS	2.0	-	-	-	-	4.0
Dox NPs #4	STS	-	2.0	-	-	-	4.0
PX G78 NPs	none	-	-	1.7	-	-	4.0
PX BTM NPs	none	-	-	-	2.5	1.5	3.5

Final concentrations of Dox and PX in drug-loaded NPs were 300 µg/ml and 150 µg/ml, respectively.

Table 7.1.B. Summary of the physicochemical properties of Dox NPs and PX NPs

Formulations	Mean diameter (nm)	% Drug loading (w/w, drug/oil)	% Drug entrapment efficiency	% Drug released in 2 h
Dox NPs #1	102.3 ± 3.9	10	87.2	77.0 ± 1.1
Dox NPs #2	103.3 ± 1.2	15	86.2 ± 5.9	45.5 ± 7.1
Dox NPs #3	84.9 ± 3.3	15	91.0 ± 5.9	56.9 ± 2.4
Dox NPs #4	68.8 ± 2.5	15	91.8 ± 4.6	52.8 ± 2.4
PX G78 NPs	138.7 ± 1.3	7.5	85.4 ± 3.3	5.5 ± 1.1
PX BTM NPs	177.3 ± 1.4	6	97.5 ± 2.6	8.7 ± 4.0

Table 7.2 Characterization of concentrated PX BTM NPs

before and after 0.2 μm filtration

Formulations	3x concentrated		4x concentrated		5x concentrated	
	Blank BTM NPs	PX BTM NPs	Blank BTM NPs	PX BTM NPs	Blank BTM NPs	PX BTM NPs
Light scattering count (cps) before	6.27×10^6	6.68×10^6	N.D	6.34×10^6	6.50×10^6	6.34×10^6
[% change before/after filtration]	[-3.5%]	[0%]		[-0.3%]	[-1.5%]	[-3.9%]
PX concentration (μg/ml) before		504.5 ± 1.0		689.6 ± 1.5		773.7 ± 1.1
[% change before/after filtration]		[-2.7%]		[-0.3%]		[-2.6%]

Table 7.3 Characterization of 3× pegylated PX BTM NPs

before and after 0.2 μm filtration

Formulations	Batch #1	Batch #2	Batch #3	Batch #4
PX concentration (μg/ml) before	449.3	465.8	477.7	404.8
[% change before/after filtration]	[-1.7%]	[-1.5%]	[-2.0%]	[4.4%]
EE%[a] of PX in filtered pegylated PX BTM NPs	97	98	97	95

[a] EE means entrapment efficiency.

Figure 7.1
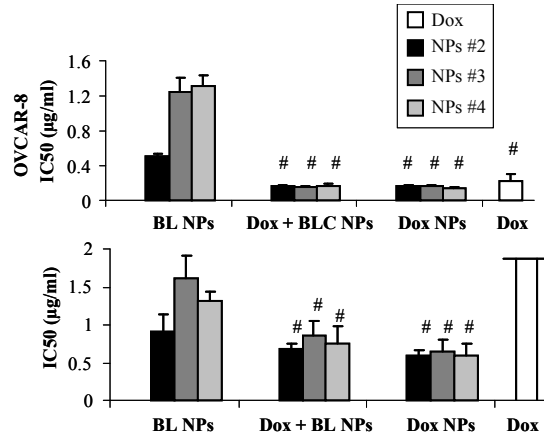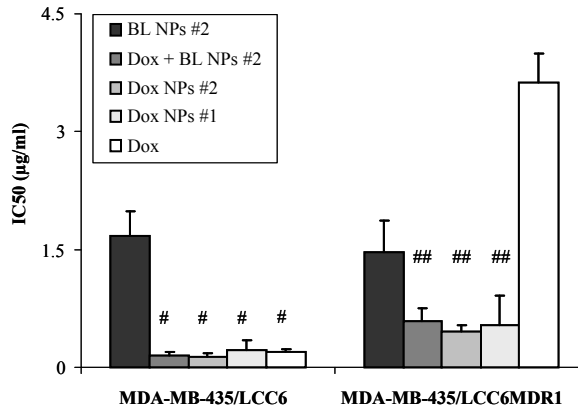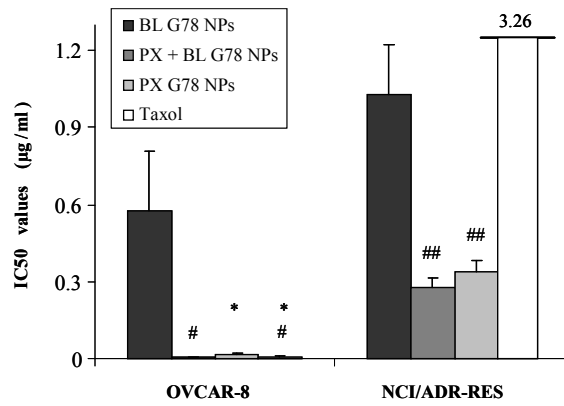
D
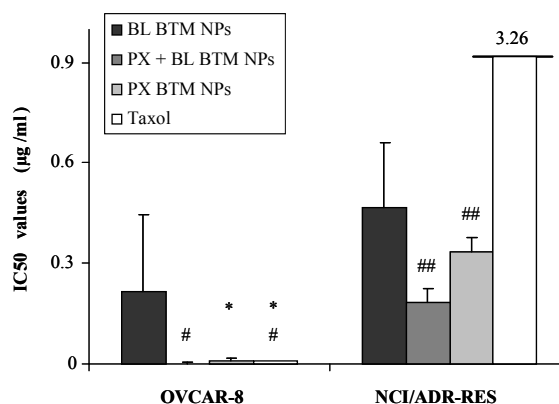
Figure 7.1: Dox and PX cytotoxicity studies at 48 h. IC50 values (µg/ml) of Dox and Dox NPs in (**A**) OVCAR-8 and NCI/ADR-RES cells, and (**B**) MDA-MB-435/LCC6 and MDA-MB-435/LCC6MDR1 cells. (**C**) IC50 values (µg/ml) of PX and PX G78 NPs in OVCAR-8 and NCI/ADR-RES cells. (**D**) IC50 values (µg/ml) of PX and PX BTM NPs in OVCAR-8 and NCI/ADR-RES cells. Data are presented as the mean ± SD of three independent experiments (N=3) with triplicate (n=3) measurements for each experiment. * $p < 0.05$; # and ## $p > 0.05$. "Drug equivalent dose" of NPs and excipients are calculated from the composition shown in Table 7.1.
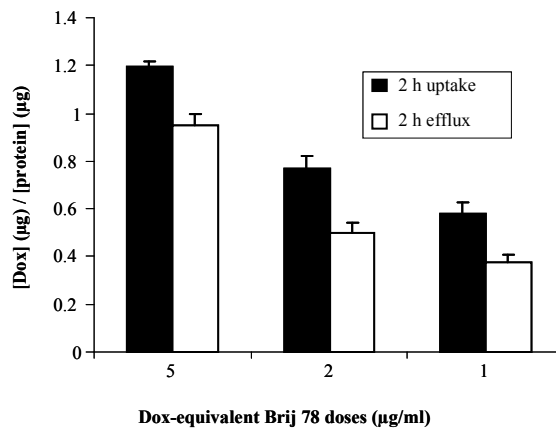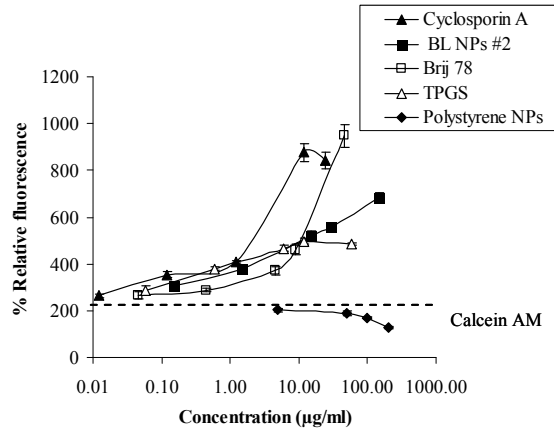
Figure 7.2

A
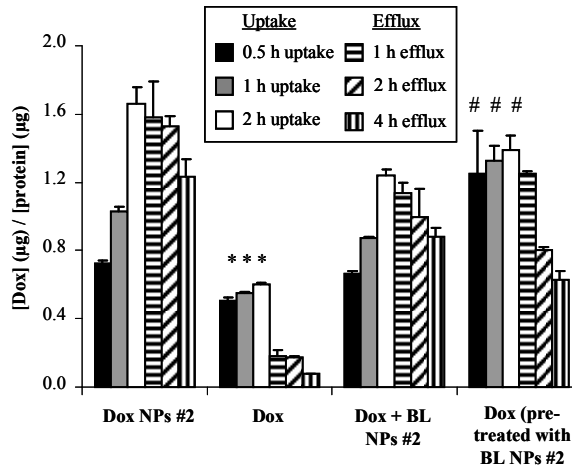
B
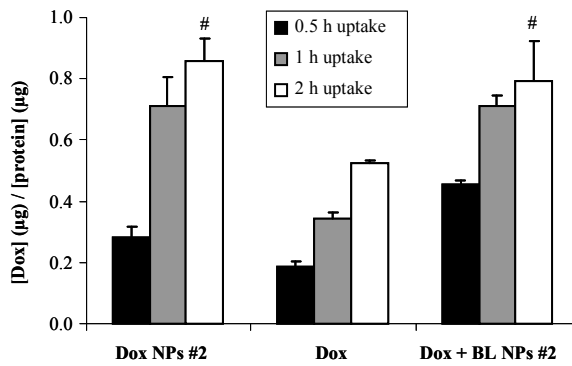
C

Figure 7.2: Cellular uptake and efflux of Dox in NCI/ADR-RES and MDA-MB-468 cells. (**A**) uptake and efflux in NCI/ADR-RES cells at 37ºC, and (**B**) uptake in MDA-MB-468 cells at 37ºC. For pre-treatment experiments, cells were pre-treated with blank NPs #2

for 0.5 h before the next step. For efflux studies, cells were treated with samples for 2 h, and then re-incubated with fresh EBSS buffer for indicated time. (**C**) Dox uptake and efflux when cells were pre-treated with Brij 78 at concentrations of 45.3, 18.1, and 9.1 µg/ml (corresponding to Dox-equivalent doses of 5, 2, and 1 µg/ml, respectively) for 0.5 h. Data are presented as the mean ± SD (n = 3). * $p < 0.05$ and # $p > 0.05$.
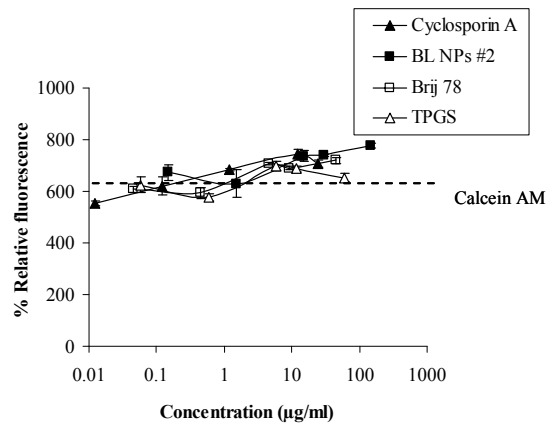
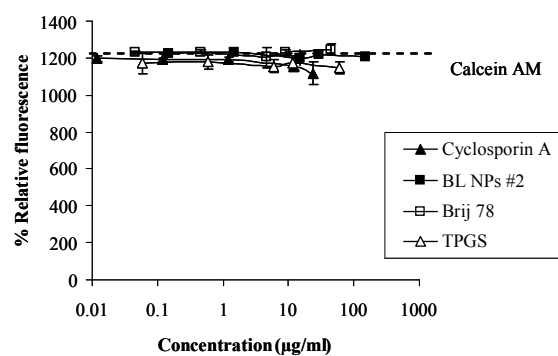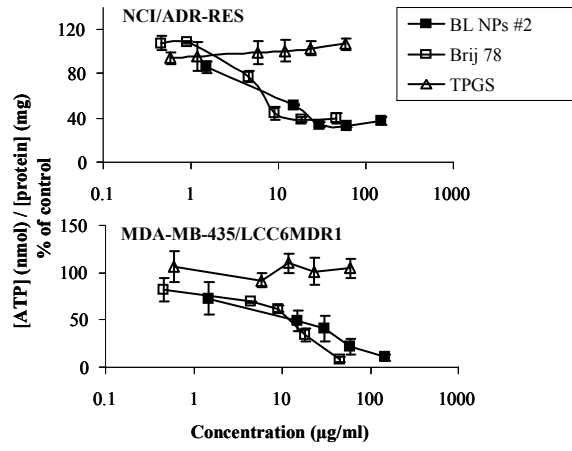**Figure 7.3**

A

B
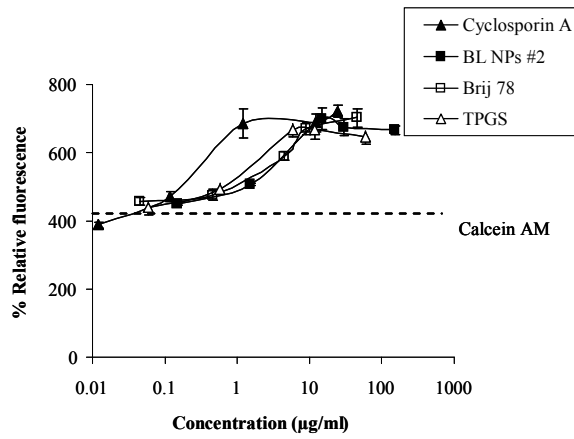
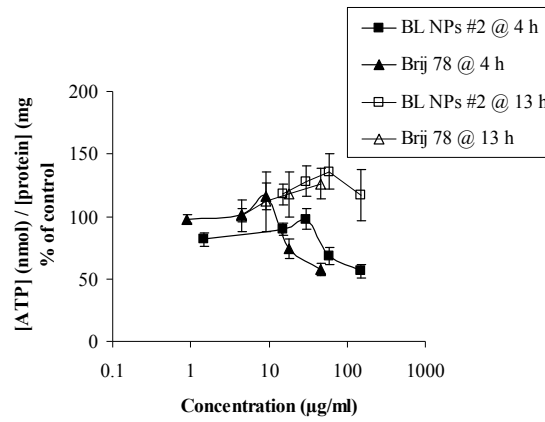**C**

D

Figure 7.3: Dose response of blank NPs #2 and surfactants in calcein AM assay in NCI/ADR-RES cells (A), MDA-MB-435/LCC6MDR1 cells (B), OVCAR-8 cells (C), and MDA-MB-435/LCC6 cells (D). Concentrations are presented as concentrations of blank NPs #2 (sum of mass of oils and surfactants) and as concentrations of free Brij 78 and TPGS. Data are presented as the mean ± SD (n = 3).
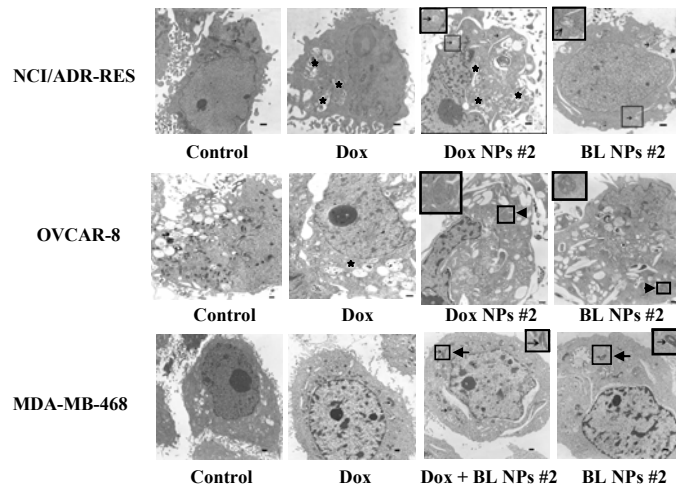
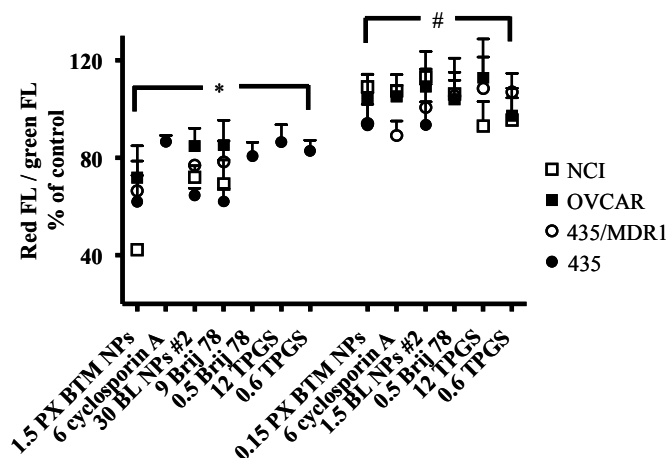# Figure 7.4

A

B

C

D

Figure 7.4: The effects of nanoparticles on ATP levels and mitochondria. (**A**) Effect of blank NPs #2 and surfactants on intracellular ATP level in NCI/ADR-RES cells and MDA-MB-435/LCC6MDR1 cells. (**B**) ATP recovery in NCI/ADR-RES cells for 4 h and 13 h. Cells were treated with test samples for 2 h at 37ºC and then samples were removed from cells. Cellular ATP levels were measured after cells were continuously incubated in fresh medium for another 4 h and 13 h. Concentrations are presented as concentrations of blank NPs #2 (sum of mass of oils and surfactants) and as concentrations of free Brij 78 and TPGS. Data are presented as the mean ± SD (n = 3). * $p < 0.05$ and # $p > 0.05$. (**C**) TEM analysis in NCI/ADR-RES, OVCAR-8 and MDA-MB-468cells treated with Dox NP #2, free Dox, and blank NP #2. Cells were treated for 1 h with samples containing Dox equivalent dose at 5 μg/ml. Treatment with Dox NPs #2 and blank NP #2 caused considerable mitochondria swelling in NCI/ADR-RES and OVCAR-8 cells, but not in MDA-MB-468 cells. The stars (✱) indicate multivesicular bodies, and the arrows (→) indicates mitochondria. Scale bar = 1 μm. (**D**) Mitochondrial potential measurement in NCI/ADR-RES cells and MDA-MB-435/LCC6MDR1 cells and their corresponding parental cells. Cells were treated with samples for 2 h at 37ºC. Mitochondrial potential detection was based on the ratio of red fluorescence caused by the accumulation of JC-1 in mitochondria and green fluorescence caused by the accumulation of JC-1 in the cytoplasm. The number before each label on x-axle indicates the concentration of tested samples (μg/ml).

Figure 7.5

Figure 7.5: The first in-vivo anti-cancer efficacy studies using pegylated PX BTM NPs in resistant mouse NCI/ADR-RES xenografts. On Day (-7), 18-19 g female nude mice (4 mice/group) received 4 x 10^6 cells by s.c. injection. Mice (n=4/group) were dosed i.v. with PX (4.5 or 2.25 mg/kg) by tail vein injection on day 0 and 7. The corresponding nanoparticle dose was 210 or 105 mg NPs/kg, respectively. Data are presented as the mean ± SD. * $p < 0.05$ and # $p > 0.05$.
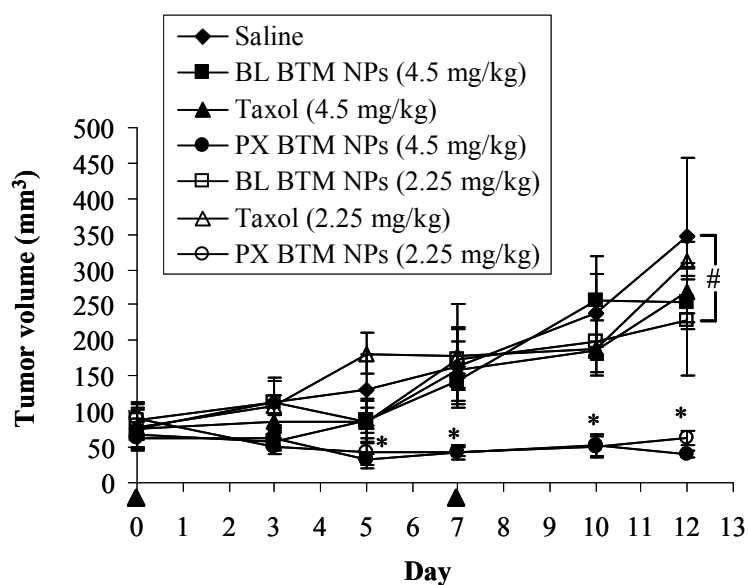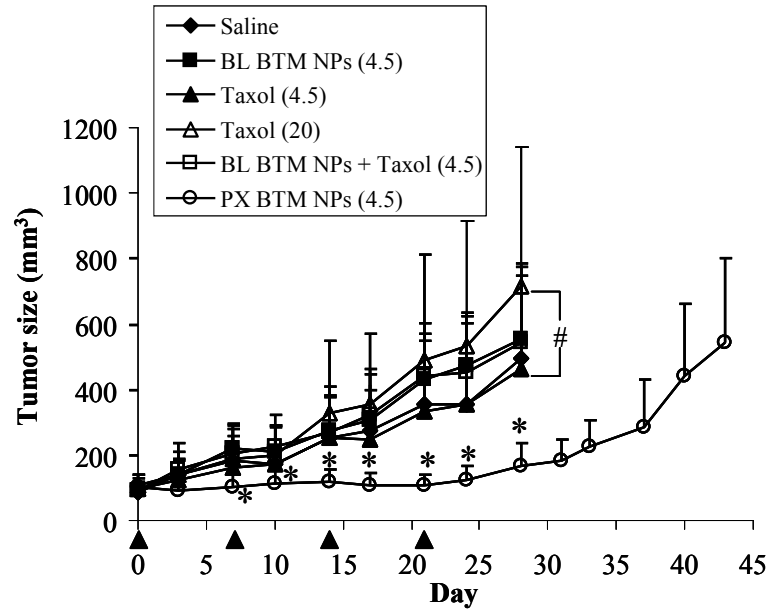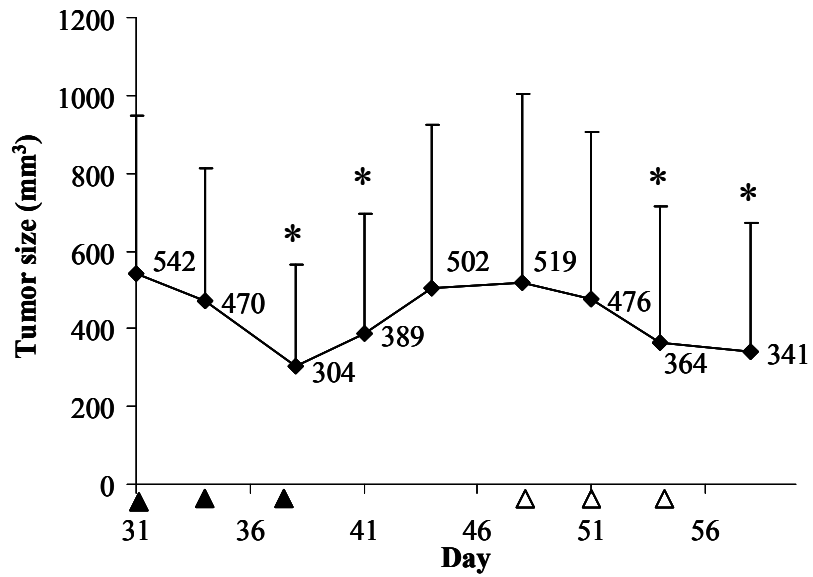
Figure 7.6

A

B

C
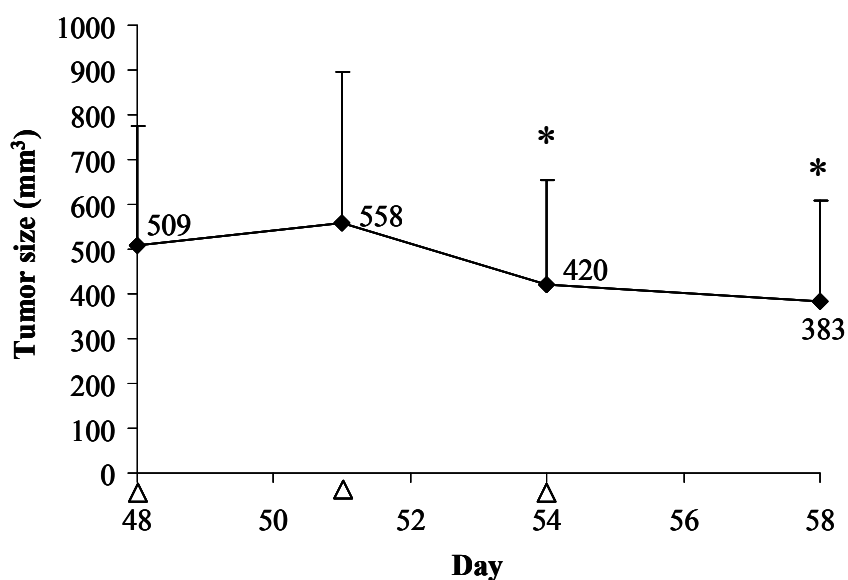
Figure 7.6: The second in-vivo anti-cancer efficacy studies using pegylated PX BTM NPs in resistant mouse NCI/ADR-RES xenografts. (**A**) The anti-cancer efficacy study. On Day (-38), 18-19 g female nude mice (6-8 mice/group) received 4×10^6 cells by s.c. injection. Mice (n=6-8/group) were dosed i.v. with PX (20 or 4.5 mg/kg) by tail vein injection on day 0, 7, 14 and 21. (**B**) Retreatment of Taxol groups with PX BTM NPs. On Day 31, Taxol groups were retreated by i.v. injection with PX BTM NPs (7.5 or 4.5 mg PX/kg) for two cycles of treatments every three days for a total of three times per cycle. (**C**) Retreatment of the PX BTM NP group. On Day 48, PX NP group was retreated by i.v. injection with PX BTM NPs (7.5 mg PX/kg) every three days for a total of three times. "▲"indicates that mice were dosed i.v. with PX BTM NPs (4.5 mg PX/kg). "Δ" indicates that mice were dosed i.v. with PX BTM NPs (7.5 mg PX/kg). Data are presented as the mean ± SD. * $p < 0.05$ and # $p > 0.05$.

Chapter 8

Summary and Conclusions

The overall goal of the studies presented herein was to investigate paclitaxel and doxorubicin-loaded nanoparticles to overcome P-gp-mediated drug resistance in solid tumors in-vivo after i.v. injection. The hypotheses driving this research were that: 1) the lipids used to form lipid nanoparticles could be metabolized in-vitro by alcohol dehydrogenase, 2) nanoparticles prepared from oil-in-water microemulsion precursors can be efficiently used to formulate paclitaxel and doxorubicin, 3) optimized nano-based paclitaxel and doxorubicin formulations will overcome P-gp-mediated tumor resistance in-vitro, and 4) paclitaxel nanoparticles will have improved anti-tumor efficacy after i.v. injection compared to free PX solution in a nude mouse xenograft model bearing P-gp-overexpressing cancer cells.

To test the metabolism of the lipids in NPs, an in-vitro study using horse liver alcohol dehydrogenase was carried out. The study demonstrated that the enzyme metabolized the lipids present in solid lipid nanoparticles. Over 80% of fatty alcohols in NPs were metabolized within 15 h in this in-vitro study. This result suggested that entrapping the lipids into solid nanoparticles did not hinder the reaction of the lipids with the enzyme. Moreover, the surfactant Brij 78 present in NPs influenced the activity of the enzyme.

In present studies, all NPs were prepared from oil-in-water microemulsion precursors. The water-insoluble drug PX was directly entrapped into lipid nanoparticles. The experimental design, a combination of Taguchi array and sequential simplex optimization, was efficiently used to develop Cremophor EL-free PX NPs. To our knowledge, this is the first report to use this combination method to optimize NP formulations via experimental design. Two injectable optimized PX NPs, including PX G78 NPs (with the solid oil glyceryl tridodecanoate) and PX BTM NPs (with the liquid oil Miglyol 812), were successfully developed. Both PX NPs had high drug loading and entrapment efficiencies with slow and sustained release profiles. Moreover, both PX NPs were physically stable at 4ºC and 37ºC. Further, both PX NPs showed similar in-vitro cytotoxicity compared to Taxol in human MDA-MB-231 breast cancer cells. Importantly,

PX BTM NPs showed unique features, such as, 1) the ability to be lyophilized without using cryoprotectants, 2) the ability to be easily sterilized by aseptic filtration with 0.2 μm filters, 3) the ability to potentially made "stealth" by adding 8% w/w/ Brij 700, and 4) good tolerability after i.v. injection in-vivo. Therefore, PX BTM NPs could be used as a novel PX formulation for i.v. injection to treat solid tumors. The water-soluble drug Dox was entrapped into lipid nanoparticles using an ion-pair complex. Several ion-pair agents were screened to quantitatively form the ion-pair complex with Dox. Finally, STS was identified as the most suitable ion-pair agent for Dox. Different compositions of NPs were developed for Dox NPs using STS as the ion-pair agent. All Dox NPs had high drug loading and entrapment efficiencies. However, relatively rapid release profiles of Dox were frequently observed in Dox NPs for all NP compositions. The variety of compositions of Dox NPs provided a number of samples to test the ability of NPs to overcome P-gp-mediated drug resistance in-vitro. These results support the hypothesis that NPs prepared from oil-in-water microemulsion precursors can be efficiently used to formulate paclitaxel and doxorubicin.

In-vitro cytotoxicity studies were performed in two paired cancer cell lines including both sensitive and resistant cells. All developed PX and Dox NPs in the present studies were tested. In the sensitive cells, PX and Dox NPs showed the same or comparable cytotoxicity. In the P-gp-overexpressing resistant cancer cells, all of Dox NPs showed 6-8-fold lower IC50 values than those of free Dox, and PX NPs decreased IC50 values up to 13-fold compared to free PX. Interestingly, even mixtures of blank NPs and free drugs showed similar cytotoxicity to drug-loaded NPs. To understand the mechanisms by which NPs could overcome P-gp-mediated resistance in-vitro, a series of in-vitro assays were carried out in both sensitive and resistant cells, including quantitative studies on uptake and efflux, inhibition of Calcein AM efflux, alteration of ATP levels, membrane integrity, mitochondrial membrane potential, apoptosis and MTT assay. Cellular uptake and efflux studies demonstrated that Dox NPs enhanced the uptake and prolonged the retention of the drug inside cells, and NPs entered cells by endocytosis pathways. Calcein AM and ATP studies demonstrated that blank NPs inhibited P-gp function and transiently depleted intracellular ATP. The surfactant Brij 78 could be the key component for ATP depletion. Further studies on apoptosis and mitochondria suggested that ATP depletion by blank NPs could be correlated to the enzyme activity in mitochondrial respiratory chain,

mitochondrial membrane potential, the observed swelling of the mitochondrial. The correlation was dominant in P-gp-overexpressing cancer cells. To the best of our knowledge, this is the first report on nanoparticles which can inhibit P-gp efflux and deplete ATP.

In-vivo anti-cancer efficacy studies were performed in mice bearing NCI/ADR-RES resistant tumors. To obtain "stealth" NPs which could escape the RES system, PX BTM NPs were pegylated with 8% w/w Brij 700 (based on the ratio of Brij 700 to the oil) using an optimized composition of PX BTM NPs. Two different doses of pegylated PX BTM NPs were used to treat these tumors after i.v. injection, and both of them significantly inhibited tumor growth compared to other control groups. Importantly, blank BTM NPs were well tolerated to mice. They did not show any clinical signs of toxicity even at the highest dose of 210 mg NPs/kg given weekly over three weeks.

These in-vitro and in-vivo studies together support the hypotheses that optimized nano-based paclitaxel and doxorubicin formulations will overcome P-gp-mediated tumor resistance in-vitro, and paclitaxel nanoparticles will have improved anti-tumor efficacy after intravenous injection compared to free PX solution in a nude mouse xenograft model bearing P-gp-overexpressing cancer cells. It was demonstrated that blank NPs themselves were P-gp inhibitors. PX BTM NPs had a slow and sustained release profile. By combining the benefits of NPs, such as long circulation and ERP effect, the properties of these NPs to inhibit P-gp and deplete ATP provide significant potential and a novel strategy to the enhance anti-cancer efficacy of drugs in resistant tumors. Therefore, P-gp inhibitors (NPs) and the anti-cancer drug (PX) could reach tumor cells at the same time and work together. This unique property of PX NPs could greatly enhance the uptake and retention of the drug in these resistant tumors to improve the therapeutic responses.

In conclusion, these studies highlight the potential application of PX and Dox-loaded NPs prepared from oil-in-water microemulsion precursors for enhancing anti-cancer efficacy of drug in P-gp-mediated resistant tumors. The combination of Taguchi array and sequential simplex optimization efficiently guided the development and optimizations of lipid-based PX NPs. Injectable PX NPs were successfully developed. Interestingly, PX BTM NPs could be lyophilized without cryoprotectants. Dox-loaded NPs were also prepared using an ion-pair strategy. PX and Dox-loaded NPs decreased IC50 values in-vitro in resistant tumor cells compared to free drugs. Of significant importance is

the demonstration that blank NPs were P-gp inhibitors and depleted intracellular ATP levels, resulting in maintaining high intracellular drug levels in resistant cancer cells. The mechanism of P-gp inhibition and ATP depletion distinguishes these Brij 78-based NPs from other known nanoparticles and liposome-based carrier systems. In-vivo anti-cancer efficacy further demonstrated the potential of PX BTM NPs containing both an anti-cancer drug and a P-gp inhibitor to enhance therapeutic responses in resistant tumors. Therefore, the use of PX-loaded NPs could provide an excellent alternative and a novel therapeutic strategy to overcome P-gp-mediated drug resistance in solid tumors.

The studies presented in the dissertation illustrate the potential application of drug-loaded NPs for overcoming P-gp-mediated drug resistance and have established the underlying in-vitro mechanisms. However, additional experiments will be necessary to further characterize and optimize these systems. Although novel PX BTM NPs were developed, pegylation of PX BTM NPs was not well optimized in these studies, especially to make pegylated PX BTM NPs in 10% lactose for i.v. injection. Furthermore, the current mechanistic studies were based on in-vitro assays. It must be recognized that there are difference between in-vitro and in-vivo mechanisms. Additional in-vivo studies are needed to further understand why pegylated PX BTM NPs showed marked anti-cancer efficacy in resistant tumors. The answers discussed above, such as the utilization of EPR effect and synergetic action of blank NPs and drugs, are only hypotheses. At this point, information on the biodistribution and pharmacokinetics of PX NPs are missing. In addition, other in-vitro mechanistic studies are worthy of investigation. Besides inhibition of P-gp function, blank NPs may influence other biological responses such as GSH/GST detoxification system, cell apoptosis signaling and cellular defensive mechanisms (Table. 3.2). These further studies may provide new opportunities for NPs to overcome drug resistance caused by other mechanisms, not just P-gp-mediated resistance. Moreover, the present studies on the mechanism demonstrated that blank NPs depleted ATP. Most of transporters involved in MDR are ATP-dependent. Thus, it is worthy to test drug-loaded NPs in other transporter-mediated MDR, e.g. MRP-mediated resistance. NPs could overcome these MDR in term of the same mechanisms presented in the dissertation. These additional studies together could extend and reveal further improvements or alternative formulation approaches to overcome MDR.

Appendices

This section contains the following additional experiments:

Appendix A: Development of TGF-α-coated nanoparticles to target EGF
receptors in cancer cells

Appendix B: Subset of figures in Chapter 7

Appendix A

Development of TGF-α-coated nanoparticles to target
EGF receptors on cancer cells

A.1   Introduction

EGFR is a cell surface transmembrane receptor overexpressed in various cancers and in many cases the extent of expression has been correlated with the stage of disease and poor prognosis. TGF-α, a biologically active polypeptide, is one of the ligands that bind to the EGF receptor. After TGF-α binding, the ligand-occupied EGFR is rapidly internalized in a process termed ligand-induced endocytosis, and TGF-α dissociates from EGFR very shortly after internalization. The recycling of EGFR to the cell surface will sustain the original ligand-binding ability of the cells.

In previous sections, we developed new lipid-based BTM NPs. Pegylated PX-loaded BTM NPs showed enhanced anti-cancer efficacy in mice bearing resistant xenograft tumors. To further improve the efficacy, this study investigated the active targeting delivery using TGF-α as a ligand attached on NP surface to target EGFR-overexpressing cancer cells. BTM NPs were selected as the prototype NPs. TGF-α was first conjugated with tresylated Brij 700 (or Steareth-100) which contains a lipid chain and PEG moiety with molecular weight of 4400. Brij 700-TGF-α conjugate was coated on fluorescent-labeled BTM NPs by a post-insertion method. Cell uptake of targeted and non-targeted fluorescent-labeled BTM NPs was quantitatively measured by a microplate reader and also evaluated by fluorescence microscopy.

A.2   Stability of TGF-α after exposure to different temperatures

TGF-α is a peptide with MW 5500 Da. Biological stability of TGF-α is a concern for the preparation and storage of TGF-α-coated NPs. To prepare TGF-α-coated NPs from microemulsion precursors, TGF-α needs to be heated at least for 10-20 min at 65ºC. Also, after TGF-α powder was reconstituted in an aqueous solution, the stability of TGF-α in the aqueous solution may become a problem. To understand the biological stability of TGF-α after exposure to different temperatures in the process of preparation of NPs, a competition binding assay of TGF-α was developed to evaluate binding activity of TGF-α to EGFR. The binding activity was used as an indicator for the biological stability of TGF-α for the targeting purpose.

The binding assay was performed in human epidermal carcinoma A431 cells which are known to overexpress EGFR (2×10^6 receptors/cell). A431 cells were seeded onto 96-well plates at a density of 1×10^5 cells/well. The cells were incubated in 100 μl DMEM medium supplemented with 10% fetal bovine serum (FBS) at 37ºC for 24 h. The medium was removed and the cells were washed twice with binding buffer (DMEM containing 20 mM HEPES, pH 7.4, and 0.1% BSA). TGF-α and EGF-Biotin samples were applied to cells in binding buffer. In saturation binding experiments, serial dilutions of EGF-Biotin were added into the wells. In competition binding experiments, mixtures of a fixed concentration of EGF-Biotin with different concentrations of TGF-α were added into the wells. A high concentration of EGF-Biotin was used to measure non-specific binding. After incubation for 2 h on ice, the cells were washed twice with binding buffer. A fixed concentration of HRP-conjugated streptavidin was added into each well and incubated for 1 h at room temperature. The cells were then washed twice with ice-cold PBS supplemented with 0.1% BSA and twice with ice-cold PBS. One hundred microliters of TMB reagent were added to the wells and incubated for 15 min at room temperature, and then 100 μl of 2 M sulfuric acid were added to stop the reaction. The absorbance of each well was measured at 450 nm by a microplate reader. Each concentration was performed in duplicate. The binding constant (K_d) of EGF-Biotin was obtained using Prism by fitting the curve with non-linear regression and the inhibition constant (K_i) of TGF-α was calculated based on the competition binding assay using following equation:

$$K_i = \frac{EC50}{1 + \dfrac{D}{K_d}}$$

where D is the concentration of EGF-Biotin, K_d is the binding constant of EGF-Biotin, and EC50 is the concentration of TGF-α at 50% of the maximum OD value. The saturation binding of EGF-Biotin and the competition binding of TGF-α are shown in Figure A.1.A and Figure A.1.B, respectively. The binding constant of EGF-Biotin to EGFR was 1.15 nM. The inhibition constant of TGF-α was 15.6 nM.

TGF-α was stored at room temperature and -4ºC for 24 h, -20ºC for one week, and was heated at 70ºC for 45 min, respectively. After these treatments, the competition binding was carried out for these treated TGF-α. The binding activities of TGF-α to EGFR were compared based on the binding constants of TGF-α. Under all tested conditions, the results of the competition binding assays demonstrated that the inhibition constants of TGF-α had slight difference (Figure A.2). Therefore, the binding activity of TGF-α to EGFR remained the same after the treatments.

A.3 Conjugation of TGF-α with tresylated-Brij 700

There are several ways to attach ligands on a NP surface. A common method called pre-insertion is to prepare activated NPs and then conjugate the ligand to the activated surface. This method sometime is problematic not only due to exposure of the functionalized NPs but also due to the possible reaction of the functional groups with other components on the NPs. A post-insertion method could avoid the problems from the pre-insertion method. Thus, in these studies, the post-insertion method was utilized to attach TGF-α to the surface of NPs. First, the targeting ligand was conjugated to the functionalized terminus of PEG. Then, the lipid-PEG ligand conjugate was inserted into NPs using the lipid as an anchor. Generally, the ligand is covalently linked to a PEG, molecule that has been functionalized with a thiol-, amine-, or carboxyl- group. However, the conjugation efficiency generally is not high. The hydroxyl group of PEG-sterol was activated with a tresyl group and reacted with the amine group on a protein [354]. After 12 h, the conjugation of protein with the activated PEG-sterol was almost complete. In our lab, the hydroxyl group of the surfactant Brij 78 was functionalized using tresyl chloride. The tresylated Brij 78 further reacted with the primary amine of the model antigen ovalbumin (OVA) to yield Brij 78-OVA conjugate. Brij 700 containing a lipid chain and PEG moiety has a similar chemical structure with Brij 78 although the one difference between them is the length of PEG moiety which has molecular weight of 4400 in Brij 700 and 880 in Brij 78. It was proposed that tresyl chemistry could be used to conjugate TGF-α to Brij 700, and that Brij 700 could improve the loading of TGF-α conjugate onto the surface of the BTM NPs. It has been reported that the A and C loops and the C-terminal tail of TGF-α contain residues that form the major binding interface with EGFR. To retain the activity of TGF-α, an N-terminal site-specific conjugation of TGF-α with PEG was desired. The competition binding assay was performed to evaluate the binding activity of TGF-α conjugate.

Tresylated Brij 700 (T-Brij 700) was synthesized as previously described with some modification [355]. Brij 700 (2.56 g) was dissolved in 20 ml of dichloromethane and incubated at 0ºC. One gram of tresyl chloride and 500 μl of pyridine were added to Brij 700 solution by a drop-wise method. The reaction solution was stirred for 18 h at room temperature under nitrogen atmosphere. Then, the organic solvents were removed by a rotary evaporator and the precipitates were dissolved in 100 ml of ethanol acidized with

163

420 μl of HCl at room temperature. The solution was kept at -20ºC overnight. Reformed precipitates were centrifuged at -5ºC. After removing the supernatant, the precipitates were redissolved in 100 ml of acidic ethanol. The supernatant was tested for UV absorbance at 255 nm for trace pyridine. The washing steps were repeated until the UV absorbance of pyridine was minimum and constant. The T-Brij 700 was dried over desiccators and stored at -20°C under nitrogen.

To prepare Brij 700-TGF-α conjugate, 1.5 mg of T-Brij 700 and 180 μg of TGF-α (about 100:1 molar ratio, T-Brij 700: TGF-α) were mixed and dissolved into 600 μl of 0.1 M HEPES buffer (pH 7.4). The reaction was kept for 18 h at room temperature. After 18 h reaction, the unreacted tresyl groups were blocked using 100 μl of 20 mM Tris-HCl buffer (pH 8.0) for 1 h. After reaction, free TGF-α and Brij 700-TGF-α conjugate were separated on a Sephedex G-100 column using 0.1M HEPES buffer pH 7.4 as the mobile phase. Thirty fractions (about 1 ml for each) were collected and tested using a Duoset ELISA kit for TGF-α (R&D System, Minneapolis, MN). In a separate experiment, 100 μg of free TGF-α were eluted from the same column to determine the fractions containing free TGF-α. The chromatographs of free TGF-α and Brij 700-TGF-α conjugate were compared to estimate the conjugation efficiency. Fractions 1-8 containing the conjugate were concentrated using Centriplus YM-3 (MWCO 3000 Da) to 700 μl of the conjugate solution. The concentration of TGF-α in the conjugate solution was measured using a Duoset ELISA kit for TGF-α. The binding activity of the conjugate was tested using the competition binding assay so as to determine if the conjugate could compete with EGF-Biotin for binding to the EGFR.

Brij 700-TGF-α conjugate was successfully synthesized using tresyl chemistry as the band of Brij 700-TGF-α conjugate (MW 10 kDa) was clearly shown on the gel (Figure A.5). Very small fractions of free TGF-α in the solution of the conjugation were observed (Figure A.3). Moreover, on the gel, the band of free TGF-α was not detected in the solution of the conjugation (Figure A.5). These results indicated that the conjugation efficiency was high. Sixty seven (67) micrograms of TGF-α were detected in the 700 μl of final purified Brij 700-TGF-α conjugate. Therefore, the total conjugation yield was 29.3% (n=2). This low yield may be due to the lost of Brij 700-TGF-α conjugate during the process of the purification and concentration. The competition binding of Brij 700-TGF-α conjugate is

shown in Figure A.4. There was no difference in the inhibition constant of Brij 700-TGF-α conjugate compared to free TGF-α.

A.4 Preparation and characterization of TGF-α-coated BTM NPs containing BODIPY 558/568 C12

To efficiently load TGF-α on BTM NPs, the composition of the optimized BTM NP formulation for the in-vivo efficacy studies was used to make TGF-α-coated BTM NPs. To label BTM NPs with a fluorescent molecule, 50 μg/ml BODIPY 558/568 C12 were entrapped into the BTM NPs. To prepare non-targeted BTM NPs containing BODIPY 558/568 C12, 2.5 mg of Miglyol 812, 1.5 mg of TPGS and 2.8 mg of Brij 78 were weighed into a glass vial and heated to 65ºC. Fifty micrograms of BODIPY 558/568 C12 dissolved in ethanol were added into the melted oil and surfactants. The ethanol was removed using a nitrogen stream. One (1) ml of filtered and D.I. water pre-heated at 65ºC was added into the mixture of melted oil and surfactants. The mixture were stirred for 20 min at 65ºC and then cooled to room temperature. To prepare TGF-α-coated NPs, different volumes of water (950 μl, 900 μl or 800 μl) were, respectively, added into the melted excipients with BODIPY 558/568 C12 and stirred for 15 min at 65ºC, and then the Brij 700-TGF-α conjugate at different volumes (50 μl, 100 μl or 200 μl) was added into the warm microemulsion to make a final volume of 1 ml TGF-α-coated NPs containing different concentrations of TGF-α. The warm microemulsion was continually stirred at 65ºC for another 10 min before cooling to room temperature. After cooling, the NP suspension was stirred for 4 h at room temperature. The particle size and size distribution of NPs were measured using a N5 Coulter Submicron Particle Size Analyzer. To measure the entrapment efficiency of BODIPY 558/568 C12 in NPs, non-targeted BODIPY 558/568 C12 BTM NPs were purified using a Centriplus Y-100 (MWCO 100 kDa). The non-purified and purified NPs were measured at 480 nm using a microplate reader to determine the entrapment efficiency of BODIPY 558/568 C12. To measure the loading efficiency of TGF-α in NPs, TGF-α-coated NPs were separated from the free Brij 700-TGF-α conjugate using a Centriplus Y-100 and reconstituted to make a 1 ml suspension. The concentration of TGF-α in the filtrate was determined using the ELISA kit above and the loading efficiency of TGF-α was calculated. To evaluate the purification efficiency of the Brij 700-TGF-α conjugate and TGF-α-coated NPs, PAGE gel separation was performed using a tris-tricine natural gel. Defined amounts of free TGF-α, the reaction solution of the conjugation, purified Brij 700-TGF-α conjugate and

TGF-α-coated NPs were loaded into the well of Ready Gel 16.5% Tris Tricine gel (Bio-rad, Hercules, CA). Also, TGF-α-coated NPs were heated for 30 min at 90ºC before loaded to the gel in order to release TGF-α from NPs and compared with non-heated TGF-α-coated NPs. The gel was soaked into running buffer and a voltage of 100 v was applied for 1.5 h. After separation, the gel was stained by SilverSNAP Stain kit (Pierce, Rockford, IL).

All resulting NPs had particle sizes less than 220 nm. The entrapment efficiency of BODIPY 558/568 C12 in BTM NPs was 90%. Different concentrations of Brij 700-TGF-α conjugate were coated on BODIPY BTM NPs. The final concentrations of TGF-α and the loading efficiencies are shown on Table A.1. Up to 16.6 µg/ml of TGF-α were coated on the surface of BTM NPs with a loading efficiency higher than 80%. Also, gel electrophoresis showed that there was no free TGF-α or Brij 700-TGF-α conjugate in purified TGF-α-coated NP suspension (Figure A.5). After heating, TGF-α on TGF-α-coated NP surface was released from Brij 700-TGF-α conjugate, or the Brij 700-TGF-α conjugate was released from NPs. Two clear bands, one for TGF-α (5.5 kDa) and the other for Brij 700-TGF-α conjugate (10 kDa), were shown on the gel for heated TGF-α-coated NPs.

A.5 Cellular uptake of TGF-α-coated BODIPY 558/568 C12 BTM NPs in NCI/ADR-RES and MDA-MB-468 cells

NCI/ADR-RES or MDA-MB-468 cells were seeded in 48-well plates at a density of 2×10^5 cells/well overnight. After washing with PBS, cells were incubated with BTM NPs for 2 h. The NPs contained BODIPY 558/568 C12 (0.4 µg/ml) and had different concentrations of TGF-α on the surface. To test the influence of EGF on the targeting, EGF was added into TGF-α-coated NPs to compete with TGF-α in the uptake study. Then cells were washed with ice-cold PBS twice and lysed with PBS containing 1% Triton X-100. The fluorescence in the lysates was measured using a fluorescence microplate reader. The total proteins in cell lysates were measured by BCA assay. The uptake was normalized with protein content. Cellular uptake in NCI/ADR-RES cells was also measured using fluorescence microscopy.

TGF-α-coated BTM NPs did not show enhanced uptake in both NCI/ADR-RES and MDA-MB-468 cells as shown in Figure A.6.A and Figure A.6.B as compared to non-targeted BTM NPs (BL C12 BTM NPs) ($p > 0.05$). Actually, the uptake of TGF-α-coated BTM NP decreased when cells treated with the NPs containing the highest TGF-α concentration on the surface ($p < 0.05$) (Figure A.6.A). In the presence of EGF, the uptake also increased compared with non-targeted NPs. Moreover, TGF-α-coated NPs did not show stronger fluorescent density on the fluorescence images compared with non-targeted NPs (Figure A.7). Based on the uptake of non-targeted NPs in NCI/ADR-RES, the uptake of non-targeted BTM NPs was 27% of the total added NPs. This was a very high uptake ratio compared to other NPs in literature or even NPs #2 in Chapter 6 which normally had cellular uptake of about 5-10% of the total dose. Thus, it is possible that the reason for no difference between TGF-α-coated NPs and non-targeted NPs in the uptake study may be the high uptake of non-targeted NPs with no ligand.

A.6　Conclusions

These studies demonstrated that the Brij 700-TGF-α conjugate could be synthesized using tresylated Brij 700. The Brij 700-TGF-α conjugate could be successfully coated on the surface of optimized BTM NPs with different concentrations of TGF-α. Moreover, BODIPY 558/568 C12 could be a suitable fluorescent molecule to label BTM NPs with very high entrapment efficiency. The cellular uptake studies indicated that uptake of TGF-α-coated BTM NPs was similar as that of non-targeted BTM NPs, probably due to the intrinsic high uptake of non-targeted BTM NPs.
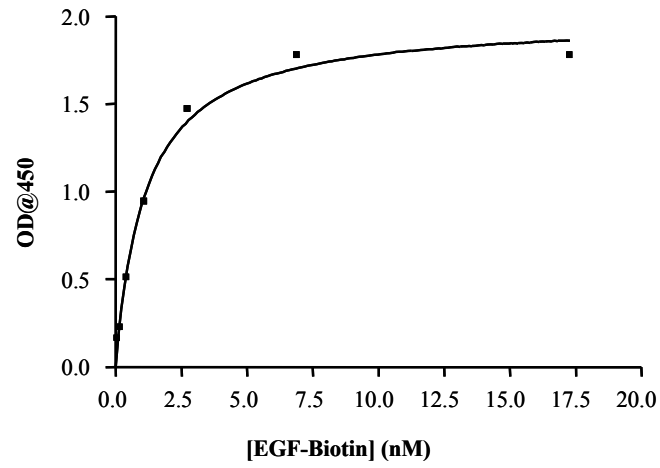
Table A.1. Characterization of TGF-α-coated BTM NPs containing different concentrations of TGF-α on the NP surface.

(BT stands for Brij 700-TGF-α conjugate)

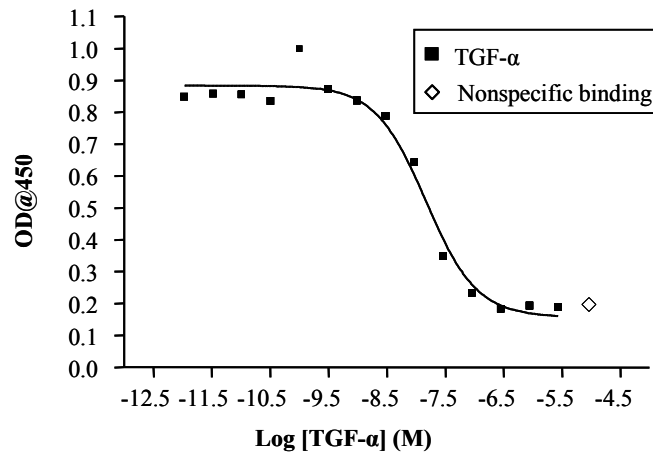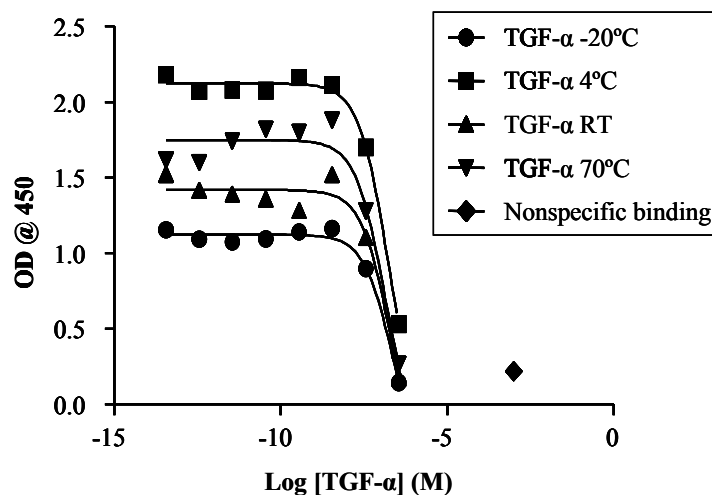| Added BT into NPs (μl)	50	100	200
TGF-α on NPs (μg/ml)	4.3	7.6	16.6
Coating %	87.9	79.3	86.5

Figure A.1

A

B

Figure A.1: The binding assays of EGF-Biotin and TGF-α in EGFR-overexpressing A431 cells. (**A**) Saturation binding of EGF-Biotin. (**B**) Competition binding studies between TGF-α and EGF-Biotin. Each experiment was done in duplicate.

Figure A.2

	TGF-α -20ºC	TGF-α 4ºC	TGF-α RT	TGF-α 70ºC
K_i (× 10^{-8} M)	6.94	5.02	6.19	4.00

Figure A.2: Stability of TGF-α after exposure to various temperatures. The stability of TGF-α was indicated by the binding activity of TGF-α to EGFR measured by the competition binding assay. TGF-α was incubated at -20ºC for one week, 4ºC and room temperature overnight and at 70ºC for 45 min (to simulate NP preparation conditions). Each experiment was done in duplicate.

Figure A.3
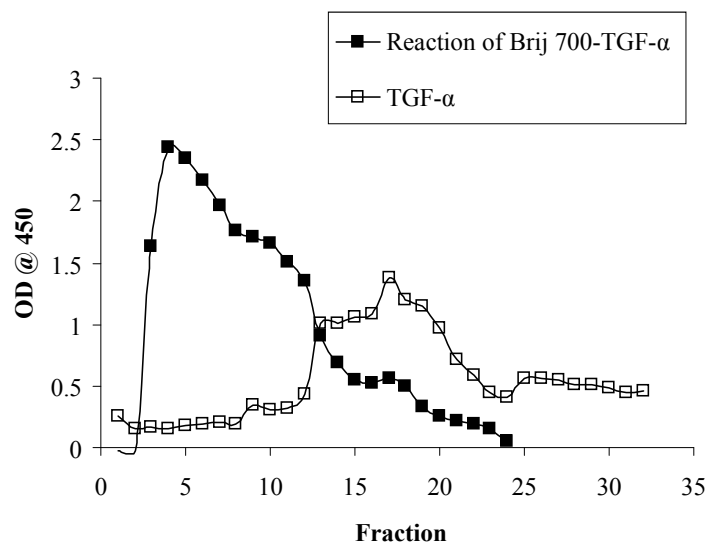
Figure A.3: Separation of the Brij 700-TGF-α conjugate and free TGF-α on a Sephedex G-100 column. The mobile phase was 0.1 M HEPES buffer (pH 7.4). Free TGF-α started to be eluted after fraction 10. Fractions 1-8 were collected as the purified conjugate to prepare TGF-α-coated NPs.
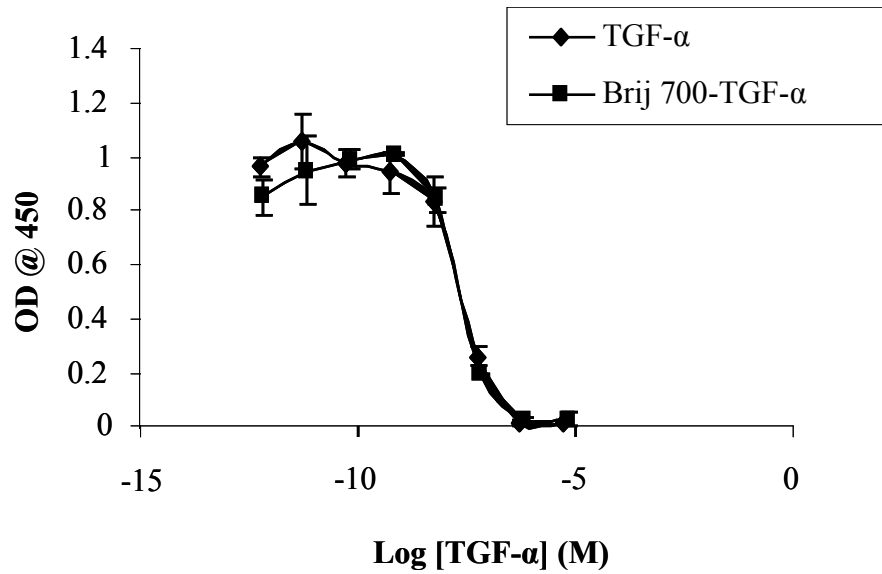
Figure A.4: Competition binding assay for the Brij 700-TGF-α conjugate compared with free TGF-α. The synthesized Brij 700-TGF-α conjugate shows similar binding activity as free TGF-α. Data are presented as the mean ± SD (n = 3).

Figure A.5
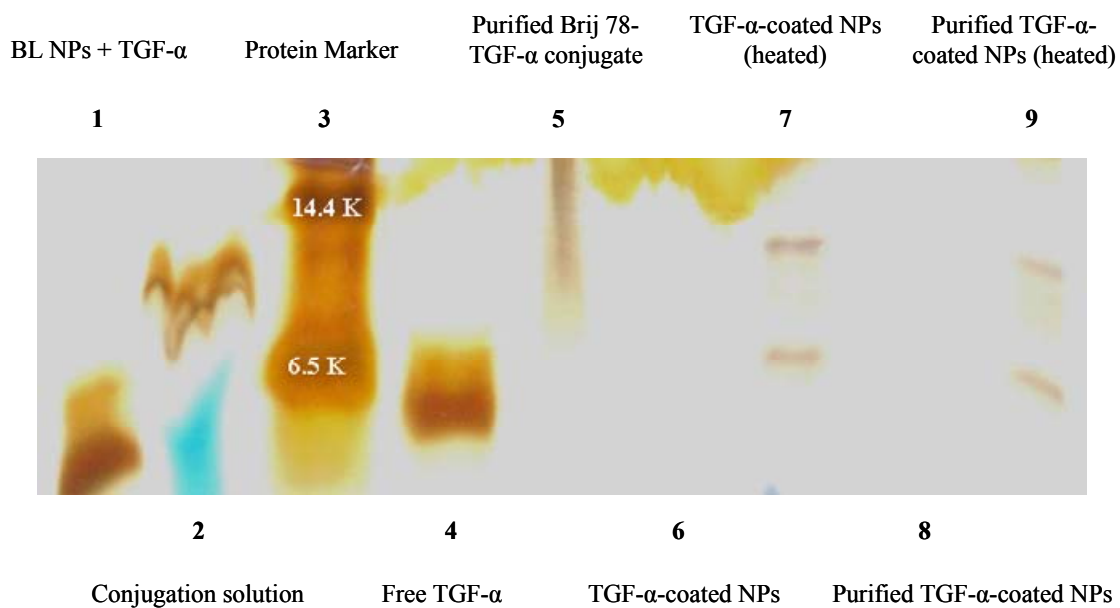
Figure A.5: **PAGE gel separation of free TGF-α, the reaction solution of the conjugation, purified Brij 700-TGF-α conjugate and TGF-α-coated NPs**. Separation was performed on a tris-tricine gel in a natural condition. The mixture of blank NPs and TGF-α was used as the control. TGF-α-coated NPs (purified and non-purified) were also heated for 30 min at 90ºC before loaded on the gel to release TGF-α or Brij 700-TGF-α conjugate from NPs.

Figure A.6

A.
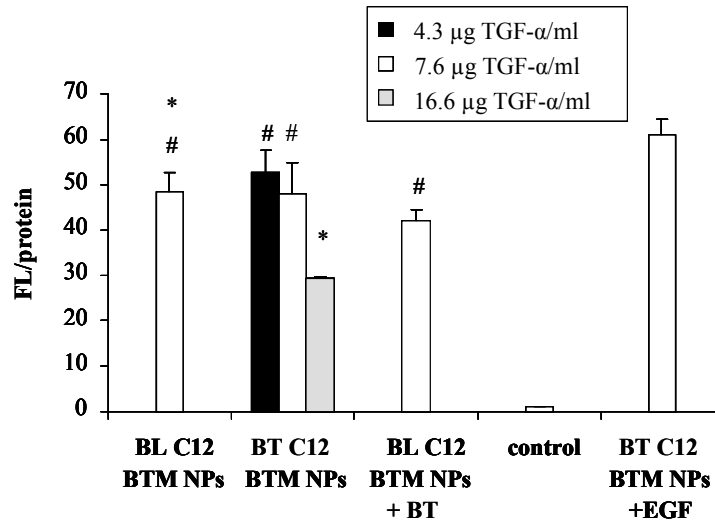
B.
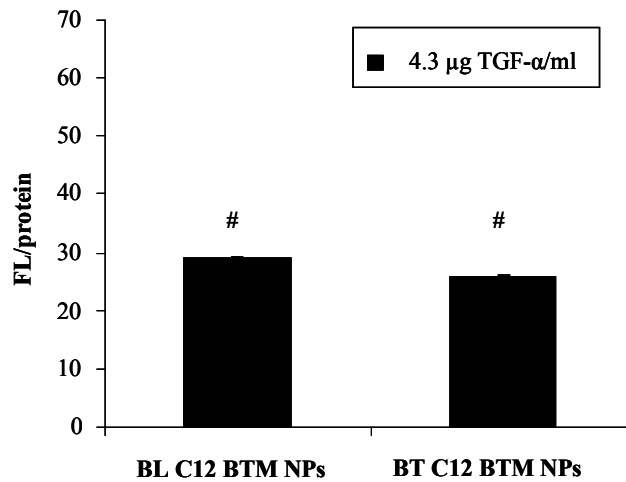
Figure A.6: **Uptake of TGF-α-coated BTM nanoparticles containing BODIPY 558/568 C12 in NCI/ADR-RES cells (A) and MDA-MB-468 cells (B).** Cells were seeded in a density of 2×10^5 cells/well on 48-well plates overnight. After washing with PBS, cells were incubated with BTM NPs containing different concentrations of TGF-α on the surface for 2 h. Then cells were washed with ice-cold PBS twice and lysed with PBS containing 1% Triton X-100. The fluorescence in the lysates was measured by a fluorescence microplate reader. The total proteins in cell lyses were measured by BCA

assay. The uptake was normalized with protein content. Data are presented as the mean $\pm$ SD (n = 3). # $p > 0.05$ and * $p < 0.05$. BT stands for Brij 700-TGF-α conjugate.

Figure A.7

| TGF-α-coated BTM NPs | BL BTM NPs |
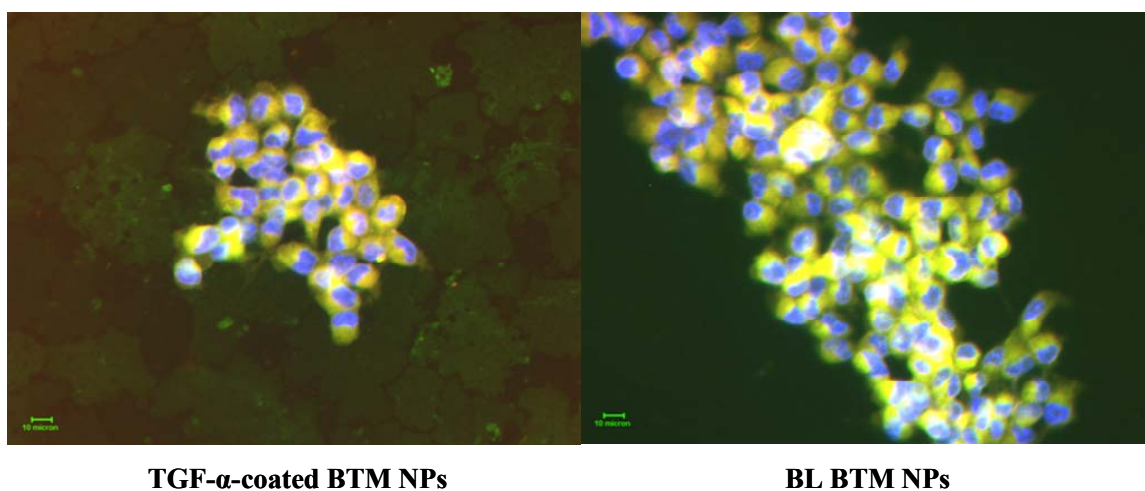
Figure A.7:   Uptake of TGF-α-coated BTM NPs and blank BTM NPs in NCI/ADR-RES at 2 h. NPs contained BODIPY 558/568 C12 (yellow color). Cell nuclei were stained with 4', 6-diamidino-2-phenylindole dihydrochloride (Dapi, 0.17 µl/ml in PBS) (blue color).

Subset of figures in Chapter 7

Figure B.1
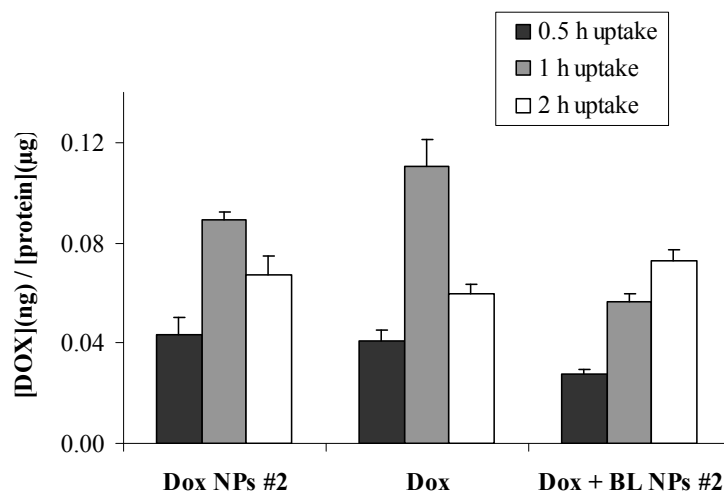
Figure B.1: Cellular uptake of Dox in NCI/ADR-RES cells at 4ºC for 2 h. Cells were incubated with samples at 5 µg/ml of Dox equivalent doses for 2 h. The uptake of Dox at 4ºC with Dox NPs #2 and free Dox was 24-fold lower and 10-fold lower than those at 37ºC, respectively. The differences between NP groups and free Dox were significantly reduced at 4ºC. Temperature-dependent uptake of Dox NPs #2 in NCI/ADR-RES cells indicates an endocytosis pathway of NP uptake. Data are presented as the mean ± SD (n = 3).

Figure B.2

| Dox NPs #2 | Dox |
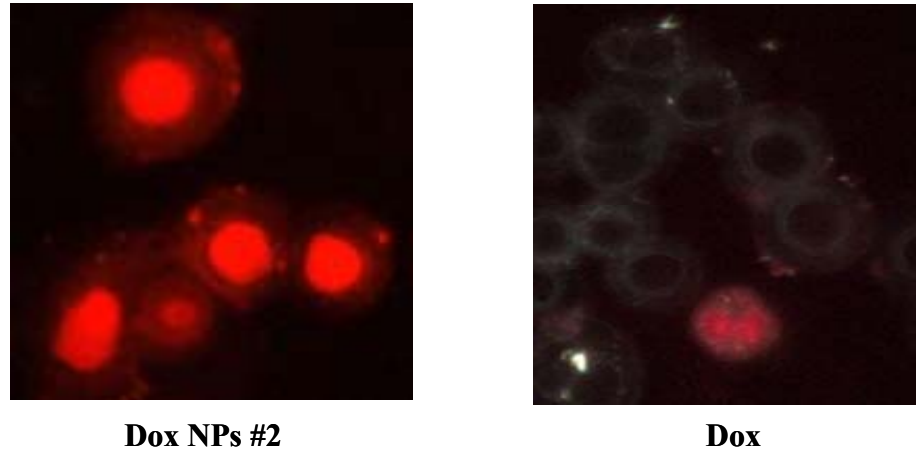
Figure B.2: Uptake of Dox NPs #2 and free Dox in MDA-MB-468 cells after 15 min of incubation as observed by Cytoviva fluorescence microscopy. MDA-MB-468 cells $(1 \times 10^5$ cells/well) in medium were plated onto glass coverslips and incubated overnight. After the coverslips were washed once with EBSS buffer, Dox NPs #2 and free Dox (5 µg/ml of Dox equivalent doses) were added on the coverslips corresponding to a Dox weight of 20 µg. Images were obtained at room temperature after 15 min using fluorescence microscopy (Cytoviva). The results show that the Dox NPs #2 very rapidly entered MDA-MB-468 cells and Dox localized quickly and extensively inside the nuclei of cells.
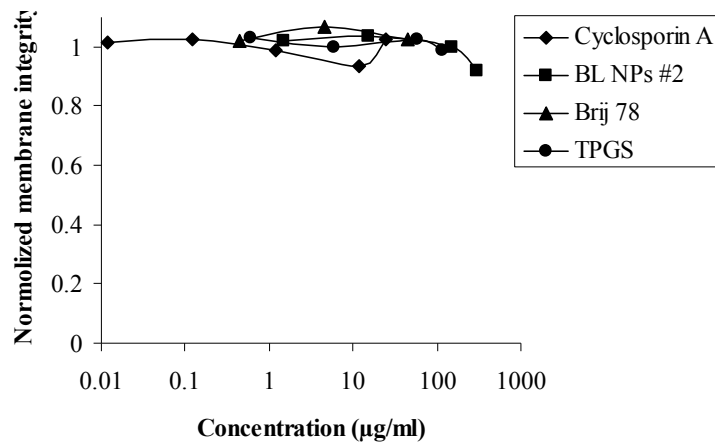
Figure B.3: Membrane integrity of NCI/ADR-RES cells treated with blank NPs #2, Brij 78 and TPGS. The integrity of the cell membrane under the conditions of the Calcein AM assay was determined using the trypan blue exclusion assay. Cells were trypsinized and plated onto 96-well plates at a density of 1×10^5 cells/well in EBSS buffer. After cells were treated with the samples under the conditions of the Calcein AM assay, 0.4% trypan blue solution were added to evaluate the membrane integrity. Each sample was measured in triplicate. Concentrations of blank NPs #2, Brij 78 and TPGS were calculated based on Dox equivalent doses.
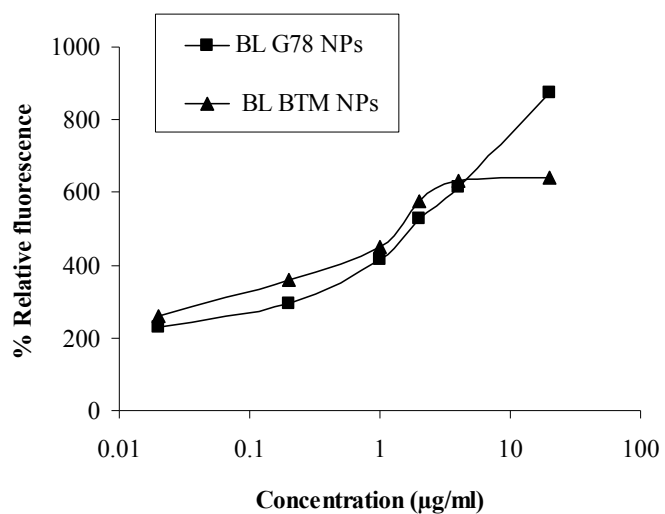
Figure B.4: Dose response of blank G78 NPs and blank BTM NPs in Calcein AM assay in NCI/ADR-RES cells. Concentrations of blank G78 NPs and BTM NPs were calculated based on PX equivalent doses. Data are presented as the mean of triplicate measurements.

Figure B.5
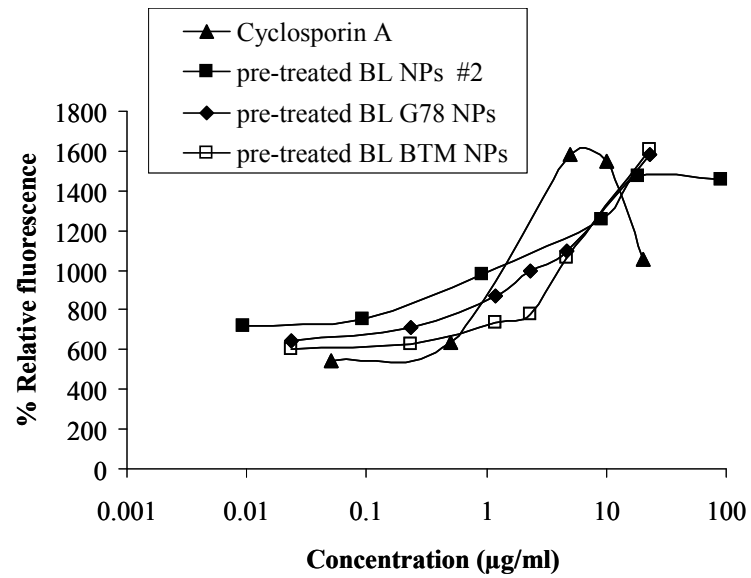
Figure B.5: Dose response of blank NPs in Calcein AM assay in NCI/ADR-RES cells in pre-treatment conditions. Cells were pretreated with blank NPs #2, blank G78 NPs and blank BTM NPs for 0.5 h, respectively. Then blank NPs were removed and Calcein AM assays were performed. Concentrations of samples were calculated based on drug equivalent doses. Data are presented as the mean of triplicate measurements.

Figure B.6
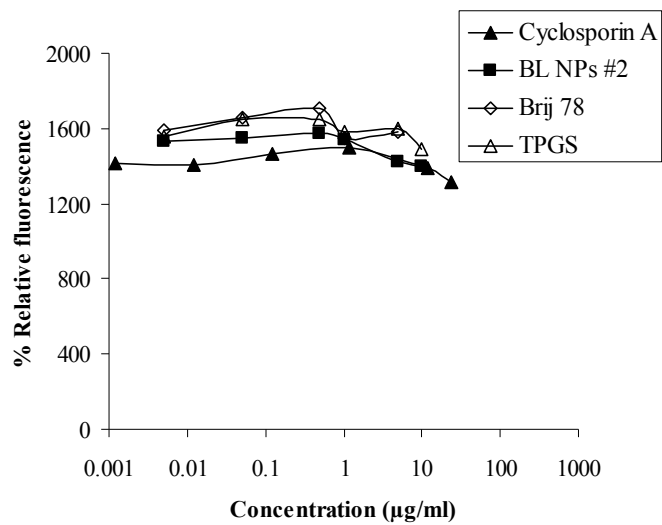
Figure B.6: Dose response of blank NPs #2 and surfactants in calcein AM assay in MDA-MB-468 cells. Concentrations of blank NPs #2, Brij 78 and TPGS were calculated based on Dox equivalent doses. Data are presented as the mean of triplicate measurements.

Figure B.7
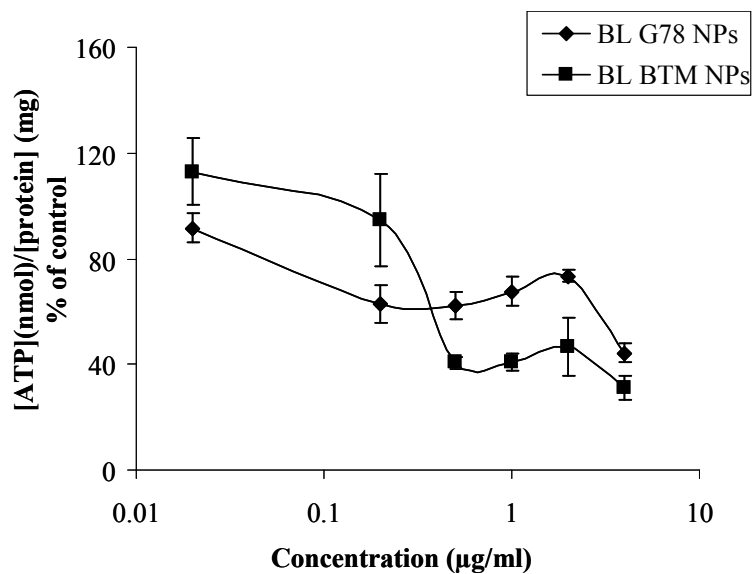
Figure B.7:   The effects of blank G78 NPs and blank BTM NPs on ATP levels in NCI/ADR-RES cells. Concentrations of blank G78 NPs and blank BTM NPs were calculated based on PX equivalent doses. The ATP levels in NCI/ADR-RES cells decreased in a dose-dependent manner. These results demonstrate that blank G78 NPs and BTM NPs also had the ability to deplete ATP in P-gp-overexpressing cancer cells. Data are presented as the mean $\pm$ SD (n = 3).

Figure B.8

A
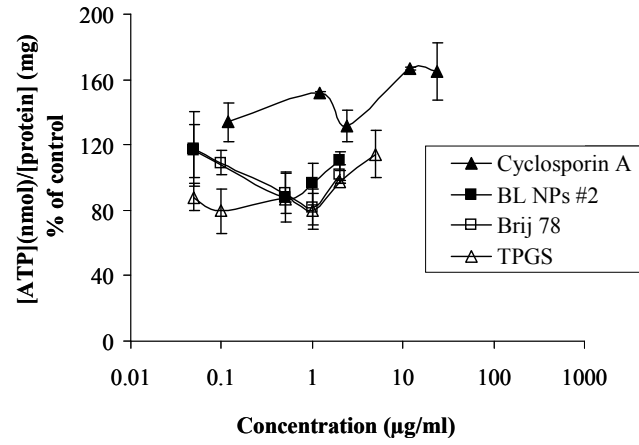
B
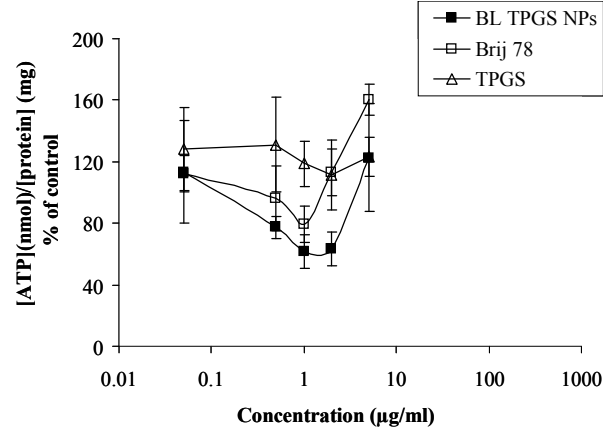
C
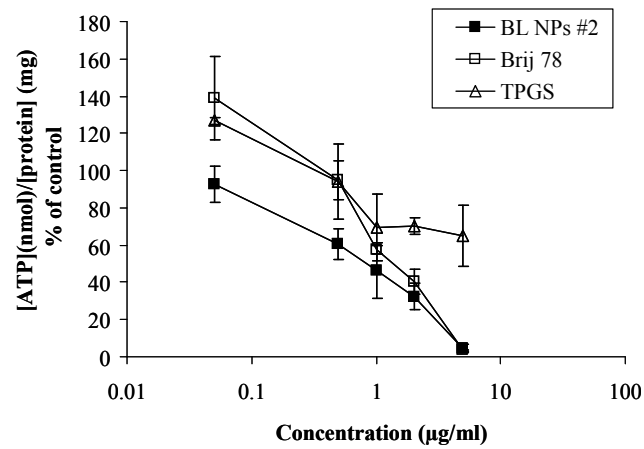
Figure B.8: The effects of nanoparticles on ATP levels in sensitive human cancer cells including, (A) MDA-MB-468 cells, (B) OVCAR-8 cells and (C) MDA-MB-435/LCC6

cells. Concentrations of blank NPs #2, Brij 78 and TPGS were calculated based on Dox equivalent doses. The ATP levels in sensitive cells responded differently to different cells. ATP levels only slightly changed in MDA-MB-468 and OVCAR-8 cells whereas ATP levels in MDA-MB-435/LCC6 cells decreased to the same extent as with the corresponding resistant cells after treatment with either blank NPs #2 or Brij 78. Even TPGS, which had no influence in other sensitive cells, decreased ATP levels in MDA-MB-435/LCC6 cells. Data are presented as the mean ± SD (n = 3).

Figure B.9
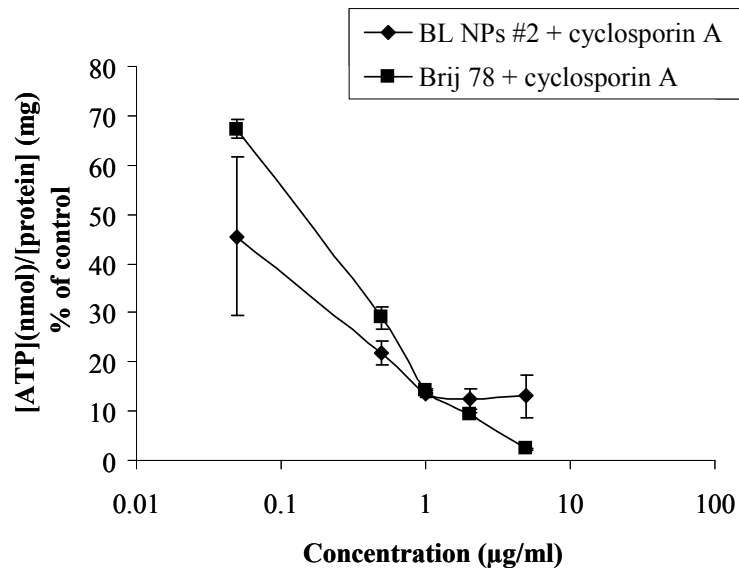
Figure B.9: The effects of blank NPs and Brij 78 on ATP levels in the present of P-gp inhibitor cyclosporin A in NCI/ADR-RES cells. In the presence of 17 μg/ml of cyclosporin A, ATP levels further decreased by an additional 20-40% at each concentration tested compared to the ATP levels tested without cyclosporin A. Concentrations of blank NPs #2 and Brij 78 were calculated based on Dox equivalent doses.

Figure B.10

| OVCAR-8 | MDA-MB-435/LCC6 | MDA-MB-435/LCC6MDR1 |
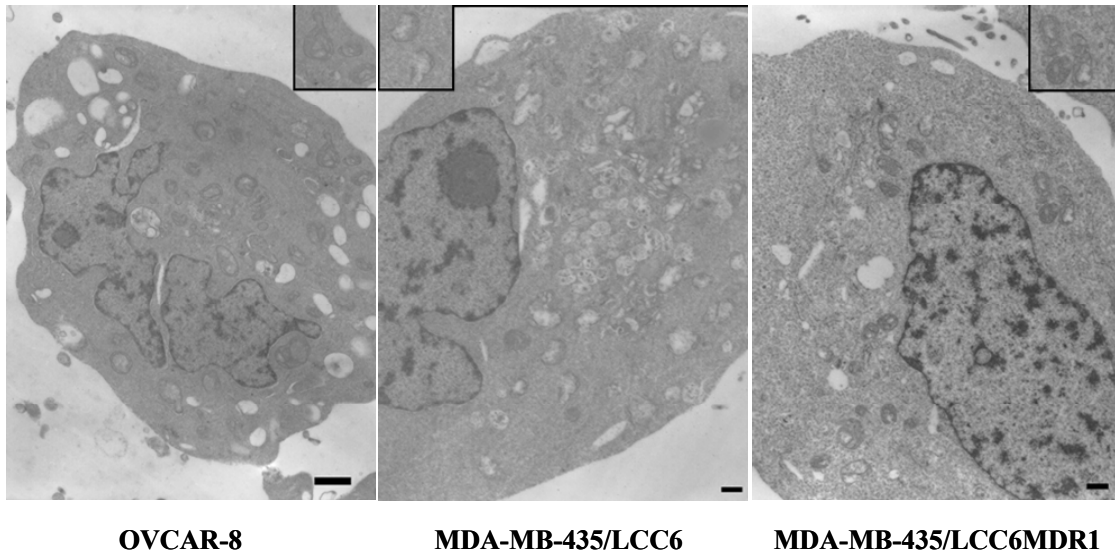
Figure B.10: The effects of Brij 78 on mitochondria analyzed by TEM. OVCAR-8, MDA-MB-435/LCC6MDR1 and MDA-MB-435/LCC6 were treated with Brij 78 at 5 µg/ml of Dox equivalent doses for 1 h at 37ºC. Brij 78 caused mitochondria swelling in all treated cells. Scale bar = 1 µm.
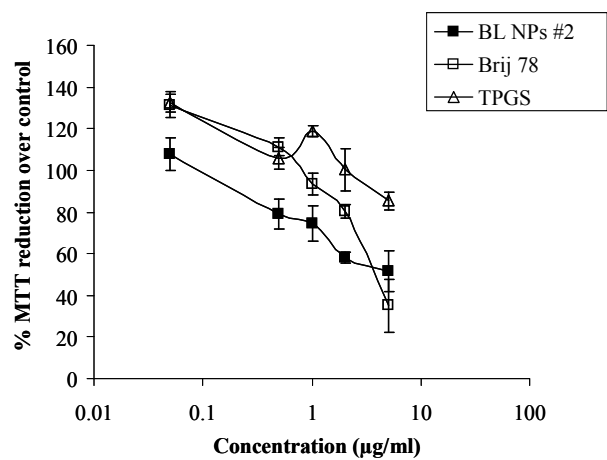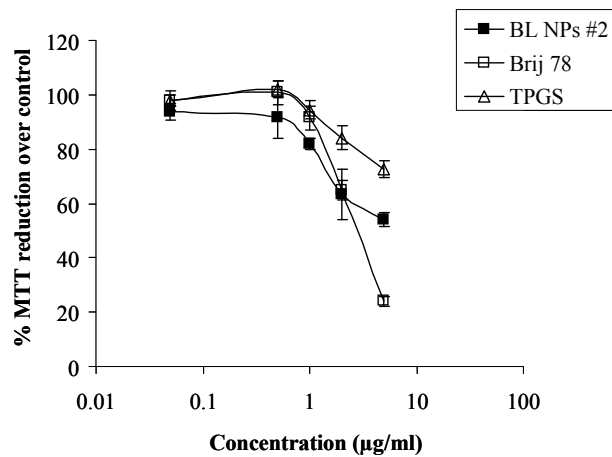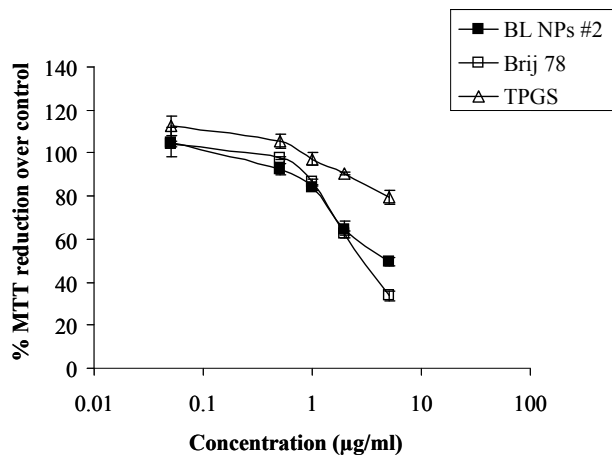
Figure B.11

D
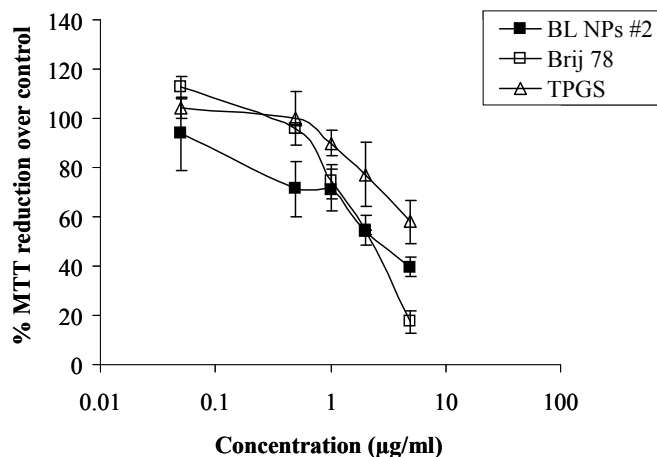
Figure B.11: **The effects of blank NPs #2, Brij 78 and TPGS on MTT reduction in human cancer cells.** MTT assays were performed in NIC/ADR-RES (**A**), MDA-MB-435/LCC6MDR1 (**B**), OVCAR-8 (**C**) and MDA-MB-435/LCC6 (**D**) cells treated with blank NPs #2 and surfactants for 2 h. MTT reduction requires catalysis of the enzymes in mitochondrial respiratory chain. Blank NPs and surfactants dramatically decreased MTT reduction within 2 h treatments, indicating the influence of blank NPs #2 and surfactants on the enzyme activity involved in the mitochondrial respiratory chain. Concentrations of blank NPs #2, Brij 78 and TPGS were calculated based on Dox equivalent doses.

References:

[1]   W.H. Organization, (2008).

[2]   H. Cortes-Funes, C. Coronado, Role of anthracyclines in the era of targeted therapy. Cardiovascular toxicology 7(2) (2007) 56-60.

[3]   M. Piccart, The role of taxanes in the adjuvant treatment of early stage breast cancer. Breast cancer research and treatment 79 Suppl 1 (2003) S25-34.

[4]   C. Bernard-Marty, F. Cardoso, M.J. Piccart, Facts and controversies in systemic treatment of metastatic breast cancer. The oncologist 9(6) (2004) 617-632.

[5]   J. O'Shaughnessy, Extending survival with chemotherapy in metastatic breast cancer. The oncologist 10 Suppl 3 (2005) 20-29.

[6]   M.C. Wani, H.L. Taylor, M.E. Wall, P. Coggon, A.T. McPhail, Plant anti-tumor agents. VI. The isolation and structure of taxol, a novel antileukemic and antitumor agent from Taxus brevifolia. Journal of the American Chemical Society 93(9) (1971) 2325-2327.

[7]   P.B. Schiff, J. Fant, S.B. Horwitz, Promotion of microtubule assembly in-vitro by taxol. Nature 277(5698) (1979) 665-667.

[8]   P.B. Schiff, S.B. Horwitz, Taxol stabilizes microtubules in mouse fibroblast cells. Proceedings of the National Academy of Sciences of the United States of America 77(3) (1980) 1561-1565.

[9]   P.B. Schiff, S.B. Horwitz, Taxol assembles tubulin in the absence of exogenous guanosine 5'-triphosphate or microtubule-associated proteins. Biochemistry 20(11) (1981) 3247-3252.

[10]   J. Parness, S.B. Horwitz, Taxol binds to polymerized tubulin in-vitro. The Journal of cell biology 91(2 Pt 1) (1981) 479-487.

[11]   J.J. Manfredi, J. Parness, S.B. Horwitz, Taxol binds to cellular microtubules. The Journal of cell biology 94(3) (1982) 688-696.

[12]   M.A. Jordan, R.J. Toso, D. Thrower, L. Wilson, Mechanism of mitotic block and inhibition of cell proliferation by taxol at low concentrations. Proceedings of the National Academy of Sciences of the United States of America 90(20) (1993) 9552-9556.

[13]   N. Kumar, Taxol-induced polymerization of purified tubulin. Mechanism of action. The Journal of biological chemistry 256(20) (1981) 10435-10441.

[14]   Y.F. Chang, L.L. Li, C.W. Wu, T.Y. Liu, W.Y. Lui, K. P'Eng F, C.W. Chi, Paclitaxel-induced apoptosis in human gastric carcinoma cell lines. Cancer 77(1) (1996) 14-18.

[15]   D.E. Saunders, W.D. Lawrence, C. Christensen, N.L. Wappler, H. Ruan, G. Deppe, Paclitaxel-induced apoptosis in MCF-7 breast-cancer cells. International journal of cancer 70(2) (1997) 214-220.

[16]   G. Griffon-Etienne, Y. Boucher, C. Brekken, H.D. Suit, R.K. Jain, Taxane-induced apoptosis decompresses blood vessels and lowers interstitial fluid pressure in solid tumors: clinical implications. Cancer research 59(15) (1999) 3776-3782.

[17]   A.G. Taghian, R. Abi-Raad, S.I. Assaad, A. Casty, M. Ancukiewicz, E. Yeh, P. Molokhia, K. Attia, T. Sullivan, I. Kuter, Y. Boucher, S.N. Powell, Paclitaxel decreases the interstitial fluid pressure and improves oxygenation in breast cancers in patients treated with neoadjuvant chemotherapy: clinical implications. Journal of clinical oncology 23(9) (2005) 1951-1961.

[18]   A.E. Mathew, M.R. Mejillano, J.P. Nath, R.H. Himes, V.J. Stella, Synthesis and evaluation of some water-soluble prodrugs and derivatives of taxol with anti-tumor activity. Journal of medicinal chemistry 35(1) (1992) 145-151.

[19]   C.S. Swindell, N.E. Krauss, Biologically active taxol analogues with deleted A-ring side chain substituents and variable C-2' configuration. Journal of medicinal chemistry 34 (1991) 1176-1184.

[20]   J.D. Adams, K.P. Flora, B.R. Goldspiel, e. al, Taxol: a history of pharmaceutical development and current pharmaceutical concerns. Journal of National Cancer Institute Monographs 15 (1993) 141-147.

[21]   A. Sparreboom, O. van Tellingen, W.J. Nooijen, J.H. Beijnen, Nonlinear pharmacokinetics of paclitaxel in mice results from the pharmaceutical vehicle Cremophor EL. Cancer research 56(9) (1996) 2112-2115.

[22]   O. van Tellingen, M.T. Huizing, V.R. Panday, J.H. Schellens, W.J. Nooijen, J.H. Beijnen, Cremophor EL causes (pseudo-) non-linear pharmacokinetics of paclitaxel in patients. British journal of cancer 81(2) (1999) 330-335.

[23]   H. Gelderblom, J. Verweij, K. Nooter, A. Sparreboom, Cremophor EL: the drawbacks and advantages of vehicle selection for drug formulation. European journal of cancer 37(13) (2001) 1590-1598.

[24]   L. van Zuylen, L. Gianni, J. Verweij, K. Mross, E. Brouwer, W.J. Loos, A. Sparreboom, Inter-relationships of paclitaxel disposition, infusion duration and cremophor EL kinetics in cancer patients. Anti-cancer drugs 11(5) (2000) 331-337.

[25]   L. van Zuylen, J. Verweij, A. Sparreboom, Role of formulation vehicles in taxane pharmacology. Investigational new drugs 19(2) (2001) 125-141.

[26]   R.B. Weiss, R.C. Donehower, P.H. Wiernik, T. Ohnuma, R.J. Gralla, D.L. Trump, J.R. Baker, Jr., D.A. Van Echo, D.D. Von Hoff, B. Leyland-Jones, Hypersensitivity reactions from taxol. Journal of clinical oncology 8(7) (1990) 1263-1268.

[27]   S. Peltier, J.M. Oger, F. Lagarce, W. Couet, J.P. Benoit, Enhanced oral paclitaxel bioavailability after administration of paclitaxel-loaded lipid nanocapsules. Pharmaceutical research 23(6) (2006) 1243-1250.

[28]   K.L. Hennenfent, R. Govindan, Novel formulations of taxanes: a review. Old wine in a new bottle? Annals of oncology 17(5) (2006) 735-749.

[29]   B. Nuijen, M. Bouma, J.H. Schellens, J.H. Beijnen, Progress in the development of alternative pharmaceutical formulations of taxanes. Investigational new drugs 19(2) (2001) 143-153.

[30]   N.K. Ibrahim, N. Desai, S. Legha, P. Soon-Shiong, R.L. Theriault, E. Rivera, B. Esmaeli, S.E. Ring, A. Bedikian, G.N. Hortobagyi, J.A. Ellerhorst, Phase I and pharmacokinetic study of ABI-007, a Cremophor-free, protein-stabilized, nanoparticle formulation of paclitaxel. Clinical cancer research 8(5) (2002) 1038-1044.

[31]   N.K. Ibrahim, B. Samuels, R. Page, D. Doval, K.M. Patel, S.C. Rao, M.K. Nair, P. Bhar, N. Desai, G.N. Hortobagyi, Multicenter phase II trial of ABI-007, an albumin-bound paclitaxel, in women with metastatic breast cancer. Journal of clinical oncology 23(25) (2005) 6019-6026.

[32]   W.J. Gradishar, S. Tjulandin, N. Davidson, H. Shaw, N. Desai, P. Bhar, M. Hawkins, J. O'Shaughnessy, Phase III trial of nanoparticle albumin-bound paclitaxel compared with polyethylated castor oil-based paclitaxel in women with breast cancer. Journal of clinical oncology 23(31) (2005) 7794-7803.

[33]   G. Minotti, P. Menna, E. Salvatorelli, G. Cairo, L. Gianni, Anthracyclines: molecular advances and pharmacologic developments in anti-tumor activity and cardiotoxicity. Pharmacological reviews 56(2) (2004) 185-229.

[34]   K.E. Reinert, Anthracycline-binding induced DNA stiffening, bending and elongation; stereochemical implications from viscometric investigations. Nucleic acids research 11(10) (1983) 3411-3430.

[35]   W.D. Meriwether, N.R. Bachur, Inhibition of DNA and RNA metabolism by daunorubicin and adriamycin in L1210 mouse leukemia. Cancer research 32(6) (1972) 1137-1142.

[36]   Y.J. Kang, Z.X. Zhou, G.W. Wang, A. Buridi, J.B. Klein, Suppression by metallothionein of doxorubicin-induced cardiomyocyte apoptosis through inhibition of p38 mitogen-activated protein kinases. The Journal of biological chemistry 275(18) (2000) 13690-13698.

[37]   J.H. Doroshow, G.Y. Locker, C.E. Myers, Enzymatic defenses of the mouse heart against reactive oxygen metabolites: alterations produced by doxorubicin. The Journal of clinical investigation 65(1) (1980) 128-135.

[38]   B. Kalyanaraman, J. Joseph, S. Kalivendi, S. Wang, E. Konorev, S. Kotamraju, Doxorubicin-induced apoptosis: implications in cardiotoxicity. Molecular and cellular biochemistry 234-235(1-2) (2002) 119-124.

[39]   M.E. O'Brien, N. Wigler, M. Inbar, R. Rosso, E. Grischke, A. Santoro, R. Catane, D.G. Kieback, P. Tomczak, S.P. Ackland, F. Orlandi, L. Mellars, L. Alland, C. Tendler, Reduced cardiotoxicity and comparable efficacy in a phase III trial of pegylated liposomal doxorubicin HCl (CAELYX/Doxil) versus conventional doxorubicin for first-line treatment of metastatic breast cancer. Annals of oncology 15(3) (2004) 440-449.

[40]   L.W. Seymour, D.R. Ferry, D. Anderson, S. Hesslewood, P.J. Julyan, R. Poyner, J. Doran, A.M. Young, S. Burtles, D.J. Kerr, Hepatic drug targeting: phase I evaluation of polymer-bound doxorubicin. Journal of clinical oncology 20(6) (2002) 1668-1676.

[41]   J.W. Hopewel, R. Duncan, D. Wilding, K. Chakrabarti, Preclinical evaluation of the cardiotoxicity of PK2: a novel HPMA copolymer-doxorubicin-galactosamine conjugate antitumour agent. Human & experimental toxicology 20(9) (2001) 461-470.

[42]   R.B. Campbell, Tumor physiology and delivery of nanopharmaceuticals. Anti-cancer agents in medicinal chemistry 6(6) (2006) 503-512.

[43]   D. Fukumura, R.K. Jain, Tumor microvasculature and microenvironment: targets for anti-angiogenesis and normalization. Microvascular research 74(2-3) (2007) 72-84.

[44]   R.K. Jain, Determinants of tumor blood flow: a review. Cancer research 48(10) (1988) 2641-2658.

[45]   B. Endrich, H.S. Reinhold, J.F. Gross, M. Intaglietta, Tissue perfusion inhomogeneity during early tumor growth in rats. Journal of the National Cancer Institute 62(2) (1979) 387-395.

[46]   L.M. Hamberg, P.E. Kristjansen, G.J. Hunter, G.L. Wolf, R.K. Jain, Spatial heterogeneity in tumor perfusion measured with functional computed tomography at 0.05 microliter resolution. Cancer research 54(23) (1994) 6032-6036.

[47]   S.K. Hobbs, W.L. Monsky, F. Yuan, W.G. Roberts, L. Griffith, V.P. Torchilin, R.K. Jain, Regulation of transport pathways in tumor vessels: role of tumor type and microenvironment. Proceedings of the National Academy of Sciences of the United States of America 95(8) (1998) 4607-4612.

[48]   P. Rubin, G. Casarett, Microcirculation of tumors. I. Anatomy, function, and necrosis. Clinical radiology 17(3) (1966) 220-229.

[49]   F. Yuan, M. Dellian, D. Fukumura, M. Leunig, D.A. Berk, V.P. Torchilin, R.K. Jain, Vascular permeability in a human tumor xenograft: molecular size dependence and cutoff size. Cancer research 55(17) (1995) 3752-3756.

[50]   P. Shubik, Vascularization of tumors: a review. Journal of cancer research and clinical oncology 103(3) (1982) 211-226.

[51]   K. Aukland, R.K. Reed, Interstitial-lymphatic mechanisms in the control of extracellular fluid volume. Physiological reviews 73(1) (1993) 1-78.

[52]   Y. Boucher, L.T. Baxter, R.K. Jain, Interstitial pressure gradients in tissue-isolated and subcutaneous tumors: implications for therapy. Cancer research 50(15) (1990) 4478-4484.

[53]   A.J. Leu, D.A. Berk, A. Lymboussaki, K. Alitalo, R.K. Jain, Absence of functional lymphatics within a murine sarcoma: a molecular and functional evaluation. Cancer research 60(16) (2000) 4324-4327.

[54]   T.P. Padera, B.R. Stoll, J.B. Tooredman, D. Capen, E. di Tomaso, R.K. Jain, Pathology: cancer cells compress intratumour vessels. Nature 427(6976) (2004) 695.

[55]   T.P. Padera, A. Kadambi, E. di Tomaso, C.M. Carreira, E.B. Brown, Y. Boucher, N.C. Choi, D. Mathisen, J. Wain, E.J. Mark, L.L. Munn, R.K. Jain, Lymphatic metastasis in the absence of functional intratumor lymphatics. Science 296 (2002) 1883-1886.

[56]   N. Saijo, Chemotherapy: the more the better? Overview. Cancer chemotherapy and pharmacology 40 Suppl (1997) S100-106.

[57]   J.C. Reed, Bcl-2: prevention of apoptosis as a mechanism of drug resistance. Hematology/oncology clinics of North America 9(2) (1995) 451-473.

[58]   C.S. Morrow, K.H. Cowan, Glutathione S-transferases and drug resistance. Cancer Cells 2(1) (1990) 15-22.

[59]   V. Ling, L.H. Thompson, Reduced permeability in CHO cells as a mechanism of resistance to colchicine. Journal of cellular physiology 83(1) (1974) 103-116.

[60]   Y.P. See, S.A. Carlsen, J.E. Till, V. Ling, Increased drug permeability in Chinese hamster ovary cells in the presence of cyanide. Biochimica et biophysica acta 373(2) (1974) 242-252.

[61]   S. Arao, H. Suwa, M. Mandai, H. Tashiro, K. Miyazaki, H. Okamura, H. Nomura, H. Hiai, M. Fukumoto, Expression of multidrug resistance gene and localization of P-glycoprotein in human primary ovarian cancer. Cancer research 54(5) (1994) 1355-1359.

[62]   R.J. Arceci, Clinical significance of P-glycoprotein in multidrug resistance malignancies. Blood 81(9) (1993) 2215-2222.

[63]   D.R. Bell, J.H. Gerlach, N. Kartner, R.N. Buick, V. Ling, Detection of P-glycoprotein in ovarian cancer: a molecular marker associated with multidrug resistance. Journal of clinical oncology 3(3) (1985) 311-315.

[64]   W.S. Dalton, T.M. Grogan, J.A. Rybski, R.J. Scheper, L. Richter, J. Kailey, H.J. Broxterman, H.M. Pinedo, S.E. Salmon, Immunohistochemical detection and quantitation of P-glycoprotein in multiple drug-resistant human myeloma cells: association with level of drug resistance and drug accumulation. Blood 73(3) (1989) 747-752.

[65]   R. Pirker, J. Wallner, K. Geissler, W. Linkesch, O.A. Haas, P. Bettelheim, M. Hopfner, R. Scherrer, P. Valent, L. Havelec, et al., MDR1 gene expression and treatment outcome in acute myeloid leukemia. Journal of the National Cancer Institute 83(10) (1991) 708-712.

[66]   H. Sato, H. Preisler, R. Day, A. Raza, R. Larson, G. Browman, J. Goldberg, R. Vogler, H. Grunwald, A. Gottlieb, et al., MDR1 transcript levels as an indication of resistant disease in acute myelogenous leukaemia. British journal of haematology 75(3) (1990) 340-345.

[67]   A.F. List, C. Spier, J. Greer, S. Wolff, J. Hutter, R. Dorr, S. Salmon, B. Futscher, M. Baier, W. Dalton, Phase I/II trial of cyclosporine as a chemotherapy-resistance modifier in acute leukemia. Journal of clinical oncology 11(9) (1993) 1652-1660.

[68]   J.P. Marie, J.N. Bastie, F. Coloma, A.M. Faussat Suberville, A. Delmer, B. Rio, B. Delmas-Marsalet, G. Leroux, P. Casassus, E. Baumelou, et al., Cyclosporin A as a modifier agent in the salvage treatment of acute leukemia (AL). Leukemia 7(6) (1993) 821-824.

[69]   C.F. Higgins, ABC transporters: from microorganisms to man. Annual review of cell biology 8 (1992) 67-113.

[70]   C. Kast, V. Canfield, R. Levenson, P. Gros, Transmembrane organization of mouse P-glycoprotein determined by epitope insertion and immunofluorescence. The Journal of biological chemistry 271(16) (1996) 9240-9248.

[71]   T.W. Loo, D.M. Clarke, Membrane topology of a cysteine-less mutant of human P-glycoprotein. The Journal of biological chemistry 270(2) (1995) 843-848.

[72]   E. Teodori, S. Dei, C. Martelli, S. Scapecchi, F. Gualtieri, The functions and structure of ABC transporters: implications for the design of new inhibitors of Pgp and MRP1 to control multidrug resistance (MDR). Current drug targets 7(7) (2006) 893-909.

[73]   A.T. Fojo, K. Ueda, D.J. Slamon, D.G. Poplack, M.M. Gottesman, I. Pastan, Expression of a multidrug-resistance gene in human tumors and tissues. Proceedings of the National Academy of Sciences of the United States of America 84(1) (1987) 265-269.

[74]   F. Thiebaut, T. Tsuruo, H. Hamada, M.M. Gottesman, I. Pastan, M.C. Willingham, Cellular localization of the multidrug-resistance gene product P-glycoprotein in normal human tissues. Proceedings of the National Academy of Sciences of the United States of America 84(21) (1987) 7735-7738.

[75]   A.H. Schinkel, C.A. Mol, E. Wagenaar, L. van Deemter, J.J. Smit, P. Borst, Multidrug resistance and the role of P-glycoprotein knockout mice. European journal of Cancer 31A(7-8) (1995) 1295-1298.

[76]   A.H. Schinkel, J.J. Smit, O. van Tellingen, J.H. Beijnen, E. Wagenaar, L. van Deemter, C.A. Mol, M.A. van der Valk, E.C. Robanus-Maandag, H.P. te Riele, et al., Disruption of the mouse mdr1a P-glycoprotein gene leads to a deficiency in the blood-brain barrier and to increased sensitivity to drugs. Cell 77(4) (1994) 491-502.

[77]   A.H. Schinkel, E. Wagenaar, L. van Deemter, C.A. Mol, P. Borst, Absence of the mdr1a P-Glycoprotein in mice affects tissue distribution and pharmacokinetics of dexamethasone, digoxin, and cyclosporin A. The Journal of clinical investigation 96(4) (1995) 1698-1705.

[78]   M.M. Gottesman, Mechanisms of cancer drug resistance. Annual review of medicine 53 (2002) 615-627.

[79]   T.W. Loo, D.M. Clarke, Recent progress in understanding the mechanism of P-glycoprotein-mediated drug efflux. The Journal of membrane biology 206(3) (2005) 173-185.

[80]   C. Ono, A. Takao, R. Atsumi, Absorption, distribution, and excretion of DJ-927, a novel orally effective taxane, in mice, dogs, and monkeys. Biological & pharmaceutical bulletin 27(3) (2004) 345-351.

[81]   M. Shionoya, T. Jimbo, M. Kitagawa, T. Soga, A. Tohgo, DJ-927, a novel oral taxane, overcomes P-glycoprotein-mediated multidrug resistance in-vitro and in-vivo. Cancer science 94(5) (2003) 459-466.

[82]   G. Cassinelli, C. Lanzi, R. Supino, G. Pratesi, V. Zuco, D. Laccabue, G. Cuccuru, E. Bombardelli, F. Zunino, Cellular bases of the anti-tumor activity of the novel taxane

IDN 5109 (BAY59-8862) on hormone-refractory prostate cancer. Clinical cancer research 8(8) (2002) 2647-2654.

[83]   D. Polizzi, G. Pratesi, S. Monestiroli, M. Tortoreto, F. Zunino, E. Bombardelli, A. Riva, P. Morazzoni, T. Colombo, M. D'Incalci, M. Zucchetti, Oral efficacy and bioavailability of a novel taxane. Clinical cancer research 6(5) (2000) 2070-2074.

[84]   T.J. Altstadt, C.R. Fairchild, J. Golik, K.A. Johnston, J.F. Kadow, F.Y. Lee, B.H. Long, W.C. Rose, D.M. Vyas, H. Wong, M.J. Wu, M.D. Wittman, Synthesis and anti-tumor activity of novel C-7 paclitaxel ethers: discovery of BMS-184476. Journal of medicinal chemistry 44(26) (2001) 4577-4583.

[85]   W.C. Rose, C. Fairchild, F.Y. Lee, Preclinical anti-tumor activity of two novel taxanes. Cancer chemotherapy and pharmacology 47(2) (2001) 97-105.

[86]   K.A. Gelmon, J. Latreille, A. Tolcher, L. Genier, B. Fisher, D. Forand, S. D'Aloisio, L. Vernillet, L. Daigneault, A. Lebecq, M. Besenval, E. Eisenhauer, Phase I dose-finding study of a new taxane, RPR 109881A, administered as a one-hour intravenous infusion days 1 and 8 to patients with advanced solid tumors. Journal of clinical oncology 18(24) (2000) 4098-4108.

[87]   T. Kurata, Y. Shimada, T. Tamura, N. Yamamoto, I. Hyodo, T. Saeki, S. Takashima, K. Fujiwara, H. Wakasugi, M. Kashimura, Phase I and pharmacokinetic study of a new taxoid, RPR 109881A, given as a 1-hour intravenous infusion in patients with advanced solid tumors. Journal of clinical oncology 18(17) (2000) 3164-3171.

[88]   D. Sadava, A. Coleman, S.E. Kane, Liposomal daunorubicin overcomes drug resistance in human breast, ovarian and lung carcinoma cells. Journal of liposome research 12(4) (2002) 301-309.

[89]   G. Gatouillat, J. Odot, E. Balasse, C. Nicolau, P.F. Tosi, D.T. Hickman, M.P. Lopez-Deber, C. Madoulet, Immunization with liposome-anchored pegylated peptides modulates doxorubicin sensitivity in P-glycoprotein-expressing P388 cells. Cancer letters 257(2) (2007) 165-171.

[90]   H. Hamada, T. Tsuruo, Functional role for the 170- to 180-kDa glycoprotein specific to drug-resistant tumor cells as revealed by monoclonal antibodies. Proceedings of the National Academy of Sciences of the United States of America 83(20) (1986) 7785-7789.

[91]   E.B. Mechetner, I.B. Roninson, Efficient inhibition of P-glycoprotein-mediated multidrug resistance with a monoclonal antibody. Proceedings of the National Academy of Sciences of the United States of America 89(13) (1992) 5824-5828.

[92]   T. Tsuruo, H. Iida, S. Tsukagoshi, Y. Sakurai, Overcoming of vincristine resistance in P388 leukemia in-vivo and in-vitro through enhanced cytotoxicity of vincristine and vinblastine by verapamil. Cancer research 41(5) (1981) 1967-1972.

[93]   T. Tsuruo, H. Iida, M. Yamashiro, S. Tsukagoshi, Y. Sakurai, Enhancement of vincristine- and adriamycin-induced cytotoxicity by verapamil in P388 leukemia and its sublines resistant to vincristine and adriamycin. Biochemical pharmacology 31(19) (1982) 3138-3140.

[94]   D.J. Kerr, J. Graham, J. Cummings, J.G. Morrison, G.G. Thompson, M.J. Brodie, S.B. Kaye, The effect of verapamil on the pharmacokinetics of adriamycin. Cancer chemotherapy and pharmacology 18(3) (1986) 239-242.

[95]   Y. Bertrand, R. Capdeville, N. Balduck, N. Philippe, Cyclosporin A used to reverse drug resistance increases vincristine neurotoxicity. American journal of hematology 40(2) (1992) 158-159.

[96]   M. Faraday, The Bakerian lecture - experimental relations of gold (and other metals) to light. philosophical transactions of the royal society of london 147 (1857) 145-181.

[97]   A.D. Bangham, M.M. Standish, J.C. Watkins, Diffusion of univalent ions across the lamellae of swollen phospholipids. Journal of molecular biology 13(1) (1965) 238-252.

[98]   F. Alexis, J.W. Rhee, J.P. Richie, A.F. Radovic-Moreno, R. Langer, O.C. Farokhzad, New frontiers in nanotechnology for cancer treatment. Urologic oncology 26(1) (2008) 74-85.

[99]   S.H. Jang, M.G. Wientjes, D. Lu, J.L. Au, Drug delivery and transport to solid tumors. Pharmaceutical research 20(9) (2003) 1337-1350.

[100] B. Haley, E. Frenkel, Nanoparticles for drug delivery in cancer treatment. Urologic oncology 26(1) (2008) 57-64.

[101] D. Peer, J.M. Karp, S. Hong, O.C. Farokhzad, R. Margalit, R. Langer, Nanocarriers as an emerging platform for cancer therapy. Nature nanotechnology 2(12) (2007) 751-760.

[102] B. Rihova, M. Bilej, V. Vetvicka, K. Ulbrich, J. Strohalm, J. Kopecek, R. Duncan, Biocompatibility of N-(2-hydroxypropyl) methacrylamide copolymers containing adriamycin. Immunogenicity, and effect on haematopoietic stem cells in bone marrow in-vivo and mouse splenocytes and human peripheral blood lymphocytes in-vitro. Biomaterials 10(5) (1989) 335-342.

[103] A. Gabizon, F. Martin, Polyethylene glycol-coated (pegylated) liposomal doxorubicin. Rationale for use in solid tumours. Drugs 54 Suppl 4 (1997) 15-21.

[104] K. Greish, J. Fang, T. Inutsuka, A. Nagamitsu, H. Maeda, Macromolecular therapeutics: advantages and prospects with special emphasis on solid tumour targeting. Clinical pharmacokinetics 42(13) (2003) 1089-1105.

[105] K. Greish, A. Nagamitsu, J. Fang, H. Maeda, Copoly(styrene-maleic acid)-pirarubicin micelles: high tumor-targeting efficiency with little toxicity. Bioconjugate chemistry 16(1) (2005) 230-236.

[106] M. Karakotchian, I.S. Fraser, An ultrastructural study of microvascular inter-endothelial tight junctions in normal endometrium. Micron 38(6) (2007) 632-636.

[107] H. Carrstensen, R.H. Muller, B.W. Muller, Particle size, surface hydrophobicity and interaction with serum of parenteral fat emulsions and model drug carriers as parameters related to RES uptake. Clinical nutrition 11(5) (1992) 289-297.

[108] M.E. Norman, P. Williams, L. Illum, Human serum albumin as a probe for surface conditioning (opsonization) of block copolymer-coated microspheres. Biomaterials 13(12) (1992) 841-849.

[109] M. Roser, D. Fischer, T. Kissel, Surface-modified biodegradable albumin nano- and microspheres. II: effect of surface charges on in-vitro phagocytosis and biodistribution in rats. European journal of pharmaceutics and biopharmaceutics 46(3) (1998) 255-263.

[110] D.E. Owens, 3rd, N.A. Peppas, Opsonization, biodistribution, and pharmacokinetics of polymeric nanoparticles. International journal of pharmaceutics 307(1) (2006) 93-102.

[111] F.K. Bedu-Addo, P. Tang, Y. Xu, L. Huang, Interaction of polyethyleneglycol-phospholipid conjugates with cholesterol-phosphatidylcholine mixtures: sterically stabilized liposome formulations. Pharmaceutical research 13(5) (1996) 718-724.

[112] L.T. Chen, L. Weiss, The role of the sinus wall in the passage of erythrocytes through the spleen. Blood 41(4) (1973) 529-537.

[113] S.M. Moghimi, A.C. Hunter, J.C. Murray, Long-circulating and target-specific nanoparticles: theory to practice. Pharmacological reviews 53(2) (2001) 283-318.

[114]   S.M. Moghimi, C.J. Porter, I.S. Muir, L. Illum, S.S. Davis, Non-phagocytic uptake of intravenously injected microspheres in rat spleen: influence of particle size and hydrophilic coating. Biochemical and biophysical research communications 177(2) (1991) 861-866.

[115]   A. Gabizon, A.T. Horowitz, D. Goren, D. Tzemach, H. Shmeeda, S. Zalipsky, In-vivo fate of folate-targeted polyethylene-glycol liposomes in tumor-bearing mice. Clinical cancer research 9(17) (2003) 6551-6559.

[116]   H. Shmeeda, L. Mak, D. Tzemach, P. Astrahan, M. Tarshish, A. Gabizon, Intracellular uptake and intracavitary targeting of folate-conjugated liposomes in a mouse lymphoma model with up-regulated folate receptors. Molecular cancer therapeutics 5(4) (2006) 818-824.

[117]   P. Sapra, T.M. Allen, Ligand-targeted liposomal anti-cancer drugs. Progress in lipid research 42(5) (2003) 439-462.

[118]   D.B. Kirpotin, D.C. Drummond, Y. Shao, M.R. Shalaby, K. Hong, U.B. Nielsen, J.D. Marks, C.C. Benz, J.W. Park, Antibody targeting of long-circulating lipidic nanoparticles does not increase tumor localization but does increase internalization in animal models. Cancer research 66(13) (2006) 6732-6740.

[119]   O.C. Farokhzad, S. Jon, A. Khademhosseini, T.N. Tran, D.A. Lavan, R. Langer, Nanoparticle-aptamer bioconjugates: a new approach for targeting prostate cancer cells. Cancer research 64(21) (2004) 7668-7672.

[120]   J. Sudimack, R.J. Lee, Targeted drug delivery via the folate receptor. Advanced drug delivery reviews 41(2) (2000) 147-162.

[121]   L. Nobs, F. Buchegger, R. Gurny, E. Allemann, Current methods for attaching targeting ligands to liposomes and nanoparticles. Journal of pharmaceutical sciences 93(8) (2004) 1980-1992.

[122]   E.H. Moase, W. Qi, T. Ishida, Z. Gabos, B.M. Longenecker, G.L. Zimmermann, L. Ding, M. Krantz, T.M. Allen, Anti-MUC-1 immunoliposomal doxorubicin in the treatment of murine models of metastatic breast cancer. Biochimica et biophysica acta 1510(1-2) (2001) 43-55.

[123]   S. Dagar, A. Krishnadas, I. Rubinstein, M.J. Blend, H. Onyuksel, VIP grafted sterically stabilized liposomes for targeted imaging of breast cancer: in-vivo studies. Journal of control release 91(1-2) (2003) 123-133.

[124]   J.H. Jeong, S.H. Kim, S.W. Kim, T.G. Park, In-vivo tumor targeting of ODN-PEG-folic acid/PEI polyelectrolyte complex micelles. Journal of biomaterials science 16(11) (2005) 1409-1419.

[125]   S. Song, D. Liu, J. Peng, Y. Sun, Z. Li, J.R. Gu, Y. Xu, Peptide ligand-mediated liposome distribution and targeting to EGFR expressing tumor in-vivo. International journal of pharmaceutics 363(1-2) (2008) 155-161.

[126]   T. Asai, K. Shimizu, M. Kondo, K. Kuromi, K. Watanabe, K. Ogino, T. Taki, S. Shuto, A. Matsuda, N. Oku, Anti-neovascular therapy by liposomal DPP-CNDAC targeted to angiogenic vessels. FEBS letters 520(1-3) (2002) 167-170.

[127]   H. Hatakeyama, H. Akita, E. Ishida, K. Hashimoto, H. Kobayashi, T. Aoki, J. Yasuda, K. Obata, H. Kikuchi, T. Ishida, H. Kiwada, H. Harashima, Tumor targeting of doxorubicin by anti-MT1-MMP antibody-modified PEG liposomes. International journal of pharmaceutics 342(1-2) (2007) 194-200.

[128]   S.D. Li, S. Chono, L. Huang, Efficient gene silencing in metastatic tumor by siRNA formulated in surface-modified nanoparticles. Journal of control release 126(1) (2008) 77-84.

[129]   J.R. Grandis, D.J. Tweardy, Elevated levels of transforming growth factor alpha and epidermal growth factor receptor messenger RNA are early markers of carcinogenesis in head and neck cancer. Cancer research 53(15) (1993) 3579-3584.

[130]   N. Prenzel, O.M. Fischer, S. Streit, S. Hart, A. Ullrich, The epidermal growth factor receptor family as a central element for cellular signal transduction and diversification. Endocrine-related cancer 8(1) (2001) 11-31.

[131]   D.S. Salomon, R. Brandt, F. Ciardiello, N. Normanno, Epidermal growth factor-related peptides and their receptors in human malignancies. Critical reviews in oncology/hematology 19(3) (1995) 183-232.

[132]   J.G. Klijn, P.M. Berns, P.I. Schmitz, J.A. Foekens, The clinical significance of epidermal growth factor receptor (EGF-R) in human breast cancer: a review on 5232 patients. Endocrine reviews 13(1) (1992) 3-17.

[133]   J. O'Dwyer P, A.B. Benson, 3rd, Epidermal growth factor receptor-targeted therapy in colorectal cancer. Seminars in oncology 29(5 Suppl 14) (2002) 10-17.

[134]   A. Wells, EGF receptor. The international journal of biochemistry & cell biology 31(6) (1999) 637-643.

[135]   J. Mendelsohn, J. Baselga, Status of epidermal growth factor receptor antagonists in the biology and treatment of cancer. Journal of clinical oncology 21(14) (2003) 2787-2799.

[136]   I. Alroy, Y. Yarden, The ErbB signaling network in embryogenesis and oncogenesis: signal diversification through combinatorial ligand-receptor interactions. FEBS letters 410(1) (1997) 83-86.

[137]   B.P. Ceresa, S.L. Schmid, Regulation of signal transduction by endocytosis. Current opinion in cell biology 12(2) (2000) 204-210.

[138]   P. Chen, R. Cameron, J. Wang, K.A. Vallis, R.M. Reilly, Anti-tumor effects and normal tissue toxicity of 111In-labeled epidermal growth factor administered to athymic mice bearing epidermal growth factor receptor-positive human breast cancer xenografts. Journal of nuclear medicine 44(9) (2003) 1469-1478.

[139]   F. Zeng, H. Lee, C. Allen, Epidermal growth factor-conjugated poly(ethylene glycol)-block- poly(delta-valerolactone) copolymer micelles for targeted delivery of chemotherapeutics. Bioconjugate chemistry 17(2) (2006) 399-409.

[140]   E. Bohl Kullberg, N. Bergstrand, J. Carlsson, K. Edwards, M. Johnsson, S. Sjoberg, L. Gedda, Development of EGF-conjugated liposomes for targeted delivery of boronated DNA-binding agents. Bioconjugate chemistry 13(4) (2002) 737-743.

[141]   C. Mamot, D.C. Drummond, U. Greiser, K. Hong, D.B. Kirpotin, J.D. Marks, J.W. Park, Epidermal growth factor receptor (EGFR)-targeted immunoliposomes mediate specific and efficient drug delivery to EGFR- and EGFRvIII-overexpressing tumor cells. Cancer research 63(12) (2003) 3154-3161.

[142]   J.E. de Larco, G.J. Todaro, Growth factors from murine sarcoma virus-transformed cells. Proceedings of the National Academy of Sciences of the United States of America 75(8) (1978) 4001-4005.

[143]   D.W. Hoyt, R.N. Harkins, M.T. Debanne, M. O'Connor-McCourt, B.D. Sykes, Interaction of transforming growth factor alpha with the epidermal growth factor receptor: binding kinetics and differential mobility within the bound TGF-α. Biochemistry 33(51) (1994) 15283-15292.

[144]   C. McInnes, J. Wang, A.E. Al Moustafa, C. Yansouni, M. O'Connor-McCourt, B.D. Sykes, Structure-based minimization of transforming growth factor-alpha (TGF-α)

through NMR analysis of the receptor-bound ligand. Design, solution structure, and activity of TGF-α 8-50. The Journal of biological chemistry 273(42) (1998) 27357-27363.

[145] G.M. Howell, L.E. Humphrey, B.L. Ziober, R. Awwad, B. Periyasamy, A. Koterba, W. Li, J.K. Willson, K. Coleman, J. Carboni, M. Lynch, M.G. Brattain, Regulation of transforming growth factor alpha expression in a growth factor-independent cell line. Molecular and cellular biology 18(1) (1998) 303-313.

[146] D. Wang, W. Li, W. Jiang, L.E. Humphrey, G.M. Howell, M.G. Brattain, Autocrine TGFalpha expression in the regulation of initiation of human colon carcinoma growth. Journal of cellular physiology 177(3) (1998) 387-395.

[147] S. Chakrabarty, S. Huang, T.L. Moskal, H.A. Fritsche, Jr., Elevated serum levels of transforming growth factor-alpha in breast cancer patients. Cancer letters 79(2) (1994) 157-160.

[148] C.B. Kienhuis, P.G. Koenders, H. Klominska, T.J. Benraad, Endogenous ligands for the epidermal growth factor receptor in human breast tumors do not interfere in an epidermal growth factor receptor radioligand binding assay. Breast cancer research and treatment 27(3) (1993) 271-275.

[149] D.C. Heimbrook, S.M. Stirdivant, J.D. Ahern, N.L. Balishin, D.R. Patrick, G.M. Edwards, D. Defeo-Jones, D.J. FitzGerald, I. Pastan, A. Oliff, Transforming growth factor alpha-Pseudomonas exotoxin fusion protein prolongs survival of nude mice bearing tumor xenografts. Proceedings of the National Academy of Sciences of the United States of America 87(12) (1990) 4697-4701.

[150] J.H. Sampson, G. Akabani, G.E. Archer, M.S. Berger, R.E. Coleman, A.H. Friedman, H.S. Friedman, K. Greer, J.E. Herndon, 2nd, S. Kunwar, R.E. McLendon, A. Paolino, N.A. Petry, J.M. Provenzale, D.A. Reardon, T.Z. Wong, M.R. Zalutsky, I. Pastan, D.D. Bigner, Intracerebral infusion of an EGFR-targeted toxin in recurrent malignant brain tumors. Neuro-oncology 10(3) (2008) 320-329.

[151] S. Stegemann, F. Leveiller, D. Franchi, H. de Jong, H. Linden, When poor solubility becomes an issue: from early stage to proof of concept. European journal of pharmaceutical sciences 31(5) (2007) 249-261.

[152] E. Bilensoy, O. Gurkaynak, A.L. Dogan, A.A. Hincal, Safety and efficacy of amphiphilic beta-cyclodextrin nanoparticles for paclitaxel delivery. International journal of pharmaceutics 347(1-2) (2008) 163-170.

[153] P. Liu, B. Wang, J.L. Weili Qiao, Multi-anti-cancer drugs encapsulated in the micelle: a novel chemotherapy to cancer. Medical hypotheses 71(3) (2008) 379-381.

[154] O. Benny, O. Fainaru, A. Adini, F. Cassiola, L. Bazinet, I. Adini, E. Pravda, Y. Nahmias, S. Koirala, G. Corfas, R.J. D'Amato, J. Folkman, An orally delivered small-molecule formulation with antiangiogenic and anti-cancer activity. Nature biotechnology 26(7) (2008) 799-807.

[155] B. Sarmento, S. Martins, D. Ferreira, E.B. Souto, Oral insulin delivery by means of solid lipid nanoparticles. International journal of nanomedicine 2(4) (2007) 743-749.

[156] D. Cosco, C. Celia, F. Cilurzo, E. Trapasso, D. Paolino, Colloidal carriers for the enhanced delivery through the skin. Expert opinion on drug delivery 5(7) (2008) 737-755.

[157] R.M. Mainardes, M.C. Urban, P.O. Cinto, N.M. Khalil, M.V. Chaud, R.C. Evangelista, M.P. Gremiao, Colloidal carriers for ophthalmic drug delivery. Current drug targets 6(3) (2005) 363-371.

[158] P.P. Constantinides, M.V. Chaubal, R. Shorr, Advances in lipid nanodispersions for parenteral drug delivery and targeting. Advanced drug delivery reviews 60(6) (2008) 757-767.

[159]   S. Tamilvanan, Oil-in-water lipid emulsions: implications for parenteral and ocular delivering systems. Progress in lipid research 43(6) (2004) 489-533.

[160]   Piskin, X. Kaitian, E.B. Denkbas, Z. Kucukyavuz, Novel PDLLA/PEG copolymer micelles as drug carriers. Journal of biomaterials science 7(4) (1995) 359-373.

[161]   S.B. La, T. Okano, K. Kataoka, Preparation and characterization of the micelle-forming polymeric drug indomethacin-incorporated poly(ethylene oxide)-poly(beta-benzyl L-aspartate) block copolymer micelles. Journal of pharmaceutical sciences 85(1) (1996) 85-90.

[162]   A.L. Klibanov, K. Maruyama, V.P. Torchilin, L. Huang, Amphipathic polyethyleneglycols effectively prolong the circulation time of liposomes. FEBS letters 268(1) (1990) 235-237.

[163]   V.P. Torchilin, Micellar nanocarriers: pharmaceutical perspectives. Pharmaceutical research 24(1) (2007) 1-16.

[164]   C. Kontoyianni, Z. Sideratou, T. Theodossiou, L.A. Tziveleka, D. Tsiourvas, C.M. Paleos, A novel micellar PEGylated hyperbranched polyester as a prospective drug delivery system for paclitaxel. Macromolecular bioscience 8(9) (2008) 871-881.

[165]   D. Kim, E.S. Lee, K.T. Oh, Z.G. Gao, Y.H. Bae, Doxorubicin-loaded polymeric micelle overcomes multidrug resistance of cancer by double-targeting folate receptor and early endosomal pH. Small 4(11) (2008) 2043-2050.

[166]   D. Sutton, N. Nasongkla, E. Blanco, J. Gao, Functionalized micellar systems for cancer targeted drug delivery. Pharmaceutical research 24(6) (2007) 1029-1046.

[167]   K. Letchford, R. Liggins, K.M. Wasan, H. Burt, In-vitro human plasma distribution of nanoparticulate paclitaxel is dependent on the physicochemical properties of poly(ethylene glycol)-block-poly(caprolactone) nanoparticles. European journal of pharmaceutics and biopharmaceutics (2008).

[168]   C.R. Dass, Drug delivery in cancer using liposomes. Methods in molecular biology 437 (2008) 177-182.

[169]   T. Ishida, M. Ichihara, X. Wang, H. Kiwada, Spleen plays an important role in the induction of accelerated blood clearance of PEGylated liposomes. Journal of control release 115(3) (2006) 243-250.

[170]   T. Tadros, P. Izquierdo, J. Esquena, C. Solans, Formation and stability of nano-emulsions. Advances in colloid and interface science 108-109 (2004) 303-318.

[171]   C. Solans, P. Izquierdo, J. Nolla, N. Azemar, M.J. Garcia-Celma, Nano-emulsions. Current opinion in colloid and interface science 10 (2005) 102-110.

[172]   A. Forgiarini, J. Esquena, C. Gonzalez, C. Solans, Studies of the relation between phase behavior and emulsification methods with nanoemulsion formation. Progress in colloid and polymer science 115 (2000) 36-39.

[173]   P. Izquierdo, J. Feng, J. Esquena, T.F. Tadros, J.C. Dederen, M.J. Garcia, N. Azemar, C. Solans, The influence of surfactant mixing ratio on nano-emulsion formation by the pit method. Journal of colloid and interface science 285(1) (2005) 388-394.

[174]   F. Ganachaud, J.L. Katz, Nanoparticles and nanocapsules created using the ouzo effect: spontaneous emulsification as an alternative to ultrasonic and high-shear devices. ChemPhysChem 6 (2005) 209-216.

[175]   H.M. Courrier, T.F. Vandamme, M.P. Krafft, Reverse water-in-fluorocarbon emulsions and microemulsions obtained with a fluorinated surfactant. Colloids surfactant, a. Physicochemical engineering aspects 244 (2004) 141-148.

[176]   P.P. Constantinides, K.J. Lambert, A.K. Tustian, B. Schneider, S. Lalji, W. Ma, B. Wentzel, D. Kessler, D. Worah, S.C. Quay, Formulation development and anti-tumor

activity of a filter-sterilizable emulsion of paclitaxel. Pharmaceutical research 17(2) (2000) 175-182.

[177]   S.B. Tiwari, M.M. Amiji, Improved oral delivery of paclitaxel following administration in nanoemulsion formulations. Journal of nanoscience and nanotechnology 6(9-10) (2006) 3215-3221.

[178]   D. Goldstein, O. Gofrit, A. Nyska, S. Benita, Anti-HER2 cationic immunoemulsion as a potential targeted drug delivery system for the treatment of prostate cancer. Cancer research 67(1) (2007) 269-275.

[179]   P.P. Constantinides, A. Tustian, D.R. Kessler, Tocol emulsions for drug solubilization and parenteral delivery. Advanced drug delivery reviews 56(9) (2004) 1243-1255.

[180]   Y. Nishioka, H. Yoshino, Lymphatic targeting with nanoparticulate system. Advanced drug delivery reviews 47(1) (2001) 55-64.

[181]   A.R. Pohlmann, L.U. Soares, L. Cruz, N.P. da Silveira, S.S. Guterres, Alkaline hydrolysis as a tool to determine the association form of indomethacin in nanocapsules prepared with poly(eta-caprolactone). Current drug delivery 1(2) (2004) 103-110.

[182]   D. Quintanar-Guerrero, E. Allemann, E. Doelker, H. Fessi, Preparation and characterization of nanocapsules from preformed polymers by a new process based on emulsification-diffusion technique. Pharmaceutical research 15(7) (1998) 1056-1062.

[183]   J.M. Rollot, P. Couvreur, L. Roblot-Treupel, F. Puisieux, Physicochemical and morphological characterization of polyisobutyl cyanoacrylate nanocapsules. Journal of pharmaceutical sciences 75(4) (1986) 361-364.

[184]   V.C. Mosqueira, P. Legrand, H. Pinto-Alphandary, F. Puisieux, G. Barratt, Poly(D,L-lactide) nanocapsules prepared by a solvent displacement process: influence of the composition on physicochemical and structural properties. Journal of pharmaceutical sciences 89(5) (2000) 614-626.

[185]   B. Heurtault, P. Saulnier, B. Pech, J.E. Proust, J.P. Benoit, A novel phase inversion-based process for the preparation of lipid nanocarriers. Pharmaceutical research 19(6) (2002) 875-880.

[186]   M.H. Bartoli, M. Boitard, H. Fessi, H. Beriel, J.P. Devissaguet, F. Picot, F. Puisieux, In-vitro and in-vivo anti-tumoral activity of free, and encapsulated taxol. Journal of microencapsulation 7(2) (1990) 191-197.

[187]   W. Abdelwahed, G. Degobert, H. Fessi, A pilot study of freeze drying of poly(epsilon-caprolactone) nanocapsules stabilized by poly(vinyl alcohol): formulation and process optimization. International journal of pharmaceutics 309(1-2) (2006) 178-188.

[188]   S.R. Schaffazick, A.R. Pohlmann, T. Dalla-Costa, S.S. Guterres, Freeze-drying polymeric colloidal suspensions: nanocapsules, nanospheres and nanodispersion. A comparative study. European journal of pharmaceutics and biopharmaceutics 56(3) (2003) 501-505.

[189]   F. Lacoeuille, E. Garcion, J.P. Benoit, A. Lamprecht, Lipid nanocapsules for intracellular drug delivery of anti-cancer drugs. Journal of nanoscience and nanotechnology 7(12) (2007) 4612-4617.

[190]   B. Stella, S. Arpicco, F. Rocco, V. Marsaud, J.M. Renoir, L. Cattel, P. Couvreur, Encapsulation of gemcitabine lipophilic derivatives into polycyanoacrylate nanospheres and nanocapsules. International journal of pharmaceutics 344(1-2) (2007) 71-77.

[191]   A. Beduneau, P. Saulnier, N. Anton, F. Hindre, C. Passirani, H. Rajerison, N. Noiret, J.P. Benoit, Pegylated nanocapsules produced by an organic solvent-free method: Evaluation of their stealth properties. Pharmaceutical research 23(9) (2006) 2190-2199.

[192] M.N. Khalid, P. Simard, D. Hoarau, A. Dragomir, J.C. Leroux, Long circulating poly(ethylene glycol)-decorated lipid nanocapsules deliver docetaxel to solid tumors. Pharmaceutical research 23(4) (2006) 752-758.

[193] E. Garcion, A. Lamprecht, B. Heurtault, A. Paillard, A. Aubert-Pouessel, B. Denizot, P. Menei, J.P. Benoit, A new generation of anti-cancer, drug-loaded, colloidal vectors reverses multidrug resistance in glioma and reduces tumor progression in rats. Molecular cancer therapeutics 5(7) (2006) 1710-1722.

[194] R.H. Muller, K. Mader, S. Gohla, Solid lipid nanoparticles (SLN) for controlled drug delivery - a review of the state of the art. European journal of pharmaceutics and biopharmaceutics 50(1) (2000) 161-177.

[195] K. Manjunath, J.S. Reddy, V. Venkateswarlu, Solid lipid nanoparticles as drug delivery systems. Methods and findings in experimental and clinical pharmacology 27(2) (2005) 127-144.

[196] F.Q. Hu, M. Wu, H. Yuan, H.H. Zhang, A novel preparation of solid lipid nanoparticles with cyclosporin A for prolonged drug release. Die Pharmazie 59(9) (2004) 683-685.

[197] S.C. Yang, J.B. Zhu, Preparation and characterization of camptothecin solid lipid nanoparticles. Drug development and industrial pharmacy 28(3) (2002) 265-274.

[198] P. Ahlin, J. Kristl, M. Sentjurc, J. Strancar, S. Pecar, Influence of spin probe structure on its distribution in SLN dispersions. International journal of pharmaceutics 196(2) (2000) 241-244.

[199] R.H. Muller, M. Radtke, S.A. Wissing, Nanostructured lipid matrices for improved microencapsulation of drugs. International journal of pharmaceutics 242(1-2) (2002) 121-128.

[200] J. Pietkiewicz, M. Sznitowska, M. Placzek, The expulsion of lipophilic drugs from the cores of solid lipid microspheres in diluted suspensions and in concentrates. International journal of pharmaceutics 310(1-2) (2006) 64-71.

[201] J. Gabrielsson, N. Lindberg, T. Lundstedt, Multivariate methods in pharmaceutical applications. Journal of chemometrics 16 (2002) 141-160.

[202] J.H. De Boer, A.K. Smilde, D.A. Doombos, Introduction of multicriteria decision making in optimization procedures for pharmaceutical formulations. Acta pharmaceutica technologica 34 (1988) 140-143

[203] M.D. Bhavsar, S.B. Tiwari, M.M. Amiji, Formulation optimization for the nanoparticles-in-microsphere hybrid oral delivery system using factorial design. Journal of control release 110(2) (2006) 422-430.

[204] Y. Duan, S. Xu, Q. Wang, J. Liu, Z. Zhang, Optimization of preparation of DHAQ-loaded PEG-PLGA-PEG nonaparticles using central composite design. Journal of materials science 17(6) (2006) 559-563.

[205] A.K. Mehta, K.S. Yadav, K.K. Sawant, Nimodipine loaded PLGA nanoparticles: formulation optimization using factorial design, characterization and in-vitro evaluation. Current drug delivery 4(3) (2007) 185-193.

[206] B.S. Sachin, S.C. Sharma, S. Sethi, S.A. Tasduq, M.K. Tikoo, A.K. Tikoo, N.K. Satti, B.D. Gupta, K.A. Suri, R.K. Johri, G.N. Qazi, Herbal modulation of drug bioavailability: enhancement of rifampicin levels in plasma by herbal products and a flavonoid glycoside derived from Cuminum cyminum. Phytotherapy research 21(2) (2007) 157-163.

[207]   S. Sashmal, S. Mukherjee, S. Ray, R.S. Thakur, L.K. Ghosh, B.K. Gupta, Design and optimization of NSAID loaded nanoparticles. Pakistan journal of pharmaceutical sciences 20(2) (2007) 157-162.

[208]   R.K. Roy, Design of Experiments Using the Taguchi Approach, John Wiley & Sons, Inc., New York, NY, 2001.

[209]   J.A. Nelder, R. Mead, A simplex method for function minimization. The Computer journal 7 (1965) 308-313.

[210]   S.N. Deming, Chemometrics: an overview. Clinical chemistry 32(9) (1986) 1702-1706.

[211]   M. Ghazali, G.L. Hayward, Simplex optimization of acoustic assay for plasminogen activators. Analytical and bioanalytical chemistry 393(2) (2009) 635-642.

[212]   A.M. Siouffi, R. Phan-Tan-Luu, Optimization methods in chromatography and capillary electrophoresis. Journal of chromatography 892(1-2) (2000) 75-106.

[213]   M. Salazar de Saavedra, I.I. Saavedra Cuadra, Application of a mixed optimization strategy in the design of a pharmaceutical solid formulation at laboratory scale. Drug development and industrial pharmacy 27 (2000) 675-685.

[214]   S.T. Stern, S.E. McNeil, Nanotechnology safety concerns revisited. Toxicological sciences 101(1) (2008) 4-21.

[215]   B.G. Short, Safety evaluation of ocular drug delivery formulations: techniques and practical considerations. Toxicologic pathology 36(1) (2008) 49-62.

[216]   I. Engelberg, J. Kohn, Physico-mechanical properties of degradable polymers used in medical applications: a comparative study. Biomaterials 12(3) (1991) 292-304.

[217]   S. Shalel, S. Streichman, A. Marmur, The mechanism of hemolysis by surfactants: effect of solution composition. Journal of colloid and interface science 252(1) (2002) 66-76.

[218]   J.M. Koziara, J.J. Oh, W.S. Akers, S.P. Ferraris, R.J. Mumper, Blood compatibility of cetyl alcohol/polysorbate-based nanoparticles. Pharmaceutical research 22(11) (2005) 1821-1828.

[219]   C. Olbrich, O. Kayser, R.H. Muller, Lipase degradation of Dynasan 114 and 116 solid lipid nanoparticles (SLN)--effect of surfactants, storage time and crystallinity. International journal of pharmaceutics 237(1-2) (2002) 119-128.

[220]   C. Olbrich, R.H. Muller, Enzymatic degradation of SLN-effect of surfactant and surfactant mixtures. International journal of pharmaceutics 180(1) (1999) 31-39.

[221]   X.J. Liang, C. Chen, Y. Zhao, L. Jia, P.C. Wang, Biopharmaceutics and therapeutic potential of engineered nanomaterials. Current drug metabolism 9(8) (2008) 697-709.

[222]   P.P. Constantinides, K.M. Wasan, Lipid formulation strategies for enhancing intestinal transport and absorption of P-glycoprotein (P-gp) substrate drugs: in-vitro/in-vivo case studies. Journal of pharmaceutical sciences 96(2) (2007) 235-248.

[223]   H. Riehm, J.L. Biedler, Potentiation of drug effect by Tween 80 in Chinese hamster cells resistant to actinomycin D and daunomycin. Cancer research 32(6) (1972) 1195-1200.

[224]   A. Seelig, G. Gerebtzoff, Enhancement of drug absorption by noncharged detergents through membrane and P-glycoprotein binding. Expert opinion on drug metabolism & toxicology 2(5) (2006) 733-752.

[225]   K. Bogman, Y. Zysset, L. Degen, G. Hopfgartner, H. Gutmann, J. Alsenz, J. Drewe, P-glycoprotein and surfactants: effect on intestinal talinolol absorption. Clinical pharmacology and therapeutics 77(1) (2005) 24-32.

[226] F. Foger, H. Hoyer, K. Kafedjiiski, M. Thaurer, A. Bernkop-Schnurch, In-vivo comparison of various polymeric and low molecular mass inhibitors of intestinal P-glycoprotein. Biomaterials 27(34) (2006) 5855-5860.

[227] J.M. Dintaman, J.A. Silverman, Inhibition of P-glycoprotein by D-alpha-tocopheryl polyethylene glycol 1000 succinate (TPGS). Pharmaceutical research 16(10) (1999) 1550-1556.

[228] E.M. Collnot, C. Baldes, M.F. Wempe, J. Hyatt, L. Navarro, K.J. Edgar, U.F. Schaefer, C.M. Lehr, Influence of vitamin E TPGS poly(ethylene glycol) chain length on apical efflux transporters in Caco-2 cell monolayers. Journal of control release 111(1-2) (2006) 35-40.

[229] Y.L. Lo, Relationships between the hydrophilic-lipophilic balance values of pharmaceutical excipients and their multidrug resistance modulating effect in Caco-2 cells and rat intestines. Journal of control release 90(1) (2003) 37-48.

[230] E.V. Batrakova, S. Li, V.Y. Alakhov, D.W. Miller, A.V. Kabanov, Optimal structure requirements for pluronic block copolymers in modifying P-glycoprotein drug efflux transporter activity in bovine brain microvessel endothelial cells. The Journal of pharmacology and experimental therapeutics 304(2) (2003) 845-854.

[231] D.W. Loe, F.J. Sharom, Interaction of multidrug-resistant Chinese hamster ovary cells with amphiphiles. British journal of cancer 68(2) (1993) 342-351.

[232] B.D. Rege, J.P. Kao, J.E. Polli, Effects of nonionic surfactants on membrane transporters in Caco-2 cell monolayers. European journal of pharmaceutical sciences 16(4-5) (2002) 237-246.

[233] T. Yamazaki, Y. Sato, M. Hanai, J. Mochimaru, I. Tsujino, U. Sawada, T. Horie, Non-ionic detergent Tween 80 modulates VP-16 resistance in classical multidrug resistant K562 cells via enhancement of VP-16 influx. Cancer letters 149(1-2) (2000) 153-161.

[234] L.D. Mayer, J.A. Shabbits, The role for liposomal drug delivery in molecular and pharmacological strategies to overcome multidrug resistance. Cancer metastasis reviews 20(1-2) (2001) 87-93.

[235] A. Rahman, S.R. Husain, J. Siddiqui, M. Verma, M. Agresti, M. Center, A.R. Safa, R.I. Glazer, Liposome-mediated modulation of multidrug resistance in human HL-60 leukemia cells. Journal of the National Cancer Institute 84(24) (1992) 1909-1915.

[236] A.R. Thierry, A. Dritschilo, A. Rahman, Effect of liposomes on P-glycoprotein function in multidrug resistant cells. Biochemical and biophysical research communications 187(2) (1992) 1098-1105.

[237] L. Warren, J.C. Jardillier, A. Malarska, M.G. Akeli, Increased accumulation of drugs in multidrug-resistant cells induced by liposomes. Cancer research 52(11) (1992) 3241-3245.

[238] J.M. Ford, W.N. Hait, Pharmacology of drugs that alter multidrug resistance in cancer. Pharmacological reviews 42(3) (1990) 155-199.

[239] D.J. Booser, F.J. Esteva, E. Rivera, V. Valero, L. Esparza-Guerra, W. Priebe, G.N. Hortobagyi, Phase II study of liposomal annamycin in the treatment of doxorubicin-resistant breast cancer. Cancer chemotherapy and pharmacology 50(1) (2002) 6-8.

[240] Y.P. Hu, N. Henry-Toulme, J. Robert, Failure of liposomal encapsulation of doxorubicin to circumvent multidrug resistance in an in-vitro model of rat glioblastoma cells. European journal of cancer 31A(3) (1995) 389-394.

[241] E. Rivera, V. Valero, F.J. Esteva, L. Syrewicz, M. Cristofanilli, Z. Rahman, D.J. Booser, G.N. Hortobagyi, Lack of activity of stealth liposomal doxorubicin in the

treatment of patients with anthracycline-resistant breast cancer. Cancer chemotherapy and pharmacology 49(4) (2002) 299-302.

[242] Y. Wang, S. Eksborg, R. Lewensohn, A. Lindberg, E. Liliemark, In-vitro cellular accumulation and cytotoxicity of liposomal and conventional formulations of daunorubicin and doxorubicin in resistant K562 cells. Anti-cancer drugs 10(10) (1999) 921-928.

[243] X. Li, W.L. Lu, G.W. Liang, G.R. Ruan, H.Y. Hong, C. Long, Y.T. Zhang, Y. Liu, J.C. Wang, X. Zhang, Q. Zhang, Effect of stealthy liposomal topotecan plus amlodipine on the multidrug-resistant leukaemia cells in-vitro and xenograft in mice. European journal of clinical investigation 36(6) (2006) 409-418.

[244] J. Wu, Y. Lu, A. Lee, X. Pan, X. Yang, X. Zhao, R.J. Lee, Reversal of multidrug resistance by transferrin-conjugated liposomes co-encapsulating doxorubicin and verapamil. Journal of pharmacy and pharmaceutical sciences 10(3) (2007) 350-357.

[245] J. Wang, B. Goh, W. Lu, Q. Zhang, A. Chang, X.Y. Liu, T.M. Tan, H. Lee, In-vitro cytotoxicity of Stealth liposomes co-encapsulating doxorubicin and verapamil on doxorubicin-resistant tumor cells. Biological & pharmaceutical bulletin 28(5) (2005) 822-828.

[246] S.K. Sahoo, V. Labhasetwar, Enhanced antiproliferative activity of transferrin-conjugated paclitaxel-loaded nanoparticles is mediated via sustained intracellular drug retention. Molecular pharmaceutics 2(5) (2005) 373-383.

[247] L. Barraud, P. Merle, E. Soma, L. Lefrancois, S. Guerret, M. Chevallier, C. Dubernet, P. Couvreur, C. Trepo, L. Vitvitski, Increase of doxorubicin sensitivity by doxorubicin-loading into nanoparticles for hepatocellular carcinoma cells in-vitro and in-vivo. Journal of hepatology 42(5) (2005) 736-743.

[248] M.D. Chavanpatil, A. Khdair, B. Gerard, C. Bachmeier, D.W. Miller, M.P. Shekhar, J. Panyam, Surfactant-polymer nanoparticles overcome P-glycoprotein-mediated drug efflux. Molecular pharmaceutics 4(5) (2007) 730-738.

[249] S. Bennis, C. Chapey, P. Couvreur, J. Robert, Enhanced cytotoxicity of doxorubicin encapsulated in polyisohexylcyanoacrylate nanospheres against multidrug-resistant tumour cells in culture. European journal of cancer 30A(1) (1994) 89-93.

[250] A. Colin de Verdiere, C. Dubernet, F. Nemati, M.F. Poupon, F. Puisieux, P. Couvreur, Uptake of doxorubicin from loaded nanoparticles in multidrug-resistant leukemic murine cells. Cancer chemotherapy and pharmacology 33(6) (1994) 504-508.

[251] H.L. Wong, A.M. Rauth, R. Bendayan, J.L. Manias, M. Ramaswamy, Z. Liu, S.Z. Erhan, X.Y. Wu, A new polymer-lipid hybrid nanoparticle system increases cytotoxicity of doxorubicin against multidrug-resistant human breast cancer cells. Pharmaceutical research 23(7) (2006) 1574-1585.

[252] A. Astier, B. Doat, M.J. Ferrer, G. Benoit, J. Fleury, A. Rolland, R. Leverge, Enhancement of adriamycin anti-tumor activity by its binding with an intracellular sustained-release form, polymethacrylate nanospheres, in U-937 cells. Cancer research 48(7) (1988) 1835-1841.

[253] A. Colin de Verdiere, C. Dubernet, F. Nemati, E. Soma, M. Appel, J. Ferte, S. Bernard, F. Puisieux, P. Couvreur, Reversion of multidrug resistance with polyalkylcyanoacrylate nanoparticles: towards a mechanism of action. British journal of cancer 76(2) (1997) 198-205.

[254] X. Pepin, L. Attali, C. Domrault, S. Gallet, J.M. Metreau, Y. Reault, P.J. Cardot, M. Imalalen, C. Dubernet, E. Soma, P. Couvreur, On the use of ion-pair chromatography to elucidate doxorubicin release mechanism from polyalkylcyanoacrylate nanoparticles at

the cellular level. Journal of chromatography. B, Biomedical sciences and applications 702(1-2) (1997) 181-191.

[255] I. Brigger, C. Dubernet, P. Couvreur, Nanoparticles in cancer therapy and diagnosis. Advanced drug delivery reviews 54(5) (2002) 631-651.

[256] H.L. Wong, R. Bendayan, A.M. Rauth, H.Y. Xue, K. Babakhanian, X.Y. Wu, A mechanistic study of enhanced doxorubicin uptake and retention in multidrug resistant breast cancer cells using a polymer-lipid hybrid nanoparticle system. The Journal of pharmacology and experimental therapeutics 317(3) (2006) 1372-1381.

[257] A. Lamprecht, J.P. Benoit, Etoposide nanocarriers suppress glioma cell growth by intracellular drug delivery and simultaneous P-glycoprotein inhibition. Journal of control release 112(2) (2006) 208-213.

[258] M.D. Chavanpatil, Y. Patil, J. Panyam, Susceptibility of nanoparticle-encapsulated paclitaxel to P-glycoprotein-mediated drug efflux. International journal of pharmaceutics 320(1-2) (2006) 150-156.

[259] V. Omelyanenko, P. Kopeckova, C. Gentry, J. Kopecek, Targetable HPMA copolymer-adriamycin conjugates. Recognition, internalization, and subcellular fate. Journal of control release 53(1-3) (1998) 25-37.

[260] A. Nori, J. Kopecek, Intracellular targeting of polymer-bound drugs for cancer chemotherapy. Advanced drug delivery reviews 57(4) (2005) 609-636.

[261] J. Kopecek, P. Kopeckova, T. Minko, Z. Lu, HPMA copolymer-anti-cancer drug conjugates: design, activity, and mechanism of action. European journal of pharmaceutics and biopharmaceutics 50(1) (2000) 61-81.

[262] T. Minko, P. Kopeckova, J. Kopecek, Chronic exposure to HPMA copolymer-bound adriamycin does not induce multidrug resistance in a human ovarian carcinoma cell line. Journal of control release 59(2) (1999) 133-148.

[263] T. Minko, P. Kopeckova, J. Kopecek, Comparison of the anti-cancer effect of free and HPMA copolymer-bound adriamycin in human ovarian carcinoma cells. Pharmaceutical research 16(7) (1999) 986-996.

[264] T. Minko, P. Kopeckova, J. Kopecek, Preliminary evaluation of caspases-dependent apoptosis signaling pathways of free and HPMA copolymer-bound doxorubicin in human ovarian carcinoma cells. Journal of control release 71(3) (2001) 227-237.

[265] T. Minko, P. Kopeckova, J. Kopecek, Efficacy of the chemotherapeutic action of HPMA copolymer-bound doxorubicin in a solid tumor model of ovarian carcinoma. International journal of cancer 86(1) (2000) 108-117.

[266] V. Alakhov, E. Moskaleva, E.V. Batrakova, A.V. Kabanov, Hypersensitization of multidrug resistant human ovarian carcinoma cells by pluronic P85 block copolymer. Bioconjugate chemistry 7(2) (1996) 209-216.

[267] E.V. Batrakova, A.V. Kabanov, Pluronic block copolymers: evolution of drug delivery concept from inert nanocarriers to biological response modifiers. Journal of control release 130(2) (2008) 98-106.

[268] A.V. Kabanov, E.V. Batrakova, V.Y. Alakhov, Pluronic block copolymers for overcoming drug resistance in cancer. Advanced drug delivery reviews 54(5) (2002) 759-779.

[269] V.Y. Alakhov, E. Klinski, S. Li, G. Pietrzynski, A. Venne, E.V. Batrakova, T. Bronitch, A.V. Kabanov, Block copolymer-based formulation of doxorubicin. From cell screen to clinical trials. Colloids and surfaces B: Biointerfaces 16 (1999) 113-134.

[270] E.V. Batrakova, S. Li, Y. Li, V.Y. Alakhov, W.F. Elmquist, A.V. Kabanov, Distribution kinetics of a micelle-forming block copolymer Pluronic P85. Journal of control release 100(3) (2004) 389-397.

[271] J.D. Pruitt, G. Husseini, N. Rapoport, W.G. Pitt, Stabilization of Pluronic P-105 micelles with an interpenetrating network of N,N-diethylacrylamide. Macromolecules 33 (2000) 9306-9309

[272] T.F. Yang, C.N. Chen, M.C. Chen, C.H. Lai, H.F. Liang, H.W. Sung, Shell-crosslinked Pluronic L121 micelles as a drug delivery vehicle. Biomaterials 28(4) (2007) 725-734.

[273] E.V. Batrakova, S. Li, S.V. Vinogradov, V.Y. Alakhov, D.W. Miller, A.V. Kabanov, Mechanism of pluronic effect on P-glycoprotein efflux system in blood-brain barrier: contributions of energy depletion and membrane fluidization. The Journal of pharmacology and experimental therapeutics 299(2) (2001) 483-493.

[274] E.V. Batrakova, S. Li, Y. Li, V.Y. Alakhov, A.V. Kabanov, Effect of pluronic P85 on ATPase activity of drug efflux transporters. Pharmaceutical research 21(12) (2004) 2226-2233.

[275] E.V. Batrakova, S. Li, W.F. Elmquist, D.W. Miller, V.Y. Alakhov, A.V. Kabanov, Mechanism of sensitization of MDR cancer cells by Pluronic block copolymers: Selective energy depletion. British journal of cancer 85(12) (2001) 1987-1997.

[276] T. Minko, E.V. Batrakova, S. Li, Y. Li, R.I. Pakunlu, V.Y. Alakhov, A.V. Kabanov, Pluronic block copolymers alter apoptotic signal transduction of doxorubicin in drug-resistant cancer cells. Journal of control release 105(3) (2005) 269-278.

[277] E.V. Batrakova, S. Li, V.Y. Alakhov, W.F. Elmquist, D.W. Miller, A.V. Kabanov, Sensitization of cells overexpressing multidrug-resistant proteins by pluronic P85. Pharmaceutical research 20(10) (2003) 1581-1590.

[278] A.C. Wolff, R.C. Donehower, M.K. Carducci, M.A. Carducci, J.R. Brahmer, Y. Zabelina, M.O. Bradley, F.H. Anthony, C.S. Swindell, P.A. Witman, N.L. Webb, S.D. Baker, Phase I study of docosahexaenoic acid-paclitaxel: a taxane-fatty acid conjugate with a unique pharmacology and toxicity profile. Clinical cancer research 9(10 Pt 1) (2003) 3589-3597.

[279] T.Y. Kim, D.W. Kim, J.Y. Chung, S.G. Shin, S.C. Kim, D.S. Heo, N.K. Kim, Y.J. Bang, Phase I and pharmacokinetic study of Genexol-PM, a cremophor-free, polymeric micelle-formulated paclitaxel, in patients with advanced malignancies. Clinical cancer research 10(11) (2004) 3708-3716.

[280] J. Treat, N. Damjanov, C. Huang, S. Zrada, A. Rahman, Liposomal-encapsulated chemotherapy: preliminary results of a phase I study of a novel liposomal paclitaxel. Oncology 15(5 Suppl 7) (2001) 44-48.

[281] S.C. Spigel, S.F. Jones, F.A. Greco, S-8184 vitamin E paclitaxel emulsion: preclinical and phase I data. . Proceedings of the American Society for clinical oncology 20 (2002) 406 (Abstract).

[282] F. Nielloud, G. Marti-Mestres, Pharmaceutical Emulsions and Suspensions, Marcel Dekker, Inc. New York, 2000.

[283] F.M. Muggia, Doxorubicin-polymer conjugates: further demonstration of the concept of enhanced permeability and retention. Clinical cancer research 5(1) (1999) 7-8.

[284] K.N. Burger, R.W. Staffhorst, H.C. de Vijlder, M.J. Velinova, P.H. Bomans, P.M. Frederik, B. de Kruijff, Nanocapsules: lipid-coated aggregates of cisplatin with high cytotoxicity. Nature medicine 8(1) (2002) 81-84.

[285] G. Kaul, M. Amiji, Long-circulating poly(ethylene glycol)-modified gelatin nanoparticles for intracellular delivery. Pharmaceutical research 19(7) (2002) 1061-1067.

[286] N. Nishiyama, S. Okazaki, H. Cabral, M. Miyamoto, Y. Kato, Y. Sugiyama, K. Nishio, Y. Matsumura, K. Kataoka, Novel cisplatin-incorporated polymeric micelles can eradicate solid tumors in mice. Cancer research 63(24) (2003) 8977-8983.

[287] C.R. Dass, Improving anti-angiogenic therapy via selective delivery of cationic liposomes to tumour vasculature. International journal of pharmaceutics 267(1-2) (2003) 1-12.

[288] Y. Zhao, J. Fu, D.K. Ng, C. Wu, Formation and degradation of poly(D,L-lactide) nanoparticles and their potential application as controllable releasing devices. Macromolecular bioscience 4(9) (2004) 901-906.

[289] A. Dingler, R.P. Blum, H. Niehus, R.H. Muller, S. Gohla, Solid lipid nanoparticles (SLN/Lipopearls)--a pharmaceutical and cosmetic carrier for the application of vitamin E in dermal products. Journal of microencapsulation 16(6) (1999) 751-767.

[290] M.L. Bondi, G. Fontana, B. Carlisi, G. Giammona, Preparation and characterization of solid lipid nanoparticles containing cloricromene. Drug delivery 10(4) (2003) 245-250.

[291] R. Bodmeier, J. Wang, H. Bhagwatwar, Process and formulation variables in the preparation of wax microparticles by a melt dispersion technique. II. W/O/W multiple emulsion technique for water-soluble drugs. Journal of microencapsulation 9(1) (1992) 99-107.

[292] M. Maheshwari, A.R. Ketkar, B. Chauhan, V.B. Patil, A.R. Paradkar, Preparation and characterization of ibuprofen-cetyl alcohol beads by melt solidification technique: effect of variables. International journal of pharmaceutics 261(1-2) (2003) 57-67.

[293] J.J. Sudimack, W. Guo, W. Tjarks, R.J. Lee, A novel pH-sensitive liposome formulation containing oleyl alcohol. Biochimica et biophysica acta 1564(1) (2002) 31-37.

[294] R. Cortesi, E. Esposjto, G. Luca, C. Nastruzzi, Production of lipospheres as carriers for bioactive compounds. Biomaterials 23(11) (2002) 2283-2294.

[295] E. Ye, M. Tan, G. Wang, J. Yuan, Novel fluorescent europium chelate-doped silica nanoparticles preparation, characterization and time-resolved fluorometric application. Journal of materials chemistry 14 (2004) 851-856.

[296] R.L. DeAngelis, J.W. Findlay, Metabolism of synthetic surfactants. Clinics in perinatology 20(4) (1993) 697-710.

[297] P.R. Lockman, J.M. Koziara, R.J. Mumper, D.D. Allen, Nanoparticle surface charges alter blood-brain barrier integrity and permeability. Journal of drug targeting 12(9-10) (2004) 635-641.

[298] Z. Cui, J. Patel, M. Tuzova, P. Ray, R. Phillips, J.G. Woodward, A. Nath, R.J. Mumper, Strong T cell type-1 immune responses to HIV-1 Tat (1-72) protein-coated nanoparticles. Vaccine 22(20) (2004) 2631-2640.

[299] R.J. Mumper, Z. Cui, Genetic immunization by jet injection of targeted pDNA-coated nanoparticles. Methods 31(3) (2003) 255-262.

[300] J.M. Koziara, P.R. Lockman, D.D. Allen, R.J. Mumper, Paclitaxel nanoparticles for the potential treatment of brain tumors. Journal of control release 99(2) (2004) 259-269.

[301] M.O. Oyewumi, S. Liu, J.A. Moscow, R.J. Mumper, Specific association of thiamine-coated gadolinium nanoparticles with human breast cancer cells expressing thiamine transporters. Bioconjugate chemistry 14(2) (2003) 404-411.

[302] M.O. Oyewumi, R.A. Yokel, M. Jay, T. Coakley, R.J. Mumper, Comparison of cell uptake, biodistribution and tumor retention of folate-coated and PEG-coated gadolinium nanoparticles in tumor-bearing mice. Journal of control release 95(3) (2004) 613-626.

[303] W.B. Rizzo, D.A. Craft, A.L. Dammann, M.W. Phillips, Fatty alcohol metabolism in cultured human fibroblasts. Evidence for a fatty alcohol cycle. The Journal of biological chemistry 262(36) (1987) 17412-17419.

[304] T. Lee, Characterization of fatty alcohol:NAD+ oxidoreductase from rat liver. The Journal of biological chemistry 254(8) (1979) 2892-2896.

[305] K. Ichihara, E. Kusunose, Y. Noda, M. Kusunose, Some properties of the fatty alcohol oxidation system and reconstitution of microsomal oxidation activity in intestinal mucosa. Biochimica et biophysica acta 878(3) (1986) 412-418.

[306] G.T. Henehan, N.J. Oppenheimer, Horse liver alcohol dehydrogenase-catalyzed oxidation of aldehydes: dismutation precedes net production of reduced nicotinamide adenine dinucleotide. Biochemistry 32(3) (1993) 735-738.

[307] J.A. Hinson, R.A. Neal, An examination of octanol and octanal metabolism to octanoic acid by horse liver alcohol dehydrogenase. Biochimica et biophysica acta 384(1) (1975) 1-11.

[308] L.P. Olson, J. Luo, O. Almarsson, T.C. Bruice, Mechanism of aldehyde oxidation catalyzed by horse liver alcohol dehydrogenase. Biochemistry 35(30) (1996) 9782-9791.

[309] M.A. Longo, D. Combes, Influence of surface hydrophilic/hydrophobic balance on enzyme properties. Journal of biotechnology 58(1) (1997) 21-32.

[310] D.N. Rubingh, The influence of surfactants on enzyme activity. Current opinion in colloid and interface science 1 (1996) 598-603.

[311] R. Pasqualini, W. Arap, D.M. McDonald, Probing the structural and molecular diversity of tumor vasculature. Trends in molecular medicine 8(12) (2002) 563-571.

[312] H. Maeda, T. Sawa, T. Konno, Mechanism of tumor-targeted delivery of macromolecular drugs, including the EPR effect in solid tumor and clinical overview of the prototype polymeric drug SMANCS. Journal of control release 74(1-3) (2001) 47-61.

[313] B.K. Kang, J.S. Lee, S.K. Chon, S.Y. Jeong, S.H. Yuk, G. Khang, H.B. Lee, S.H. Cho, Development of self-microemulsifying drug delivery systems (SMEDDS) for oral bioavailability enhancement of simvastatin in beagle dogs. International journal of pharmaceutics 274(1-2) (2004) 65-73.

[314] P.M. Bummer, Physical chemical considerations of lipid-based oral drug delivery--solid lipid nanoparticles. Critical reviews in therapeutic drug carrier systems 21(1) (2004) 1-20.

[315] M.C. Gohel, A.F. Amin, Formulation optimization of controlled release diclofenac sodium microspheres using factorial design. Journal of control release 51(2-3) (1998) 115-122.

[316] J. Gabrielsson, N. Lindberg, T. Lundstedt, Multivariate methods in pharmaceutical applications. Journal of chemometrics 16 (2002) 141-160.

[317] F.H. Walters, L.R. Parker, S.L. Morgan, S.N. Deming, Sequential Simplex Optimization, CRC Press Inc., Boca Raton, Florida, 1991.

[318] X. Dong, R.J. Mumper, The metabolism of fatty alcohols in lipid nanoparticles by alcohol dehydrogenase. Drug development and industrial pharmacy 32(8) (2006) 973-980.

[319] J.M. Koziara, T.R. Whisman, M.T. Tseng, R.J. Mumper, In-vivo efficacy of novel paclitaxel nanoparticles in paclitaxel-resistant human colorectal tumors. Journal of control release 112(3) (2006) 312-319.

[320] K.A. Traul, A. Driedger, D.L. Ingle, D. Nakhasi, Review of the toxicologic properties of medium-chain triglycerides. Food and chemical toxicology 38(1) (2000) 79-98.

[321] A.B. Dhanikula, N.M. Khalid, S.D. Lee, R. Yeung, V. Risovic, K.M. Wasan, J.C. Leroux, Long circulating lipid nanocapsules for drug detoxification. Biomaterials 28(6) (2007) 1248-1257.

[322] M.O. Oyewumi, R.J. Mumper, Gadolinium-loaded nanoparticles engineered from microemulsion templates. Drug development and industrial pharmacy 28(3) (2002) 317-328.

[323] G. Derringer, R. Suich, Simultaneous optimization of several response variables. Journal of quality technology 12 (1980) 214-219.

[324] K.T. Papazisis, G.D. Geromichalos, K.A. Dimitriadis, A.H. Kortsaris, Optimization of the sulforhodamine B colorimetric assay. Journal of immunological methods 208 (1997) 151-158.

[325] G.J. MacEachern-Keith, L.J. Wagner Butterfield, M.J. Incorvia Mattina, Paclitaxel stability in solution. Analytical chemistry 69 (1997) 72-77.

[326] J. Tian, V.J. Stella, Degradation of paclitaxel and related compounds in aqueous solutions I: epimerization. Journal of pharmaceutical sciences 97(3) (2008) 1224-1235.

[327] H. Bunjes, K. Westesen, M.H.J. Koch, Crystallization tendency and polymorphic transitions in triglyceride nanoparticles. International journal of pharmaceutics 129 (1996) 159-173.

[328] B. Siekmann, K. Westesen, Thermoanalysis of the recrystallization process of melt-homogenized glyceride nanoparticles. Colloids and surfaces B. Biointerfaces 3 (1994) 159-175.

[329] J.A. Zhang, G. Anyarambhatla, L. Ma, S. Ugwu, T. Xuan, T. Sardone, I. Ahmad, Development and characterization of a novel Cremophor EL free liposome-based paclitaxel (LEP-ETU) formulation. European journal of pharmaceutics and biopharmaceutics 59(1) (2005) 177-187.

[330] M.K. Lee, S.J. Lim, C.K. Kim, Preparation, characterization and in-vitro cytotoxicity of paclitaxel-loaded sterically stabilized solid lipid nanoparticles. Biomaterials 28(12) (2007) 2137-2146.

[331] L.E. van Vlerken, Z. Duan, M.V. Seiden, M.M. Amiji, Modulation of intracellular ceramide using polymeric nanoparticles to overcome multidrug resistance in cancer. Cancer research 67(10) (2007) 4843-4850.

[332] M. Sznitowska, M. Klunder, M. Placzek, Paclitaxel solubility in aqueous dispersions and mixed micellar solutions of lecithin. Chemical & pharmaceutical bulletin 56(1) (2008) 70-74.

[333] S. Hassan, S. Dhar, M. Sandstrom, D. Arsenau, M. Budnikova, I. Lokot, N. Lobanov, M.O. Karlsson, R. Larsson, E. Lindhagen, Cytotoxic activity of a new paclitaxel formulation, Pacliex, in-vitro and in-vivo. Cancer chemotherapy and pharmacology 55(1) (2005) 47-54.

[334] P. Kan, Z.B. Chen, C.J. Lee, I.M. Chu, Development of nonionic surfactant/phospholipid o/w emulsion as a paclitaxel delivery system. Journal of control release 58(3) (1999) 271-278.

[335] M. Fresta, G. Cavallaro, G. Giammona, E. Wehrli, G. Puglisi, Preparation and characterization of polyethyl-2-cyanoacrylate nanocapsules containing antiepileptic drugs. Biomaterials 17(8) (1996) 751-758.

[336] C. Solans, P. Izquierdo, J. Nolla, N. Azemar, M.J. Garacia-Celema, Nano-emulsions. Current opinion in colloid and interface science 10 (2005) 102-110.

[337] H.L. Wong, R. Bendayan, A.M. Rauth, X.Y. Wu, Development of solid lipid nanoparticles containing ionically complexed chemotherapeutic drugs and chemosensitizers. Journal of pharmaceutical sciences 93(8) (2004) 1993-2008.

[338] M. Volm, J. Mattern, Resistance mechanisms and their regulation in lung cancer. Critical reviews in oncogenesis 7(3-4) (1996) 227-244.

[339] M.M. Gottesman, T. Fojo, S.E. Bates, Multidrug resistance in cancer: role of ATP-dependent transporters. Nature reviws cancer 2(1) (2002) 48-58.

[340] G.C. Wishart, D. Bissett, J. Paul, D. Jodrell, A. Harnett, T. Habeshaw, D.J. Kerr, M.A. Macham, M. Soukop, R.C. Leonard, et al., Quinidine as a resistance modulator of epirubicin in advanced breast cancer: mature results of a placebo-controlled randomized trial. Journal of clinical oncology 12(9) (1994) 1771-1777.

[341] C.E. Soma, C. Dubernet, G. Barratt, F. Nemati, M. Appel, S. Benita, P. Couvreur, Ability of doxorubicin-loaded nanoparticles to overcome multidrug resistance of tumor cells after their capture by macrophages. Pharmaceutical research 16(11) (1999) 1710-1716.

[342] T. Minko, P. Kopeckova, V. Pozharov, J. Kopecek, HPMA copolymer bound adriamycin overcomes MDR1 gene encoded resistance in a human ovarian carcinoma cell line. Journal of control release 54(2) (1998) 223-233.

[343] P.K. Smith, R.I. Krohn, G.T. Hermanson, A.K. Mallia, F.H. Gartner, M.D. Provenzano, E.K. Fujimoto, N.M. Goeke, B.J. Olson, D.C. Klenk, Measurement of protein using bicinchoninic acid. Analytical biochemistry 150(1) (1985) 76-85.

[344] J.W. Polli, S.A. Wring, J.E. Humphreys, L. Huang, J.B. Morgan, L.O. Webster, C.S. Serabjit-Singh, Rational use of in-vitro P-glycoprotein assays in drug discovery. The Journal of pharmacology and experimental therapeutics 299(2) (2001) 620-628.

[345] F. Némati, C. Dubernet, A. Colin de Verdière, M. Poupon, L. Treupel-Acar, F. Puisieux, P. Couvreur, Some parameters influencing cytotoxicity of free doxorubicin and doxorubiicn-loaded nanoparticles in sensitive and multidrug resistant leucemic murine cells: incubation time, number of nanoparticles per cell. International journal of pharmaceutics 102 (1994) 55-62.

[346] E. Tomlinson, L. Malspeis, Concomitant adsorption and stability of some anthracycline antibiotics. Journal of pharmaceutical sciences 71(10) (1982) 1121-1125.

[347] A.C. de Verdiere, C. Dubernet, F. Nemati, E. Soma, M. Appel, J. Ferte, S. Bernard, F. Puisieux, P. Couvreur, Reversion of multidrug resistance with polyalkylcyanoacrylate nanoparticles: towards a mechanism of action. British journal of cancer 76(2) (1997) 198-205.

[348] K. Bogman, F. Erne-Brand, J. Alsenz, J. Drewe, The role of surfactants in the reversal of active transport mediated by multidrug resistance proteins. Journal of pharmaceutical sciences 92(6) (2003) 1250-1261.

[349] A.V. Kabanov, E.V. Batrakova, V.Y. Alakhov, An essential relationship between ATP depletion and chemosensitizing activity of Pluronic block copolymers. Journal of control release 91(1-2) (2003) 75-83.

[350] A.P. Halestrap, The regulation of the oxidation of fatty acids and other substrates in rat heart mitochondria by changes in the matrix volume induced by osmotic strength, valinomycin and Ca2+. The Biochemical journal 244(1) (1987) 159-164.

[351] A. Kaasik, D. Safiulina, A. Zharkovsky, V. Veksler, Regulation of mitochondrial matrix volume. American journal of physiology 292(1) (2007) C157-163.

[352] M.V. Berridge, P.M. Herst, A.S. Tan, Tetrazolium dyes as tools in cell biology: new insights into their cellular reduction. Biotechnology annual review 11 (2005) 127-152.

[353] R. Stowe, D.W. Koening, S.K. Mishra, D.L. Piersonb, Nondestructive and continuous spectrophotometric measurement of cell respiration using a tetrazolium-formazan microemulsion. Journal of microbial methods 22 (1995) 283-292.

[354] T. Steenpass, A. Lung, R. Schubert, Tresylated PEG-sterols for coupling of proteins to preformed plain or PEGylated liposomes. Biochimica et biophysica acta 1758(1) (2006) 20-28.

[355] K. Nilsson, K. Mosbach, Immobilization of ligands with organic sulfonyl chlorides. Methods in enzymology 104 (1984) 56-69.

Vita

Xiaowei Dong was born on April 11, 1973 in Xi'an, China. She received her Bachelor of Science degree (1994) from Sichuan Institute of Light Industry and Chemical Technology (Sichuan, China). She received her Master's in Science (Applied Chemistry) degree (1999) from East China University of Science and Technology (Shanghai, China). Xiaowei worked under the supervision of Prof. Guizhen Li. Her master's thesis was titled *"Determination of Major Phospholipids in Soybean Lecithin by HPLC and Their Structure Research"*. In August of 1999, Xiaowei accepted a position as an assistant researcher in State Key Laboratory of Organometallic Chemistry, Shanghai Institute of Organic Chemistry (SIOC), Chinese Academy of Sciences (Shanghai, China). She joined the Department of Pharmaceutical Sciences Graduate Program at the University of Kentucky in the fall of 2004. Xiaowei was the recipient of 2008 AAPS Graduate Student Symposium in Drug Delivery and Pharmaceutical Technology sponsored by Bristol Myers Squibb. Xiaowei is an author or co-author of ten peer reviewed publications and three patent applications. The most important paper of her publications was her first- authored publication in *Cancer Research* (with impact factor 2007: 7.67) about overcoming P-gp-mediated drug resistance using drug-loaded NPs. She has one additional manuscript in preparation.

Publications:

1. **X. Dong**, C.A. Mattingly, M. Tseng, M. Cho, Y. Liu, V. Adams and R.J. Mumper. Doxorubicin and paclitaxel-loaded lipid-based nanoparticles overcome multidrug resistance by inhibiting P-gp and depleting ATP. Cancer research 69 (2009) 3918-3926.

2. **X. Dong**, C.A. Mattingly, M. Tseng, M. Cho, V. Adams and R.J. Mumper. Development of new lipid-based paclitaxel nanoparticles using sequential simplex optimization. European journal of pharmaceutics and biopharmaceutics 72 (2008) 9-17.

3. **X. Dong**, P. Ma, C.A. Mattingly, M. Tseng, M. Cho, V. Adams and R.J. Mumper. In-vivo anticancer efficacy of paclitaxel-loaded nanoparticles to overcome P-gp-mediated drug resistance in human ovarian tumors. In preparation

4. **X. Dong** and R.J. Mumper. The metabolism of fatty alcohols in lipid nanoparticles by alcohol dehydrogenase. Drug development and industrial pharmacy 32(8) (2006) 973-980.

5. P. Ma, **X. Dong**, C.L. Swadley, A. Gupte, M. Leggas, H.C. Ledebur and R.J. Mumper. Development of idarubicin and doxorubicin solid lipid nanoparticles to overcome Pgp-mediated multiple drug resistance in Leukemia. Journal of biomedical nanotechnology 5 (2009) 151-161

6. **X. Dong**, X. Xu, H. Jin, and Z. Li. Separation of chloro-substituted and bromo-substituted styrene oxide by chiral GC. Chinese journal of organic chemistry 24(3) (2004) 306-310.

7. X. Xu, **X. Dong** and P. Mao. Precipitation reaction between berberine and rheinic acid by capillary electrophoresis. Acta pharmaceutica sinica 38(10) (2003) 779-782.

8. X. Xu, X. Bao, **X. Dong**, Z. Shi, Z. Yu and S. Ma. Chiral separation of 2, 3-allenice acid by capillary zone electrophoresis using cyclodextrin derivatives. Chirality 15 (2003) 201-205.

9. **X. Dong**, X. Xu, H. Hou, Q. Wei, D. Xu, S. Zhao, A. Zhang, N. Jiao, and S. Ma. Gas chromatographic enantiomeric separation of propargylic alcohols and 2, 3-allenic alcohols. Chinese journal of organic chemistry 21 (2001) 1142.

10. **X. Dong**, X. Feng and G. Li. Determination of phospholipids in soy phospholipids by high performance liquid chromatography. Journal of east China university of science and technology 26 (2000) 315-318.

11. W. Deng, X. Hou, L. Dai and **X. Dong**. Efficient planar chiral 2'-substituted 1, 1'-P, N-ferrocene ligands for the asymmetric heck reaction: control of enantioselectivity and configuration by planar chiral substituent. Chemical communications (2000) 1483-1484.

<div style="text-align: right;">

Xiaowei Dong
_____
Author

May 20, 2009
_____
Date

</div>